Durham E-Theses

A study of turbulent diffusion in the lower atmosphere using artificially produced electric space charge

Jones, C. D.

How to cite:

Use policy

A STUDY OF TURBULENT DIFFUSION

IN THE LOWER ATMOSPHERE USING

ARTIFICIALLY PRODUCED ELECTRIC SPACE CHARGE

by

C. D. JONES, M. Inst. P., F.R. Met. Soc., of
the Graduate Society of the University of Durham

Presented in candidature for the degree of Doctor
of Philosophy in the University of Durham

January 1974

ABSTRACT

An investigation into the behaviour of artificially produced
ions, released from a point source a few metres above the
Earth's surface, is presented. It is shown both experimentally
and theoretically that the ions form a plume downwind of the
ion source and, moreover, that the nature of this plume is
rather similar to that of a smoke plume. Electric field and
ion concentration measurements have been used to deduce certain
features about ion plumes and distinct connexions between ion
plume behaviour and the local meteorological conditions have
been observed. In particular, the use of bidirectional vane
techniques has indicated that ions can be used quite success-
fully as a tracer in short range atmospheric diffusion experi-.
ments. The technique does, however, possess certain limita-
tions, the details of which are included in the text.

In accordance with modern practice, I have used the rationalized MKS system of units throughout this thesis. Apart from any adherence to convention, the employment of this system is both convenient and simple and thus the choice seemed obvious.

Considerable confusion has arisen in Atmospheric Electricity when discussing electric fields and potential gradients. Unfortunately, quite often, the term 'field' has been used to denote dV/dz and not, as the definition strictly requires $- dV/dz$. Here z is the height, measured vertically upward. In this work both the terms potential gradient and electric field have been used, but great care has been taken to employ these correctly. When discussing experimental results the numerical observations are, where appropriate, expressed in terms of potential gradient to facilitate comparisons with other work.

The descriptions ion plume and space charge plume are used virtually synonomously in the text. Strictly speaking, the term space charge plume is more accurate because the artificial ions, on leaving the generator, become mixed with natural ions of both signs. In cases where it is necessary to distinguish between the two concepts this has been done.

ACKNOWLEDGEMENTS

my appreciation to the entire staff of the Physics Department.

I would like to express my gratitude to my wife, whose under-standing, tolerance and encouragement have been of inestimable value in the last three years.

Finally, thanks are due to Mrs. Diana MUNRO for the speed and efficiency with which she typed this thesis.

LIST OF SECTION HEADINGS

Chapter 1: INTRODUCTION

1.1
General Background

The lower atmosphere consists of a uniform mixture of gases, the chief of these being nitrogen, oxygen, argon and carbon dioxide. In addition, there is always present a relatively small, but nonetheless highly significant, proportion of water vapour. Unlike the gases, the concentration of this vapour varies both from time to time and from place to place. It is, in fact, these constant variations of water vapour content which are, to a great extent, responsible for the various types of weather.

As well as the substances referred to above, the atmosphere, and particularly the lower atmosphere, always contains suspended particulate matter in considerable amounts. In times past, the origins of such matter were almost exclusively natural and arose from activities such as volcanic eruptions and the evaporation of sea-spray. However, in the last century or so, and particularly in industrial or urban environments, man's activities have resulted in very considerable increases in the concentrations of particulate, and other, materials.

In addition to the substances above, there are varying concentrations of ions present in the lower atmosphere. The existence of such entities was recognized as early as 1899 by ELSTER and GEITEL, but at that time their origin was obscure. Later EBERT (1904) found that air diffusing from

the ground contained ions, the ionization resulting presumably from radioactivity in the earth's crust. HESS (1911) discovered that ions were more plentiful at higher levels in the atmosphere. This was later attributed to an effect of cosmic rays.

A most important property of ions, particularly insofar as this project is concerned, is their ability to persist for periods of up to several minutes (or even longer) in the lower atmosphere. CHALMERS (1967) gives values of 20 - 300 S for the lifetime of a small ion (see Sec. 3.2), depending on the locality. Any ion, being electrically charged, will, of course, move in an electric field. It has been known since 1752 (LEMONNIER) that such a field exists near the earth's surface. However, the magnitude of this field is such that, except perhaps in stormy conditions, resulting ion motions are only in the order of a few centimetres per second. Consequently, the movement of ions, at least in the lower atmosphere, is often largely determined by the wind.

The actual concentration of ions near the surface is small, only about one molecule in 10^{17} being ionized at any one time. This implies that there are in the order of 10^9 ions of each sign in a cubic metre of air.

1.2
Artificially produced ions and the concept of a space charge plume

We can readily envisage the existence of a cloud of ions in
the atmosphere, such an entity being, in all probability,
rather similar in nature to a puff of smoke. The origin of
the ion cloud could be either natural or artificial, but in
both cases the cloud will be blown along with the wind.
Like a smoke puff, the ion cloud will become more dilute as
it moves downwind. If the numbers of ions of each sign
(assuming they are singly charged) within the cloud are equal,
then the total net charge will be zero. However, if ions of
one sign are in the majority, the cloud will possess a net
space charge. Elementary electrostatic theory predicts that
there will be an electric field in the vicinity of all space
charges and consequently electric field observation may be a
useful technique for the *detection* and measurement of such
charges.

KELVIN (1860) was the first to recognize the effects of man-
made space charges. He measured the electrical disturbances
due to locomotive steam and concluded that it was always
positively charged. Much later, WHITLOCK and CHALMERS (1956)
observed that these space charge "packets" from steam loco-
motives were detectable as far as 1 km from their source.
In fact, many combustion processes produce space charge.
MUEHLEISEN (1953) found large positive charges in diesel
exhaust gases and negative charges in the effluents of chemi-
cal factories and gasworks. OGDEN (1967) has also reported
positive charges near diesel engines.

The high electric fields during showers and thunderstorms
often result in copious ion production by point discharge
processes. In this case, the ionization results from
electron-molecule and ion-molecule collision phenomena
in the high field region near the point. The ions, once
produced, are blown away from the point by the wind. In
many respects this is a very similar situation to that of
smoke being blown from a chimney stack, it being a matter
of familiar experience that, usually, a long plume is
formed downwind of the source. Observations show that
the size of a smoke plume steadily increases as it moves
downwind, this diffusion process being intimately connec-
ted with the gusty, or turbulent, character of the wind.
Similarly, when point discharge occurs, we might reasonably
expect that an ion plume will be formed downwind of the
point. As in the case of the smoke plume, the dimensions
of the ion plume will increase at greater distances from the
ion source.

MAUND (1958) has shown that, at horizontal distances less
than about twice the height of a discharging point, the ion
or space charge plume may be regarded as a line charge.
That is, the effects of turbulent diffusion can be ignored
relatively near the source. MAUND, in fact, wanted to
estimate the current flowing through the point by comparing
the upwind and downwind electric fields. Considering the
ion plume as a line charge, therefore, greatly facilitated
his theoretical calculations of electric field.

CHALMERS (1967) suggested that if space charge could be gene-
rated artificially, then measurements of charge density down-
wind of an ion source might provide useful information on
atmospheric diffusion. In fact, CRAMER, GILL and RECORD
(1954) had already used an electrically charged smoke, rather
than ions, to conduct just such an investigation into the
effects of turbulent diffusion. However, experiments invol-
ving the use of ions, although also suggested by LARGE and
PIERCE (1957) and OGDEN (1967), do not appear to have ever
been carried out. Techniques involving ions would in many
ways be closely analogous to more familiar methods using
such substances as sulphur dioxide. Space charge density
measurements in ion plumes have their counterpart in SO_2
concentration measurements in those plumes, but electric
field measurements offer a unique tool for the investigation
of ion plumes, no analogous measurement being possible with
uncharged plumes. The value of the electric field at a par-
ticular point is determined by both the total charge present
and its distribution in space relative to that point. There-
fore, electric field measurements near ion plumes might pro-
vide useful, certainly interesting, information regarding the
behaviour of plumes in general.

Point discharge currents depend, to a considerable extent,
on the wind speed as well as the prevailing electric field.
Consequently, a discharging point, being therefore a variable-
output ion source, would hardly be suitable for an investiga-
tion of turbulent diffusion. In order to minimize the effects
of the earth's potential gradient, LARGE and PIERCE (1957)
connected a raised point to a high voltage supply in their

studies of point discharge. These workers were interested
in the effects of wind on point discharge currents and
therefore the point was left exposed. However, if a dis-
charging point were shielded from both the wind and exter-
nal electric fields, it might be possible to construct a
constant-output ion source suitable for use in diffusion
studies.

DAYARATNA (1969) investigated the behaviour of artifi-
cially produced ions in a wind tunnel. However, his
design of ion generator, being specifically intended for
work in wind tunnel environments, could not readily be
adapted to the needs of the current project. Details of
the constant-output ion generator specially developed for
use in the diffusion studies conducted here can be found
in *Sec.* 4.4.

1.3
The nature of the proposed investigation and the choice of experimental sites

The basis of the proposed investigation has already been intimated in the previous section. Considerable interest has always been centred on the dispersal of atmospheric pollutants, usually produced by point sources, and thus it was thought that an analogous study, involving the use of a point source of ions, might be very worthwhile.

Much previous work on turbulent diffusion has required the expenditure of considerable resources, both in terms of man-hours and equipment. Many research programmes have been really ambitious, notably the Project Prairie Grass in 1956. In this study several hundred sampling stations were placed in a series of arcs downwind of a point source of sulphur dioxide. However, as the present investigation had to be conducted virtually single-handed, relatively modest goals were set.

It was proposed to design and construct a constant output ion source capable of producing either negative or positive ions, the choice being that of the experimenter. This ion source was to be mounted on a mast, and, at various distances downwind, the electric field and ion concentration were to be measured. It was hoped that measurements would be feasible up to about 500 m. from the ion source.

At this stage, it was clear that certain meteorological observations would be necessary in order to make the best use of the electrical measurements. The wind speed and

direction both have a considerable effect on any plume and, initially, it was proposed that just these quantities be measured. Later, it was expected that, as experimental work advanced, more sophisticated meteorological data would be required.

The experimental technique was entirely novel and therefore, to some extent, the investigation was open-ended, that is, no precise objectives were defined. The aim of the project was to investigate the behaviour of ion plumes in as much detail as possible, and then to try to draw comparisons between these and plumes of uncharged material.

Clearly, an investigation of the type proposed demands the use of a site where pollution levels are low, otherwise the effects mentioned in sec. 1.2 might produce erroneous results.

Previous workers at Durham, e.g. SHARPLESS (1968), have conducted extensive investigations at Lanehead, which is situated high in the Pennine hills in West County Durham. SHARPLESS concluded, from his electrical measurements, that atmospheric pollution levels were minimal in this area and consequently it appeared suitable for the current project. In particular, the existence of a large, and substantially level area near the top of the hill, 1 km NNW of the centre seemed an ideal location for the experimental work. In fact, initial work was carried out at this site, but owing to the altitude (600 m), severe weather was often experienced, even in Summer, and efforts were therefore made to seek a more congenial environment in which to conduct the experiments.

THE OXEN LAW SITE

1km
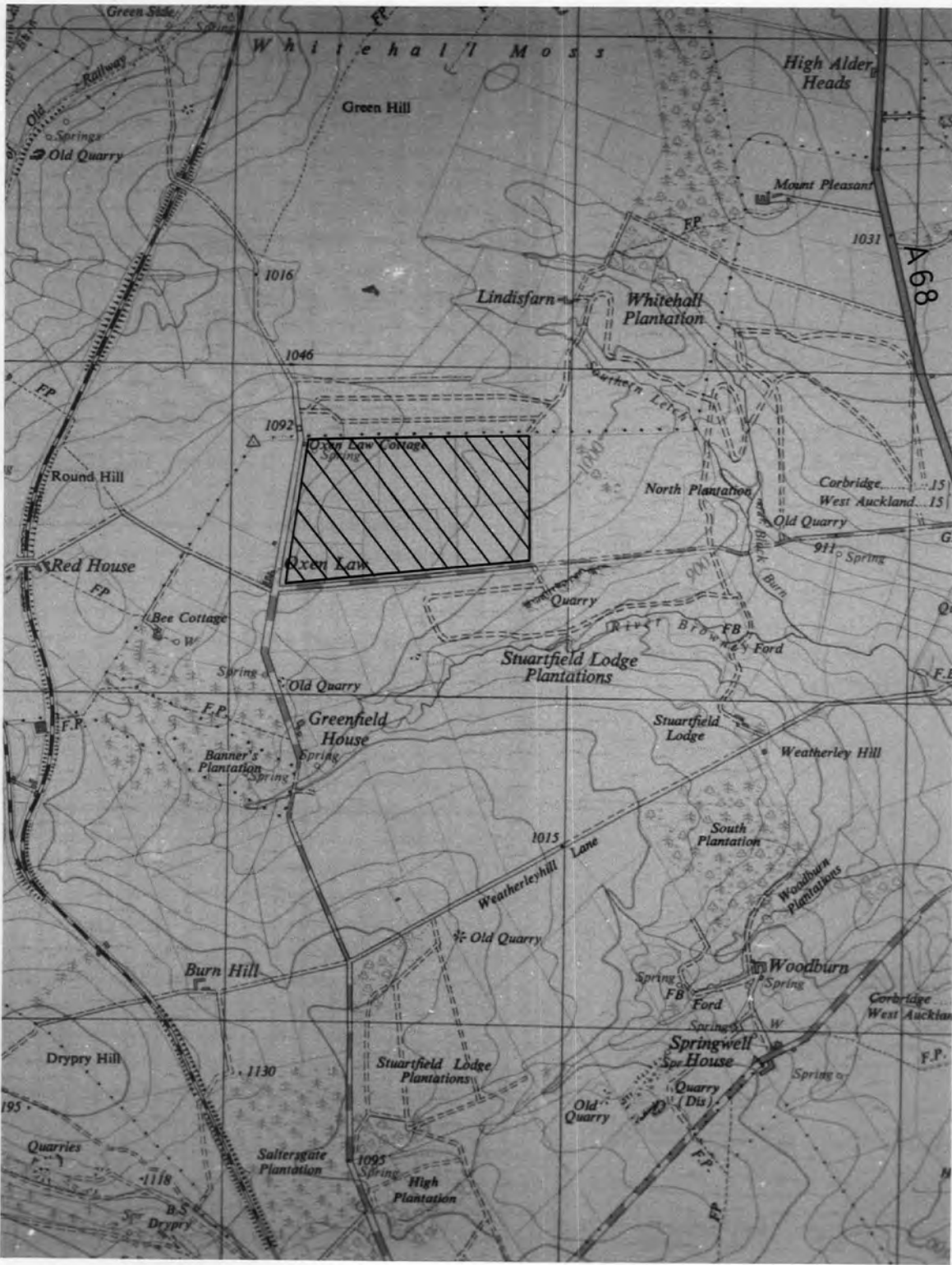
THE MAIDEN CASTLE SITE

1km

The use of a site at Oxen Law, about 6 km SW of Consett, was obtained. The terrain in this locality consists of gently rolling grass and moorland, with relatively few trees or other projections likely to disturb the air flow. The elevation of this site is only 300 m. and, together with the fact that it is only half the distance from the University (30 km) as is Lanehead, made it an attractive proposition for experimental work. The details of this site are shown in Fig. P1.

Some investigations were also carried out in a large field at the University Sports Centre, Maiden Castle, Durham. Details are shown in Fig. P2. The Centre, which is located in a very shallow region of the Wear Valley, is only 1 km from the University, thus making it a very convenient field work site.

Despite the proximity of Consett in the case of the Oxen Law site, and Durham in that of the Maiden Castle site, surprisingly little trouble was experienced from air pollution. Occasionally difficulties did arise, however, and these are discussed further in Sec. 3.2.

Chapter 2: THE DISPERSAL OF IONS BY TURBULENT DIFFUSION

2.1
Purpose of the Chapter

It soon became obvious that the behaviour of the ion plume,
in common with that of smoke plumes, was largely determined
by the local air motion. It is my intention in this chapter
to present first a brief account of the general nature of
winds and secondly to examine in detail features of turbulent
flow relevant to this project. A steady state plume model,
based on traditional methods, is first presented and then,
in view of the statistical nature of turbulence, more reali-
stic "fluctuating plume" models are proposed. The electric
fields due to the ion plume may then be computed by applying
an appropriate model.

Certain electrostatic effects are also capable of influencing
the behaviour of the ion plume. These will be discussed in
the following chapter.

2.2
Initial Considerations

REYNOLDS (1883) showed that two distinct types of flow exist;
at relatively low velocities the fluid moves in a steady,
quiet manner - laminar flow, whilst at higher velocities the
flow becomes irregular and unpredictable - turbulent flow.
It has been found in the lower atmosphere that winds are
nearly always turbulent, observation of a smoke plume readily
confirming this.

Any flow requires a continuous input of energy to maintain it,
otherwise its kinetic energy would decrease, being ultimately
dissipated by viscosity as heat. Solar radiation is the
driving force as far as the earth's winds are concerned.
The sun's heat produces large-scale convective systems which
are modified by the Coriolis force into the extensive vortices
known in our latitude as depressions and anticyclones.

At heights above 500 m., it is possible to neglect the fric-
tional effect of the earth's surface on the air flow. At
these levels the flow is the result of a balance between the
pressure gradient and Coriolis forces and is referred to as
the geostrophic wind. Further details on this and other
aspects of synoptic scale meteorology can be found in BRUNT
(1939) and are therefore not discussed here.

The increasing effect of friction at the lower levels causes
the relatively steady geostrophic flow to be broken down into
a series of irregular vortices near the ground. The mean
velocity of the air gradually reduces until at the surface it

is close to zero. This layer between the surface and the geostrophic flow region is known as the planetary boundary or friction layer. It is the physics of this layer which is of most interest to us in this project.

The Transport of Material and Momentum in the Earth's Boundary Layer

This is a region in which momentum from the geostrophic layer is continually transferred downward towards the earth's surface. The flow is turbulent and thus the momentum flux takes the form of eddies.

Let us now examine mathematically some of the consequences of the velocity fluctuations which occur in all turbulent flows. It is customary, both in the measurement and analysis of atmospheric turbulence, to choose the co-ordinate directions (x, y and z) so that the mean velocity ($\bar{u}$) lies along the x-axis, thus making the y and z directions those of the lateral and vertical components respectively. This is represented in Fig. 2.1(a). It is also conventional to regard an instantaneous value of velocity at a particular point as being the sum of a mean and a fluctuating component (see Fig. 2.1(b).). It is, of course, perfectly feasible to consider other varying quantities in a similar manner; this approach being used extensively later.

In the case of the longitudinal velocity component , we may write its mean value $\bar{u}$ as,

$$\bar{u} = \frac{1}{T} \int_{o}^{T} u \, dt \qquad (2.1)$$

by definition, similar relations holding for the other two components v and w.

Suppose we were measuring the concentration χ of a pollutant as a function of time. Then, by employing the above method, we can write:

$$\chi(t) = \bar{\chi} + \chi'(t) \qquad (2.2)$$

where the overbar and prime refer to the mean and fluctuating components as before.

Consider now the effect of a turbulent flow on the distribution of material, the system being assumed horizontally homogeneous for the sake of simplicity. This implies that χ is function of the height, z, only. The amount of material crossing a small horizontal surface in the upward direction is given by:

$$M_z = \chi w \qquad (2.3)$$

that is, the flux is equal to the instantaneous concentration multiplied by the vertical velocity.

Expanding 2.3, we obtain:

$$M_z = (\bar{\chi} + \chi')(\bar{w} + w')$$

and upon multiplying out and taking the time mean value, we find:

$$\overline{M_z} = \overline{\bar{\chi}\bar{w}} + \overline{\bar{\chi}w'} + \overline{\chi'\bar{w}} + \overline{\chi'w'} \qquad (2.4)$$

Certain of the terms in 2.4 can be shown to be zero. In the calculation of the product $\overline{\chi'\bar{w}}$, for instance, it is clear that:

$$\overline{\chi'\bar{w}} = \bar{\chi'}\bar{w}$$

since the quantity $\bar{w}$ acts only as a constant coefficient for the fluctuating portion χ'. Further, the mean value of χ' is zero by definition. In view of this, equation 2.4 simplifies to:

$$\overline{M_z} = \overline{\bar{\chi}\bar{w}} + \overline{\chi'w'} \qquad (2.5)$$

Conventions used in studies of atmospheric turbulence

(a) Choice of co-ordinate system
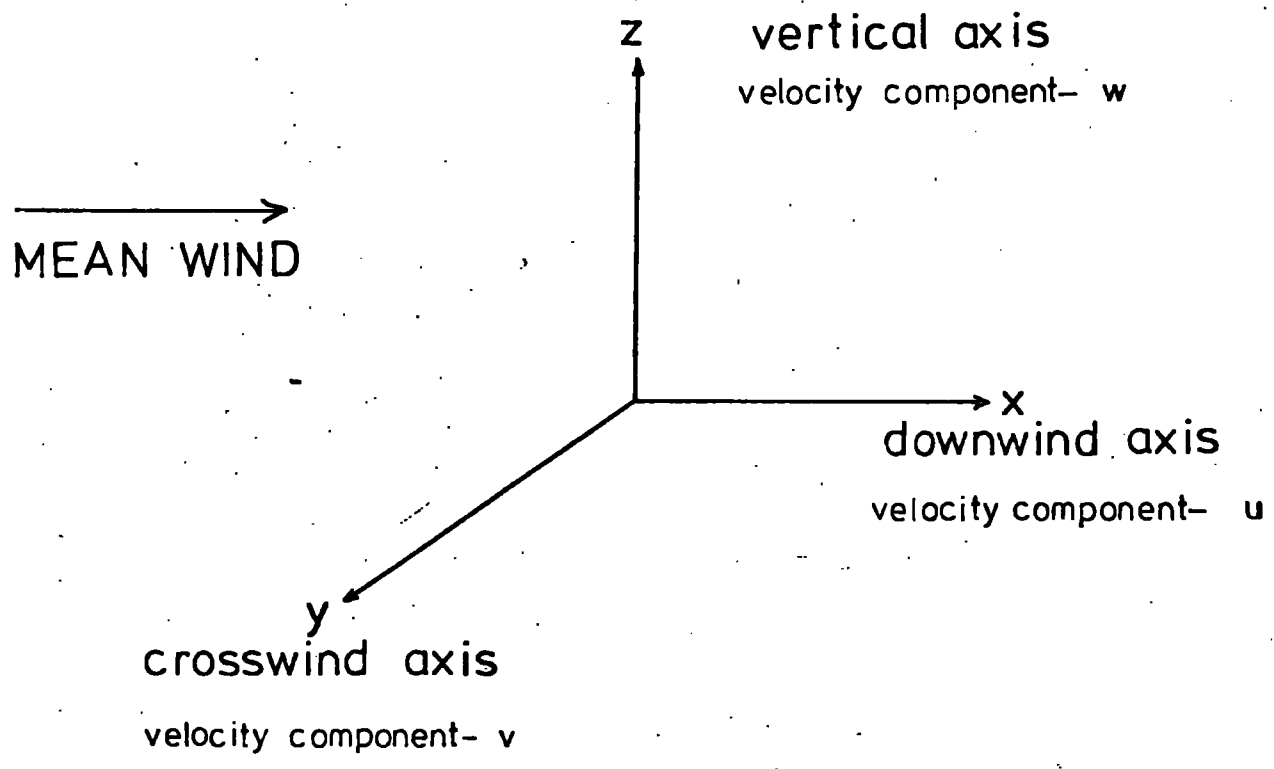
z — vertical axis
velocity component— w

MEAN WIND →

x → downwind axis
velocity component— u

y
crosswind axis
velocity component— v

(b) Mean and fluctuating values

velocity component

u

fluctuation u′

mean velocity over time T

Ū

time

T
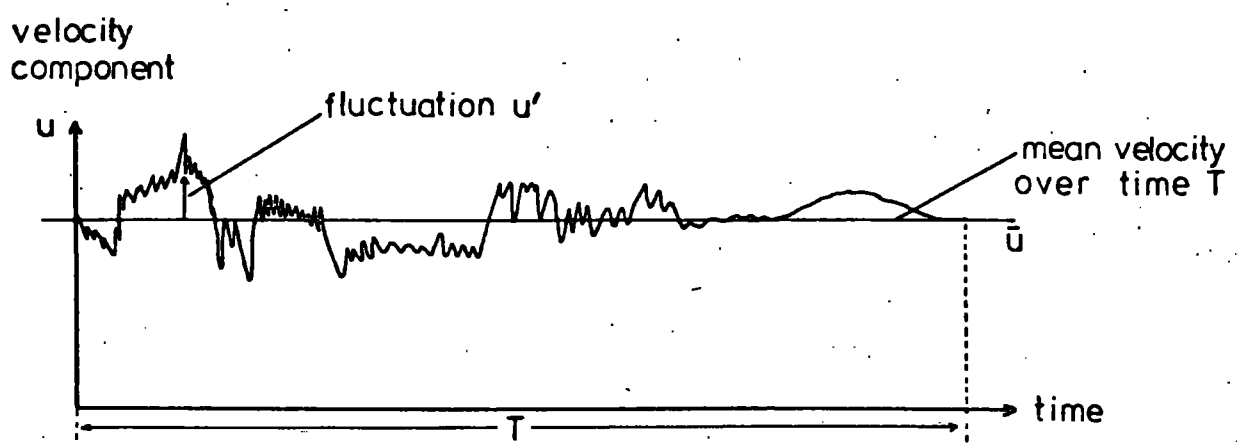
$$U(t) = \bar{U} + U'(t)$$

actual value   mean value   fluctuation

The first term represents the flux to be associated with the mean vertical motion and would have appeared even if the flow had been laminar. The second term, which is not necessarily zero, is apparently a transfer caused by the fluctuations themselves.

In the lower atmosphere, the mean vertical velocity $\overline{w}$ is usually small and can normally be ignored in comparison with w' . Hence, 2.5 reduces to:

$$\boxed{\overline{M_z} = \overline{\mathcal{X}'w'}} \qquad (2.6)$$

We may generalize equation 2.6 to represent the transport of other entities by turbulence. In particular, we could write:

$$\boxed{\Upsilon = d\overline{u'w'}} \qquad (2.7)$$

to represent the transfer of momentum in the boundary layer. The density, d , appears because the instantaneous momentum is du per unit volume, this, therefore, replacing $\mathcal{X}$ in 2.6. The quantity Υ refers to the amount of momentum crossing a unit horizontal surface and is known as the turbulent or Reynolds stress.

The viscous stress is, as usual, given by an expression of the type:

$$\boxed{\Upsilon_v = \eta \, \frac{du}{dz}} \qquad (2.8)$$

where η is the coefficient of viscosity.

There is no physical reason why viscous and turbulent effects cannot occur together. However, it so happens in the atmosphere that the Reynolds stress is much larger than any viscous

stresses. Thus, in most cases, it is quite satisfactory to
consider the Reynolds stress as if it were acting alone.

The Concepts of Eddy Diffusivity and Viscosity

In the previous section, we established a simple relation
for the flux of material that is transferred by the turbu-
lent eddies. Naturally, our main interest here is the trans-
port and diffusion of space charge, rather than these more
familiar entities.

Apart from certain electrostatic factors to be discussed
later, there would seem to be no reason why equation 2.6
cannot be generalized to include space charge transfer.
Hence we may write:

$$\overline{S}_z = \overline{\rho' w'} \qquad (2.9)$$

where ρ is the instantaneous space charge concentration
at a particular point and S_z the space charge flux (equi-
valent to current per unit area). We now recall the rela-
tionship between flux and concentration for a simple molecu-
lar diffusion process. Fick's first law states that the flux
of material is proportional to the concentration gradient,
thus:

$$m_z = -D_m \frac{dx}{dz} \qquad (2.10)$$

where m_z is the upward flux of material due to molecular dif-
fusion and D_m the appropriate coefficient. Similarly, in
the special case of space charge, we can write, by analogy,
that:

$$s_z = -D_s \frac{d\rho}{dz} \qquad (2.11)$$

Early workers, notably SCHIMDT (1918), explored the possibi-
lity of representing the turbulent fluxes in a way mathemati-
cally similar to their molecular counterparts. This is, of

course, largely just a mathematical artifice because the mechanisms of molecular and turbulent transfer are so different.

On this basis, we can rewrite equation 2.6 in the form:

$$\boxed{\overline{M}_z = - K_m \frac{d\overline{x}}{dz}} \qquad (2.12)$$

where K_m is a turbulent diffusion coefficient for the material and $d\overline{x}/dz$ the gradient of <u>mean</u> concentration.

A cautionary note should be sounded here regarding the nature of K_m. The reader is probably aware that a molecular diffusion coefficient is essentially a property of the fluid and diffusing species. This is not, however, the case with turbulent diffusion coefficients as their values depend on the nature of the flow rather than on that of the fluid itself. We shall see that in the lower atmosphere K_m can vary by as much as two orders of magnitude as the conditions change.

We may extend the exchange coefficient hypothesis, as it is known, to include the transfer of momentum and presumably ions. In the case of momentum we write:

$$\boxed{\overline{\tau} = - K_v \frac{d\overline{u}}{dz}} \qquad (2.13)$$

where K_v is referred to as the eddy viscosity. Similarly, for the turbulent transfer of space charge we obtain:

$$\boxed{\overline{S}_z = - K_s \frac{d\overline{\rho}}{dz}} \qquad (2.14)$$

Provided that the ions are in low concentration, so that the electrostatic effects are small, we may assume that there will be no difference between the transfer mechanisms of ions and those of any other material. This implies that:

$$K_s = K_m.$$

KAWANO (1957) has determined a value for K_s indirectly by measurements of electric field, conductivity and space-charge, whilst HOPPEL and GATHMAN (1972) performed a similar measurement by a slightly different method. All three workers find values of K_s not far removed from those of K_m and we may assume that the similarity in transfer mechanisms is experimentally established.

2.5.1
The Basic Equations

It is the purpose of this section to apply the results obtained previously to describe the behaviour of space charge clouds. As a point source of ions was employed, it is obvious that diffusion will proceed in all three co-ordinate directions and, therefore, we must generalize the transfer relations to include those cases. Hence we write:

$$
\begin{aligned}
\bar{S}_x &= - K_x \frac{\partial \bar{\rho}}{\partial x} \\[2mm]
\bar{S}_y &= - K_y \frac{\partial \bar{\rho}}{\partial y} \\[2mm]
\bar{S}_z &= - K_z \frac{\partial \bar{\rho}}{\partial z}
\end{aligned}
\qquad (2.15)
$$

The subscript s has been omitted from the diffusivity because, in future, we shall only be concerned with the diffusion of space charge. The possibility of non-isotropic diffusion has, however, been allowed for by inclusion of the directional subscripts x, y, and z. In practice, atmospheric diffusion processes are rarely isotropic, particularly in the boundary layer.

Equations of the type 2.15, whilst being mathematically simple, are not, from our point of view, in a very helpful form. We wish to know, if possible, how the space charge concentration varies downwind of the source. Suppose we consider the flux of space charge through a small volume and at the same time, apply the principle of conservation of charge. It is found that:

$$
\frac{d\bar{\rho}}{dt} = \frac{\partial}{\partial x}\left(K_x \frac{\partial \bar{\rho}}{\partial x} \right) + \frac{\partial}{\partial y}\left(K_y \frac{\partial \bar{\rho}}{\partial y} \right) + \frac{\partial}{\partial z}\left(K_z \frac{\partial \bar{\rho}}{\partial z} \right) \qquad (2.16)
$$

the
~~The~~ details of a similar derivation being given by SUTTON

(1953). If K_x, K_y and K_z are independent of position, we

may simplify 2.16 to:

$$\frac{d\bar{\rho}}{dt} = K_x \frac{\partial^2 \bar{\rho}}{\partial x^2} + K_y \frac{\partial^2 \bar{\rho}}{\partial y^2} + K_z \frac{\partial^2 \bar{\rho}}{\partial z^2}$$

(2.17)

and, if the diffusion process if also isotropic, that is

$K_x = K_y = K_z = K$ say, then:

$$\frac{d\bar{\rho}}{dt} = K \nabla^2 \bar{\rho}$$

(2.18)

where ∇^2 is the Laplacian Operator.

We now consider some relevant solutions of these equations.

2.5.2
Diffusion from an Instantaneous Point Source

This type of source is exemplified in practice by a smoke

bomb or shell burst. We imagine a source that suddenly

releases a quantity Q of space charge and thereafter ceases

to produce ions. We further assume, for mathematical simpli-

city, that the ion source is far above ground. The boundary

conditions in this case are:

$\rho \longrightarrow 0$ as $t \longrightarrow 0$ at $r > 0$,

$\rho \longrightarrow 0$ as $t \longrightarrow \infty$,

r being the radial distance from the source.

If we assume that the total space charge is conserved, we may
write:

$$\int_V \rho\, dV = Q \qquad (2.19)$$

where the integral is with respect to volume.

We also assume the diffusion process is isotropic, and, bearing
in mind the symmetry of the system, we can rewrite equation
2.18 in the form:

$$\frac{\partial \bar{\rho}}{\partial t} = \frac{K}{r^2} \frac{\partial}{\partial r}\left(r^2 \frac{\partial \bar{\rho}}{\partial r} \right) \qquad (2.20)$$

The solution of 2.20 was first given by ROBERTS (1923) and is

$$\bar{\rho}(x,y,z,t) = \frac{Q}{8(\pi K t)^{3/2}} \exp\left(-\frac{r^2}{4Kt}\right) \qquad (2.21)$$

We observe that the concentration, at any particular time, is
a gaussian function of the radial distance, a feature which is
invariably present in the solutions of diffusion equations of
this type.

A situation of more interest to ourselves is the dispersal of
a puff of ions in a wind. ROBERTS assumed that the diffusion
process continues in this case as before, the diffusing puff
being merely carried bodily forward by the wind.

In certain circumstances, it might be possible for small por-
tions of a plume to become virtually detached from the main
system. Equation 2.21 may therefore be of assistance when
discussing the behaviour of these separated elements.

2.5.3
Diffusion from a Continuous Point Source
2.5.3.1
Ion Source in Calm Conditions for Above Ground

We can find the solution quite simply in this case by integrating 2.21 with respect to time. This is equivalent to considering a continuous ion source as being the sum of an infinite number of instantaneous sources. (More details of this technique can be found in works on the conduction of heat, e.g. CARSLAW and JAEGER, 1959). We rewrite the integral in the form:

$$\bar{\rho}(x,y,z,t) = \frac{Q}{8(\pi K)^{3/2}} \int_0^t t^{-3/2} \exp\left(\frac{-r^2}{4Kt}\right) dt,$$

which has the solution:

$$\bar{\rho}(x,y,z,t) = \frac{i}{4\pi K r} \, erfc\left(\frac{r}{(4Kt)^{1/2}}\right) \tag{2.22}$$

where $erfc$ denotes the complementary error function and i is the net current output of the ion generator.

The behaviour of 2.22 is illustrated in Fig. 2.2(a) and this shows clearly how the charge builds up around the source. At large values of time expression 2.22 takes the form:

$$\bar{\rho}(r) \longrightarrow \frac{i}{4\pi K r} \tag{2.23}$$

This case of diffusion in calm conditions is, although of interest, rather unlikely to happen in practice. Occasionally, the wind speed may be low enough for the process to commence but it is thought that certain electrostatic factors would intervene, and as a result, prevent such a build-up of charge actually occurring. This point is discussed further in the next chapter.

2.5.3.2
Continuous Ion Source in a Wind

We turn now to a much more familiar situation - that of a
continuous source in a wind. It is a matter of common expe-
rience that in these circumstances, a long plume of material
is formed downwind of the source, see Fig. 2.2(b). We assume,
as before, that we can describe the diffusion process in
terms of equation 2.18. However, in this case we must also
allow for the advection of ions by the wind. Making this
adjustment we find that:

$$\frac{\partial \bar{\rho}}{\partial t} + u\frac{\partial \bar{\rho}}{\partial x} = K \nabla^2 \bar{\rho} \qquad (2.24)$$

where u is the wind velocity, assumed constant.

Equation 2.24 is difficult to solve as it stands and therefore
we shall only consider the steady state solution obtained by
setting $\partial \bar{\rho}/\partial t$ equal to zero. Any solution can only give
mean values of the concentration, and it should be clearly
appreciated that, in reality, the concentration fluctuates in
the vicinity of all sources. (The diffusion theory employed
cannot possibly predict the fluctuations because, at the out-
set, we deliberately expressed the instantaneous fluxes in
terms of the gradients of mean concentration).

The steady state solution, first given by ROBERTS (1923) is:

$$\bar{\rho}(x,y,z) = \frac{i}{4\pi K x} \exp[-\frac{u(y^2 + z^2)}{4Kx}] \qquad (2.25)$$

Equation 2.25, which expresses the concentration downwind of
an isolated point source, can be readily adapted to the case
where the source is near the ground, a situation which is,
of course, of particular importance here. The details of
the modification are not discussed as a full account is given

The ion concentration due to a continuous point source

(a) conditions:- zero wind, far above ground, electrostatic effects negligible

r decreasing

r_1

r_2

$\dfrac{Q}{4\pi A\, r_1}$

$r_1 < r_2$

CHARGE CONCENTRATION

TIME →

ion source switched on.

r = radial distance from source.
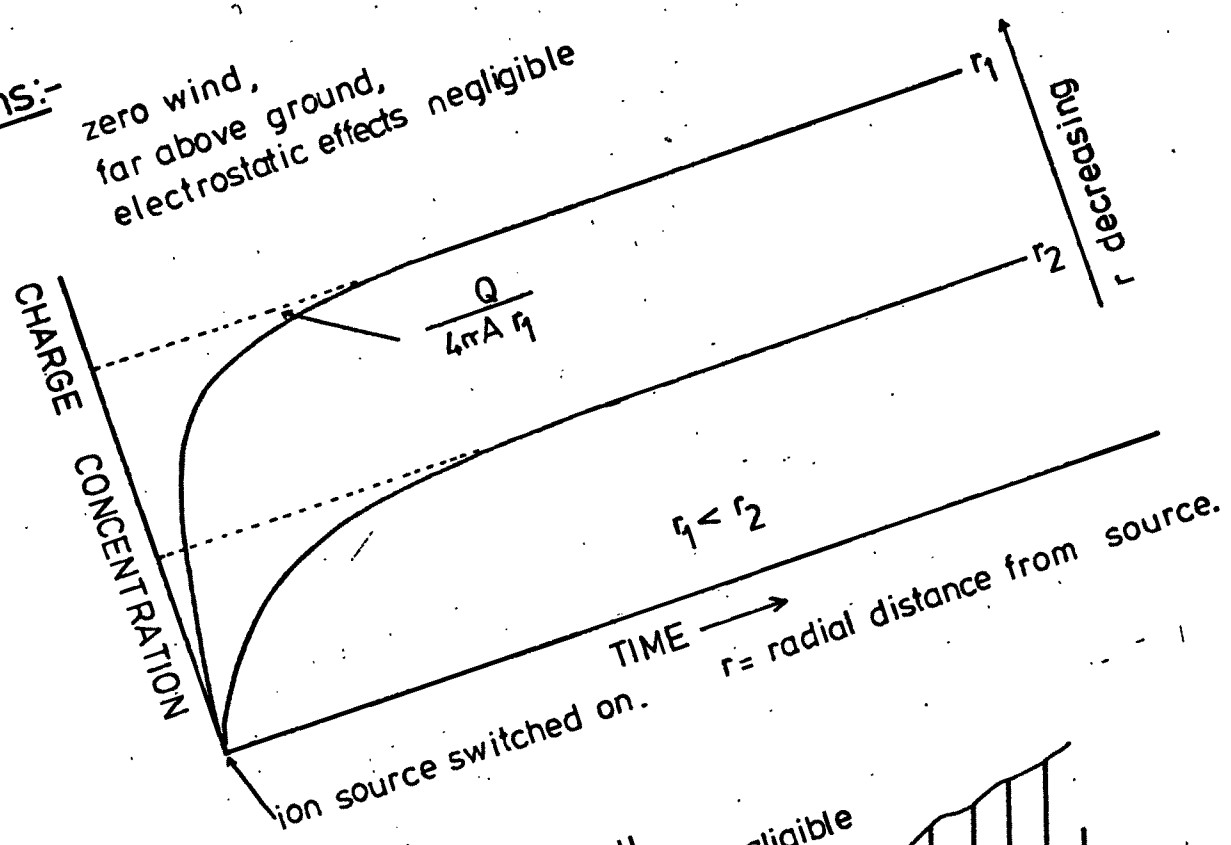
(b) conditions:- wind speed u, electrostatic effects negligible

ION PLUME

plume axis

ION SOURCE

z

x

y

h

wind direction
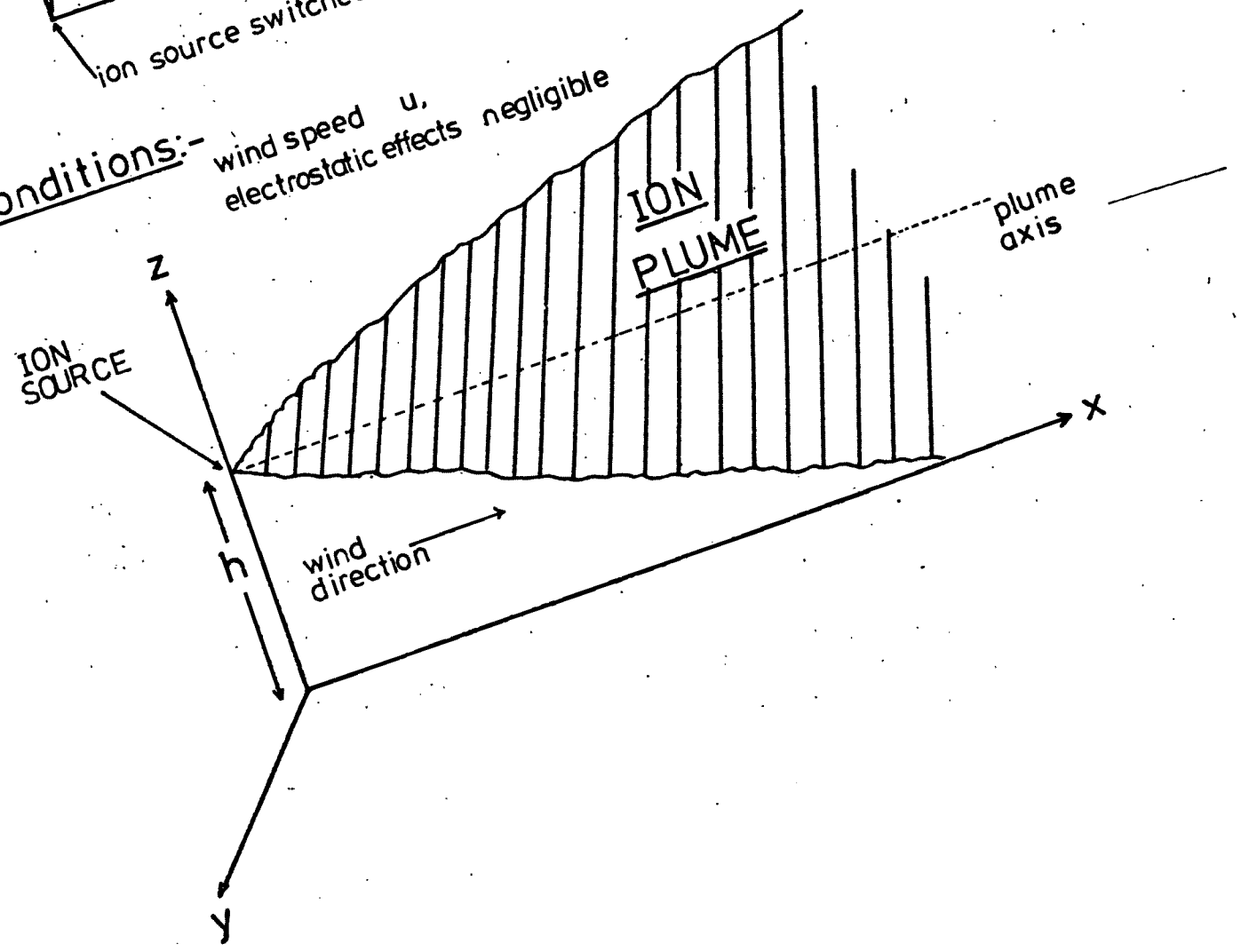
by SUTTON (1953). It is found that:

$$\bar{\rho}(x,y,z) = \frac{i}{4\pi Kx} \exp[\frac{-uy^2}{4Kx}] \left[\exp[\frac{-u(z-h)^2}{4Kx}] + \exp[\frac{-u(z+h)^2}{4Kx}] \right] \quad (2.26)$$

where h is the source height.

MAUND (1958) used an equation similar to 2.26 to estimate the electric field under an ion plume. In his case, the ions were produced by a point discharging during stormy conditions, his requirement being to estimate the point discharge current by making electric field measurements under the plume.

The implications of equation 2.26 are difficult to visualize. As it stands, however, it is clear that both the crosswind and vertical concentration profiles are gaussian. As a simplification, consider the variation of concentration directly under the plume axis, this being obtained by setting y and z equal to zero. Thus:

$$\bar{\rho}(x,0,0) = \frac{i}{2\pi Kx} \exp[\frac{-uh^2}{4Kx}] \quad (2.27)$$

It is found that in all cases, equation 2.27 predicts that the concentration attains a maximum value at a certain distance downwind. This feature is found in practice although not necessarily at the distance predicted by the equation.

Equation 2.26 forms the basis of the steady state plume model and its application to electric field calculations is discussed in the next chapter. We shall now consider certain

statistical features of turbulence before proceeding with the
development of the "fluctuating plume models".

Fuller details of diffusion theory and comparison with experi-
mental results can be found in PASQUILL (1962)

2.6
The Statistics of Atmosphere Turbulence and the Complicating Effects of Radiation and Topography

2.6.1
Preliminary Remarks

The smoke from a chimney changes its direction and inclination in response to the varying wind. Observation reveals that these motions are random in nature and occupy time scales from a fraction of a second to many minutes. The ion plume was expected to behave similarly in the turbulent wind.

Previously, we absorbed the dispersing effect of the fluctuations into an eddy diffusion coefficient. However, the use of this technique can only provide mean concentration values. It is my intention now to develop more sophisticated plume models which can predict the fluctuating values of space charge concentration downwind of source. We shall first digress a little to discuss the topic of atmospheric stability.

2.6.2
A brief note on Atmospheric Stability

During the daytime, particularly if the sky is clear, incoming solar radiation warms the ground. Air is virtually transparent to the radiation and thus the ground temperature rises more rapidly than that of the air. Close to the surface, however, the air is warmed in addition by the proximity of the hot ground. The effect is, of course, largest at the lowest levels and we therefore would expect the air temperature to fall rapidly with increasing height in these circumstances. Conversely, at night, under a clear sky, the earth radiates heat and the ground cools more quickly than the air. If the

radiation effect is strong enough, the temperature of the air may even increase with height for a short distance above the surface.

When the sky is clouded and the net radiation reduced to low levels, the vertical temperature gradient assumes a small negative value - the dry adiabatic lapse rate. This lapse rate is, in fact, determined solely by thermodynamic processes and is numerically about 1° C. per 100 m.

The three cases above are those of unstable, stable and neutral conditions respectively.

It is felt that the majority of readers will be familiar with these effects hence the brevity of this discussion. Further details are to be found in SUTTON (1953).

2.6.3
Fundamental Characteristics of the Velocity Fluctuations

The mean and standard deviation are of fundamental importance in a statistical description of turbulence. We denote the mean by an overbar as before, the standard deviation being represented by the symbol σ . A quantity which is of considerable interest is the gustiness (g). It is defined by the relations:

$$
g_x = \frac{\sigma_u}{\bar{u}}
$$
$$
g_y = \frac{\sigma_v}{\bar{u}}
$$
$$
g_z = \frac{\sigma_w}{\bar{u}}
$$

(2.28)

and is a measure of the intensity of turbulence in the three co-ordinate directions.

In the lower atmosphere it is normally found that gustiness values lie between 0.1 and 0.2 for the g_x and g_y components, while g_z tends to be more variable. Early researchers, notably SCRASE (1930) and BEST (1935), soon discovered that, near the ground, g_y was usually larger than g_z, the difference becoming more accentuated at lower levels. This was attributed to the presence of the ground inhibiting vertical motion, and thus, near the surface, the turbulence is anisotropic.

At higher levels within the boundary layer it was discovered that the turbulent energy was more equally distributed among its components. In practice, this equipartition is only attained at heights above 50 m. or so and thus all the experimental work in this project was conducted in the lower, anisotropic region.

In unstable conditions we would expect the vertical velocity component, in particular, to be enhanced by convective effects and the level of turbulence to be augmented generally. Conversely, in stable conditions, the vertical motions tend to be suppressed and thus turbulent activity diminishes. It was mentioned that turbulence arose as a result of the frictional effects of the earth's surface, and in neutral and stable conditions this is undoubtedly true. In unstable conditions convective effects also contribute to the turbulent energy and thus, in this case, our original statement needs modification.

A very useful parameter, introduced by RICHARDSON (1925) enables one to compare the relative importance of the thermal and mechanical parts of the turbulence. Richardson, in his analysis, compares the dissipation (or production) of energy by mechanical and thermal processes and concludes that the quantity:

$$Ri = \frac{g}{T} \frac{\frac{\partial \bar{T}}{\partial z} + \Gamma}{(\frac{\partial \bar{u}}{\partial z})^2}$$

(2.29)

is of considerable importance.

In the above T is the absolute temperature,

$\partial \bar{T}/\partial z$ the mean temperature gradient,

$\partial \bar{u}/\partial z$ the mean wind speed gradient,

Γ the dry adiabatic lapse rate,

and g the acceleration due to gravity.

He suggested if Ri were less than unity, the flow would remain turbulent, but that if Ri were greater than unity, the flow would become laminar. This criterion, although slightly incorrect numerically, does provide a valuable indication of the atmospheric stability and has been used extensively in this investigation.

It is possible, by appropriate mathematical techniques, to present a velocity fluctuation record in the form of a spectrum, this approach being used widely in practice. Spectral analysis has been a very effective probe with which to uncover the mechanisms of turbulence and we now consider a result of direct relevance to this project. Analysis of the velocity variations has revealed that the thermal (i.e. convective)

processes are responsible for variations of frequency lower than those caused by mechanical (i.e. frictional) effects. Typical spectra illustrating this point are shown in Fig.2.3. Generally speaking, "convective" eddies have periodicities of a few minutes whilst those of "mechanical" eddies are measured in tens of seconds. This implies that the convective systems, as we might expect, are rather larger than those of mechanical origin. The reader is referred to PRIESTLEY (1959) for a fuller discussion of this topic.

2.6.4
Topographic and other effects

The majority of theoretical work on the turbulent boundary layer has assumed the system to be horizontally uniform. Further, most of the experimental work has, until recently, been conducted at locations where there was a considerable expanse of flat ground. The implications are that, strictly, the results discussed above should only be applied to large flat areas. Although this is apparently a severe limitation, fortunately the essential features of turbulence are retained even over quite undulating terrain.

One must bear in mind that topographic effects will super-impose themselves on the turbulent variations in a complex way. Consequently, the observer must be able to recognise the presence of orographic, anabatic and katabatic effects on his data. Additionally, if the site is near the coast, then sea breezes may alter the conditions further.

The proximity of local obstructions had also to be considered when choosing a site. Clearly siting instruments too near

trees or houses is most undesirable because of the disturbance
such objects would have on the local air flow. In both sites
chosen for this project (see Sec.1.3) it is not thought that
this effect has caused any trouble.

Finally, the fact that meteorological conditions are never
steady for long, at least in this country, must also be taken
into consideration. The wind, for example, may be veering or
backing quite systematically during an experiment, or perhaps
periods of sunshine and cloudiness are alternating with each
other.

Unfortunately, as it is virtually impossible to quantify any
of the highly variable factors mentioned above, the onus rests
very much on the observer to assess the prevailing conditions.
However, by choosing one or two sites and working frequently
at them, the author suggests that it is possible to become
familiar with a location and thus know in a rough, but useful,
way what is likely to happen.

Showing the effect of atmospheric stability on the velocity component spectra

(a) u spectra
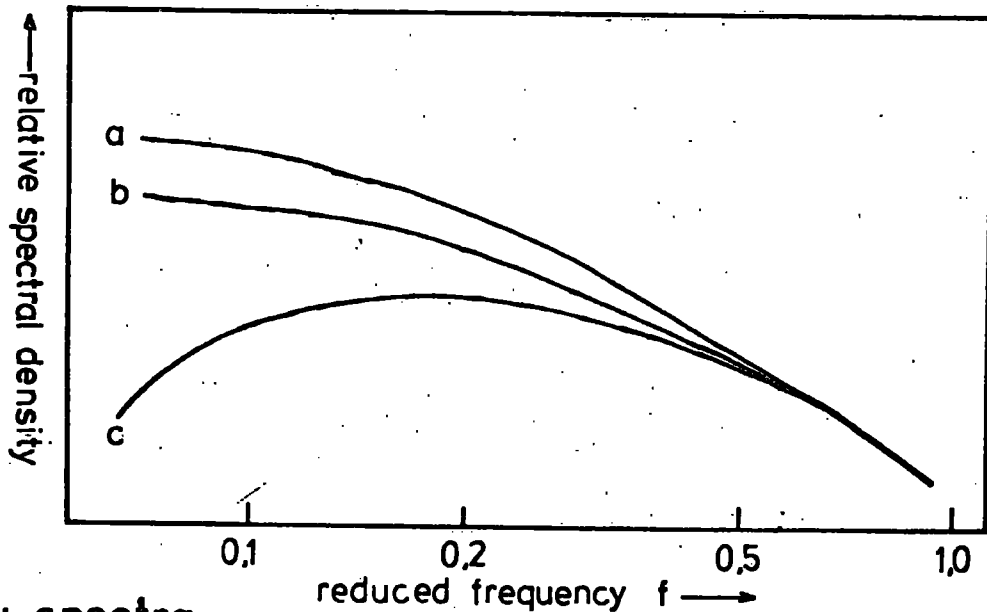
(b) w spectra
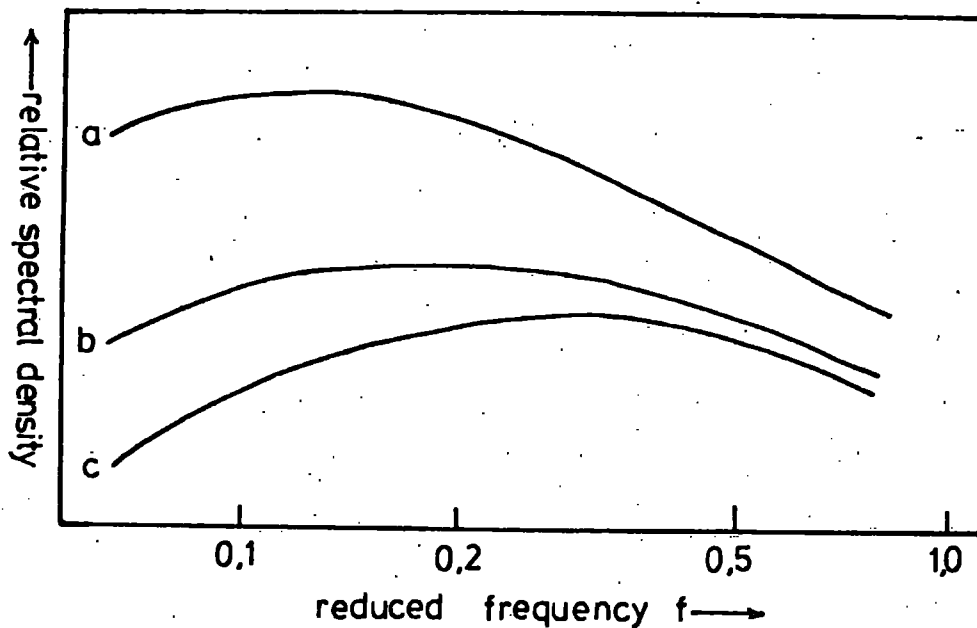
KEY
a strong instability
b moderate instability
c weak instability

where $f = \dfrac{nz}{\bar{u}}$

n measured frequency
z height of measurement
$\bar{u}$ mean wind speed

The Influence of Atmospheric Stability on the Form of Plumes

Systematic observation of smoke plumes indicates that their behaviour depends on the nature of the turbulence and consequently on the atmospheric stability. The three types of plume behaviour, shown in Fig. 2.4., are known as looping, *coning* and fanning, and can be associated with unstable, neutral and stable conditions respectively.

In unstable conditions, the vertical movements are strongly accentuated by convective effects. There is more turbulent energy present generally, particularly at low frequencies. These large low frequency variations displace the plume bodily, forming the loops. The higher frequency components, which are responsible for the smaller scale diffusive effects, produce a progressive increase in width as the plume is blown downwind.

During neutral conditions, the mechanically produced turbulence is neither suppressed nor augmented because thermal effects are absent. Large, low frequency eddies are absent and therefore the plume shows little tendency to loop. The neutral stability encourages the variations to become isotropic because the distinction between vertical and horizontal motion is, effectively, removed. These factors result in the material spreading away from the source in the form of a cone.

The onset of stable conditions results in turbulent activity being suppressed, particularly the vertical component fluctuations. Horizontal eddies still exist, to a limited extent,

but very little energy is available for vertical movement. The plume, almost unable to diffuse vertically, takes the form of a thin "fan" lying horizontally downwind of the source.

It should be mentioned that the distinction between these types of behaviour is not always as marked as indicated above, and therefore caution must be exercised in applying these conclusions to the analysis of experimental situations. Nevertheless, the concepts described here have been of considerable assistance in understanding the ion plume behaviour.

The influence of stability on the form of a plume

ELEVATIONS

PLANS

UNSTABLE

LOOPING

NEUTRAL

CONING

STABLE

FANNING
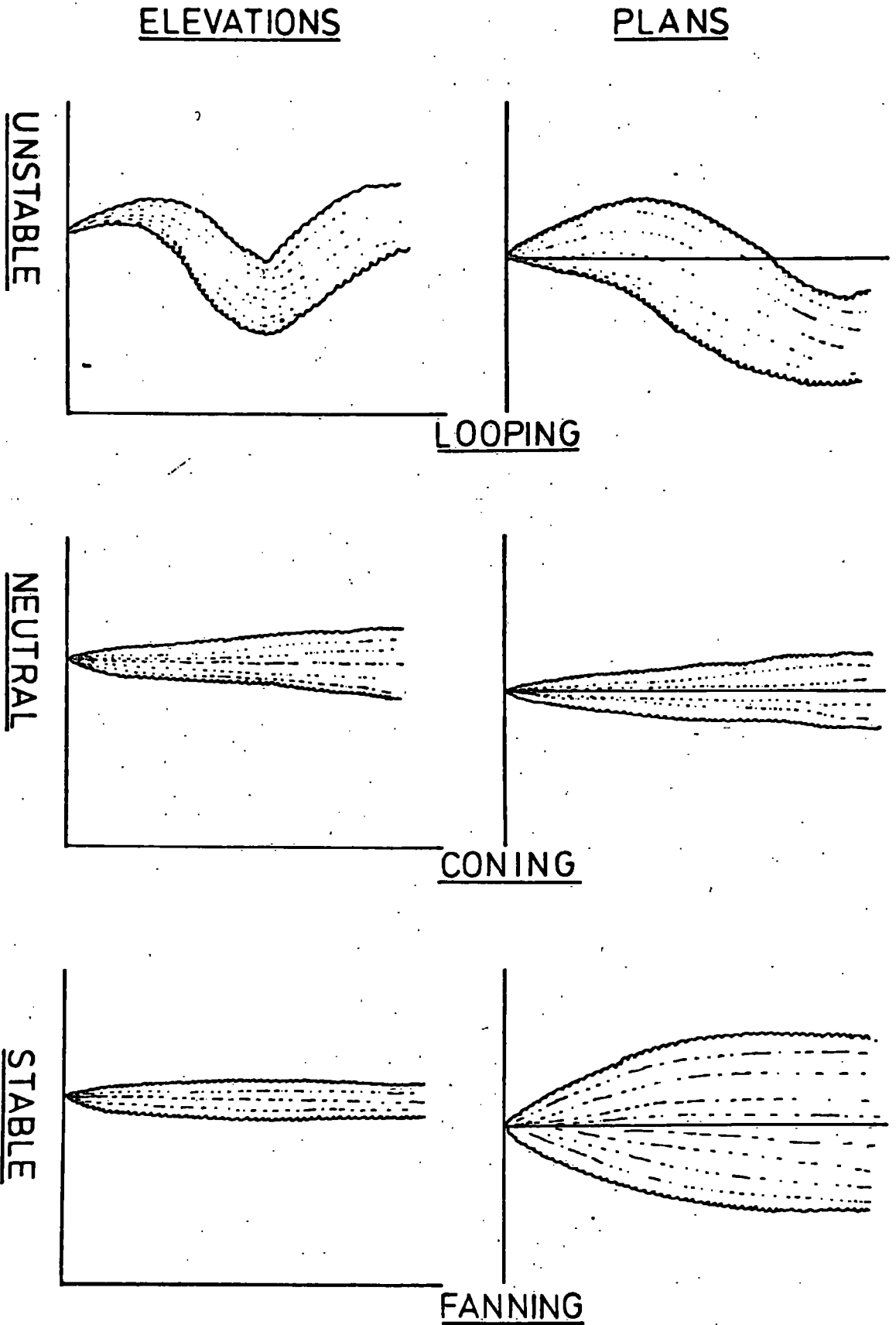
2.8
The Evolvement of Plume Models

2.8.1
The Rôle of Plume Models

The principal object of this project was to assess the feasibility of using ions, rather than more conventional materials, in small-scale atmospheric diffusion experiments. It was found that, whilst the ion plume behaviour could be roughly correlated with the atmospheric stability, a more precise knowledge of the changing plume configuration would have been very useful. These requirements prompted the development of plume models which, when supplied with the necessary meteorological data, would realistically simulate the ion plume behaviour.

2.8.2
The BIVANE Data Model

DAVIDSON and HALITSKY (1957) discovered that, if smoke plumes were photographed on cine film and the film then wound backwards, an interesting feature became apparent. Portions of the plume which were identifiable appeared to travel back to the source in straight lines. As the author's experiments were conducted at much lower levels than those of Davidson and Halitsky, it was necessary to establish whether this "straight line effect" still occurred nearer the ground. Some field tests were conducted and it was found that the effect was maintained with source heights down to about 5 m., but, below this the presence of the ground caused a plume to depart radically from the straight line behaviour.

It was Davidson and Halitsky's intention to reconstruct the
plume configuration with the aid of bidirectional vane
(bivane) data. A bivane, in conjunction with a suitable
anenometer, measures the instantaneous values of the three
velocity components, thus making it possible to predict the
direction of the plume as it leaves the source. By invoking
the straight line hypothesis, we may then predict the tra-
jectory of the plume element as it moves away downwind.
The technique can be extended by computing the paths of the
succession of elements which comprise the plume. This is the
basis of the bivane data model.

The approach is shown in Fig. 2.5(a), where only the $X—Z$
plane is shown for reasons of clarity. Let us suppose we
have u, v and w data from a bivane near the ion source, and
that the values of these components are averages over the sam-
pling interval s . We list these values below:

Time	Velocity Components			Plume Element just leaving Source
$-4s$	u_4	v_4	w_4	P_4
$-3s$	u_3	v_3	w_3	P_3
$-2s$	u_2	v_2	w_2	P_2
$-s$	u_1	v_1	w_1	P_1
0	u_0	v_0	w_0	P_0

Consider the situation at $-s$ when the plume element P_1
was just leaving the source. From the velocity component
values we may write down the co-ordinates of P_1 when the time
is zero. These are:

$$x_1 = u_1 \cdot s$$
$$y_1 = v_1 \cdot s$$
$$z_1 = w_1 \cdot s$$

At time $-2s$ the plume element P_2 was leaving the source and hence at zero
time the co-ordinates of P_2 are:

PLUME MODELS USED TO SIMULATE ION PLUME BEHAVIOUR

(a) Bivane data model

computed plume configuration

source

x_1

x_2

x_3

x_4

downwind axis

(b) Oscillating plume model

source

simulated plume configurations

downwind axis
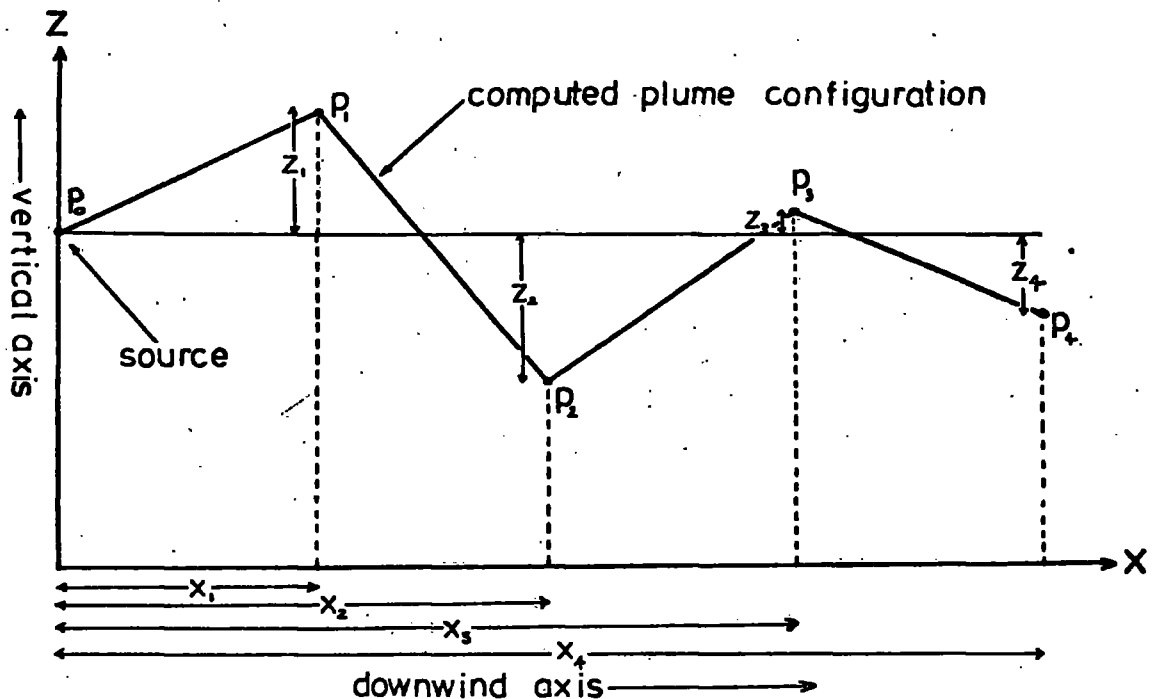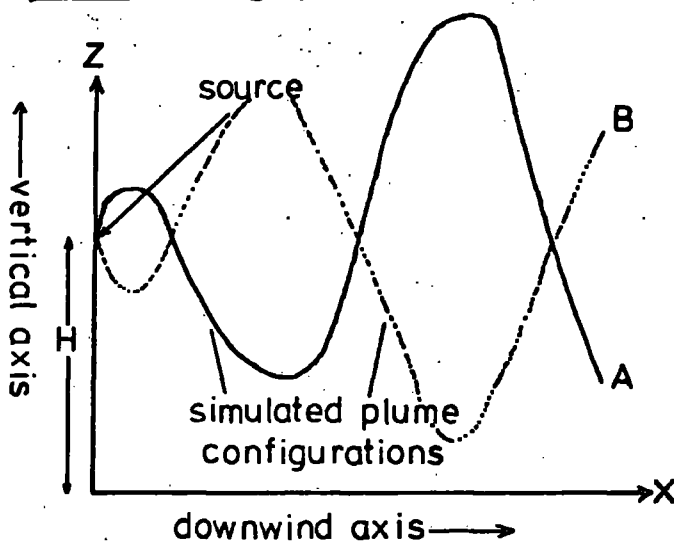
relations used to depict plume co-ordinates

$$X = U.P$$

$$Y = A_y.P\sin(2\pi.F_y.(P+T))$$

$$Z = H + A_z.P\sin(2\pi.F_z.(P+T))$$

A_y, A_z horizontal and vertical amplitude factors.

F_y, F_z frequency factors.

U wind speed.

P parameter having the dimensions of time.

T time.

H source height

$$x_2 = u_2 \cdot 2s$$
$$y_2 = v_2 \cdot 2s$$
$$z_2 = w_2 \cdot 2s$$

We may extend the process to compute the co-ordinates of P_3, P_4..... at this time. The above method thus allowes us to calculate the position of the plume elements, and from this we can assemble a picture of the plume as it was at any particular time. After this, we may, by advancing the entire calculating process by one sampling interval at a time, produce a sequence of computed plume configurations.

In later experimental work, once the bivane was serviceable, the above technique was adopted and proved very helpful in understanding the electric field variations measured under plumes. A discussion of the application of this model will be found in Chapter 3.

2.8.3
The Oscillating Plume Model

It was originally hoped that the steady state model described in *Sec.* 2.5 would be capable of providing realistic electric field values downwind of ion sources in neutral and stable conditions. No steady-state model could possibly give usable information to assist in the analysis of data obtained in unstable conditions, the oscillating plume model being an attempt to imitate both the shape and the movement of the looping plume of these circumstances.

The basis of the model is illustrated in Fig. 2.5(b). The usual system of axes is employed and three equations set-up to generate a series of co-ordinates appropriate to a looping

plume. These are shown in the figure. The model was designed
to be used on a digital computer, a special programme
(OSCPLMPROG - see Chapter 6) being written for the purpose.
It was necessary to specify six variables in order to charac-
terize the plume completely, these being the amplitude and
frequencies of the oscillations in both the horizontal and
vertical, requiring four constants A_y, A_z, F_y, F_z , the
source height, H, and the wind speed, U . In use the arbi-
trary parameter P (having the dimensions of time) was increa-
sed from zero up to a sufficiently large value to generate
enough plume for the particular application in view. Usually
P was increased until the x co-ordinate of the simulated
plume attained 50 m. During this process, the y and z
co-ordinates would vary as required by the equations; typi-
cally the z values behaved as shown by Plume A.

It was also possible, by varying T , the time, in the equa-
tions, to make plumes undergo oscillations in terms of time
as well as space, and, for example, with an appropriate value
of T , the configuration B would be produced.

The model was not used as much as the bivane data model,
mainly due to lack of adequate data needed to set realistic
values for the amplitude and frequency constants. The effects
of crosswind and vertical diffusion were not incorporated in
the model and this detracted from the validity of predicted
electric field values. The application of the model is dis-
cussed in Chapter 3, whilst results obtained with it are con-
sidered in Chapter 6.

Chapter 3: <u>ELECTRICAL ASPECTS OF ION PLUMES</u>

3.1
<u>Introduction</u>

The previous chapter was concerned only with those features of ion plume behaviour which were determined by turbulent diffusion processes. However, it is fairly obvious, particularly with the relatively high ion concentrations used in this project, that electrostatic forces may be sufficiently large to substantially modify the form of the plume. Before embarking on a discussion of this topic, we must first consider certain fundamental features of ions and space charges in general. In addition, we cannot afford to ignore the effect of the Earth's natural electric field, both on the plume itself and on the electrical measurements to be made near the plume.

3.2
<u>Basic Principles</u>
3.2.1
<u>Forces and Fields</u>

We begin by quoting Coulomb's law, which expresses the force between two point charges of magnitude q_1 and q_2 as a function of r their distance apart. Mathematically, we can write,

$$F = \frac{q_1 q_2}{4 \pi \epsilon_. \epsilon_r r^2} \qquad (3.1)$$

where F is the force between the charges,

     $\epsilon_.$ the *permittivity of* free space,

 and ϵ_r the relative *permittivity*

(The relative *permittivity* of air is very close to unity and for our purposes any small difference can be safely ignored.)

The electric field vector, $\underline{E}$, due to a charge q is given by the expression,

$$\underline{E} = \frac{q}{4\pi\epsilon_o r^3} \underline{r}$$ (3.2)

where $\underline{r}$ is directed away from the charge if it is positive and vice-versa.

According to an earlier convention, the atmospheric electric field at the Earth's surface was directed oppositely to that used in electrostatic theory. To avoid this ambiguity it is often better not to use the term "field" but instead to refer to the potential gradient dV/dr . These quantities are related by the expression,

$$\underline{E} = - dV/d\underline{r}$$ (3.3)

The electric field and the potential gradient possess both magnitude and direction and are, of course, vector quantities.

3.2.2
Gauss's Theorem

This theorem is often of considerable assistance when we try to understand the nature of electrical effects in the atmosphere. The theorem can be stated in the form that the total integrated normal component of flux over a closed surface is equal to the total charge contained in the volume bounded by that surface. The reasoning upon which this conclusion depends will not be discussed here as it has been widely treated in the literature, an excellent paper on the subject being given by CHALMERS (1963). The theorem can be expressed mathematically in the form,

$$\int_V \rho \, dV = \epsilon_o \int_S \underline{E}.d\underline{s}$$ (3.4)

where ρ is the space charge density,

 $d\underline{s}$ an element of area, the direction being that of the
 outward normal,

and dV an element of volume.

Further, it can be shown that,

$$\boxed{\frac{\rho}{\epsilon_o} = div\,\underline{E}}$$ (3.5)

where

$$div\,\underline{E} = \frac{\partial E_x}{\partial x} + \frac{\partial E_y}{\partial y} + \frac{\partial E_z}{\partial z}$$

A further and very useful implication of Gauss's theorem,
admittedly not obvious from the above, is that it allows
us to consider certain charge distributions as if they
were, at least in some respects, line or point charges.
As a consequence of this, we could for example, compute
the electric field due to a uniformly concentrated spheri-
cal cloud of ions by assuming that the total charge in the
system resided entirely at the cloud centre. Clearly this
is an important and useful simplification in the treatment
of electrical phenomena and the approach has been employed
extensively in the theoretical work associated with this
project.

3.2.3
The Effect of Boundaries and the Method of Images

Until now we have considered ions and charges as being completely isolated and
far away from any boundaries. This state of affairs is clearly unrealistic insofar
as this project is concerned and therefore we must consider the implications of
the plume being within a few metres of the Earth's surface. In electrostatic
terms the earth is a good conductor and although it is, of course, spherical,
we may, because of the relatively small scale of this field work investigation,
consider its conducting surface to be planar. It is a familiar boundary condition
of electrostatic theory that a parallel component of electric field cannot exist
at a conducting boundary.

- 41 -

In atmospheric electric terms, this means that, at the Earth's surface, the electric field is entirely vertical. Of course, above the surface there is no reason why horizontal components of electric field cannot exist and, although these have not been measured, the existence of very large horizontal fields in the vicinity of ion plumes has been demonstrated theoretically.

The method of images enables one to incorporate, in a simple way, the effect of the presence of boundaries near to arrangements of charges. In essence, the conducting surface is considered as if it were a mirror, an image charge of the opposite sign to the real charge then being placed at the appropriate point on the other side of this mirror. The use of such an approach is illustrated in Fig.3.1(a). It should be noted that the presence of this oppositely charged image associated with the real charge implies the existence of an attractive force towards the boundary. This actually occurs in practice and thus in this sense (and only this sense) the image charge is very "real". More details of the method of images as applied to the solution of electrostatic problems can be found in BLEANEY & BLEANEY (1965).

3.2.4
The Movement of Ions in Electric Fields - Mobility

The presence of an electric field exerts a force on an ion. In a gas, however, an ion is not able to accelerate continuously under the influence of the field because of the incessant collisions it makes with the molecules comprising the gas. These collisions result in the ion, after a very short time, attaining a terminal velocity, v_t, say. It has been found

experimentally that v is proportional to E , the applied electric field, for any particular ion and gas combination. Hence we may write that,

$$v = \mu E \qquad (3.6)$$

where μ is a constant known as the mobility. This relationship is of considerable importance, because we can, knowing E and μ , compute the velocities of ions in or near the plume.

3.2.5
The Nature and Concentration of Natural Ions and Nuclei

ELSTER & GEITEL (1899) and WILSON (1900) discovered the existence of atmospheric ions but it was not until some years later that the distinction between ions of various mobilities was appreciated.

Small ions, as they are known, are believed to consist of a few neutral molecules clustered around a singly charged molecule. Such a system was kept together by its charge polarizing the surrounding molecules, thus producing the necessary attractive forces. WRIGHT (1936) considered the mass of a small ion to be equal to about that of ten water molecules, while TORREDON (1939) estimated an ion to be about the size of four oxygen molecules. The mobility of small ions lies between 1×10^{4} and 2×10^{4} MKS units. There are, in fact, about 7 x 10^{8} of each sign in a cubic metre of air at an "average land station", (CHALMERS 1967).

The "large" ions were discovered by LANGEVIN (1905) and have mobilities about 0.002 that of the small ions. These ions are considerably larger than the small ions and are charge-

bearing particles of the same type as condensation nuclei.
It is probable that they are comprised of such substances as
evaporated sea-salt or residues from industrial and domestic
pollution. Consequently large ions (and uncharged nuclei)
are much more abundant in urban than rural areas. CHALMERS
(1967) indicates that, at an "average land station", there are
approximately 10^9 large ions of each sign and about 4×10^9
uncharged condensation nuclei in a cubic metre of air.

Clearly an ion may remain as such until it is neutralized by an encounter with an
ion of the opposite sign. Ions may however combine with each other in various wa
for instance, a small ion could combine with a similar ion of opposite sign and
the result would be neutral molecules. Alternatively the small ion might interac
with a large ion of the opposite sign this process resulting in an uncharged
condensation nucleus plus some neutral molecules. A small ion might also become
attached to a neutral nucleus and thus become a large ion of the same sign.

We can, in fact, expect the number of interactions that occur
in unit time in a given volume to be proportional to the num-
bers present of both types of particle involved. On this basis
we can define a "combination coefficient" for the process in
which we are interested. Following CHALMERS (1967) we may
write for small positive ions,

$$\frac{dn_i}{dt} = q - \alpha n_1 n_2 - \eta_{12} n_1 N_2 - \eta_{10} n_1 N_o \qquad (3.7a)$$

and for negative ions,

$$\frac{dn_2}{dt} = q - \alpha n_1 n_2 - \eta_{21} n_2 N_1 - \eta_{20} n_2 N_o \qquad (3.7b)$$

In the above:
  q denotes the rate of production of small ion pairs per unit
        volume per unit time,

  n_1 the positive small ion concentration,

  n_2 the negative small ion concentration,

  N_1 the positive large ion concentration

  N_2 the negative large ion concentration

and N_o the neutral nucleus concentration.

The small ion recombination coefficient is α , whilst the
other coefficients are as follows,

η_{12} combination coefficient for small positive - large negative ions

η_{21} combination coefficient for small negative - large positive ions

The combination coefficients between small ions and neutral
nuclei are denoted by,

η_{10} coefficient for small positive ions and nuclei,

η_{20} coefficient for small negative ions and nuclei.

The values of the combination coefficient are not discussed
here as details can be found in CHALMERS (1967). Equations
(3.7a) and (3.7b) are of considerable importance because they
enable us to make various deductions concerning the behaviour
of the artificially produced ions used in this project. A
discussion of this topic now follows.

3.2.6
The Nature and Fate of the Artificially Produced Ions

The ions used for the experimental studies in this project
were produced by the application of a very large electric
field to a current of air. The discharge processes occurring
in the ion generator involve ionized gas molecules (general
reference LOEB 1965) and consequently only small ions were
produced by the ion source. These artificially produced ions
will, like their natural counterparts, be subject to all of the
combination processes referred to previously. It is, there-
fore, of considerable importance to estimate, at least appro-
ximately, the effectiveness of the various processes in remo-
ving these ions as the plume travels downwind.

It seems logical that near the ion source, say within 20 m,
where the artificial ion concentration is very high, there
will be, relatively speaking, very few natural ions (of oppo -

site sign) and nuclei available for combination processes. Further calculations show that at distances of $50\,m$ or greater from the source the artificial ion concentration will have fallen to $10^{-9}\,cm^{-3}$ or less. If these typical figures are then substituted into equation $(3.7a)$ or $(3.7b)$ whichever is appropriate, together with suitable values for the various combination coefficients, the rate of small ion removal is found to be about 1 per cent per second. Of this 1 per cent approximately 0.7 per cent is absorbed in conversion to new large ions, whilst the remaining 0.3 per cent is destroyed by neutralization. For a typical plume, therefore, travelling downwind at a few metres per second, it appears a reasonable assumption that these depletion processes will not, under most circumstances, remove more than a few per cent of the ions from the plume in its first hundred metres of travel.

One should appreciate that, whilst the artificially produced ions may be slowly removed from the plume, this does not necessarily imply that the total space charge is decreasing. To illustrate this point consider the following situation. In the lower atmosphere ambient ionization levels are very low; however there, unlike the ion plume, there are, to a reasonable approximation, equal numbers of positive and negative ions. (very near the ground the electrode effect can disturb this equality - see CROZIER 1963). An artificially produced ion, travelling downwind, may encounter an oppositely charged *natural* ion and combine with it. However, when this occurs there still must remain somewhere a surplus natural ion of the same sign as the original artificial ion and thus the net space charge of the ion plume would appear to have been maintained.

On this argument it would seem that recombination processes are in themselves incapable of dissipating the space charge of the plume although, of course, the artificial ions are gradually replaced by natural small and large ions. In actual fact, it is thought that a considerable number of ions are removed from the plume by image forces *-see Sec. (3.5.5)*

OGDEN (1967) estimated, using a different method, that the small ions from a $1\mu A$ source will nearly all be converted into large ions within 1 km downwind of that source. In the case of the ion source used in this project, which had an output of about $0.3\mu A$, it can be computed on the basis of OGDEN's formula that most of the conversion to large ions would be achieved within $500m$ of the source.

In practice, electric field measurements were always made within $100m$ of the ion source, and consequently it is reasonably certain that a small-ion plume was being investigated. However, on a few occasions at the Maiden Castle site it was thought that the nucleus concentration might have been rather higher than the figures given by CHALMERS. If this was indeed so, then the conversion rates deduced previously will be underestimates and thus there could be a significant number of large ions nearer the ion source. Unfortunately, no nucleus concentration measurements were made during this project, the high nucleus concentrations being inferred from relatively high natural fields observed on these occasions.

3.3
The Electric Fields Due to Various Space Charge Distributions

3.3.1
Opening Note

In this section we shall consider the electric fields to be expected in the vicinity of simple charge distributions. The results will, of course, be of considerable interest in themselves but moreover they will serve as a useful prelude to the discussions on the estimation of the electric fields due to ion plumes.

3.3.2
Spherical Space Charge Cloud

This is illustrated in Fig. 3.1(a). A spherical space charge, O, of uniform density ρ_s and radius r_s is at a height h above flat ground. The general point M, at which we wish to know the electric field, is situated a horizontal distance x from the space charge centre. The total charge present is, in accordance with Gauss's theorem, considered to act as if it were entirely at the centre point. In the diagram the image charge, i, is also shown together with the various electric field vectors and their components. The vectors from the real and image charges are indicated by E_o and E_i respectively and we observe that the horizontal components of these, i.e. E_{x_o} and E_{x_i}, are equal and opposite. Hence the horizontal component of field is zero as required by the boundary conditions.

We can write for the vertical component, E_z,

$$E_z = \frac{2q}{4\pi\epsilon_o} \frac{1}{R^2} \sin\alpha \qquad (3.8)$$

However, we can express the total charge q in the form

$$q = \frac{4}{3}\pi r_s^3 \rho_s$$

and R^2 and $\sin\alpha$ in terms of x and h. As a result we find

$$E_z = \frac{2 r_s^3 \rho_s}{3\epsilon_o} \frac{h}{(x^2 + h^2)^{3/2}} \qquad (3.9)$$

The electric field due to:-

(a) spherical space charge (elevation)
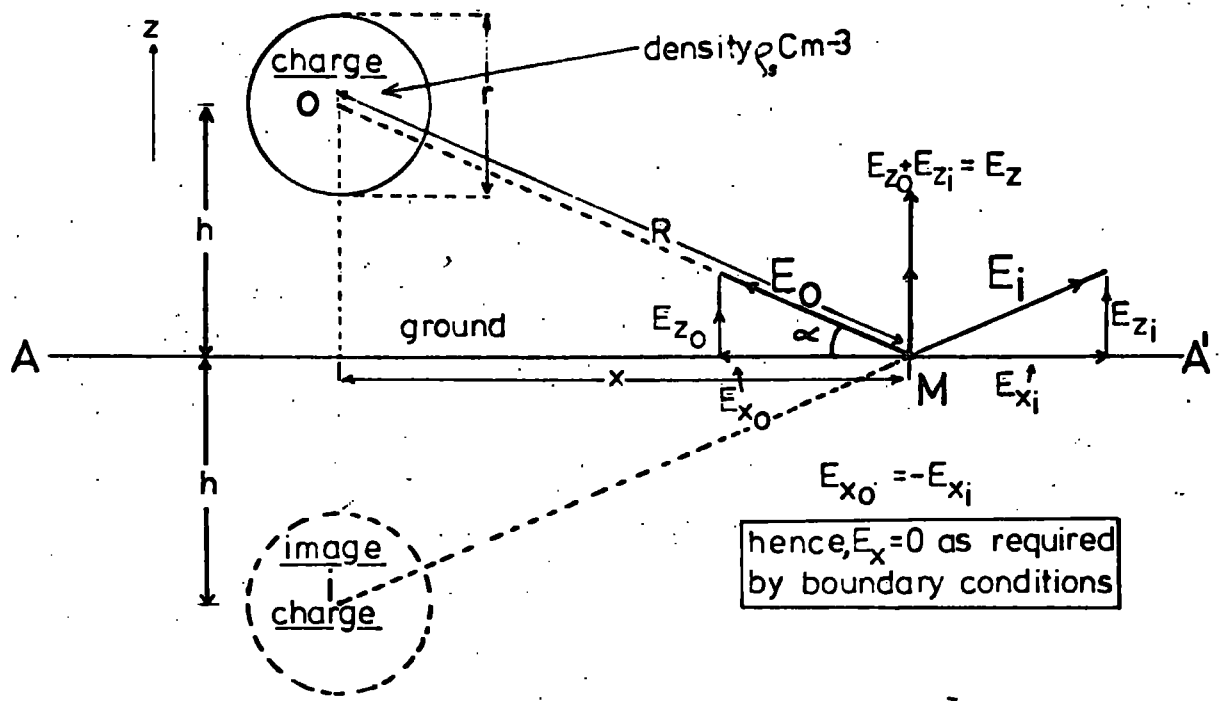
(b) infinite cylindrical space charge (plan)
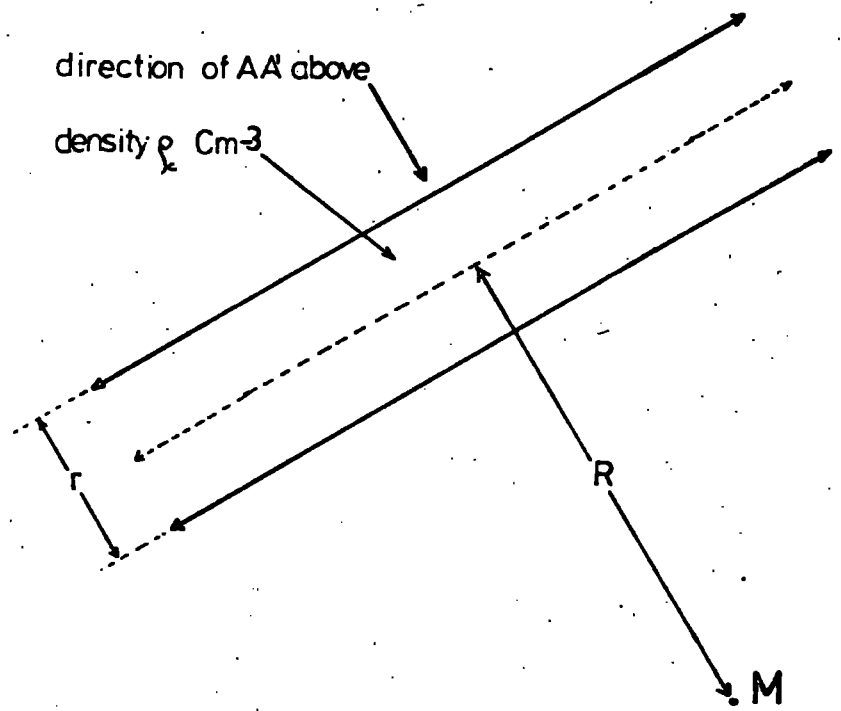
N.B. A negative space charge is considered above. This is convenient as the electric field vector is then upward.

Now E_z attains a maximum value when x is zero, i.e. when the charge is overhead, and this is given by

$$E_z \; (max) \; = \; \frac{2 \, r_s^3 \, \rho_s}{3 \epsilon_0 \, h^2}$$

(3.10)

Let us now consider a numerical example with values appropriate to this *project*. Suppose we set $r_s = 1m$, $\rho_s = 1 \mu Cm^{-3}$ and $h = 10m$.

It is found from equation (3.10) that in this case,

$$E_z \; (max) \; = \; 750 Vm^{-1}$$

We note immediately that the relatively small space charge, a few micro-coulombs, produces a substantial electric field at the Earth's surface. In fact, it would take the ion generator used in this project about ten seconds to produce this amount of charge.

3.3.3
Cylindrical Space Charge (Infinite Length)

This is illustrated in plan in Fig. 3.1(b). Fig. 3.1(a), although originally drawn to represent a spherical space charge cloud, will also be used to describe the cylindrical charge cloud now under consideration.

In the case of a cylindrical charge cloud, the method used to determine the electric field is essentially no different from the previous one. Hence the derivation of the formulae is not included here, the reader being asked to consult BLEANEY & BLEANEY for the details. The vertical field component at M is given by

$$E_z \; = \frac{\lambda}{\epsilon_0 \pi R} \; sin \propto$$

(3.11)

where λ is the charge per unit length.

As before we can write

$$\lambda = \pi r_c^2 \rho_c$$

and by expressing R and $sin\alpha$ in terms of x and h we find that

$$E_z = \frac{r_c^2 \rho_c}{\epsilon_o} \frac{h}{(x^2 + h^2)} \qquad (3.12)$$

As in the previous case E_z attains a maximum when the charge is overhead. This is given by

$$E_z (max) = \frac{r_c^2 \rho_c}{\epsilon_o h} \qquad (3.13)$$

Again we consider a simple numerical example in order to form an idea of the magnitude of the quantities involved. Typical values might be

$$r_c = 1m, \quad \rho_c = 0.1 \mu Cm^{-3} \quad and \quad h = 10 m.$$

Using (3.13) we find that

$$E (max) = 1130 Vm^{-1}$$

In conditions where turbulent diffusion effects are small it may be possible to regard the ion plume as an infinite (or semi-infinite) line-charge. This possibility was recognized by MAUND (1958) in his investigations of point discharge. Clearly our ion plume is not infinitely long but, in practice, provided its length subtends an angle within a few degrees of $180°$ (or $90°$) at the point (M) the assumption can be shown to be acceptable.

3.3.4
Electric Fields Due to Moving Space Charges

A space charge produced in the atmosphere will not, of course, remain stationary but will be blown along by the prevailing wind. Naturally the charge will also be diffused by turbulent

Electric field associated with passing space charges

Point/Sphere Charge

$$E_s = \frac{q}{2\pi \varepsilon_o} \frac{h}{(x^2 + h^2)^{3/2}}$$

$$q = \frac{4\pi r^3 \rho}{3}$$

at $x=0$ $E_s = E_s(max)$ hence,

$$E_s(max) = \frac{q}{2\pi \varepsilon_o h^2}$$

Line/Cylinder Charge

$$E_c = \frac{\lambda}{\pi \varepsilon_o} \frac{h}{(x^2 + h^2)}$$

$$\lambda = \pi r^2 \rho$$

at $x=0$ $E_c = E_c(max)$ hence,

$$E_c(max) = \frac{\lambda}{\pi \varepsilon_o h}$$

line charge
$E_c/E_c(max)$

point charge
$E_s/E_s(max)$

Normalized electric field ⟶

1,0
0,8
0,7
0,6
0,5
0,4
0,3
0,2
0,1

-3,0   -2,0   -1,0   0   1,0   2,0   3,0

Relative distance of space charge in units of x/h
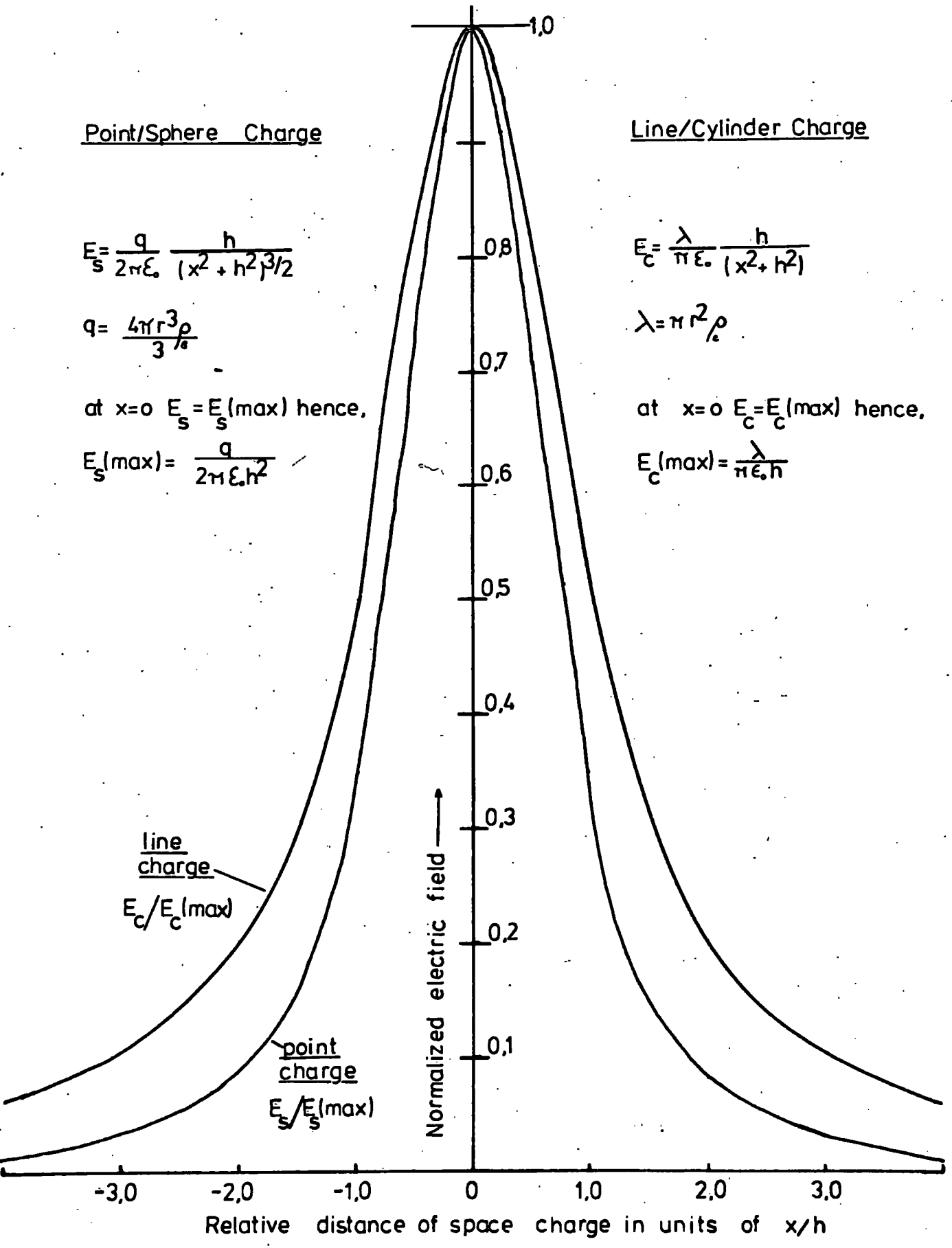
processes but we shall ignore this complication while we are
considering the basic principles. It is of great interest to
compute the variation of electric field as a space charge cloud
passes by. The results of such a calculation, employing equa-
tions (3.9) and (3.12) are shown in Fig. 3.2. (In the figure
the notation has been changed slightly to emphasize the dis-
tinction between the cylindrical case, subscripted c, and the
spherical, subscripted s.) We note from the equations that
in the case of the spherical charge the shape of the curve in
the figure is determined by the quantity

$$h / (x^2 + h^2)^{3/2}$$

whilst in the cylindrical system the shape is given by the
function

$$h / (x^2 + h^2)$$

Accordingly the relationship between the value of the field
due to the charge at a distance x and its overhead value
depends only on the ratio x / h . This applies in both cases.

We note from the diagram that relatively little effect is felt
from the charges until they are within about 2h of the point
in question. Thereafter the electric field varies rapidly as
the charge system passes overhead. It can be deduced that the
variation is most rapid when $x = 0.5h$ in the case of the spheri-
cal charge and when $x = h / (\sqrt{3})$ for the cylindrical case.

We should also consider the spherical charge cloud that does
not pass directly over M . Suppose the perpendicular distance
from the projection of the charge trajectory on the ground to
the point M were p . Further let us suppose that the projection

of the actual position of the charge is at a distance q from the point where this perpendicular intersects the projected trajectory. Then we may write

$$x = \sqrt{q^2 + p^2}$$

and we may proceed as before and write the electric field as

$$E_z = \frac{2 r_s^3 \rho_s}{3 \epsilon_o} \frac{h}{(q^2 + p^2 + h^2)} \qquad (3.14)$$

In practice, the electric field at a particular point would be measured as a function of time, but by employing the transformation $x = ut$, where u is the wind velocity, we can amend our equation accordingly. For example, in the above $q = ut$ and therefore

$$E_z(t) = \frac{r_s^3 \rho_s}{3 \epsilon_o} \frac{h}{(u^2 t^2 + p^2 + h^2)^{3/2}} \qquad (3.15)$$

3.4
Calculation of Electric Fields Using the Plume Models

3.4.1
Introduction

In the previous section we established, quite simply, the electric field using the plume models described in Secs. 2.5 and 2.8.

In practice the manner of application of all three models is much the same. The electric field due to a plume element is first calculated and then the total field computed by some type of integration or summation process. MAUND (1958) discovered whilst using a similar steady state model to mine that an analytical integration was virtually impossible. MAUND did not have a digital computer at his disposal and was therefore forced

to grossly simplify his equations in order to proceed with an integration. Fortunately, this restriction did not apply as an adequate computer was available to perform the numerical work.

The results obtained with these models are not discussed here. They will be presented immediately before the field data in order to facilitate comparisons.

3.4.2
The Steady State Model

The space charge concentration distribution in this model is based on equation (2.26). The principles of this and the other two models are illustrated in Fig. 3.3.

Consider the plume element $S(p,q,r)$. Suppose its volume were δV and the concentration within the element $\rho(p,q,r)$. The concentration is determined, of course, from equation (2.26) after specifying appropriate values for the ion source strength and height, wind speed and eddy diffusivity. The total charge in the element S is given by

$$\boxed{\delta Q = \rho(p,q,r)\, \delta V} \qquad (3.16)$$

Consequently, the electric field at the general point $M(x,y,z)$ is found to be

$$\boxed{\delta E = \frac{\rho(p,q,r)\delta V}{4\pi \epsilon_o} \frac{1}{R^2}} \qquad (3.17)$$

the elemental electric field, δE , being parallel to the line SM in the figure. Let us denote the x, y and z components of this vector by δE_x , δE_y and δE_z respectively. Then, by application of simple trigonometry we can write

$$\boxed{\begin{aligned} \delta E_x &= \delta E \cos\alpha \cos\beta \\ \delta E_y &= \delta E \cos\alpha \sin\beta \\ \delta E_z &= \delta E \sin\alpha \end{aligned}} \qquad (3.18)$$

- 53 -

where α and β are as shown in Fig. 3.3(a), and δE is the magnitude of $\delta \underline{E}$. Now let us derive the field contributions made by the image element at $S'(p,q,r')$. Employing a dashed notation for distances and angles pertaining to the charge image, we can write

$$\delta \underline{E}' = \frac{-\rho(p,q,r)\,\delta V}{4\pi\epsilon_o}\,\frac{1}{R'^2} \qquad (3.19)$$

and here, of course, $r' = -r$ because of the symmetry.

In a similar manner, we may list the components of $\delta \underline{E}'$, these being

$$\begin{aligned}
\delta E'_x &= \delta E' \cos\alpha' \cos\beta' \\
\delta E'_y &= \delta E' \cos\alpha' \sin\beta' \\
\delta E'_z &= \delta E' \sin\alpha'
\end{aligned} \qquad (3.20)$$

where α' and β' are the angles of elevation and azimuth of the charge element image with respect to the point M. $(N.B.\ \beta' = \beta)$.

It is now possible to determine the field components present at M due to the charge element and its image. Denoting these components by DE_x, DE_y and DE_z we may write,

$$\begin{aligned}
DE_x &= \delta E_x + \delta E'_x \\
DE_y &= \delta E_y + \delta E'_y \\
DE_z &= \delta E_z + \delta E'_z
\end{aligned} \qquad (3.21)$$

If, and only if, the z coordinate of M is zero the equations reduce to

$$\begin{aligned}
DE_x &= 0 \\
DE_y &= 0 \\
DE_z &= 2\delta E_z
\end{aligned} \qquad (3.22)$$

We have deduced expressions for the elemental field due to the typical element S and its image S'. Therefore, at least in principle, it should be a straightforward matter to divide the plume into a sufficiently large number of similar elements, usually about 10^4, sum all the field contributions and deduce

Calculation of electric field values from plume models

(a) the steady-state model
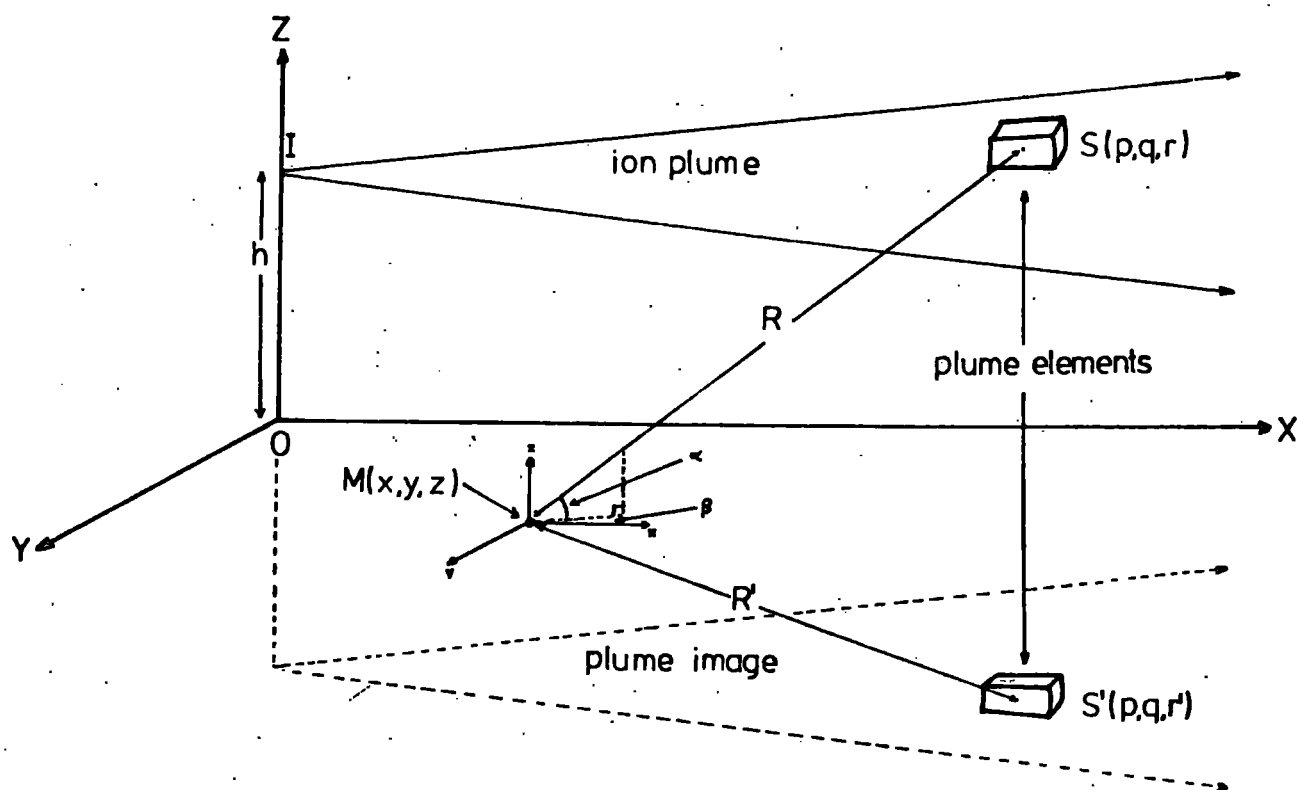
(b) the bivane data model
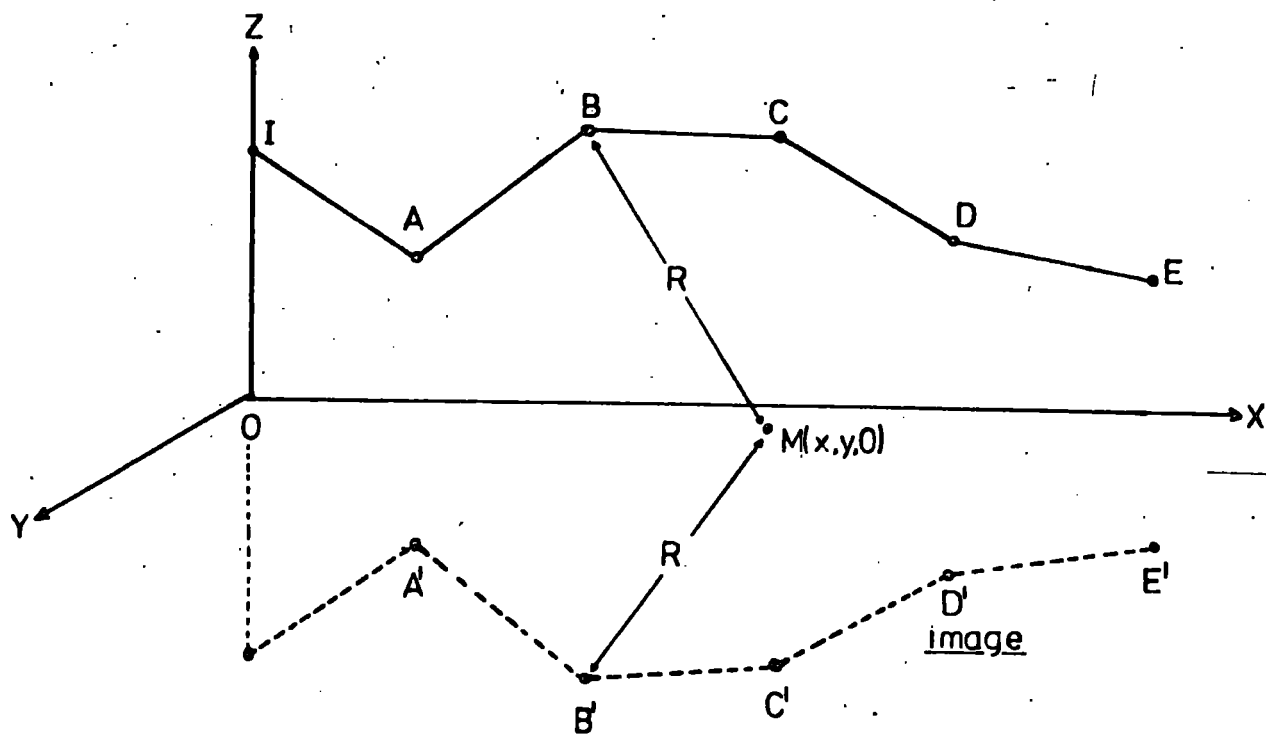
the total field components. A special program (PLMPROG) was written for this purpose. In computing these electric field values the angles of elevation of the real charge and of depression of its image (α and α') together with the azimuth angle (β). were all expressed in terms of the coordinates of M, S and S'. It was also found expedient to express these various coordinates needed in computation on the basis of a spherical polar system, the pole being at M.

A further point was the necessity to "limit" the physical size of the plume in this model. The concentration cross-section implied by equation (2.26) only becomes zero at infinite values of y or z. Thus, in the case of the crosswind and vertical profiles, it was decided that summations should be performed only up to the distance where the concentration had fallen to $0,1$ of its axial value. For similar reasons, the plume in the downwind (x) direction was "stopped" at $300\,m$. The implications of making these somewhat arbitrary truncations were thoroughly investigaed and were found to have a negligible effect on the validity of the results obtained.

3.4.3
The Bivane Data Model

The development of this model was described in Sec. 2.8. Its method of use is indicated in Fig. 3.3(b).

It should be borne in mind that this model was devised to directly simulate actual conditions. Consequently, the cooordinates ascribed to M were those of the field mill in the particular run being analysed. These mills were always placed at ground level and therefore we shall only be concerned with the vertical electric field, E_z, here. This is a considerable simplification as compared with the previous model. We now discuss

briefly the method adopted for the electric field calculations.

Ultimately, it was hoped that this model would be used to com--
pute electric field values for entire experimental runs. A
typical field run lasted 25 minutes, bivane readings being
recorded every 1.5 s throughout the run. Consequently, in the
region of 10^3 different plume configurations had to be derived
from the data in order to calculate the electric field varia-
tions. Even with the very large IBM 360/67 computer at my dis-
posal the computing time required to perform these tasks was
rather long. As a result of this the application of the model
had to be restricted to some extent. It was not, for instance,
possible to incorporate crosswind and vertical diffusion as had
been originally intended. In fact, the derived plume was consi-
dered to be a series of discrete point charges for the purposes
of this model. However, despite all these restrictions quite
good results were obtained.

It will be recalled that the points A,B,C, etc. (Fig.3.3(b))
are derived from the bivane readings. These points represent
the position of successive plume elements at a particular
moment in time. The ion generator used in this project gave
a continuous output, but because of the restrictions referred
to earlier, it was necessary to assume that the ion plume con-
tained its charge in parcels which resided at the points A, B,
C, etc. The magnitude of the charges placed at the points is
given directly by the expression $i s$, i being the generator out-
put and s the sampling interval. (The alternative procedure,
that is to imagine the charge to be uniformly distributed along
the lines joining the points, and then to perform a numerical

line integration, unfortunately would have also demanded too much computer time). In many ways the approach used was a rather drastic simplification but it is vindicated, at least to some extent, by the fact that it gave quite good results.

Once the plume configuration had been determined it was a simple matter to evaluate the electric field at any particular point. An image plume was first "constructed", as shown in the figure. Now consider the parcel of charge at the point B, for example. The element of vertical field, DE_z , due to the charge at B and its image at B' is given by

$$DE_z = \frac{is}{2\pi\epsilon_o} \frac{\sin\alpha}{R^2}$$ (3.23)

where α is the angle of elevation of B with respect to the point M. The total electric field can then be determined by adding the contributions from the points A, B, C, etc.

Field mills were never placed at more than $30m$ from the ion source in the experiments which this model was designed to simulate. Thus, in order to consider all the plume segments likely to affect the computed electric field values, the summation process was continued until the simulated plume attained a distance of $50m$ from the source. Computer trials indicated that this was a satisfactory limit.

3.4.4
The Oscillating Plume Model

The basic features of this model were described in Sec.2.8 and are illustrated in Fig. 2.5(b). The method of field computation is indicated in Fig.3.3(c), and is, in fact, very similar to that used for the bivane data model. In

view of this procedure is only noted in outline here.

The oscillating plume is considered as if it were a deformed line charge, crosswind and vertical diffusion having to be excluded for the same reasons as before. In use, the point M, at which the electric field was to be calculated, was always at ground level and thus, as before, we are only dealing with vertical fields. The plume, and its image, were divided into a number of small elements and the field due to a typical element-image pair calculated. We can write:

$$DE = \frac{\lambda \delta s}{2\pi \epsilon_0 R^2} \sin\alpha \qquad (3.24)$$

where λ is the linear charge density and

δs the length of the element.

The quantity λ can be determined from straightforward trigonometry as soon as the various constants for the particular computer run have been specified. The total electric field was found, as usual, by summing the field due to the elements along a sufficient length of plume.

It may be remembered that the configuration of this plume was made to vary with time and thus it was necessary to perform an entirely new summation for each time step. As field work progressed interest was taken in the cross-correlation obtaining between electric field values recorded by various pairs of field mills. In order to investigate these correlations the model was extended to enable calculation of the electric field at three points to proceed simultaneously. (See also Sec. 3.6)

(c) <u>the oscillating plume model</u>
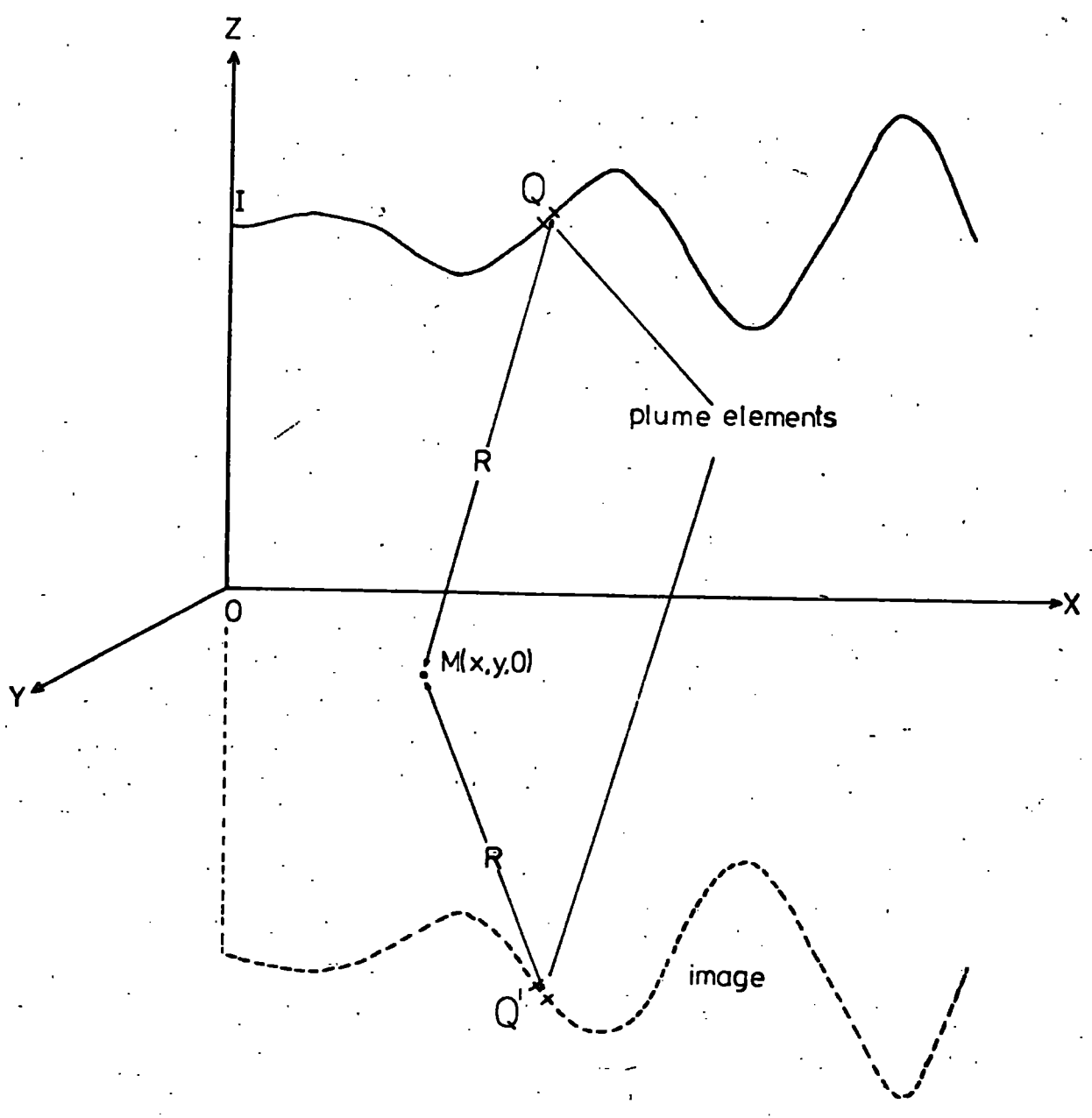
3.5
The Effect of Electrostatic Forces on Simple Charge Systems

3.5.1
Introduction

So far the rôle of electrostatic forces in determining the
behaviour of ion plumes, for reasons of simplicity, has been
largely suppressed. In the previous chapter the effects of
turbulent diffusion were described, and in this chapter we
have considered certain fundamentals of electrostatics rele-
vant to ion plumes. As a result, we are now in a position to
discuss the effects of these electrostatic forces in some
detail. It should be added here, of course, that the turbu-
lent and electrostatic forces do not act separately on the
ion plume but together. The plume behaviour is therefore
very complex.

The nature of the electrostatic forces is illustrated in
Fig.3.4. We note that the ion plume is subjected both to
outward radial repulsive forces and to a general downward
image force. The origin of these forces was discussed in
Sec.3.2 and now we wish to estimate their magnitude and,
wherever possible, compare their effects with those of tur-
bulent diffusion.

My early investigations soon revealed that it would be a very
complex task to apply equations describing these electrostatic
effects directly to a plume. As an alternative, therefore, it
was decided to apply such equations to much simpler charge
systems, explore their behaviour, and then attempt to inter-
pret the results in terms of ion plumes.

The Electrostatic Expansion of an Instantaneously Produced Spherical Charge Cloud

Let us imagine that such a cloud becomes detached from an ion plume as a result of turbulence and then moves downwind without too much further diffusion occurring. The outward radial electrostatic forces will cause the space charge to expand as it travels downwind and clearly this effect is thus, at least superficially, rather similar to turbulent diffusion (see Sec. 2.5).

In this analysis we shall use the notation that any quantity bearing the subscript 'o' refers to the value of that quantity at time, t, equals zero. Thus, for example, ρ_o indicates the initial charge concentration (supposed uniform) within the charge under consideration. Using this notation we thus refer to the initial radius of the charge cloud as R_o , and consequently the total charge (Q_o) present is

$$\boxed{\frac{4}{3} \pi R_o^3 \rho_o} \qquad (3.25)$$

and we assume, for simplicity, that this is conserved during the process. Let us fix attention (Fig. 3.5) on the sphere A_o , of radius r_o , within the charge cloud, i.e. $r_o < R_o$. We assume that as the expansion proceeds, after a particular time t, A_o will have reached A, a radius r from the charge centre. In a similar way the sphere B_o will expand so as to be at B in the same time. At $t = 0$, the distance $A_o B_o$ is δr_o , whilst at the time t, AB is equal to δr .

Now consider the charge (q_o) enclosed by A_o . We have

$$\boxed{q_o = \frac{4}{3} \pi r_o^3 \rho_o} \qquad (3.26)$$

Electrical forces influencing ion plumes

outward radial forces of
electrostatic repulsion

Wind⟶

positive
ion plume

+ve ion
source

downward image forces

H

GROUND

H

negative
plume image
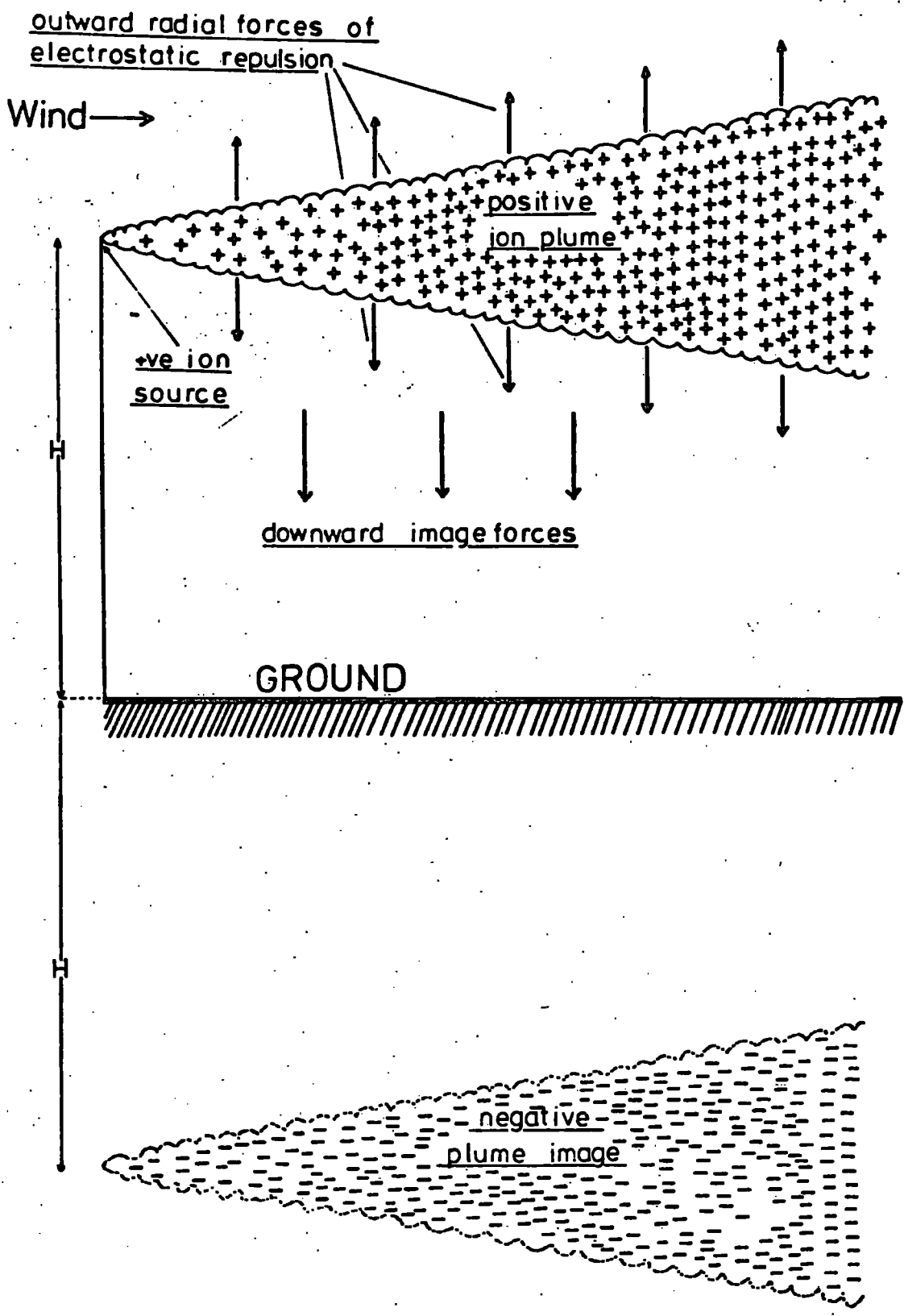
Electrostatic forces acting on simple charge systems

(a) Outward repulsive force

$r_0 + \delta r_0$ $r + \delta r$

A_0 B_0 A B

O
charge centre

charge density ρ_0 charge density ρ

r_0 r

(b) Image force

O 1

O' 2

O'' 3

h

h'

h''

I''

I'

I
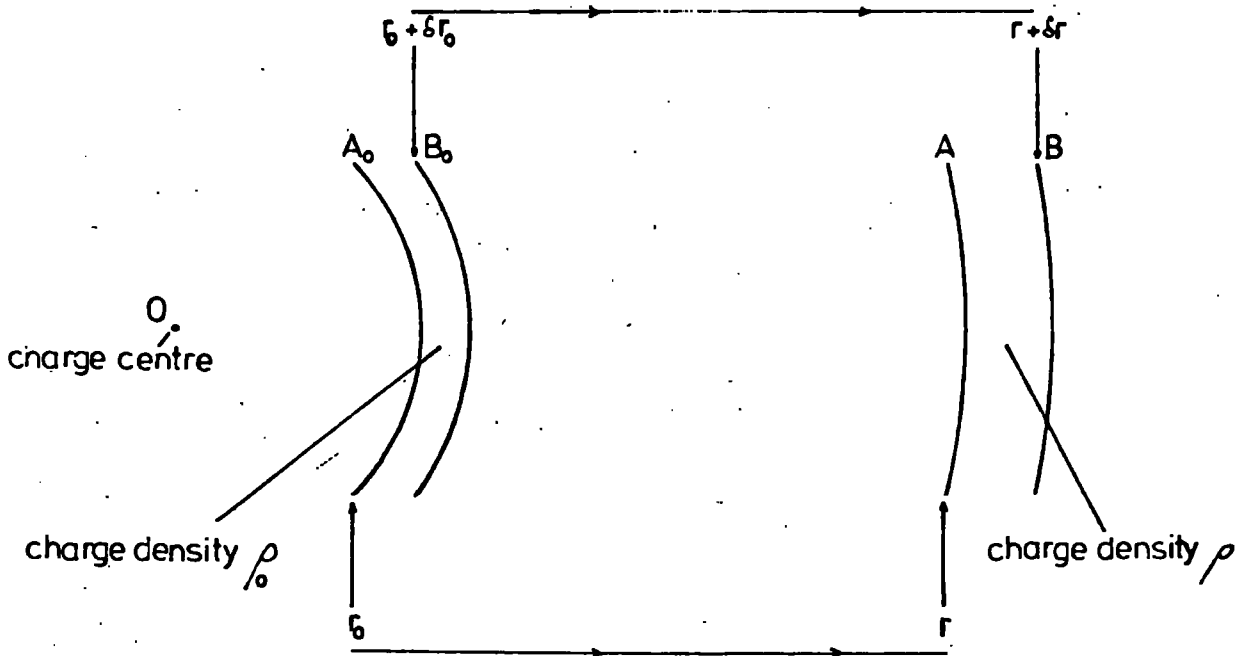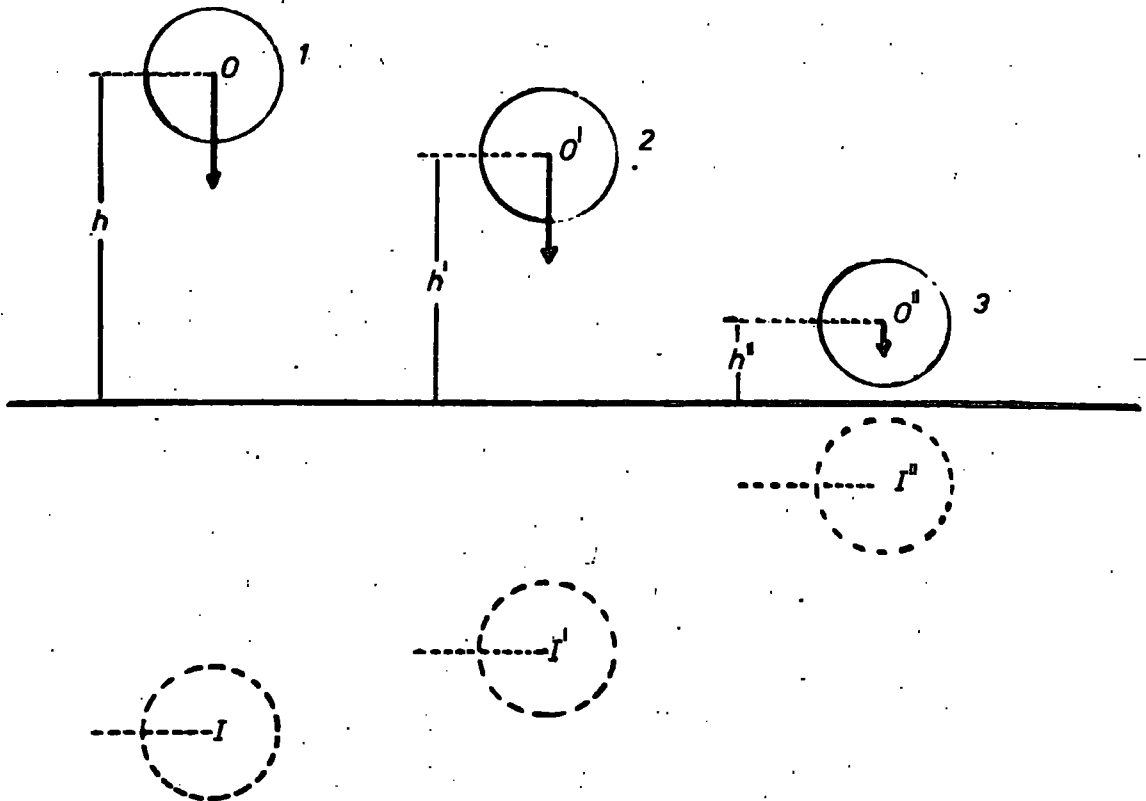
Consider the electric field, E , at the surface of the expanding charge cloud. In time t the cloud has increased its radius from r_o to r and hence

$$E_r = \frac{q}{4\pi\epsilon_o r^2} = \frac{r_o^3 \rho}{3\epsilon_o r^2} \qquad (3.27)$$

If the mobility of the ions is μ then we may write immediately that

$$\frac{dr}{dt} = \mu E_r \qquad (3.28)$$

Using (3.27) and (3.28) we find that

$$\frac{dr}{dt} = \frac{\mu \rho r_o^3}{3\epsilon_o r^2} \qquad (3.29)$$

and we may integrate this equation, not forgetting that at $t = 0, r = r_o$.

Thus

$$\int r^2 dr = \frac{\mu \rho r_o^3}{3\epsilon_o} \int dt + C$$

which gives after some algebra

$$r = r_o \left[1 + \frac{\mu \rho t}{\epsilon_o} \right]^{1/3} \qquad (3.30)$$

Equation (3.30) is therefore the relation sought between the charge cloud radius and the time. If now we differentiate (3.30) with respect to r_o , we find that

$$\frac{dr}{dr_o} = \left[1 + \frac{\mu \rho t}{\epsilon_o} \right]^{1/3} \qquad (3.31)$$

Referring to Fig. 3.5 we note that the quantity of charge contained in the spherical shell $A.B.$, say q_{r_o} , is given by the expression

$$q_{r_o} = 4\pi r_o^2 \delta r_o \rho \qquad (3.32)$$

Since charge is conserved in the expansion process, we know that the charge contained in the shell AB must also equal q_{r_o}.

Hence

$$q_{r_e} = 4\pi r^2 \delta r \, \rho \qquad (3.33)$$

Equating (3.32) and (3.33) we see that in the limit

$$\rho = \frac{r_e^2}{r^2} \frac{dr_e}{dr} \rho_e \qquad (3.34)$$

Then, from (3.34), (3.30) and (3.31),

$$\rho = \rho_e \left[1 + \frac{\mu \rho_e t}{\epsilon_o} \right]^{-1} \qquad (3.35)$$

With the aid of equations (3.30) and (3.35) we may now investigate the behaviour of this expanding space charge. However, we have not yet discussed the situation which occurs when the point under consideration is at a distance D, which is greater than R_e , the initial radius of the charge. Under these circumstances the concentration will remain zero until R equals D . Let us suppose that the time taken for R to attain this value is t_1 . We can find t_1 by inverting (3.30) and solving for t . Consequently

$$t_1 = \frac{\epsilon_o}{\mu \rho_e} \left[\left[\frac{D}{R_e} \right]^3 - 1 \right] \qquad (3.36)$$

At times greater than t_1 the charge density obeys equation (3.35).

The immediate implications of equations (3.30), (3.35) and (3.36) in the context of this project are not easy to visualize. The behaviour of the ratios r/r_e and ρ/ρ_e as functions of the relevant parameters is therefore shown in Figs. 3.6 (a) and 3.7. As mentioned in Sec. 3.1 the plume consisted of small ions, at least near the source, and therefore the small ion mobility has been used in the construction of these graphs. The expansion rates with large ion systems are, of course, very much less.

ELECTROSTATIC EXPANSION

(a) 'Instantaneous' spherical space charge cloud
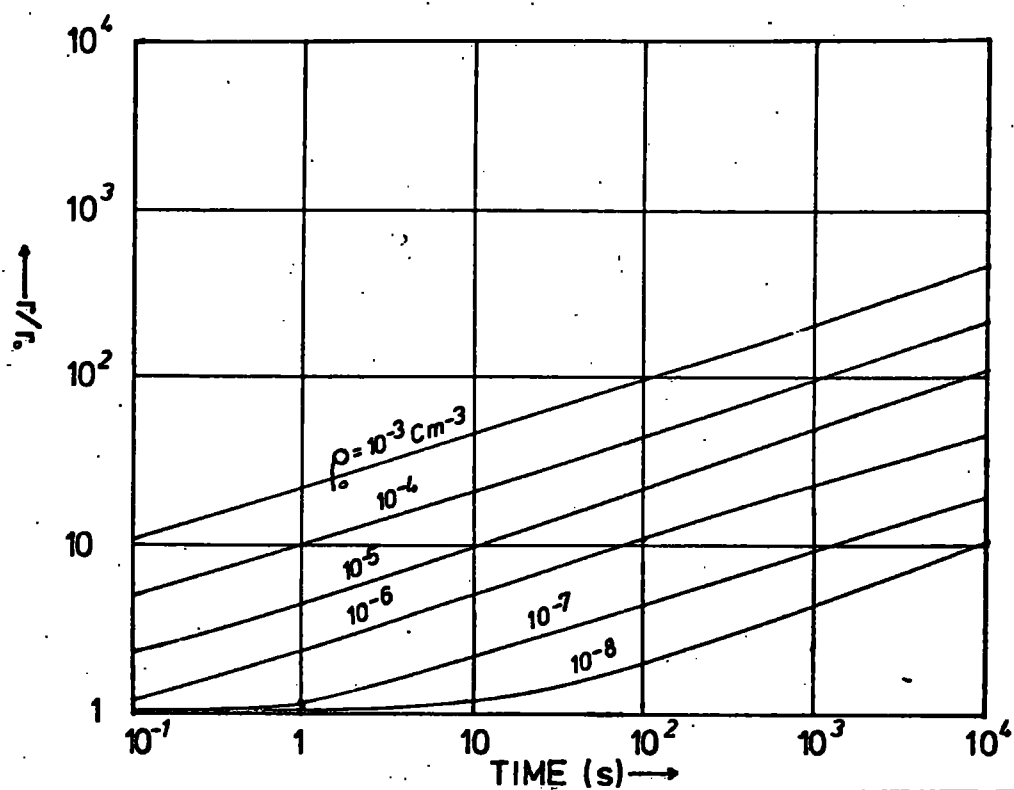
(b) 'Instantaneous' cylindrical space charge cloud
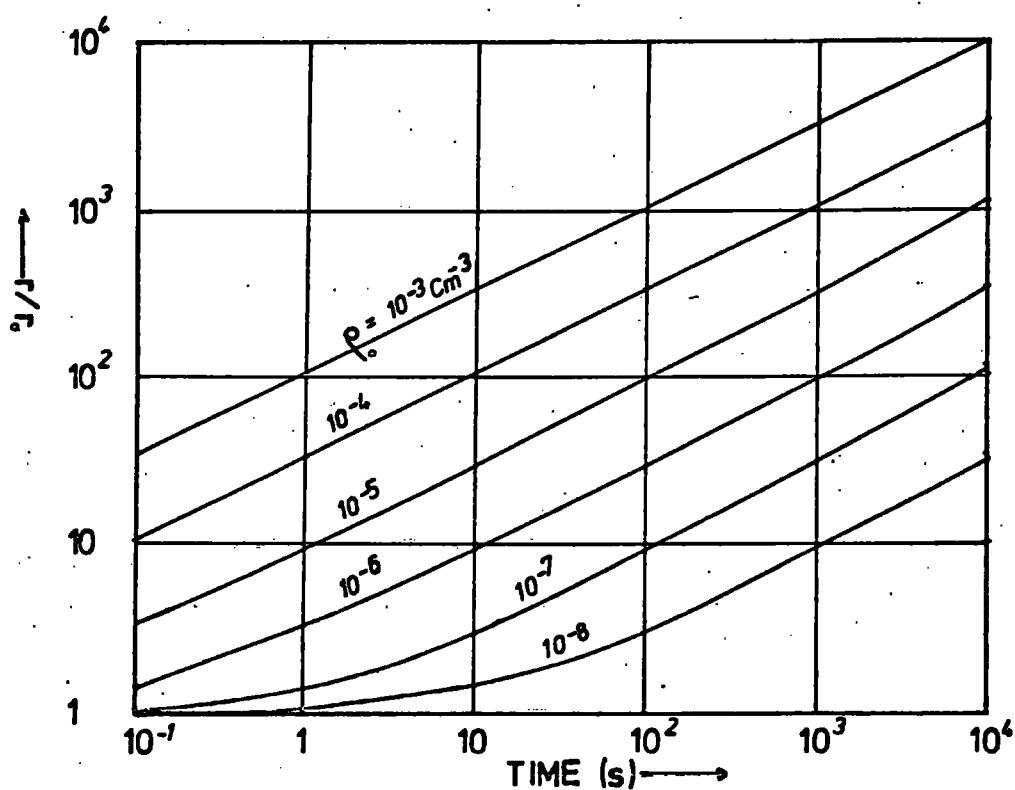
ELECTROSTATIC EXPANSION

'Instantaneous' spherical/cylindrical space charge clouds
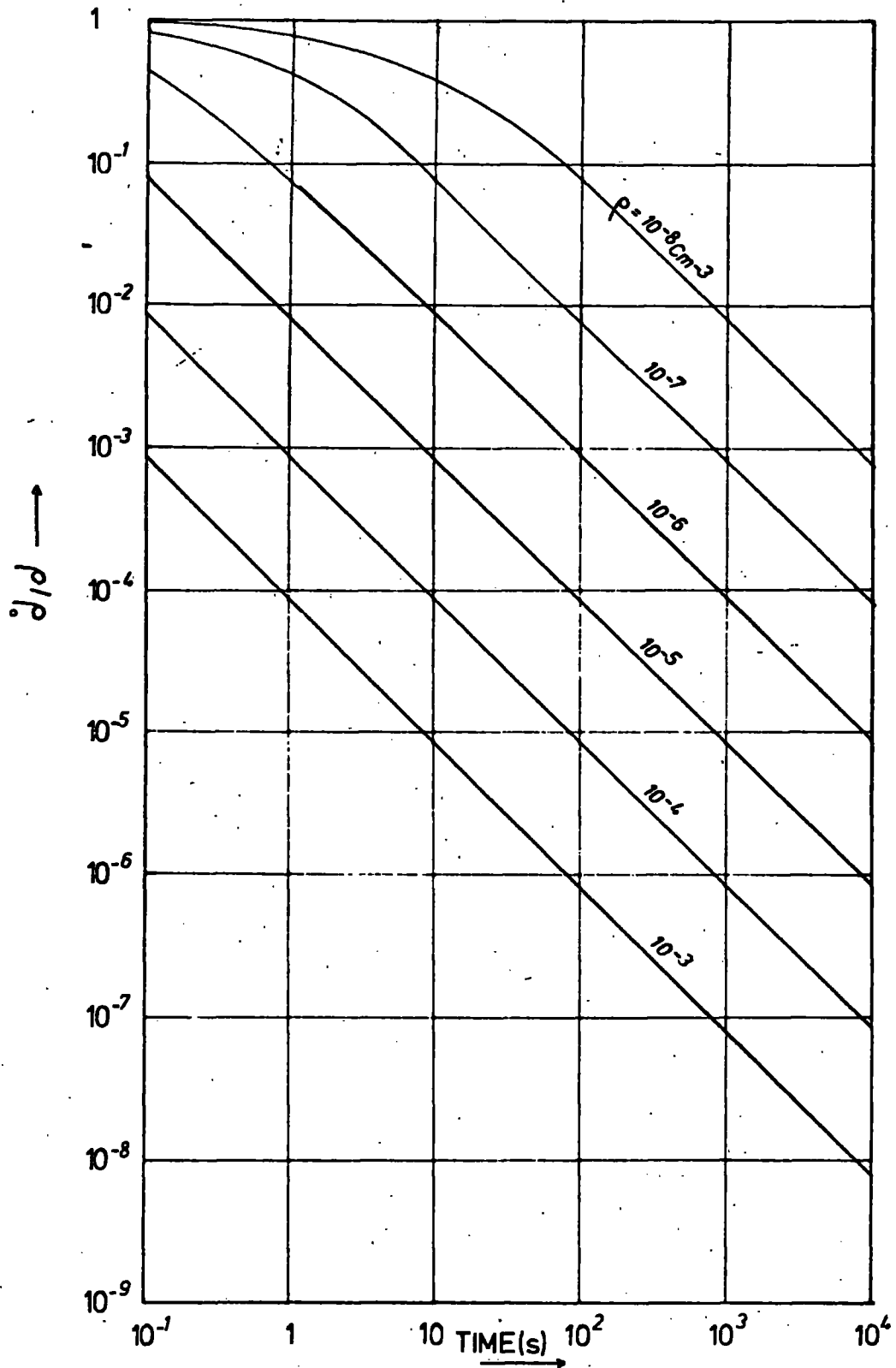
In a typical situation we might consider the expansion of a
spherical charge cloud initially of 1 m outer radius and con-
centration $10^{-8} Cm^{-3}$. Figures of this magnitude have
actually been measured in the field work associated with this
project. Referring to the 10^{-8} curve on Fig. 3.6(a) we note
that, after 100 s for instance, the charge has expanded so
that its outermost radius is now 2.3 m. From a knowledge of
the increase in radius we can calculate the decrease in con-
centration directly without reference to Fig. 3.7. It is
worth noting also, that during the expansion process the con-
centration, although falling all the time, remains uniform
within the entire sphere at any particular time. (See equa-
tion (3.35) which shows that ρ is independent of r).

It is clear then, from this simple example, that the electro-
static expansion effects are substantial, and therefore must
be taken into account when estimating the behaviour of an ion
plume. Having considered the case of an isolated instanta-
neous spherical charge cloud we now discuss an isolated instan-
taneous cylindrical charge cloud.

3.5.3
The Electrostatic Expansion of an Isolated, Instantaneously Produced Cylindrical Space Charge Cloud

We imagine that the charge is brought, somehow, into existence
instantaneously and then left to expand under the action of its
own electrostatic forces. It will be shown later that the
results obtained with this charge configuration can be adapted
to indicate, very approximately, the behaviour of an ion plume.
Because of the similarity of the analysis with that of the pre-
vious case only the results are quoted here.

The radius, as a function of time, of the cylindrical charge
is given by the expression

$$r = r_o \left[1 + \frac{\mu \varrho_o t}{\epsilon_o} \right]^{1/2} \qquad (3.37)$$

and the decrease in charge density with time by

$$\varrho = \varrho_o \left[1 + \frac{\mu \varrho_o t}{\epsilon_o} \right]^{-1} \qquad (3.38)$$

In the above r_o refers to the original radius of a cylindrical
shell drawn within the charge cloud, whilst r is the radius
of that shell after time t.

These expressions are plotted in Figs. 3.6(b) and 3.7. We note
that the radius expansion of the cylindrical charge is more
rapid that that of a spherical system having the same initial
charge density. It is also worth noting that the expressions
describing the expansions in the two cases are very similar,
only the indices being different, whilst those describing the
behaviour of charge density are identical.

We now rearrange (3.37) and (3.38) in order to discuss the
behaviour of a plume. Consider the outermost radius, R, of
the expanding cylindrical charge. We may write immediately
a similar equation to (3.37) describing the behaviour of R
in terms of R_o and t. If the linear charge density within
the cylinder were λ, we could also write.

$$\varrho_o = \lambda / \pi R_o^2 \qquad (3.39)$$

Applying these ideas to equation (3.37) we find that

$$R = \left[R_o^2 + \frac{\mu \lambda t}{\pi \epsilon_o} \right]^{1/2} \qquad (3.40)$$

In the case of an ion plume, the ions are produced at a par-
ticular point and are then blown downwind. However, if we
were to consider a particular plume segment travelling along
we would observe that, once it had been formed, there was no

further charge generation within it. At least in this res-
pect therefore, the portion of plume corresponds quite closely
to a segment of an instantaneous cylindrical charge. Conse-
quently it might not be too unreasonable to imagine that the
actual electrostatic expansion of an ion plume would be rather
similar to that of a cylindrical charge.

Suppose the wind speed is u , then after a time t the plume
segment will have travelled a distance ut away from the source.
For an ion generator of constant output current i , we can write

$$\lambda = i/u \qquad (3.41)$$

and on substituting the above relations involving t and λ
into equation (3.40) we find

$$R = \left[R_\circ^2 + \frac{\mu i x}{u^2 \pi \epsilon_\circ} \right]^{1/2} \qquad (3.42)$$

where $x = ut$, the distance downwind.

Equation (3.42) is of great importance as it enables us to com-
pare the electrostatic and turbulent effects directly. In order
to facilitate these comparisons both now, and in the analysis of
field work, the two effects are contrasted in Figs. 3.8(a) and
(b). In Fig. 3.8(a) the curves are appropriate to a source at
10 m above the ground. The turbulent diffusivities associated
with the three classes of stability were based on the results of
DEACON (1955). (See also PRIESTLEY 1959). Inspection of the
curves indicates that on many occasions we might reasonably expect
the turbulent and electrostatic effects to be of roughly equal
magnitude. In very low wind speeds the electrostatic expansion
obviously dominates the turbulent effects whilst at higher wind
speeds the converse is true. This interesting feature was actually
found in practice and consequently further discussion is postponed
until the experimental results are presented in Chs. 7 and 8.

In the previous chapter we considered the turbulent diffusion of ions from a *continuous* point source in calm conditions. However, in very low wind speeds, turbulent effects tend to be rather small and consequently the validity of the approach in Sec. 2.5 is questionable. As an interesting alternative we shall consider here the effect that the electrostatic forces alone have on such a system and disregard turbulent diffusion effects entirely. In practice, such a situation might arise during a strong inversion with dead calm, any turbulence being virtually eliminated in these circumstances.

It is found, after an analysis rather similar to the previous cases, that once a steady state has been established, the space charge concentration ρ , at a point distance r from the ion source, is given by the expression

$$\rho = \left[\frac{3 \epsilon i}{8 \pi \mu r^3} \right]^{1/2} \qquad (3.43)$$

where i is the current output of the source. The behaviour of (3.43) is indicated in Fig. 3.9(a). The analysis here has only been concerned with an isolated point source, and thus, in the circumstances of this project, the presence of image forces may seriously disturb the validity of (3.43). Nevertheless, as these results are certainly of relevance to the behaviour of ion clouds at higher levels, where image effects are much smaller, they are included.

It is of interest to calculate the value of the electric field E_r , that would exist at a distance r from the ion source. A simple analysis shows that

$$E_r = \left[\frac{i}{6 \pi \mu \epsilon r} \right]^{1/2} \qquad (3.44)$$

ION PLUME EXPANSION

(a) by turbulent diffusion (using steady state model)
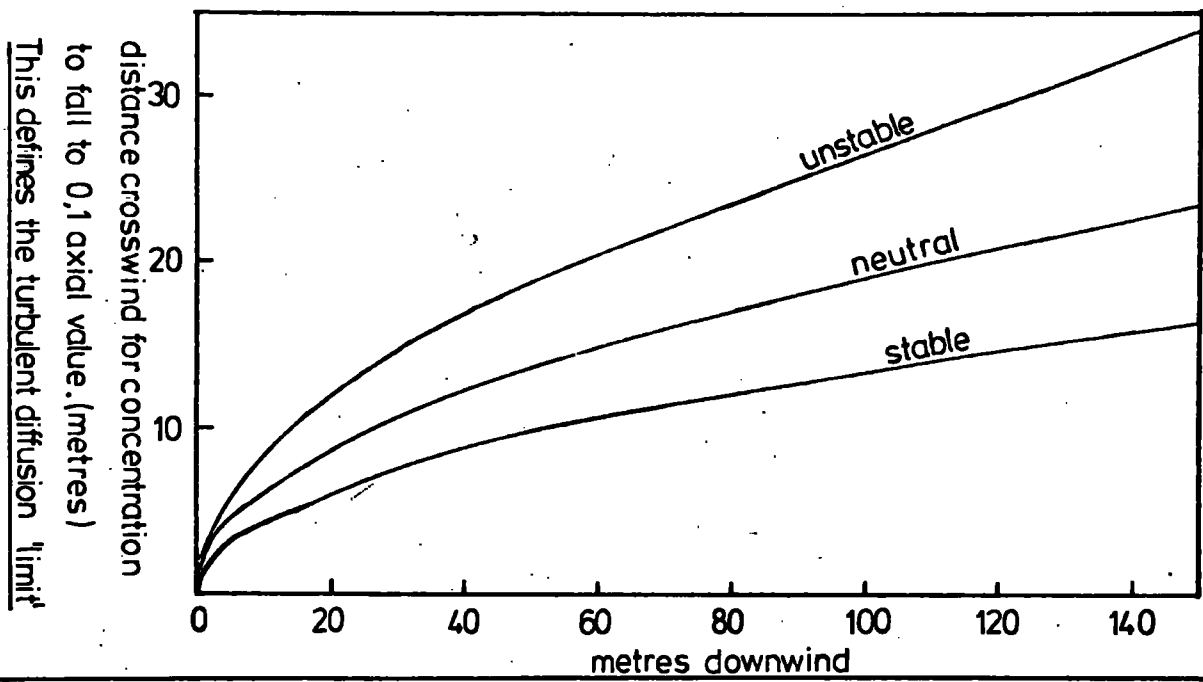
(b) by electrostatic repulsion effect
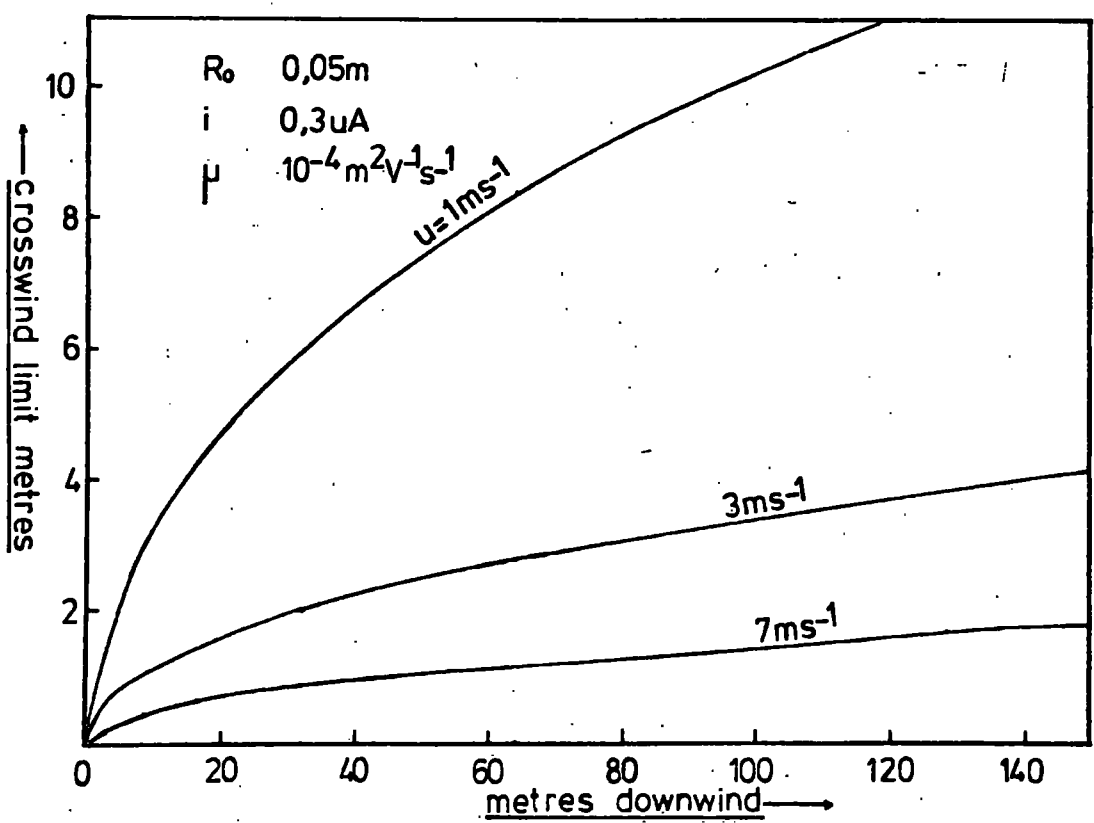
Continuous point source in calm conditions
(a) behaviour of charge concentration

← charge concentration Cm⁻³

distance from source (m) →
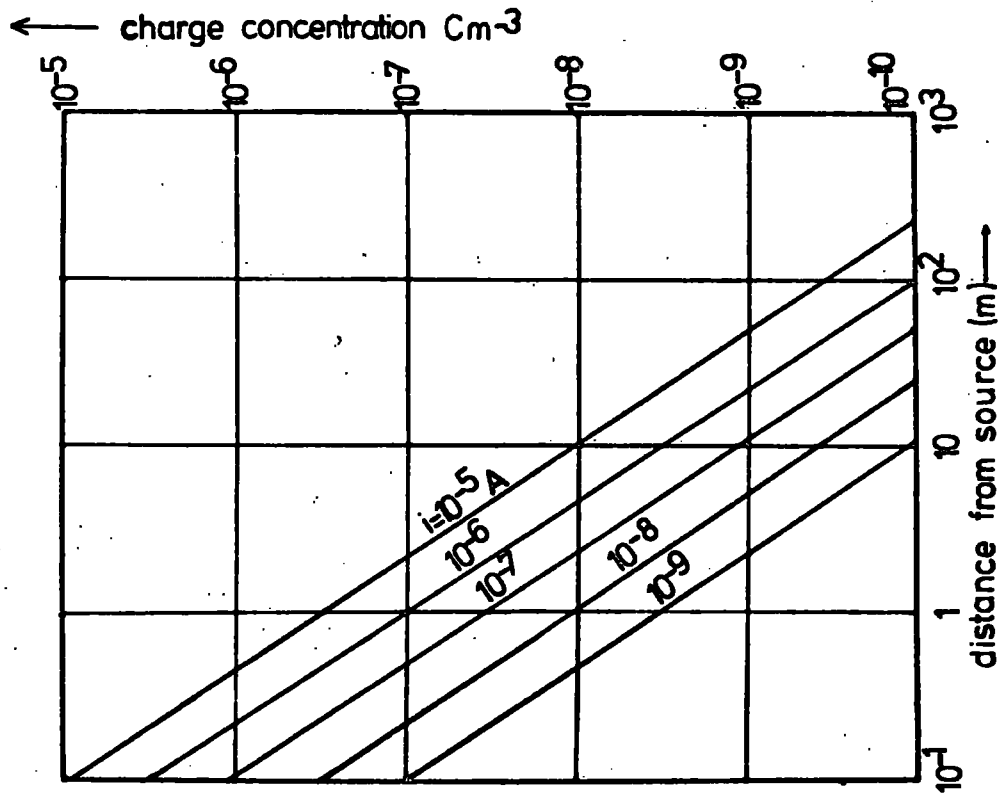
(b) behaviour of electric field

distance from source (m) →
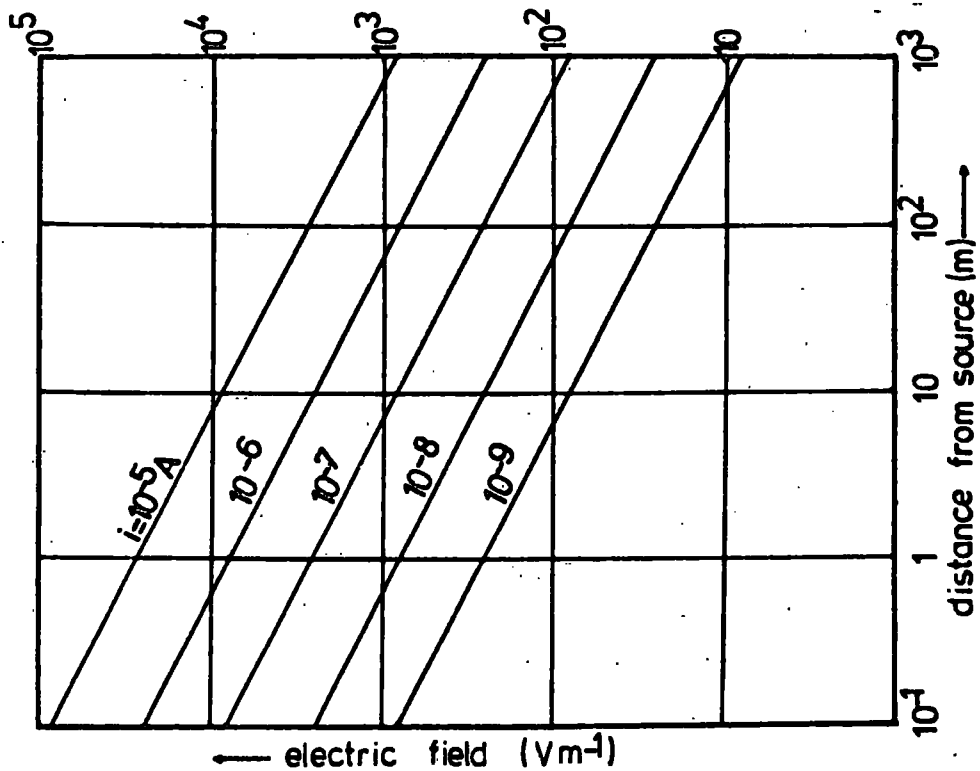
← electric field (Vm⁻¹)

This equation is plotted, for various values of i , in Fig. 3.9(b). In this project the ion generator output was $0.3\mu A$, and for example, we note from the figure that at $10\,m$ from the source the electric field predicted is about $1\,kVm^{-1}$. A field of this magnitude would be readily detectable and accordingly there should be no experimental difficulty in establishing the validity, or otherwise, of equation (3.44).

We may also estimate, using Fig. 3.9(b), the outward radial velocity of the ions. In the situation above, for instance, where E_r was $1\,kVm^{-1}$, we find that, with a small ion mobility of $10^{-4}\,ms^{-1}\,per\,Vm^{-1}$ their radial velocity is $0.1\,ms^{-1}$. This illustrates in a very practical way that the analysis applies for only extremely low wind speeds.

Finally, we must consider, and this also applies to the previous cases, the effect of the ion motion on the air through which they pass. To establish whether any effect is present, we shall investigate the circumstances in which we suspect it to occur most markedly. It seems reasonable, on common sense grounds, that such effects, if any, are most likely to occur at short distances from powerful ion sources. Let us therefore consider a point $1m$ away from a $10\,\mu A$ source. We note from Fig. 3.9(a) that at this distance the ion concentration is $3 \times 10^{-7}\,Cm^{-3}$, whilst from Fig. 3.9(b) we observe that the electric field is $30\,kVm^{-1}$. Hence the outward velocity of the ions is

$$v_r = \mu E_r = 3\,ms^{-1}$$

With this charge density, assuming singly charged ions, the
number of ions, n , per cubic metre is given by

$$n = \frac{3 \times 10^{-7}}{1.6 \times 10^{19}} = 2 \times 10^{12} \quad \text{approx.}$$

By comparison, the number of molecules, N , in a cubic metre
of air at NTP is

$$N = 2.7 \times 10^{25}$$

and we note that the ratio n/N is approximately 10^{-13} .
Therefore we conclude that if any electrically driven air
motion does actually occur it will be a very small effect.

3.5.5
The Effect of Image Forces on Simple Charge Systems
3.5.5.1
Opening Note

A precise theoretical investigation of the effect of these
forces, even on quite simple systems, is, because of its
complexity, beyond the scope of this project. In this sec-
tion we shall consider, as before, two simple cases and then
apply the results obtained from them to ion plumes. It must,
of course, always be borne in mind that the expansion processes
discussed previously will operate in addition to the image
effects now being considered.

3.5.5.2
Spherical Charge

This is shown in Fig. 3.5(b), the labels 1, 2 and 3 indicating
successive positions of the spherical charge as it moves down-
ward under the action of image forces. In reality, the upper
part of this charge will, to some extent, be screened from
image forces by the lower part. As a result of this, the image
forces will exert a stronger effect on the lower parts of the
charge and therefore will cause it to be distorted from its
original spherical shape. Ultimately, as the charge descends

it will become pear-shaped, or even cigar-shaped. For the purposes of this analysis we shall not consider this aspect any further but content ourselves with a very simple analysis of the image effect.

Suppose the distributed space charge illustrated in Fig. 3.5(b) were reduced to an equivalent point charge q . This charge is placed at O , a height h above the ground. The electric field E_i at the charge due to its own image is given by

$$E_i = \frac{q}{4 \pi \epsilon_\circ (2h)^2}$$ (3.45)

Therefore, for a cloud of ions of mobility μ , the initial downward speed is given by

$$\frac{dh}{dt} = -\frac{\mu q}{16 \pi \epsilon_\circ h^2}$$ (3.46)

Integrating (3.46), and remembering that at $t=0, h=h_\circ$, we find that

$$h = \left[h_\circ^3 - \frac{3 \mu q t}{16 \pi \epsilon_\circ} \right]^{1/3}$$

If the charge is being blown along by a wind of velocity u we can replace t by x/u in the above equation. Here x is the distance of travel from the point where the charge was at the original height $h_\circ$.

Hence

$$h = \left[h_\circ^3 - \frac{3 \mu q x}{16 \pi \epsilon_\circ u} \right]^{1/3}$$ (3.47)

We illustrate the magnitude of the effect predicted by (3.47) by considering two simple examples. Suppose $h = 10,00\,m$, $q = 0,1\,\mu C$, $u = 5\,ms^{-1}$ and $x = 50\,m$. In these circumstances h is found to be $9.99\,m$ and the image effect is negligible. Now suppose $h_\circ = 1\,m$, with the remaining quantities as before.

Here we find that h is now $0.67m$ and in this case the image effect is substantial.

It is clear that we cannot always ignore image effects and, in fact, with low level ion sources the progressive reduction in height of the space charges must be taken into account. Ultimately some of the ions will arrive at the ground and, in so doing, will either remain there or be discharged. Moreover even if any undischarged ions reside at the ground they can no longer produce any electrical effects and thus, effectively, have also been removed from the plume.

We now move on to consider a simple plume analogy derived from a line charge concept.

3.5.5.3
Cylindrical Charge

If we consider the image force on a line, instead of a point, charge, we find that the height decreases with time according to

$$h = \left[h_o^2 - \frac{\mu \lambda t}{\pi \epsilon_o} \right]^{1/2} \qquad (3.48)$$

(λ is the charge per unit length)

By employing similar arguments to those used in Sec. 3.5.3. we may apply this result, albeit rather naively, to an ion plume. It is found that

$$h = \left[h_o^2 - \frac{\mu i x}{\pi \epsilon_o u^2} \right]^{1/2} \qquad (3.49)$$

The predictions of this important equation in regard to the particular conditions of this project are shown in Figs. 3.10 (a) and (b). The implications of the results are not discussed here as they will be fully dealt with later. Nevertheless, it should be pointed out that, particularly when the

The effect of image forces on ion plumes

(a) ion source 0,3μA at 10m

Plume height, h (m) vs downwind distance, x (m). Curves labelled u=2ms⁻¹, 0,5ms⁻¹, 1ms⁻¹.

(b) ion source 0,3μA at 2m

Plume height, h (m) vs downwind distance, x (m). Curves labelled u=10ms⁻¹, 2ms⁻¹, 5ms⁻¹.
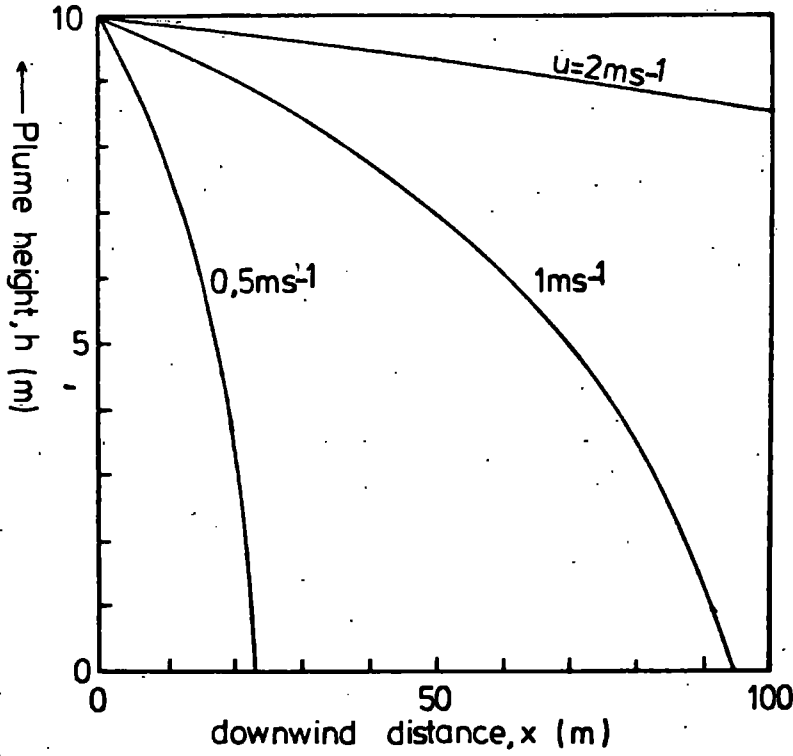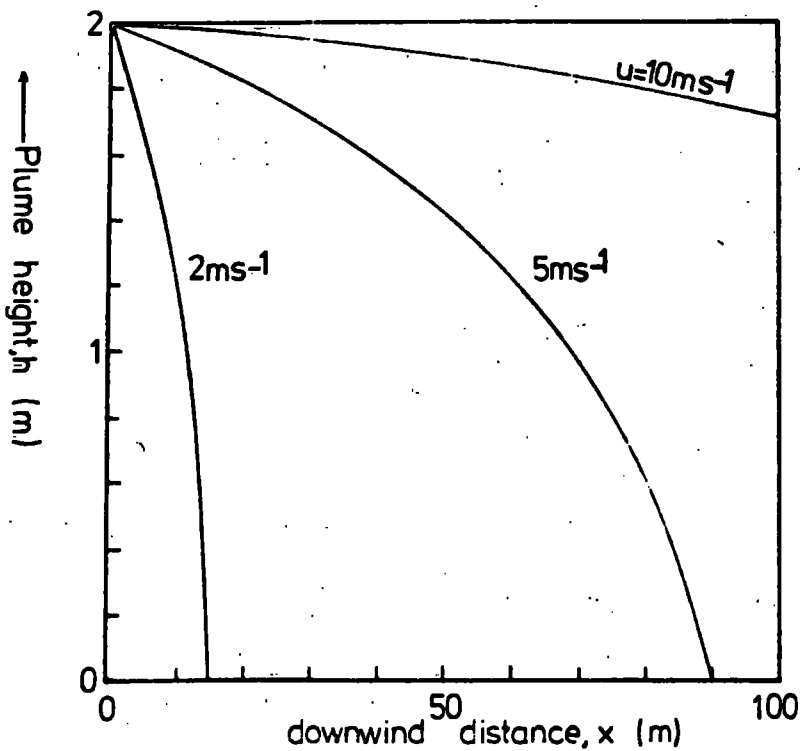
ion source was at $2m$ the image forces were evidently of
considerable importance in determining the plume behaviour.

3.6
The Relation between the Electric Fields at Different Points under an Ion Plume

So far we have considered techniques for estimating the elec-
tric field at any given point under an ion plume. In this
project four field mills were operated simultaneously and
therefore it is of interest to be aware of any relationships
that might exist between the various field records.

At any point under the plume the electric field changes con-
stantly in response to the varying charge distribution. How-
ever, quite frequently, certain features such as kinks and
loops (see Sec. 2.7) develop in plumes, and, when features
of this nature pass over a given point distinctive electric
field patterns are often produced. In addition, if the kink
passes over (or near) two points in succession we would expect
similar field patterns to be recorded but with an appropriate
time displacement between them.

One type of behaviour is illustrated in Fig. 3.11(a). A verti-
cal kink (k) develops in a plume and then travels downwind.
This situation might result from a sudden short-lived burst
in the downward velocity component ($\overset{\bullet}{w}$). It is fairly obvious
that the presence of such a kink near a measuring point would
result in an enhanced electric field. In the diagram M1 and
M2 represent the positions of typical recording stations and
the graph indicates the type of electric field variations to
be expected. The electric field records will each attain a
maximum as the feature passes overhead but these maxima will

be displaced by an amount t_d depending on the separation
of the points M1 M2 and the mean wind speed (u). A cross-
correlation analysis (see Sec. 6.2) of the field records would
therefore reveal a maximum value at a lag number corresponding
to t_d . In practice, a kink or loop will usually become less
well-defined as it travels downwind and, as a result, the cross-
correlation coefficient at t_d will reflect, in a sensitive
manner, the relative "power" of the turbulent diffusion pro-
cesses operating.

A second possibility is shown in Fig. 3.11(b). In this case a
horizontal kink develops and travels downwind. Let us suppose
that field mills are arranged across wind as illustrated. It
is clear that, as the kink moves downwind towards M2 , the elec-
tric field will increase there, ultimately reaching a maximum
value and then declining as the feature moves away. During
this time, however, the field mill at position M1 has seen the
plume first recede and then advance after the passage of the
kink. Consequently the electric field here falls to a minimum
as the feature passes by. A cross-correlation analysis of the
M1 and M2 records would therefore show a negative value at zero
time lag, as a result of the out-of-phase nature of the two
records. It is also possible, with this arrangement of field
mills, to make certain deductions about the ion plume width.
For example, if there were negative correlation between records
such as M1 and M2 then the plume could not have been wider than
the distance y between M1 and M2 . Therefore if we place field
mills at various distances apart in a cross-wind line and then
examine the cross-correlation coefficients between their records
it should be possible to arrive at useful conclusions about the

The relation between the electric fields at different points under an ion plume

(a) the effect of vertical kinks

in elevation

←height

M2

x

M1

downwind distance →

K

u

M2

M1

t_d

←electric field

time →
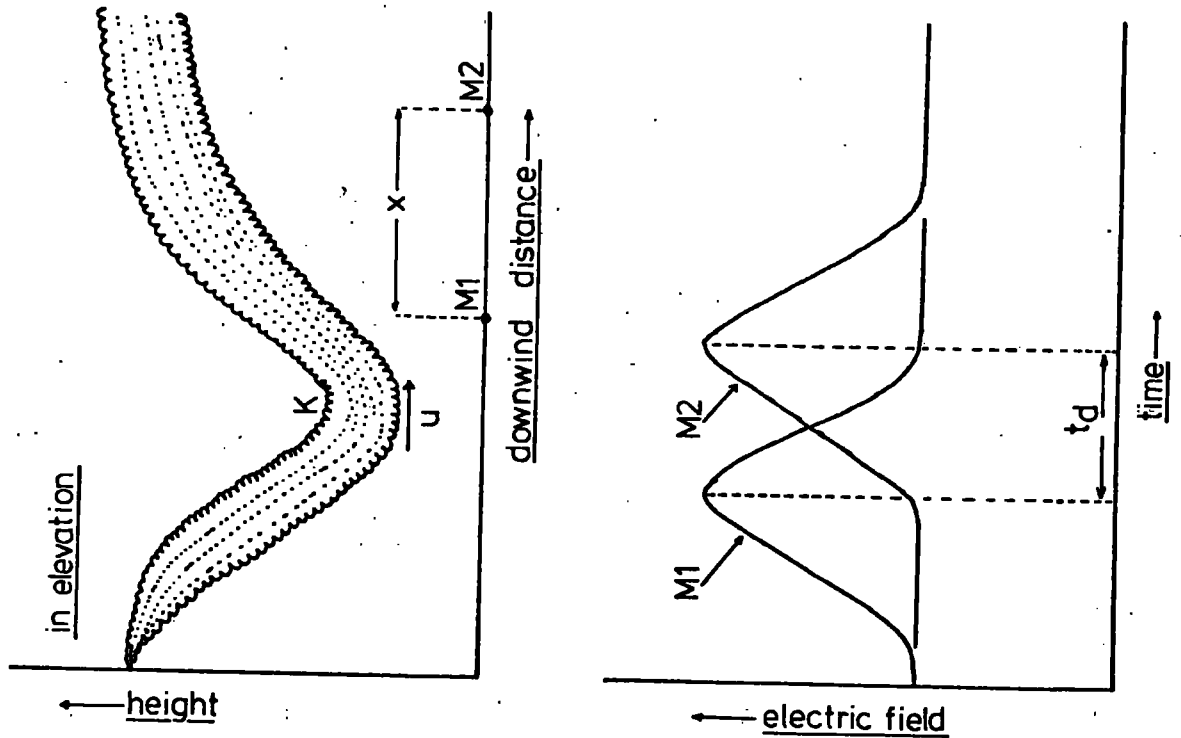
(b) the effect of horizontal kinks

in plan

←crosswind distance→

M1

plume width

M2

K

downwind distance →

M1

M2

←electric field

time →
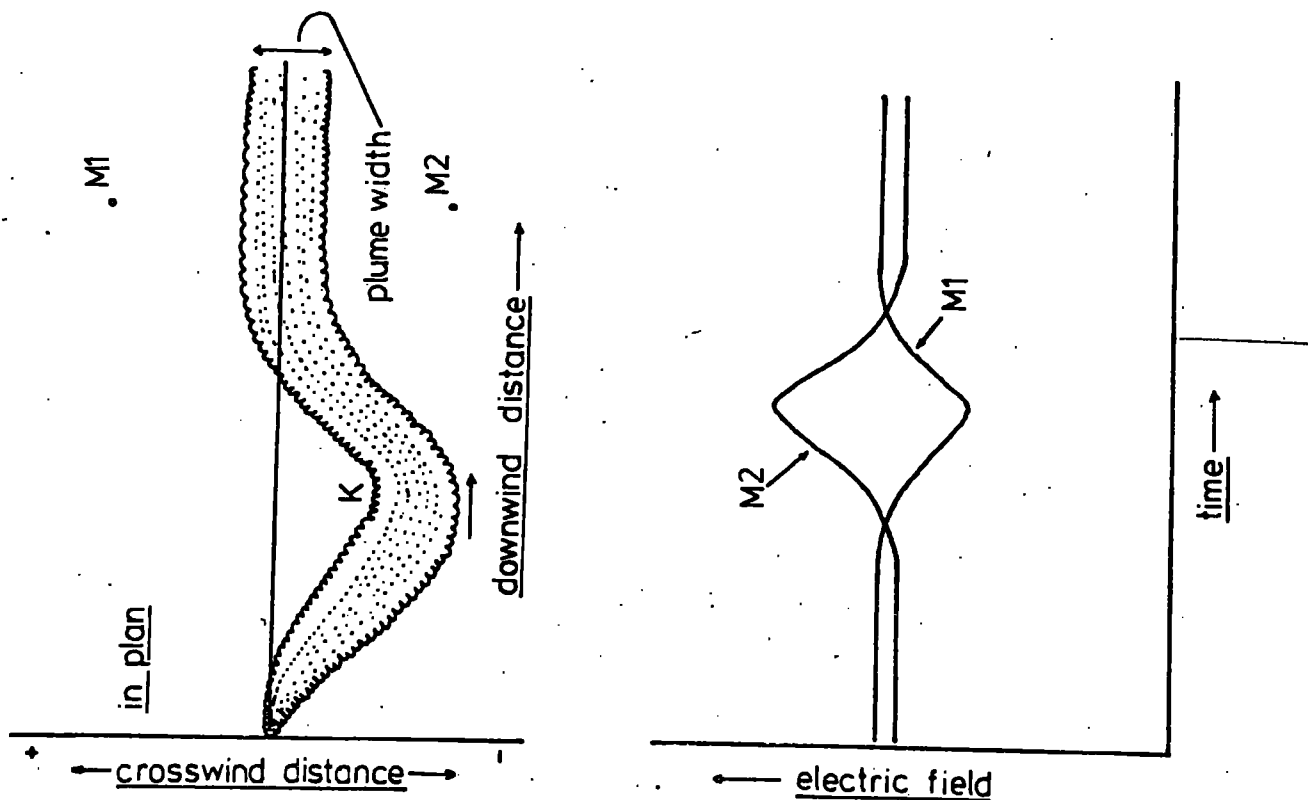
ion plume dimensions.

The above concepts have been found invaluable in the analysis of experimental results and will be referred to again in Ch.7.

3.7
The Presence of the Natural Electric Field

The existence of a natural electric field at the Earth's surface is well known, having been first detected by LEMONNIER as early as 1752. The presence of an "external" electric field in addition to that of the ion plume might possibly confuse any experimental results and therefore the likelihood of interference from this cause had to be investigated.

SHARPLESS (1968) carefully observed the behaviour of the natural field at an unpolluted site and concluded that, during fine weather, the average potential gradient was approximately $100 \ Vm^{-1}$. WHITLOCK and CHALMERS (1956) made a special study of the short period variations and discovered that, in fine weather and with little low cloud present, any changes were relatively small. On the other hand, in disturbed weather conditions, mostly frontal precipitation, showers and thunderstorms, the potential gradient is large and often displays rapid fluctuations - see ASPINALL (1969). Very frequently potential gradients exceed $1 \ kVm^{-1}$ and, during thundery weather, values as large as $10 \ kVm^{-1}$ are not uncommon.

It was expected, largely on the basis of the plume models described herein, that the electric fields associated with ion plumes would range up to approximately $2 \ kVm^{-1}$. Consequently, it seemed evident that the variations of the natural field

occurring in disturbed weather would often be large enough to mask those fields caused by the ion plume. Apart from this problem, there would also be considerable difficulties in operating the equipment during wet weather. It was therefore necessary, for both these reasons, to restrict all field work to dry conditions.

On the basis of the results of SHARPLESS and WHITLOCK little interference was expected from the natural field in fine weather conditions. As a precaution, however, the relevant characteristics of the natural field were investigated early in this project. It was found that, in practice, slight interference did occur but it detracted little from the quality of the experimental results. The characteristics of the natural field, as found in this project, are presented with the rest of the experimental data, in Chs. 7 and 8.

Chapter 4: <u>THE MEASURING EQUIPMENT</u>

<u>4.1</u>
<u>Introduction</u>

The following items of equipment were required:-

(a) Ion generator,

(b) Ion detectors - in the form of field mills or ion collectors,

(c) Apparatus for monitoring the micro-meteorological environment,

(d) Certain photographic equipment for the smoke plume investigations,

(e) A suitable mast to support certain of the above items.

(The mast used for this project, made by A. C. CLARKE & CO.,
Binstead, Isle of Wight, consisted of six telescopic sections.
It could be raised to a maximum height of $12m$ by air pressure
generated from an attached hand pump. The mast gave no trouble
throughout the project.)

<u>4.2</u>
<u>General Design Criteria</u>

Ideally for this investigation a permanent installation would
have been desirable but the only location where this might
have been possible, Durham University Observatory field, was
too small and insufficiently level. Therefore, there was no
choice but to design and construct instruments which could be
transported to a site, be set out and operate independently of
a mains supply. At one stage use of the Group's Honda genera-
tor , giving $240 \, V$ AC, was considered, but this idea was rejected
when it was discovered that its internal combustion engine was
a prolific source of ions. Hence the employment of batteries
as the means of power supply appeared the only solution. It
was necessary that the equipment should be capable of running

for at least 5 hr before requiring renewal or recharging of batteries. Certain items of equipment requiring only small currents were powered by conventional dry batteries, whilst apparatus needing larger currents, such as field mill motors, were supplied by rechargeable batteries. This approach enabled costs to be kept to a minimum commensurate with satisfactory equipment performance. One of the most undesirable features of all batteries is their progressive reduction in voltage which takes place as discharge proceeds. Much of the equipment was sensitive to supply voltage alterations and therefore great care had to be taken to minimise any effects due to this.

The apparatus needed to be mechanically robust as it would be transported long distances by Land Rover over rough ground. Overall system reliability needed to be good as only the most minor of breakdowns could be repaired in the field.

At this stage it was also necessary to decide on the type of output signal that the measuring instruments should produce. It was proposed that each instrument should give a small direct voltage output, the value of which was linearly proportional to the magnitude of the parameter being measured. The actual voltage range employed was 0 to 1.0 V, the lower figure always corresponding to the minimum value of the parameter, the upper to the maximum.

4.3
The Field Mills

4.3.1
Design and construction

The fundamental principles of field mills have been thoroughly documented elsewhere and therefore will not be discussed here. The field mills used in this project, although largely of standard design, do, however, incorporate one or two innovations which were a result of the particular requirements of this project. We now examine these features in more detail.

Early work indicated that electric fields as large as $3\,kVm^{-1}$ occurred near ion plumes. In contrast, if a field mill were placed a considerable distance from such a plume it would register an electric field close to the natural value ($100-300\ Vm^{-1}$ in fine weather). It was clear therefore that the field mills would need various ranges if accurate measurements were desired. The nominal ranges chosen, giving a 0 - 1.0 volt output were (1) $0 - 200\,Vm^{-1}$, (2) $0 - 400\,Vm^{-1}$, (3) $0 - 1kVm^{-1}$, (4) $0 - 1.6\,kVm^{-1}$ (5) $0 - 3\,kVm^{-1}$ and (6) $0 - 6\,kVm^{-1}$. The type of field mill used responded equally to potential gradients of either sign as it consisted of a simple rotor and stator system without bias plate. It was originally hoped to incorporate sign discrimination by modifying the existing stator to act as a bias plate, at the same time introducing a new stator. However, this modification was never performed. This lack of sign discrimination was of no importance when studying positive ion plumes in fair weather as the resulting potential gradients were always positive. However, on those few occasions when negative ion plumes were investigated, sign ambiguities, although present, were not too troublesome.

OGDEN (1967) has constructed portable field mills but in my opinion his design seemed unnecessarily cumbersome. Portable field mills, using DC motors, are inevitably very susceptible to electrostatic interference from the motor commutator brushes. Ogden overcame this problem by isolating the motor from the field mill proper by means of a long flexible coupling. It was hoped that, by using a high speed motor with a reduction gearbox and modifying the standard amplifier design (see SHARPLESS 1968), this long coupling could be eliminated. Such modifications were most desirable as they would considerably reduce the size of the instrument. In practice a $6V$ DC motor, with a nominal speed of 7500 RPM, was used to drive the field mill rotor via a 5:1 reduction gearbox. In this way it was thought that most of the brush interference from such a system would be at frequencies considerably higher than the mill signal frequency. After construction it was found that there was still some brush noise present, even though the motor had been carefully shielded. As development continued it appeared that the only really satisfactory method by which the interference could be eliminated was by reducing the input impedance of the amplifier to about $5M\Omega$. This, however, immediately raised another difficulty. MAPLESON & WHITLOCK (1955) have shown that, for a field mill output to be independent of signal frequency, f , the criterion $fCR > 1$, where C is the input capacitance and R the input resistance, must be met. Reducing the input impedance to $5M\Omega$ drastically violated the above relation and hence a compromise solution had to be found. This was achieved by using a tuned field mill amplifier, shown in Fig. 4.1. The amplifier gain was arranged to change with frequency in such a way that as

THE FIELD MILL AMPLIFIER

CURRENT AMPLIFIER   HIGH STABILITY   TUNED AMPLIFIER
                     VOLTAGE AMPLIFIER

the rotor speed varied the output voltage, for a given electric field, would tend to remain constant. Independence of mill output from changes in rotor speed is, of course, very important with battery-driven mills as the rotor speed progressively decreases as the battery discharges. By carefully tuning the amplifier it was possible to maintain a mill output within 5 per cent of its calibration value.

The rotor and stator were constructed from 20 SWG aluminium sheet and were of 0.17 m diameter. A small phosphor-bronze brush was used to make an earthing contact to the rotor shaft. Very occasionally trouble was experienced with contact potentials between the rotor and stator. Stripping down and thoroughly cleaning the rotor and stator assemblies invariably cured this difficulty.

Four field mills were constructed for this investigation and, complete with batteries, a field mill weighed just under 3 kg.

4.3.2
Calibration and Performance

It was anticipated that electric field in the vicinity of ion plumes would exhibit large and rapid fluctuations; further, field measured at two points separated by only a short distance might be quite different. We would expect, however, that as the distance between a field mill pair was decreased their readings would become progressively more similar. It was hoped to be able to calculate means and standard deviations of the electric field at various points and, later, possibly to investigate the correlation between the records of pairs of mills in order to test certain hypotheses about ion plume behaviour (see Sec. 3.6.).

Taken together the above experimental desiderata imply quite stringent performance criteria for the field mills. Consequently, in these mills, factors such as accuracy, short-term stability and frequency response were particularly important. It was hoped that the absolute accuracy of the mills would be better than 10 per cent whilst to make meaningful comparisons between pairs of records the short-term stability should be no worse than 2 per cent. (In this context the expression short-term refers to the duration of one run, i.e. 24 min.). Relevant features of the calibration and performance are now discussed.

The four field mills were individually calibrated on each of their six ranges for electric fields of both positive and negative polarities. A uniform electric field was set up in the laboratory by applying a stabilized voltage between two large parallel circular plates. These plates were separated by perspex insulators, 0.1 m long, and in the centre of the lower plate there was a circular hole of 0.18 m diamter. A field mill was placed under the apparatus in such a way as to render the stator flush with the lower plate. It was then possible, by varying the voltage between the plates, to impose any desired field on the mill. Early calibration work was carried out with the system housed in a Faraday cage. Later, however, it was discovered that the cage was not really necessary as the upper plate was an effective shield from external fields. During calibration the output voltage of the mill amplifier was plotted against various values of applied field, the procedure being repeated over the six ranges of each instrument. Calibration curves were then constructed. These curves

were found to be linear within a few per cent and, as the field
mill readings were to be ultimately processed by computer, it
was convenient to represent the mill transfer characteristic in
the form of a linear equation. Thus

$$\boxed{F = mV + C}$$ (4.1)

where F is the potential gradient,

V the mill output voltage

and m and C are constants for any particular
mill and range.

The value of the offset electric field (C), most likely the
result of contact potential effects, was nearly always less than
$20\ Vm^{-1}$ and, except on the lowest ranges, could be ignored.

The quantity m in the relation above is a function of the sen-
sitivity of the particular field mill. Consequently values of
m had to be calculated for each mill and each sensitivity
range, making 24 values in all. The calibration curves were
found to be symmetrical about the origin and hence if negative
potential gradients were being recorded these could be catered
for simply by reversing the sign of m in the computer programmes.

Calibration checks were performed at monthly intervals during
the early service of the field mills. Little change was noted
in the characteristics of the mills over such periods and, as
re-calibration was a lengthy procedure, later checks were
undertaken every three months. On one occasion, after the
equipment had suffered very severe mechanical shocks when the
Land Rover was driven into a deep pot-hole, a special cali-
bration check was thought advisable. Although slight depar-
tures from the nominal calibrations were detected from time
to time none of these was large enough to warrant amending the

calibration equations.

A feature of particular interest in this investigation was the frequency response of the field mills. Portions of the ion plume passing close to a mill could readily produce field variations as fast as 0.2 Hz or possibly even faster. Hence the field mills had to respond adequately to variations of such frequencies. In practice, the effective frequency response of the mills and other measuring systems was further complicated by the characteristics of the data sampling system. It is sufficient to say here that mill time constant needed to be no longer than 2s to ensure a satisfactory high frequency performance. An inspection of Fig. 4.1. indicates that the time constant of the mill amplifier is, to a large extent, determined by R_1 and C_1 . It was necessary to maintain R_1 at $10k\Omega$ to correctly match the input circuits of the sampling system (see Sec. 5.3). Thus in theory a time constant of 2s could be achieved by setting C_1 at $140\mu F$. The value of this time constant also controls the degree of smoothing that is applied to the alternating signal after rectification by D_x . An insufficiently large time constant would, whilst providing a very swift mill response, unfortunately produce a signal with an intolerable ripple content. Such a signal would, of course, be quite unsuitable for recording. Calculations show that for a signal frequency of 100 Hz the ripple signal will be less than 1 per cent of the mean value when the time constant is 2 s. This was quite acceptable.

It was thought worthwhile to determine the frequency response of the field mills experimentally. Undirectional, but sinusoidally varying, voltages were applied to the parallel plate

FIELD MILLS - FREQUENCY RESPONSE
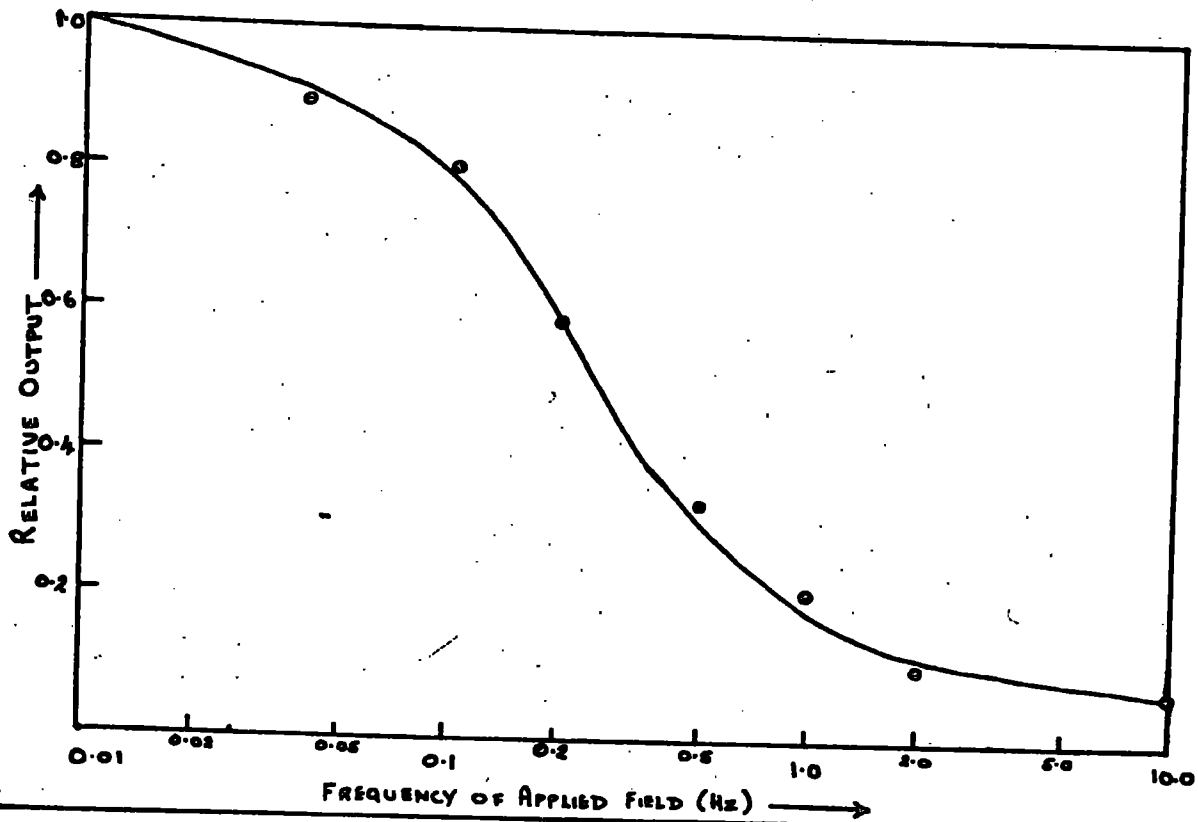
THE ION COLLECTOR - CIRCUIT PRINCIPLES
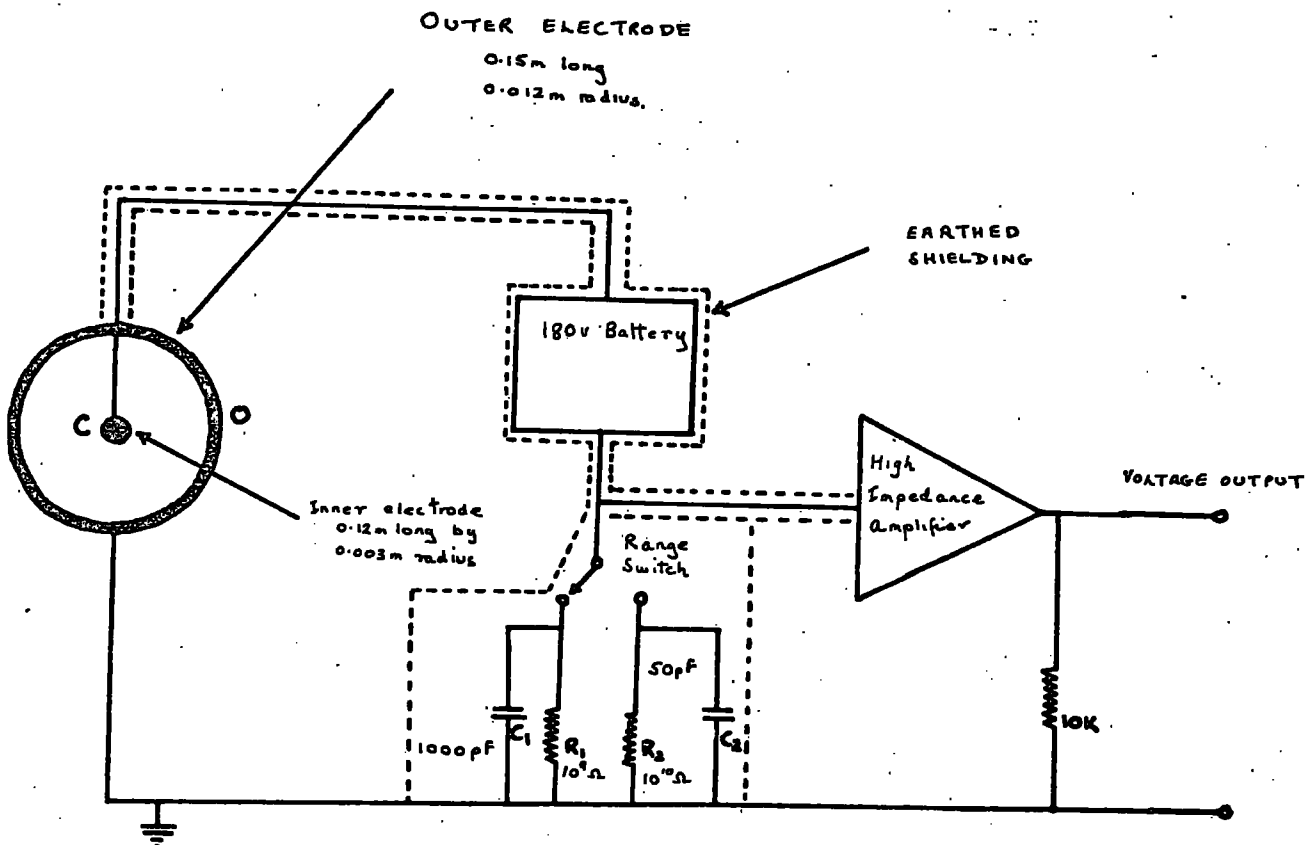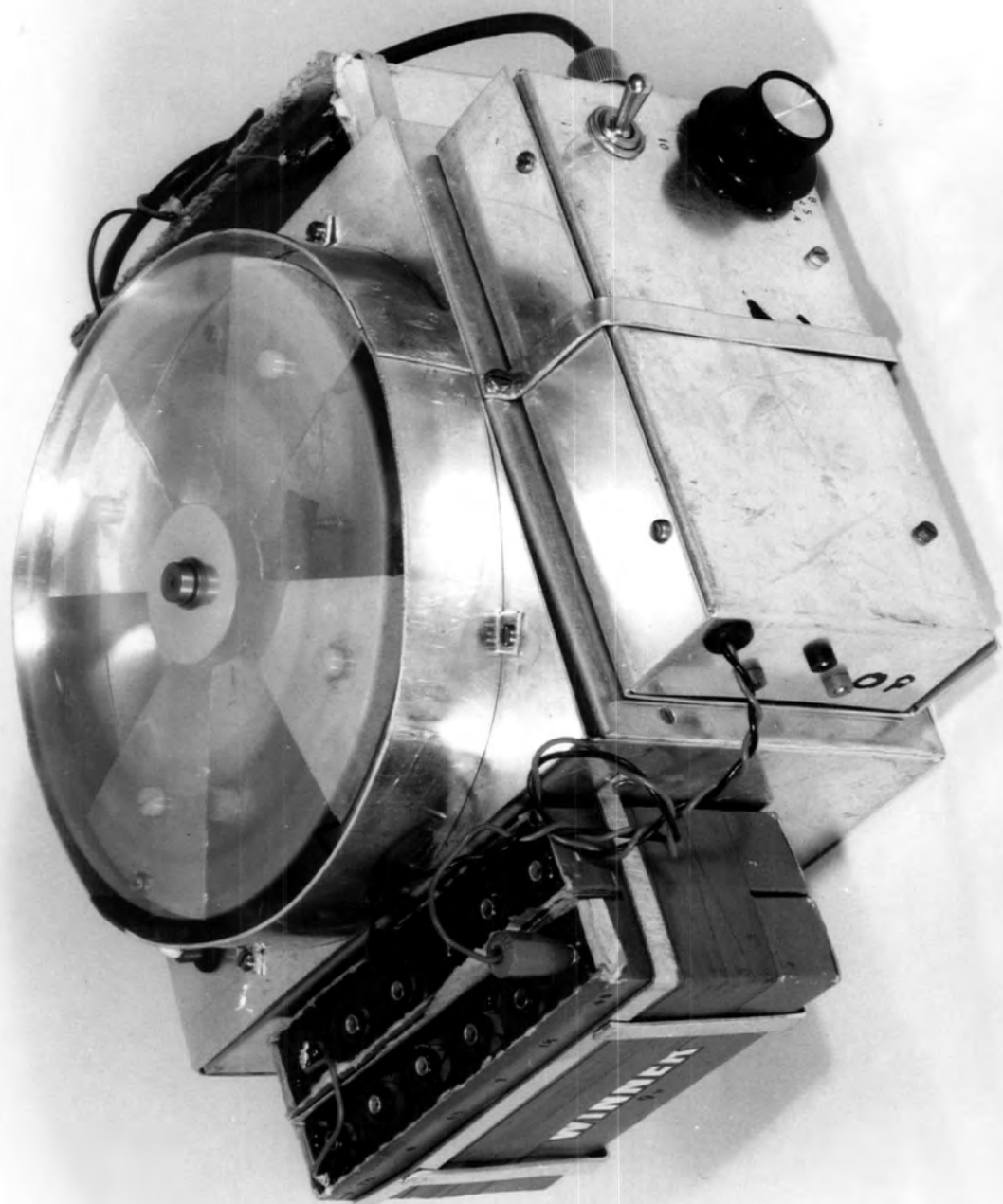
A portable field mill

calibration system by means of a special function generator.
By maintaining the amplitude of the imposed field variations
constant and measuring the output voltage of the mill ampli-
fier as the field frequency was altered, it was possible to
derive the frequency response of the field mills. The mills
differed very little from one and another and the averaged
response is shown in Fig. 4.2. These results accord well with
theoretical calculations based on a 2s value for the time con-
stant.

A characteristic of considerable relevance was the degree of
similarity that could be expected between the readings of two
field mills experiencing identical field variations. Alterna-
tively, if one obtained a low cross-correlation (see Sec. 6.2.)
between a pair of mills for a particular run one must know
whether it was real or just a result of limitations in field
mill performance. In order to investigate this, pairs of mills
were subjected to identical, but varying, electric fields in
the laboratory. This *test* field had a frequency of 1 cycle
min^{-1} and a mean amplitude of 100 Vm^{-1} . Table I shows the
results of these investigations. The coefficient of variation
(see Sec. 6.2) of the applied field is listed against the
correlation coefficient obtained. Average values for all four
mills are presented.

TABLE I

Coefficient of Variation	Cross-correlation Coefficient
0.3	1.00
0.1	0.99
0.06	0.89
0.02	0.57

We note . the excellent correlation between mill pairs when the coefficient of variation exceeds 10 per cent. On all but very few occasions the coefficient of variation of fields measured near the ion plume greatly exceeded 10 per cent. Therefore, the mill performance imposed little restriction on the validity of correlation measurements in these circumstances.

Some investigations were made of the Earth's natural electric field and the mill limitations had, of course, also to be borne in mind on these occasions. It is worth noting also that as these cross-correlation tests were performed with a low frequency field, it was anticipated that, near the high frequency limit of the mills, correlations would be lower due to signal phase shift effects in the amplifiers. The results of some mill correlations checks performed in the field are presented in Ch. 7.

As can be seen, the field mills have been subjected to stringent tests to ensure their fitness for this project. Their performance in the field has been excellent.

4.4
The Ion generator

4.4.1
Basic theory and principles of design

It is quite easy to ionize air by the application of a sufficiently large electric field. Such a field would normally be produced by the use of a high voltage supply connected to a suitable electrode system. In this project ions of only one sign were required at any particular time and these ions, once created, had then to be somehow removed from the electric field that produced them. In practice a coaxial cylinder

electrode system is very convenient for producing large electric fields without risk of breakdown. The feasibility of such a system was duly investigated and, after considerable experimentation, was finally chosen for the ion generator.

We now review the underlying principles of operation of the generator and, perhaps it should be stated at the outset, that as the physics of gas discharges is very complex, only the basic physics of the apparatus can be discussed here. A fuller description of this, and related, topics can be found in LOEB (1965).

It can be shown from elementary principles that the electric field, E , between coaxial cylinders is given by

$$E = V/(r \ln(b/a))$$ (4.2)

where V is the applied voltage,

   r the radius at which the electric field is to be calculated, and

a and b the inner and outer radii, respectively of the coaxial system.

Strictly, this relation applies only to infinitely long cylinders and to systems in which there is no space charge present. Clearly these are somewhat severe limitations, particularly in the present case, but equation (4.2) will, however, suffice for the approximate analysis given here.

In designing the ion generator the radii of the outer and inner cylinders could be varied but their dimensions could obviously not exceed certain limits. Naturally it was hoped that the ion generator could be made quite small so that it might be easily placed on a light mast. Ideally therefore the radius of the

outer cylinder should not be greater than about 0.1 *m* Also
the inner cylinder, or wire, should not be too small, because
if it were, it would not withstand normal mechanical shocks.
In fact, it proved possible to use a tungsten wire of only
6 μm radius in the ion generator; the advantage of using such
a thin wire being, of course, that even with a relatively
modest high voltage supply, very large electric fields could
be produced, thus causing intense ionization. At this stage
the design of the high voltage supply had therefore to be con-
sidered. It is, in fact, possible to construct, quite easily,
portable power supplies capable of giving 100 *kV DC*. However,
I did not wish to use such high voltages, mainly for reasons
of safety. Consequently it was decided that a 20 *kV* supply was
the maximum that could be handled in the field.

Substantial ionization occurs in regions where the electric
field exceeds some critical value, say E_c . The ions are, of
course, produced by collision processes and, in air at normal
pressures, E_c is about $10^6\,Vm^{-1}$. In the present ion genera-
tor this field is exceeded within about 2 *mm* of the central
wire. (This figure was obtained by inverting equation (4.2),
specifying appropriate values for *a(6 μm)* , *b(50 mm)* and *V(20 kV)*,
and then solving for *r* .) Consequently all ionization is con-
fined to a cylindrical region around this central wire.

Let us now consider how those ions that are created in this
region behave under the influence of the electric field that
is present. For the sake of argument, imagine that the central
wire is positive with respect to the outer cylinder. (The outer
cylinder was, in practice, always earthed.) Ions of both pola-
rities are created in the inner region and the prevailing electric

field will cause negative ions to be attracted toward the central wire whilst positive ions will be repelled toward the outer cylinder. The electric field is, however, very large near the inner wire but relatively small in the vicinity of the outer cylinder. Therefore the transit time of a positive ion to the outer cylinder will be very much larger than that of a negative ion to the central wire. Theoretical calculations (see CHALMERS 1967) show that a positive ion will require about 5 ms to reach the outer electrode whereas a negative ion (or electron) will be discharged at the central wire only a few μs after its creation. It appears therefore that the region from the outer cylinder to within 2 mm of the inner wire will be filled with relatively slow moving positive ions. In view of this it seemed there might be a possibility of expelling some of these positive ions from the system by blowing a brisk current of air along the axis of the apparatus. We can test this idea by means of a very simple calculation. Suppose the length of electrode system were L , the transit of time of the positive ions across the system t and velocity of air through the generator v . Then if

$$\boxed{v \geq L/t}$$ (4.3)

all the positive ions generated should clear the outer cylinder. The above reasoning, admittedly crude, does provide us with an idea of the practicability, or otherwise, of the proposed technique for expelling the ions. Substitution of appropriate values into equation (4.3) indicates that an air velocity of 5 ms^{-1} should be sufficient for the design contemplated. Fortunately, this is a realistic figure for a blower and thus the construction of an ion generator seemed a feasible proposition.

It should be added here that a similar analysis can be performed in the event of the central wire being at a negative potential and this suggests the interesting alternative possibility of generating negative ions.

In conclusion, I would like to point out that some factors have been deliberately omitted in the above theory. It is, for instance, possible to treat the system in a more sophisticated manner by considering the effect of space charge on the electric field distribution inside the generator. However, theoretical treatments rapidly become involved and, from my point of view, it was thought better, having established the basic principles of the device, to proceed with the construction of an ion generator.

4.4.2
Construction and Performance

An ion generator was constructed in accordance with the ideas discussed in the last section. The electrode assembly, expeller motor and fan were all mounted in a perspex tube 0.3 m long and 0.1 m in diameter. The arrangement is illustrated in Fig. 4.3. Three rectangular windows were cut in the perspex cylinder thereby permitting the earthed cylindrical electrode to be mounted on the outside of the tube. A small, easily removable, carrier was used to support the central wire. The framework of the carrier was made of thin perspex rod whilst copper pins mounted in PTFE bushes were provided at two suitable points at which to solder the gold-plated tungsten wire. The length of the central wire was 2.5 cm.

It was hoped to determine the ion output of the generator by monitoring the current flowing in the high voltage circuit.

ION SOURCE - EHT SUPPLY - RECTIFIER

Early experiments soon convinced me that this idea was not feasible because the total discharge current bore little relation to the actual quantity of ions being expelled by the generator. It appeared that many of the ions produced were not blown out but instead were ultimately collected by the outer electrode. The blower unfortunately produced a very turbulent air flow through the electrode system and it is felt that the enhanced ion transport due to this turbulence may have considerably increased the collection efficiency of the outer cylinder. Some attempt was made to improve the performance by placing straightening vanes in the air flow but this did not remedy the situation.

The output of the ion generator could, however, be readily assessed by an indirect method. The generator was mounted on a suitable mast at a few metres above ground level and a field mill was placed approximately 10 m downwind of the mast. Theoretical calculations (the steady-state model) had already provided values for the magnitude of the electric field disturbance to be expected from the presence of the ion plume. Hence it was possible, in theory at least, to deduce the ion generator output from the field mill readings. In practice this method, although a little cumbersome, worked very well and was invariably used to estimate the generator performance whilst development was proceeding.

It was later discovered accidentally that the output of the ion generator could be considerably increased by coating the outer electrode with a thin layer of varnish. It is thought that this varnish layer, whilst not materially affecting the electric field distribution within the generator, may consi-

derably decrease the collection efficiency of the outer electrode, thereby resulting in an increase in the ion output. It should be emphasised that this explanation has not been verified experimentally and may, therefore, be incorrect.

The blower used in the generator consisted of a 12-bladed rotor fan powered by a 6 V DC 6000 RPM motor. The current consumption was 1 A and the flow velocity exceeded 7 ms^{-1}.

The ion generator has been in service for over a year and, except for one occasion, has functioned quite satisfactorily. The generator failed late one evening in very damp conditions, probably only after the perspex insulation had absorbed considerable moisture. A more serious fault, however, was only noticed after the generator had been in use several months. It had become apparent that the ion output was rather erratic in high winds. This behaviour was, after some investigation, attributed to the action of strong winds disturbing the air flow over the electrode system. The problem was solved by mounting the generator with its axis horizontal, instead of vertical as previously, and then attaching a right-angle cowl over the air intake.

The output of the ion generator, estimated from numerous observations, is 0.3 μA when producing positive ions and 0.5 μA when producing negative. (The difference between the positive and negative ion outputs is not determined by the generator itself but depends on the differing mobilities, and other properties, of ions of the two signs.)

4.4.3
The High Voltage Supply

A schematic drawing of this is shown in Fig. 4.3. The high voltage supply was powered by a 12 V 4.5 Ah rechargeable battery, the current consumption of the system being o.4 A. The operation of the supply is now briefly discussed.

The inverter converts the 12 V DC supply into a 250 V 15 kHz alternating voltage which is then rectified and smoothed by D_1 and C_1 respectively. In the absence of a positive pulse from the multivibrator, the thyristor T is effectively an open-circuit between the points X and Y. The capacitor C_2 is thus charged to approximately 350 V via R_2, the primary of the ignition coil being of negligible resistance. The arrival of a short positive pulse at the gate electrode, G, of the thyristor causes it to rapidly become conducting. Hence X and Y are now effectively connected together. This results in the capacitor C_2 being discharged into the primary of the igni-tion coil thereby producing a very high voltage at the secon-dary terminal. After this the thyristor again becomes non-conducting, allowing C_2 to recharge. The process is then repeated at a frequency determined by the time constant of the multivibrator. In practice, of course, the charging time con-stant of R_2 and C_2 must be made sufficiently small so that C_2 is fully charged each time the thyristor conducts. The repeti-tion frequency in this apparatus was 30 Hz.

The secondary output was rectified by a special "silicon stack" enclosed in a separate perspex box. This arrangement was neces-sary so that the rectifier could be connected either way round into the high voltage system. This enabled negative or posi-tive ions to be generated as required. Initially a capacitance

of 500 pF was placed across the rectifier so as to provide a smoothed supply. However, the presence of a 500 pF capacitor charged to a potential difference of 20 kV was most undesirable as it could give a serious, possibly even fatal, electric shock to anyone accidentally touching it. As an alternative the distributed capacitance, amounting to 150 pF, between the cable carrying the high voltages and the earth return wire was used for smoothing. Whilst considerable charge was retained in the cables, their self inductance obviated, to a large extent, the risk of a dangerous shock.

4.5
The Ion Collector

This simple device was designed to supplement the field mill observations. After theoretical investigations it had emerged that the ion plume would initially expand very rapidly, both laterally and vertically, as a result of electrostatic forces (see Sec.3.5). It was hoped that the ion collector could be used to determine the ion concentration profile in the region within about 10 m of the source. A simple calculation shows that, at this distance, ion concentrations of the order of 10^{-8} Cm^{-3} were to be expected, a figure approximately one hundred times greater than the fair weather ambient values. (See CHALMERS 1967). Consequently, it was not anticipated that the presence of relatively small numbers of natural ions would cause any difficulties.

The collector was based on the original design of EBERT (1901) and is, in principle, almost identical. Air is drawn through a coaxial cylinder electrode system, as shown in Fig. 4.2, by a suitable motor driven fan. The central electrode C is main-

HIGH VOLTAGE SUPPLY

AND
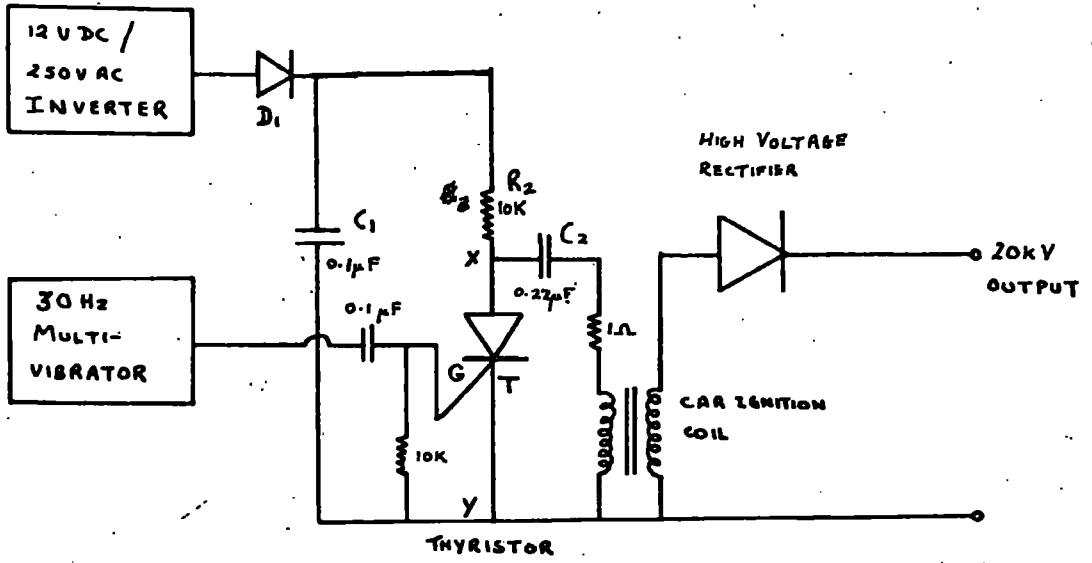
THE ION GENERATOR
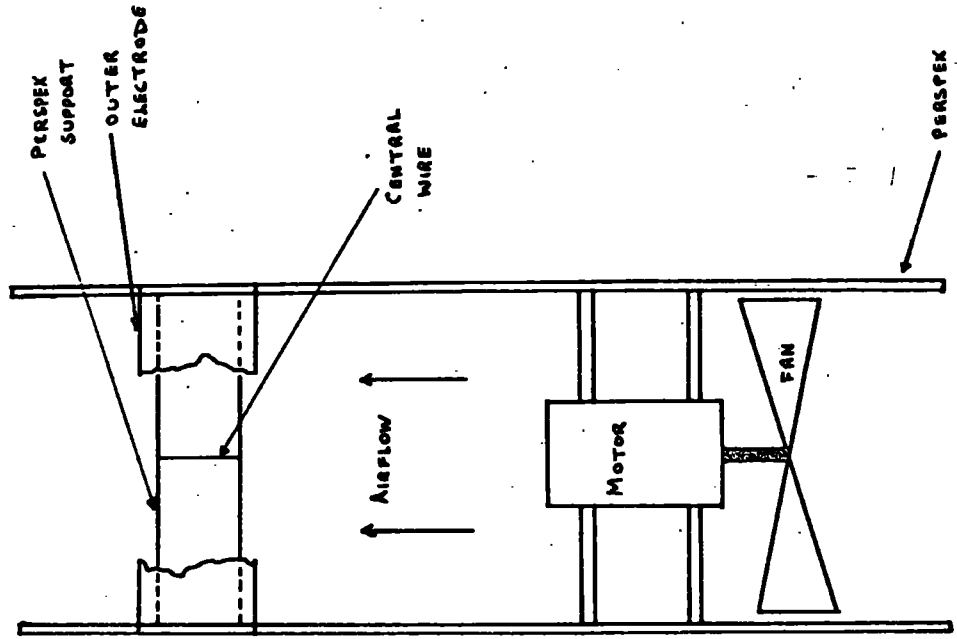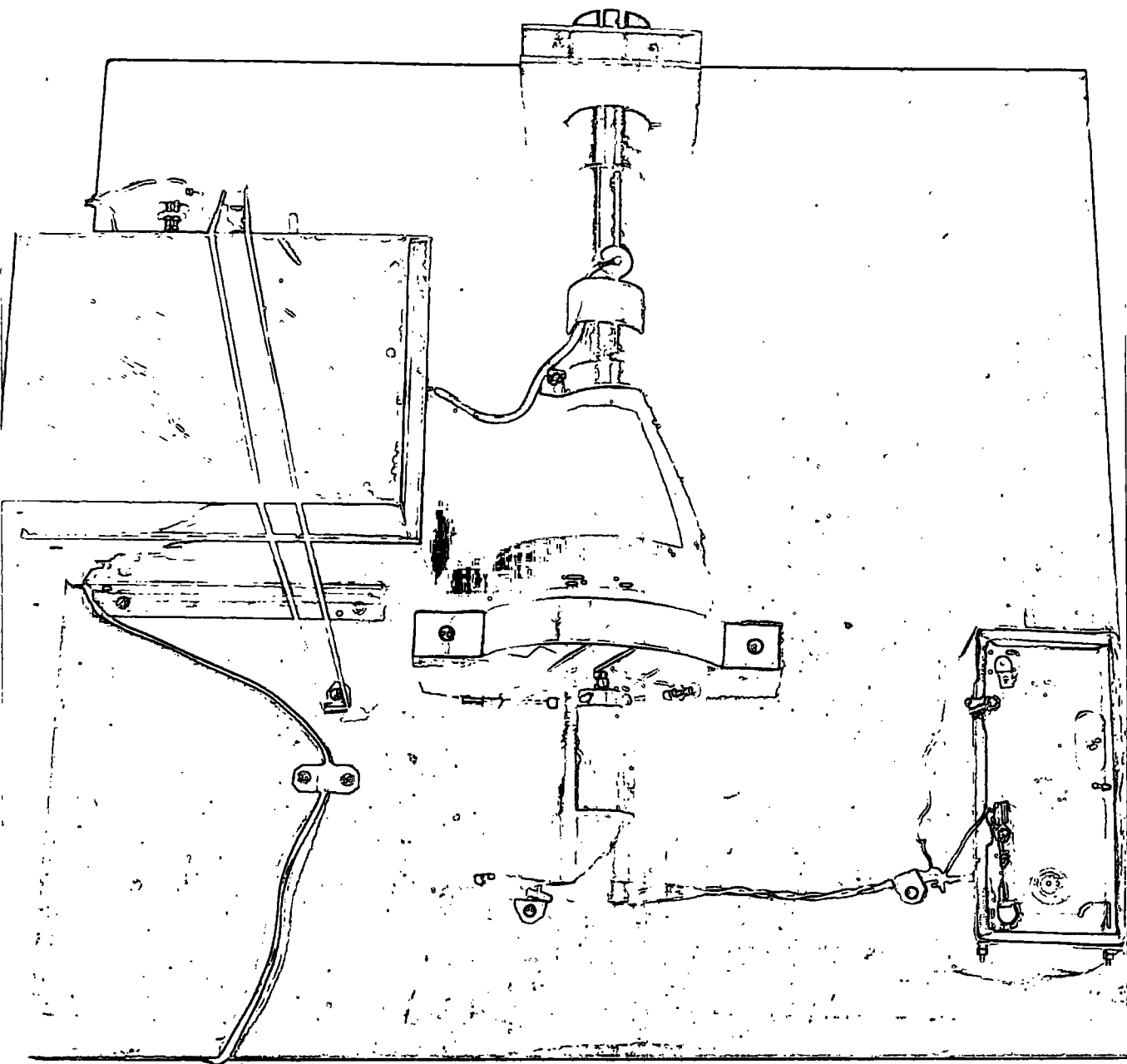
The ion collector

tained at a constant potential with respect to the outer elec-
trode O. Ions entering the device will therefore either be
attracted to or repelled from the central electrode depending
on their sign. Those ions which reach this electrode before
passing out of the device constitute an electric current.
This current flows through the external resistor R and pro-
duces a small voltage. Ions of the opposite sign reaching
the outer electrode flow to earth and play no part in the func-
tioning of the apparatus. It is, of course, essential for
quantitative work that the central electrode collects all the
ions which are drawn into the apparatus. Suppose the velocity
of air flow through the system were v and the length of the
electrode system were L; then the incoming ions must reach the
central rod in a time less than or equal to

$$L/v$$

Now by employing similar reasoning to that used in designing
the ion generator, we can show that the transit time, t, of an
ion from the outer cylinder to the central rod is given by

$$t = (\ln(b/a)(b^2 - a^2))/2\mu V \qquad (4.4)$$

where μ is the mobility of the ions,

   V the central electrode potential and

   a and b the inner and outer radii respectively.

Using the two relations above, we are now in a position to
design an ion collector. The mobility μ of the small ions
is, of course, fixed, but the quantities L, v, V, a and b are
all, within reason, left to our choice. As is usual, in prac-
tice these quantities are not independent and therefore a com-
promise must be reached. A suggested upper limit for V was
about 200 volts, as a battery of higher voltage would have

been cumbersome. It was thought that the inlet velocity, v, should be not less than 15 ms^{-1} otherwise gusty winds might adversely affect the performance of the apparatus. The length, L, was set to 0.15 m and, from equation (4.4), it was found that the dimensions of a and b were perfectly reasonable. (The exact dimensions are shown on the figure.)

Capacitors C_1 and C_2 were placed across the input resistors R_1 and R_2 to establish a definite time constant for the collector. A value of 1s was, in fact, chosen. (It should be remarked that as the self capacitance of the electrode system and wiring was approximately 50 pF C_2 only needed to be 50 pF to obtain the desired time constant). The voltage across $R_1 C_1$ (or $R_2 C_2$) was then amplified by a special FET integrated circuit DC amplifier having an input impedance of not less than $10^{11} \Omega$. The output current from this device was fed to earth via a 10 $k\Omega$ resistor, thus producing a voltage output suitable for recording. In the final design a commutating switch was provided so that the polarity of the voltage on the central electrode could be reversed. This enabled the concentrations of both positive and negative ions to be determined, though not, of course, simultaneously.

After construction, the collector was checked to make certain that it was responding to all the small ions which passed through it. A small radioactive source, of Americium 241, was placed near the inlet tube of the device and the 200 V battery was replaced by an isolated variable voltage supply. The voltage applied to the central electrode was then altered and the effect on the output voltage noted. The results of this test

indicated that at the normal working voltage 99 per cent of incoming negative and 95 per cent of incoming positive ions were collected.

This ion collector responds to the rate of arrival of ions of one sign at the central rod. From a knowledge of the air flow rate through the apparatus, it is therefore possible to calculate the charge concentration. Previous workers, e.g. OGDEN (1967), have measured the flow rate through their much larger space-charge collectors by means of gas meters. The use of such a technique was thought most unlikely to succeed in this case because gas meters require a comparatively large pressure drop to operate them satisfactorily. A crude estimate of the flow rate was, however, obtained by using a sensitive small probe hot wire anemometer to establish the mean velocity profile across the collector inlet. This was not an accurate measurement and the volume flow rate derived from it could be as much as 20 per cent in error. The mean intake velocity was found to be 14 ms^{-1} , which is close to the design figure.

The ion collector functioned quite well in the field, although the output signal was rather noisy on the more sensitive range.

4.6
The Micrometeorological System
4.6.1
Purpose of the System

Clearly the behaviour of the ion plume depended to a great extent on its local meteorological environment. It was the purpose of the instruments described herein to monitor that environment by the measurement of appropriate physical quantities. In Sec. 2.7 it was shown how the atmospheric stability had a marked effect on the behaviour of a plume. For

this reason it was decided to measure the wind speed and temperature gradients near the ground so that the Richardson number could be determined. Obviously the wind speed itself is also of considerable importance and therefore this too was measured.

Later experiments featured the use of a bivane as it was found that stability measurements, although useful, were not providing as much information as was originally hoped.

The individual instruments are now discussed.

4.6.2
The Anemometer System
4.6.2.1
General Features

Two Casella type T 16108/2 sensitive cup anemometers were obtained for this project. These anemometers were compact, simple to use and proved very reliable. The manufacturer specified a starting speed of not more than $10\ cms^{-1}$ and an accuracy of better than $0.3\ ms^{-1}$. Hence their performance was adequate for the application envisaged. These anemometers provided a single $12V$ pulse per cup shaft revolution. This pulse was derived from the rotation of a sectored disc, attached to the cup shaft, which interrupted the light beam between a photo cell and lamp. The photo cell output was fed into a Schmitt trigger circuit which produced the $12\ V$ pulses.

The anemometers were attached to the Clarke mast by suitable clamps and booms. Care was always taken to site the anemometers upwind of the mast in order to minimize the effects of wind flow disturbance on the observations. The anemometers were placed at

4.4

MICROMETEOROLOGICAL INSTRUMENTS - Electronics system

output voltage is
proportional to :-

CHOPPER DRIVE UNIT

ANEMOMETER 1 → MONOSTABLE (A) → CHOPPER (A) → HIGH STABILITY AMPLIFIER (A) → $U_1 - U_2$

ANEMOMETER 2 → MONOSTABLE (B) → CHOPPER (B) → HIGH STABILITY AMPLIFIER (B) → U_1

THERMISTOR SENSOR 1, THERMISTOR SENSOR 2 → WHEATSTONE BRIDGE → CHOPPER (C) → HIGH STABILITY AMPLIFIER (C) → $T_1 - T_2$
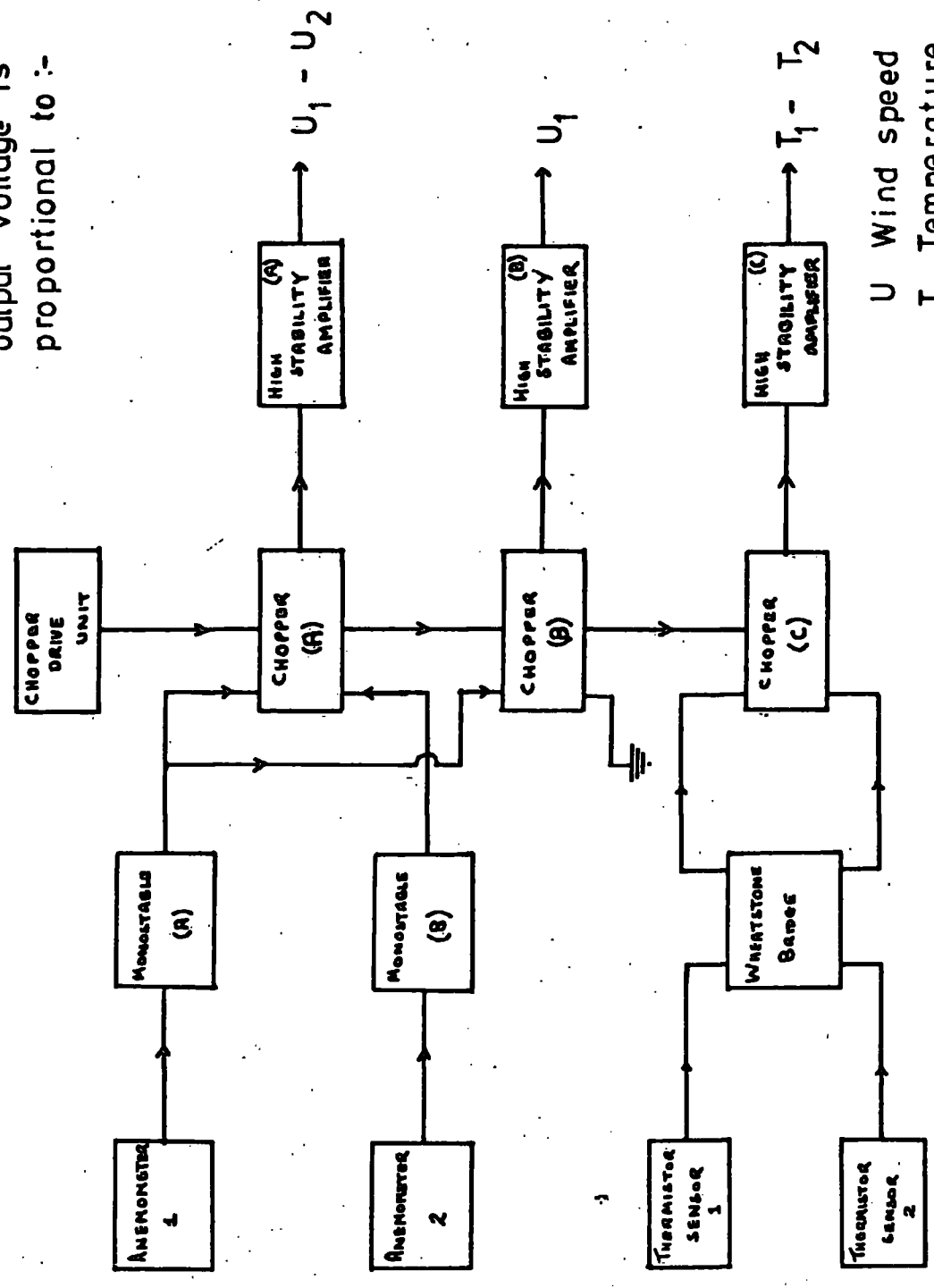
U Wind speed
T Temperature

The subscripts 1, 2 denote different
heights of the measuring instruments.
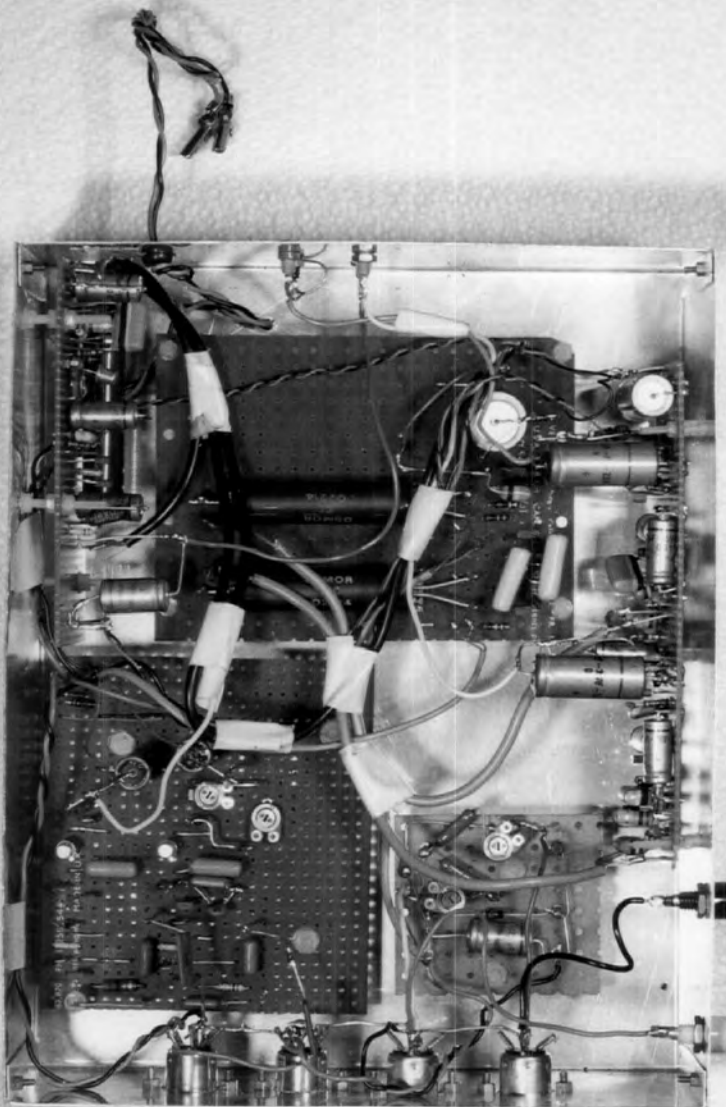
THE MICRO METEOROLOGICAL
SYSTEM ELECTRONICS

standard heights, 2 m and 9 m, and were connected to their
electronics system, which was at ground level, by lengths
of twin core shielded microphone cable. No trouble was
experienced with *interference* from the 20 kV ion generator
power supply although it had been expected.

4.6.2.2
The Electronics System

A schematic diagram of the anemometer signal processing
arrangements is shown in Fig. 4.4, whilst details of the
individual circuits can be seen in Fig. 4.5. The anemometer
electronics system was designed to produce two outputs.
Firstly a 0 to 1.0 V analogue output proportional to the
wind speed at 9 m and secondly, a similar output propor-
tional to the difference between wind speeds at 9 m and 2 m.
It would, of course, have been possible to measure and record
the wind speeds at these heights entirely independently and
then later compute the wind speed difference by substraction.
In retrospect I would now consider the latter alternative as
the more satisfactory. However, mainly due to lack of expe-
rience, it was not unfortunately adopted. Nevertheless the
system based on the original proposal, despite its unnecessary
complexity, did work well.

The 12 V pulses appearing at the anemometer outputs were not of
standard width, the actual pulse width being a function of wind
speed. In the pulse counting system contemplated it was, how-
ever, necessary that the incoming pulses were of constant
width. To achieve this the pulses from the two anemometers
were shaped by the monostable multivibrators A and B. After
conversion to standard width the pulses were integrated and DC

outputs proportional to their repetition rates were produced at point B. The time constant of the integrating circuits was 3.5 s, this being determined by the value of R_1 and C_1 in Fig. 4.5.1.

The DC voltage appearing at B was not suitable for recording because the input impedance of the recording system would have seriously disturbed the action of the integrating circuit. Thus some type of buffer amplifier was needed to give a suitable output. A simple DC amplifier was constructed but, unfortunately, output voltage drift, due largely to temperature changes, precluded its use. This, of course, was especially so in field work where hot sunshine anc cool breezes might alternate thus producing large temperature variations. After some experimentation a chopped DC amplifier was found to offer the most promise. The input of such an amplifier is alternately switched from the DC voltage to be amplified to a fixed reference voltage and vice-versa. Thus a square wave is produced at the input and this can, of course, be handled by a conventional AC amplifier. The advantages of such a system are, firstly drift is eliminated and, secondly, it is possible to design sensitive and stable circuits quite simply. A major disadvantage is that there is a difficulty in establishing the sense of the input signal as the amplifier responds only to the magnitude of the difference between the input and reference signals. In practice, this was not serious because it was found that the wind speed at 9 m was invariably greater than that at 2 m. Hence, by employing two chopper DC amplifiers it was quite simple to produce the desired output signals. Inter-connexion details of the various amplifiers are shown in Figs. 4.4 and 4.5.

MICROMETEOROLOGICAL SYSTEM ELECTRONICS I

1. Anemometer pulse convertor

MONOSTABLE

INTEGRATOR

To anemometer

2. High stability amplifier

set gain

CHOPPER—
REED SWITCH
(INPUTS 1+2)

4.5
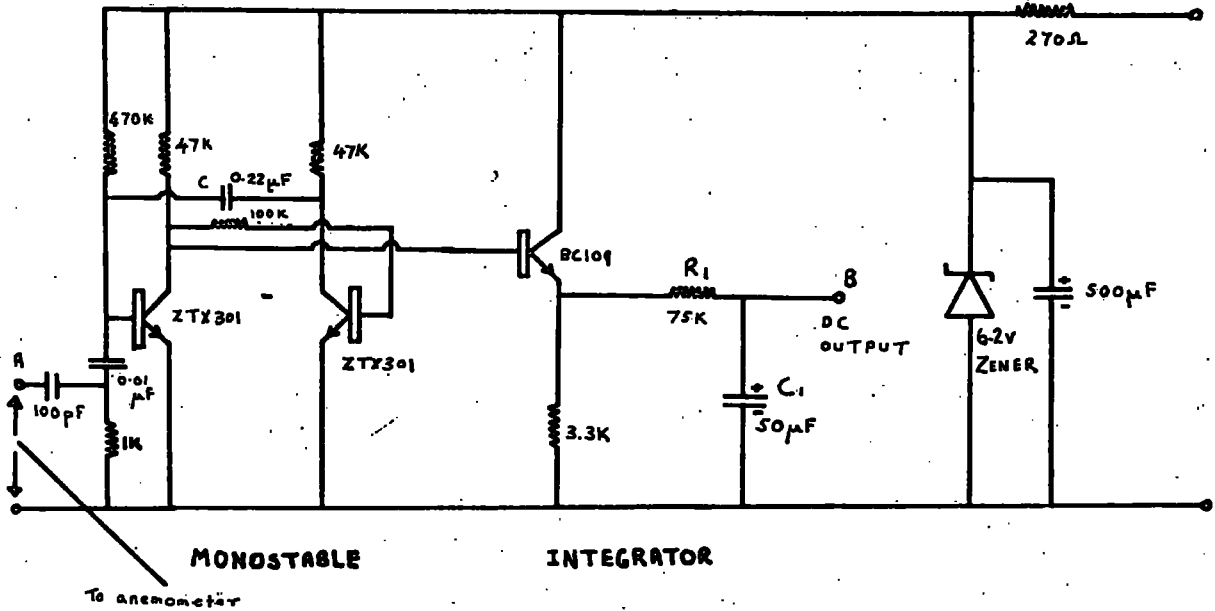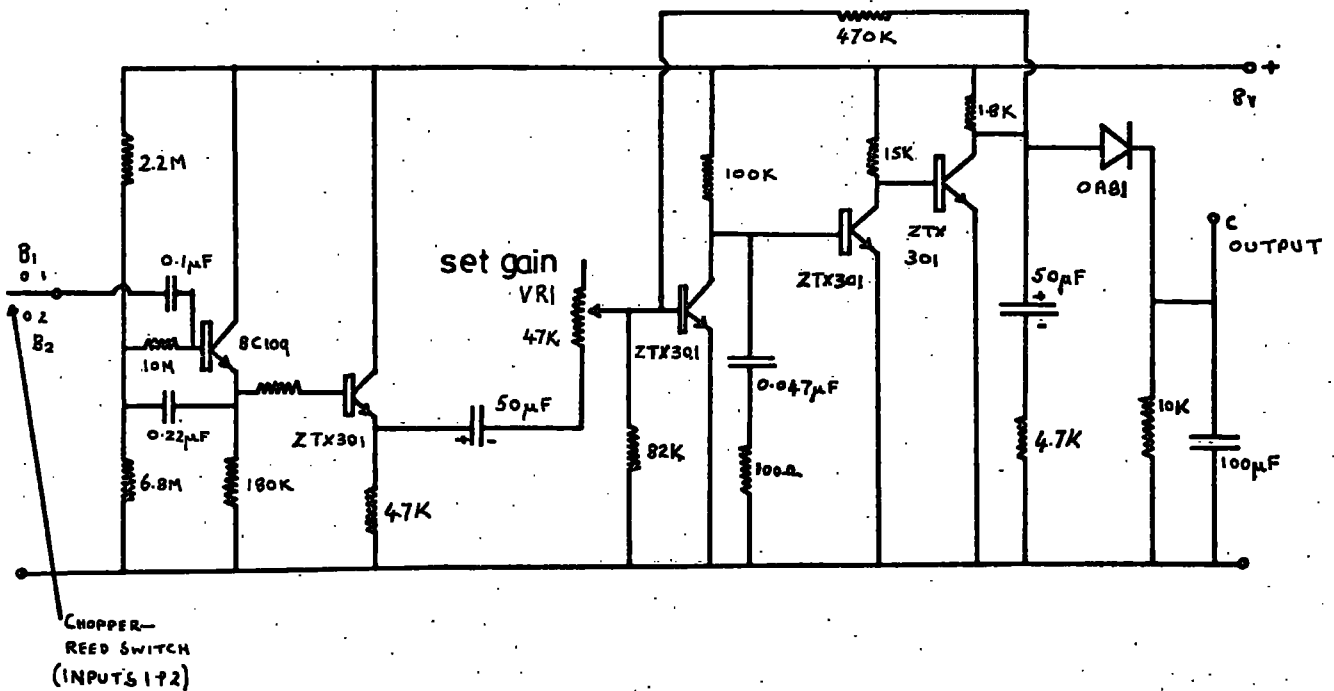
MICROMETEOROLOGICAL SYSTEM
ELECTRONICS II

3. Chopper drive unit

astable multivibrator   emitter follower
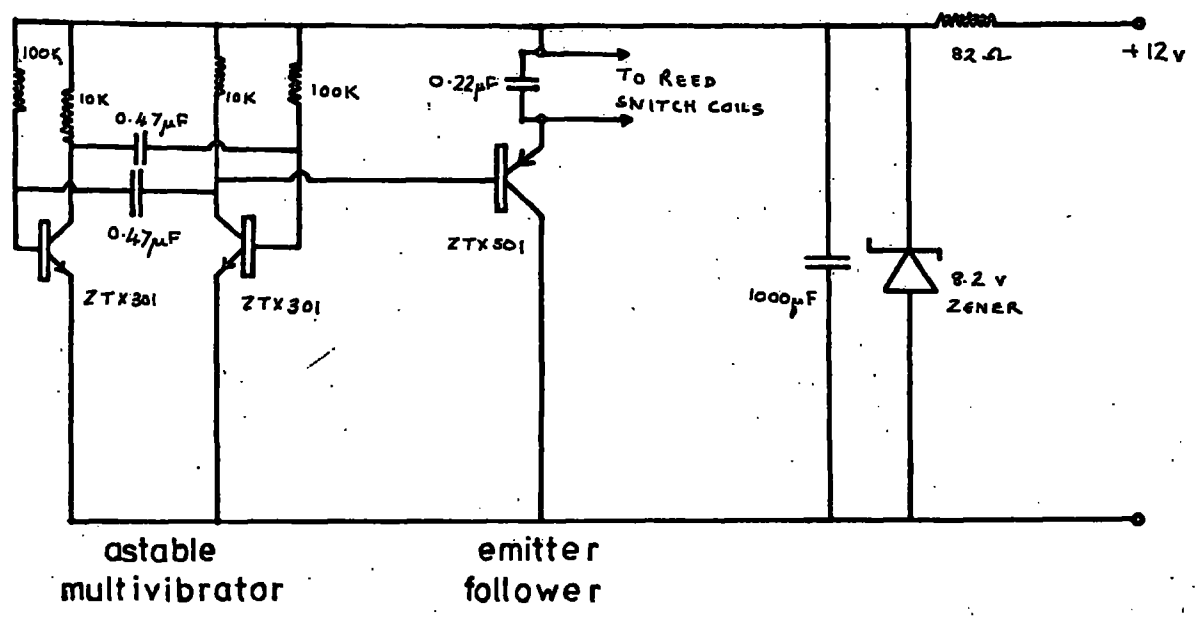
4. Thermistor bridge circuit

TH1,TH2 THERMISTOR SENSORS   Wheatstone bridge
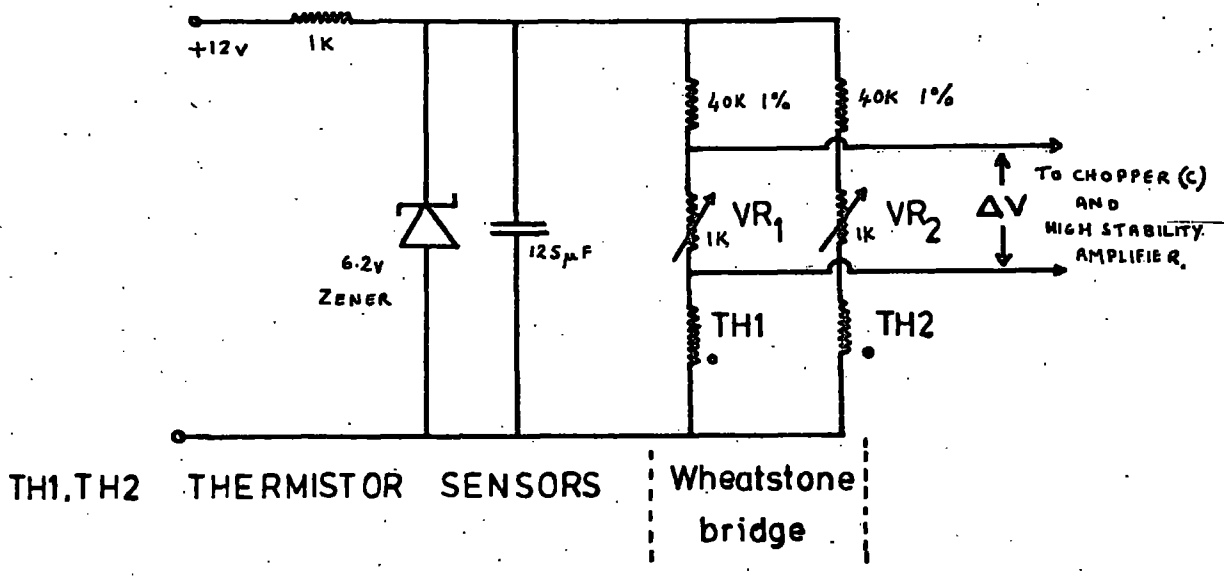
In the anemometer system two changeoever reed switch choppers
were used. The driver circuit for the chopper system is shown
in Fig. 4.5.3., and is conventional in all respects. The
chopping frequency was approximately 30 Hz. A small 0.22 μF
capacitor was placed across the reed switch to ensure that
inductive effects did not damage the driver transistor.

4.6.2.3
Calibration and Performance

The manufacturer supplied standard calibration curves with
these anemometers. These curves consisted of output pulse
rate plotted against the actual wind and were substantially
linear within the range 1-10 ms^{-1} . The two anemometers used
in this investigation were never checked in a wind tunnel
but, later, a third, individually calibrated, anemometer was
acquired and the readings of all three anemometers were very
carefully compared. It was concluded that the original two
anemometers were well within their nominal calibration even
after two years of service.

The output pulse rate of the anemometers was 40 pulses per
minute per ms^{-1} , and thus at a wind speed of 1 ms^{-1} , a
pulse occurred every 1.5 s. As the time constant of the
integrating circuit was 3.5 s, considerable ripple was appa-
rent on the output signal at very low wind speeds. This was
of little importance however, as few observations were made in
wind speeds of less than 2 ms^{-1} .

The anemometer electronics system was calibrated by means of
a specially designed pulse generator having two individually
variable pulse rate outputs. Such a pulse generator enabled
both different wind speeds and wind speed gradients to be

precisely simulated. The gain of the high stability amplifiers was controlled by VR 1 (see Fig. 4.5.2.) and setting this controlled the calibration span of both systems. The calibration curves for the anemometer systems are shown in Fig. 4.6. Some slight non-linearity is evident in the curves, but it was not large enough to be of great importance. These curves were, in fact, expressed in the form of a linear equation, this being convenient for computer processing of the data.

The electronics system, although complex, worked quite successfully in the field and suffered no major faults throughout the duration of the project. Calibration checks were performed at three-monthly intervals, very little alteration in the system being evident.

A further check of the wind speed gradient system could be made in the field. If the anemometers were placed as close as possible together, then, theoretically, they should indicate a zero wind speed difference. In practice a figure of 0.2 ms^{-1} or less was usually achieved. This was regarded as quite satisfactory.

4.6.3
The Differential Thermistor System

4.6.3.1
General Features

Two aspirated temperature sensors were constructed to enable the mean temperature gradient between 9 m and 2 m to be determined. The aspirated thermistor systems were similar in design to those of OGDEN (1967) although in this case a cylindrical rather than rectangular, arrangement was employed to facilitate

ANEMOMETER SYSTEM - Performance curves
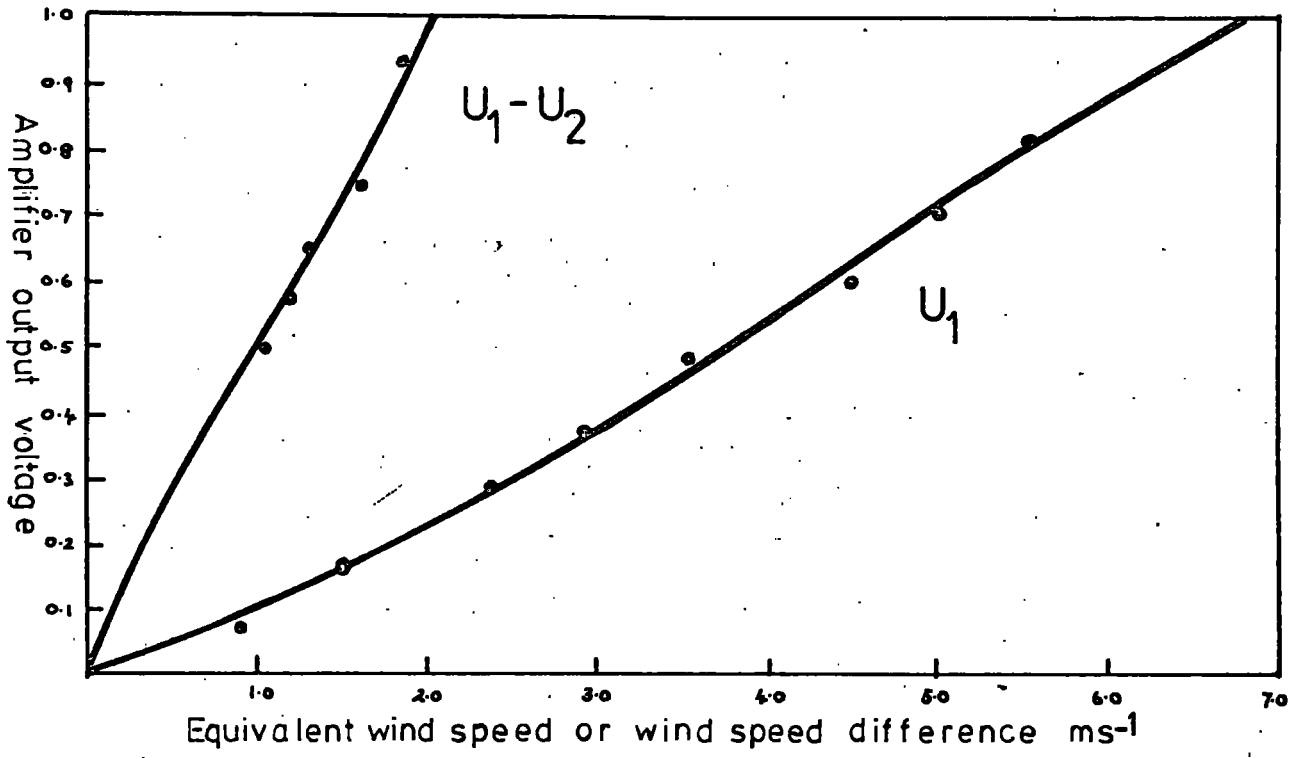
DIFFERENTIAL THERMISTOR SYSTEM
Performance curve
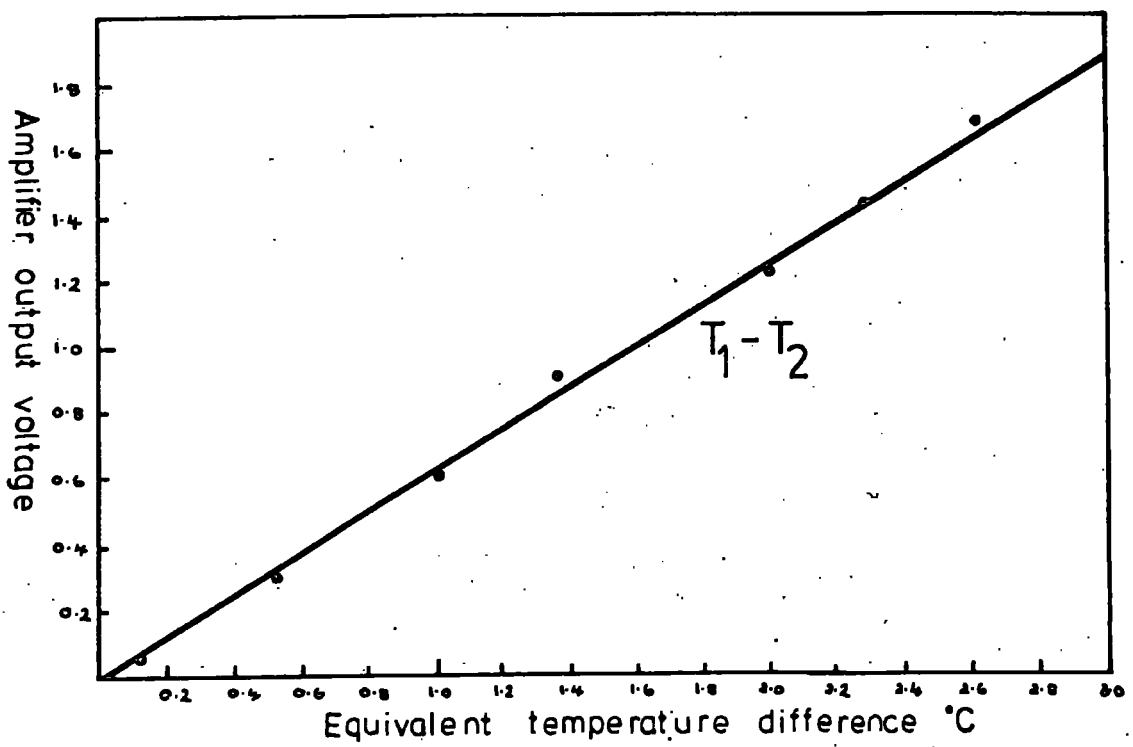
construction. A sectioned drawing of an instrument is shown
in Fig. 4.7, the external surface being, as usual, painted
white to minimize radiation effects.

The thermistors used, manufactured by the Yellow Springs
Instrument Co., have the following specification:-

TYPE YSI 44032

INTERCHANGEABILITY $0.1^{\circ}C$ in the range $-20^{\circ}C$ to $+ 70^{\circ}C$

RESISTANCE $30.00\ k\Omega$ at $25^{\circ}C$

RESPONSE TIME IN STILL AIR 10 s

DISSIPATION CONSTANT 1 $mW\ c^{-1}$

The thermistors were aspirated throughout a field run by means
of a small motor and fan. The air velocity in the large tube
was $0.6\ ms^{-1}$ and, a simple calculation shows, in the region of
the thermistors the flow velocity was about 3 ms^{-1} . Experi-
ments indicated that, at this aspiration rate, the time con-
stant of a thermistor was less than 2 s. This was satisfac-
tory.

The two thermistor sensors were connected, by means of ordinary
twin wire, into the bridge circuit shown in Fig. 4.5.4. As the
thermistors were matched to within $0.1^{\circ}C$ they could be used
directly to indicate temperature difference. Nevertheless
small trimming resistors, VR1, 2, were included in the bridge
to balance out any slight differences between the thermistors.
In fact no differences were ever found and consequently the
trimmers were never used. Precision resistors were, of course,
employed in the two remaining arms of the bridge. The voltage
supply to the bridge was fully stabilized by means of the
$6.2\ V$ zener diode arrangement shown.

The voltage difference, ΔV, produced at the bridge output was
73.0 mV per deg. C difference between the thermistors. It
was, in fact, possible to calculate accurately the voltage out-
put for given termperature differences at various temperatures
as the manufacturer supplied very precise resistance tables
with the thermistors. When such calculations were performed
it was discovered that the value of the output voltage, per
unit temperature difference, depended little on the actual
temperature. Within the range 5-20°C the change in ΔV for
a given temperature difference was less than 3 per cent and
could therefore be ignored. A further, and very useful, fea-
ture of this bridge circuit was that for relatively small
temperature differences, say less than 3°C, the output vol-
tage versus temperature difference characteristic was linear.

4.6.3.2
The Electronics System

The chopper amplifier used to process the temperature diffe-
rence signal produced by the thermistor bridge was virtually
identical with that in the anemometer electronics system.
Consequently the remarks made in Sec. 4.6.2.2. also apply,
mutatis mutandis, here.

4.6.3.3
Calibration and Performance

The temperature difference sensing system was calibrated by
substituting the thermistors with precision resistance boxes
and, by varying the resistance, various temperature difference
could be readily simulated. The results of such a calibration
are shown in Fig. 4.6, the high degree of linearity being
clearly evident. Calibration checks were undertaken at three-
monthly intervals, no indication of any charge in the perfor-
mance was ever apparent.

THERMISTOR TEMPERATURE SENSORS

A

B

A'

brass
tubing

thermistor
bead

perspex
annuli

aspirator motor
and   fan
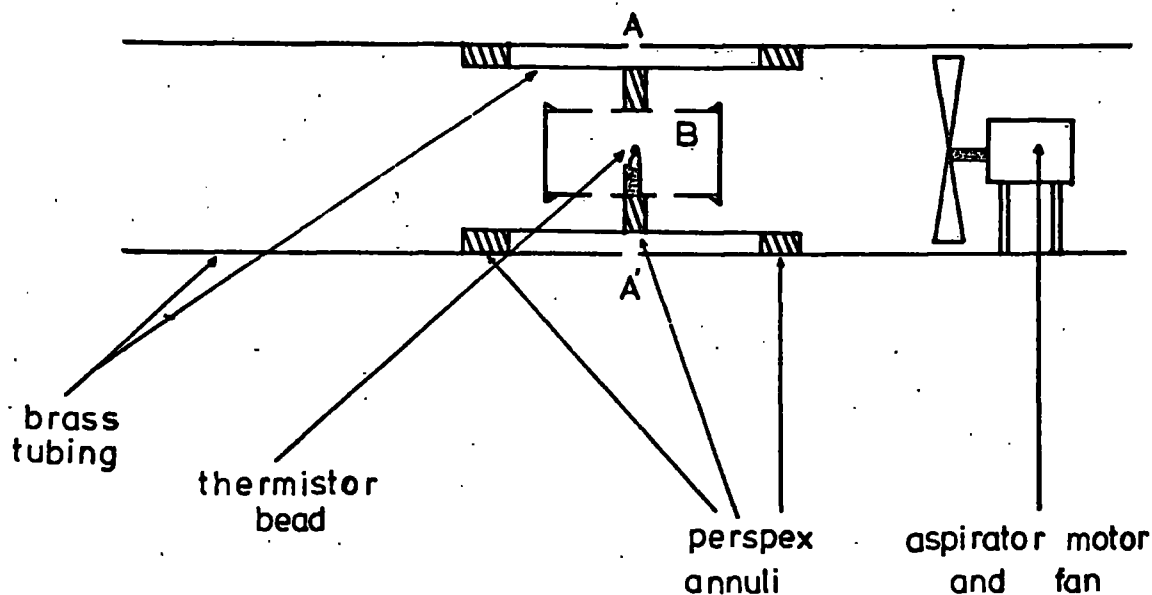
Dwg to 1/2 scale

BIDIRECTIONAL VANE - Sensing circuits

+6v

330 Ω

3.3v
zener

620 ±2%

10K±2%

5K± 2%

Vertical
component
sensor

Horizontal
component
sensor
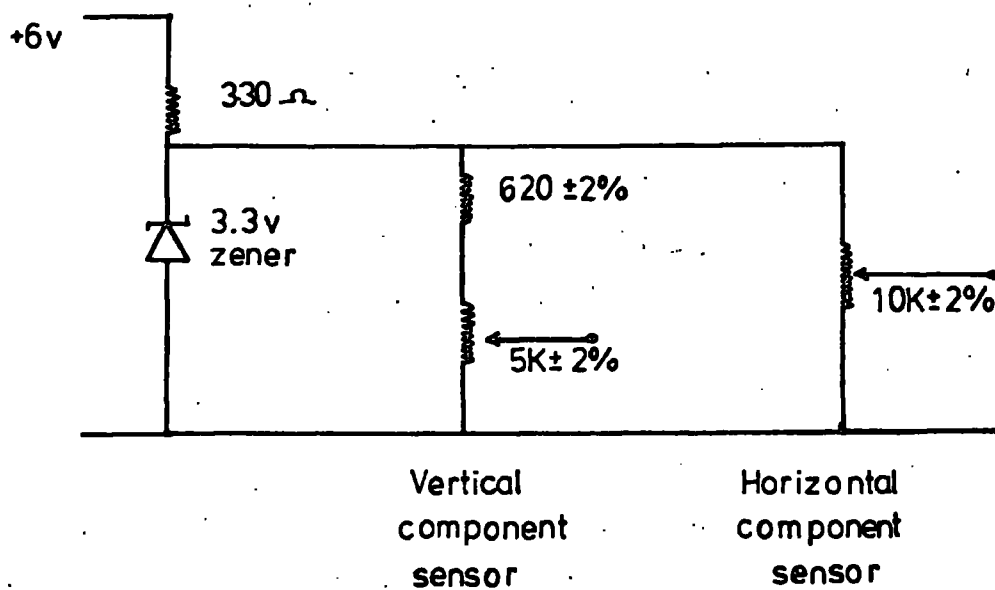
Occasionally a test was conducted in the field to check the coincidence of the thermistor characteristics. The sensors were placed at the same height on the mast and the indicated temperature difference noted. Ideally, of course, the value should be close to zero and, in fact, those observed were invariably less than $0.1^{\circ}C$. This was regarded as quite satisfactory.

It became obvious as experimental work progressed, that when designing the sensor amplifier, an importance factor had been overlooked. At that time it was not appreciated that when the conditions were near neutral (see Sec. 2.6.2.) the temperature gradient near the ground would quite frequently change from a small positive to a small negative value and vice versa. In Sec. 4.6.2.2. it was mentioned that the chopper amplifier employed only responded to the difference in voltage of the input signals, or, in other words, the amplifier indicated the magnitude of the temperature gradient but not the sign. The problem was alleviated in later work by placing a very high input impedence digital voltmeter across the bridge output whilst field work was in progress. This instrument indicated the polarity, as well as the magnitude, of the voltage across the bridge. A written note of the sign of the temperature gradient could then be taken in near neutral conditions.

Apart from this sign ambiguity, the temperature gradient system functioned very well. On one occasion, however, the system failed completely. This was later attributed to a faulty plug connector on one of the thermistor housings.

4.6.4
The Bidirectional Vane

4.6.4.1
General

Neither the author *nor* the Atmospheric Physics Group at Durham
had had any previous experience with bi-directional vanes
(bivanes). Although many published designs exist in the
literature, e.g. CRAMER, GILL AND RECORD (1957), it was felt
that these were unnecessarily complex for the project in
view. Such instruments had been designed for applications
involving surface stress measurements and, in consequence,
were required to respond to the entire spectrum of turbulent
energy. However, as far as this project was concerned, inte-
rest was centred mainly on those larger eddies which might
cause the ion plume to be displaced bodily. In order to res-
trict the response of the bivane to these lower frequencies,
its dimensions were made rather larger than usual. In fact,
the total length of the bivane was over 1 m.

4.6.4.2
Construction of the Bivane

Fig. P.7 shows clearly the construction of the device. The
horizontal and vertical sensing vanes, which were very care-
fully balanced, were attached to suitable axles and their
angular position transduced by means of specially adapted
potentiometers . (Limit stops were provided on the horizon-
tal component sensor to prevent damage if violent gusts
occurred - these were placed at 50° from the centre posi-
tion). The circuit of the system is shown in Fig. 4.7.

Potentiometers were specially adapted for this application by
bending away the wiper contact slightly, thereby relieving
some of the frictional resistance between wiper and track.

THE BIVANE

This technique was perfectly adequate for the horizontal component sensor but it was noticed, particularly in very light winds, that the vertical component sensor appeared to be sticking. Clearly this was most undesirable as it could easily lead to erroneous values for the vertical component readings. The offending potentiometer was therefore replaced by a proprietary low torque device with noble metal contacts. This potentiometer, a COLVERN type CS 08, had a starting torque of only $0.05\ gm\ wt\ m^{-1}$ and, after this had been installed, no further trouble was experienced.

The vertical sensing vane was constructed from 2 mm balsa wood sheet to achieve maximum sensitivity.

4.6.4.3
Calibration and Peformance

A ruled graticule was attached permanently to the bivane in order to enable the horizontal component sensor to be calibrated in situ. The vertical sensor was checked by fixing a protector to its axis and measuring the variation in output voltage as the sensor was manually rotated. Results of such calibrations are not shown graphically because, as was expected, they are perfectly linear. The results of the sensor calibrations were also expressed in the form of a simple equation, such a technique facilitating later data processing. The equations are given below

$$\alpha = 141 V_\alpha - 114 \qquad (4.5)$$
$$\beta = 86 V_\beta - 67 \qquad (4.6)$$

where α is the vertical component sensor angle, being positive for upward air movement and negative for downward,

β is the horizontal component sensor angle, increasing in the clockwise direction, and

V_α, V_β are the voltage outputs of the vertical and horizontal sensors respectively.

(The angles α and β were measured in degrees.)

It should be appreciated that the angles α and β are speci-
fied with reference to the appropriate axes of the bivane
itself. In the construction of the bivane great care was
taken to ensure that the axes of the two sensors were accu-
rately perpendicular. Additionally, when setting up the
bivane on the mast, considerable dexterity was needed to
ensure that it was correctly aligned. For this to be
achieved the mast needed to be accurately vertical and,
further, once the horizontal component sensor had been set,
the mast had to be prevented from any further rotation. A
second system of guy ropes, attached to the top of the mast,
was used to ensure that this could not occur. After initial
difficulties, a standard procedure for accurately siting the
bivane was eventually devised. The technique involved the
use of a prismatic compass and binoculars and, although a
little tedious, was reasonably successful.

Apart from the relatively minor difficulties of setting up
the bivane in the field, the device worked very satisfac-
torily. The results obtained from the series of experiments
using the bivane are presented in Ch. 8.

4.7
The Photographic Equipment and Smoke Generator
Cine photography of smoke plumes was employed to supplement
the bivane observations in the final stages of the project.

Smoke candles, supplied by STANDARD FIREWORKS of Huddersfield,
were placed as close to the ion generator as possible, and
then ignited by means of long fuses. When a smoke generator

was ignited, two remotely controlled automatic 8 mm cameras, the ion generator and recording system were switched on. These cameras were placed at suitable upwind and crosswind locations, and from the ensuing photographic records, it was possible to trace, accurately, the varying configuration of the smoke plume. Small tungsten bulbs, placed in the field of view of the cameras, were arranged to light once every recording cycle. In this way accurate synchronization between the photographic and data recording systems could be maintained.

In the laboratory the smoke plume configurations were compared with those computed from the bivane data. Results obtained with this technique can be found in Sec. 8.2.4.

Chapter 5: <u>THE DATA HANDLING SYSTEM</u>

<u>5.1</u>
<u>Basic Principles of Design and Operation</u>

The various instruments described in the previous chapter pro-
duced analogue voltage outputs proportional to the value of
the particular parameters they were measuring. The range
of these output voltages lay between 0 and 1.5V and any pro-
posed data handling system had therefore to accept this input.

It might have been possible to use a multichannel pen recor-
der to monitor the instrument readings directly. However,
it was hoped that an alternative system could be devised
which would provide a digital output ultimately for computer
processing. The use of a pen recorder would not have faci-
litated this objective and therefore, as well as for other
reasons, its employment was not considered any further.

It is well known that data can be stored compactly and conve-
niently on magnetic tapes and, moreover, a tape recorder would
be reasonably easy to handle in the field. Further, it was
also possible to obtain a digital output signal from a tape
recorder system. These advantages led me to the conclusion
that the most satisfactory recording medium, for this project,
would be magnetic tapes. Many previous workers, including some
at Durham, have, in fact, used this method for recording and
storing geophysical data.

An FM instrumentation recorder would, of course, have been
ideal for this project, enabling the instrumental outputs to
be recorded without further processing. Unfortunately, the
purchase of such equipment was beyond the resources of the

Atmospherics Physics Group and consequently an alternative means had to be sought. ASPINALL (1969) was, in fact, confronted with this problem and he overcame it by the employment of a system known as time division multiplexing. In such a system the output from each measuring instrument is sampled in turn and the resulting sequence of values recorded on a single channel recorder. For example, if five parameters were being measured, then the first parameter could be recorded for the first second, the sampler then advancing and the second parameter being recorded for the next second. The system is arranged to operate cyclically and, in the above example, the first parameter would again be recorded for the sixth second.

Clearly the main advantage of this technique lay in the elimination of the need for a multichannel recorder. However, as a particular quantity was only sampled for a fraction of the total time, it was inevitable that certain features present in the variations of the parameter would be lost. The effect which this loss of information has upon the overall performance of the system is discussed in Sec. 6.2.2.4.

Consideration had also to be given, at this stage, to the accuracy of the data handling system. It was decided that, in common with the requirements of previous workers, the system must not, if possible, degrade the accuracy of the individual measuring instruments in any way. In practice, the performance of the proposed system was determined by two factors, firstly the constancy of the tape speed past the heads during the recording and playback operations and secondly, the stability and linearity of the voltage to frequency and frequency to voltage

convertors. Further discussion regarding the accuracy of the system will consequently be postponed until these circuit elements have been described.

The high quality portable audio tape recorder (EMI type L4B), used by ASPINALL in his project, was still serviceable and therefore the present system was designed to operate with this recorder. Whereas an instrumentation recorder could accept DC input voltages without modification this was not the case with an ordinary audio tape recorder, which could only deal with AC signals in a range from approximately 30 Hz to 10 KHz. Consequently, it was necessary to convert the DC signals from the measuring instruments into some type of equivalent AC signal. A technique in which the frequency of an AC signal was modulated by the DC input voltage has been used by ASPINALL. Such a system, the accuracy of which depended solely on the measured frequency of a signal and not on its amplitude, would also be insensitive to changes in recording level and the effects of minor tape defects. The alternative, using amplitude modulation, suffered from both these drawbacks and was not therefore considered suitable.

Previous workers at Durham had processed their recorded tapes to produce a punched paper tape input for the computer. However, I was advised by the Computer Unit that this technique was no longer practical and it was suggested that a more up to date approach be adopted. Fortunately, at about that time, digital voltmeters with automatic printers were just appearing on the market. Further, a colleague, Mr. K. M. DAILY, was about to construct a similar data handling system and so he too might require the use of such a device for his project. The

various possibilities were explored jointly and a WEYFRINGE
type 901 "Data Capture Unit" with integral printer was finally
selected as the most suitable. The range of this voltmeter
was from zero to 199.9 mV, the accuracy being within 0.1 mV
of the indicated value. The registered value could also be
printed out (on a paper roll) by depressing the printer actua-
tor switch. The printer, which worked at the maximum rate of
one value every 3 s, could also be operated remotely and this
facility offered the possibility of completely automatic play-
back of data tapes.

5.2
The Choice of Channel Allocation and Sampling Rate

As mentioned previously, it was proposed to record the outputs
of the four field mills, the wind speed, wind speed gradient
and temperature gradient systems. Therefore, seven inputs
would be required if each instrument were to be allocated a
single channel. It occurred to the author that, of the four
different parameters chosen for recording, certain of them
might be more relevant to this investigation than others. Conse-
quently, effort was directed into assessing the most satisfac-
tory way of allocating channels to optimize data acquisition.
It was also felt desirable that a further channel be provided
in order that a marker signal could be recorded once per sam-
pling cycle. The function of this marker was to be twofold.
Firstly, appearing as it did within an ordered sequence of
sampled parameters, any omissions or duplications in the sam-
pling cycling would, on playback, be immediately obvious.
Secondly, if a standard voltage were to be applied during the
interval in which the marker was being sampled, it would enable
a useful check of the consistency of performance of the voltage

to frequency convertor to be made.

After consideration, it was decided that the field mills should be sampled twice as frequently as the micrometeorological instruments and that the inclusion of a marker was definitely worthwhile. Implementing these ideas would raise the total number of channels to twelve although, of course, four pairs of channels would be common.

Early experiments had clearly indicated the need for faster sampling than that employed in the systems used by previous workers. Even with the provision of two channels for each field mill, it was estimated, on the basis of certain theoretical relations, that the system proposed would need to cycle through all twelve channels in not more than 3 s. This relatively high sampling rate was necessary to resolve the high frequencies that were known to be present, particularly in the electric field variations.

5.3
The Sampling and Recording System

5.3.1
Purpose of the System

This system was designed to sample each of the measuring instruments in cyclic sequence and convert their output voltages into a series of AC signals suitable for tape recording. The operation of the system is represented schematically in Fig. 5.1.

THE SAMPLING

AND RECORDING SYSTEMS
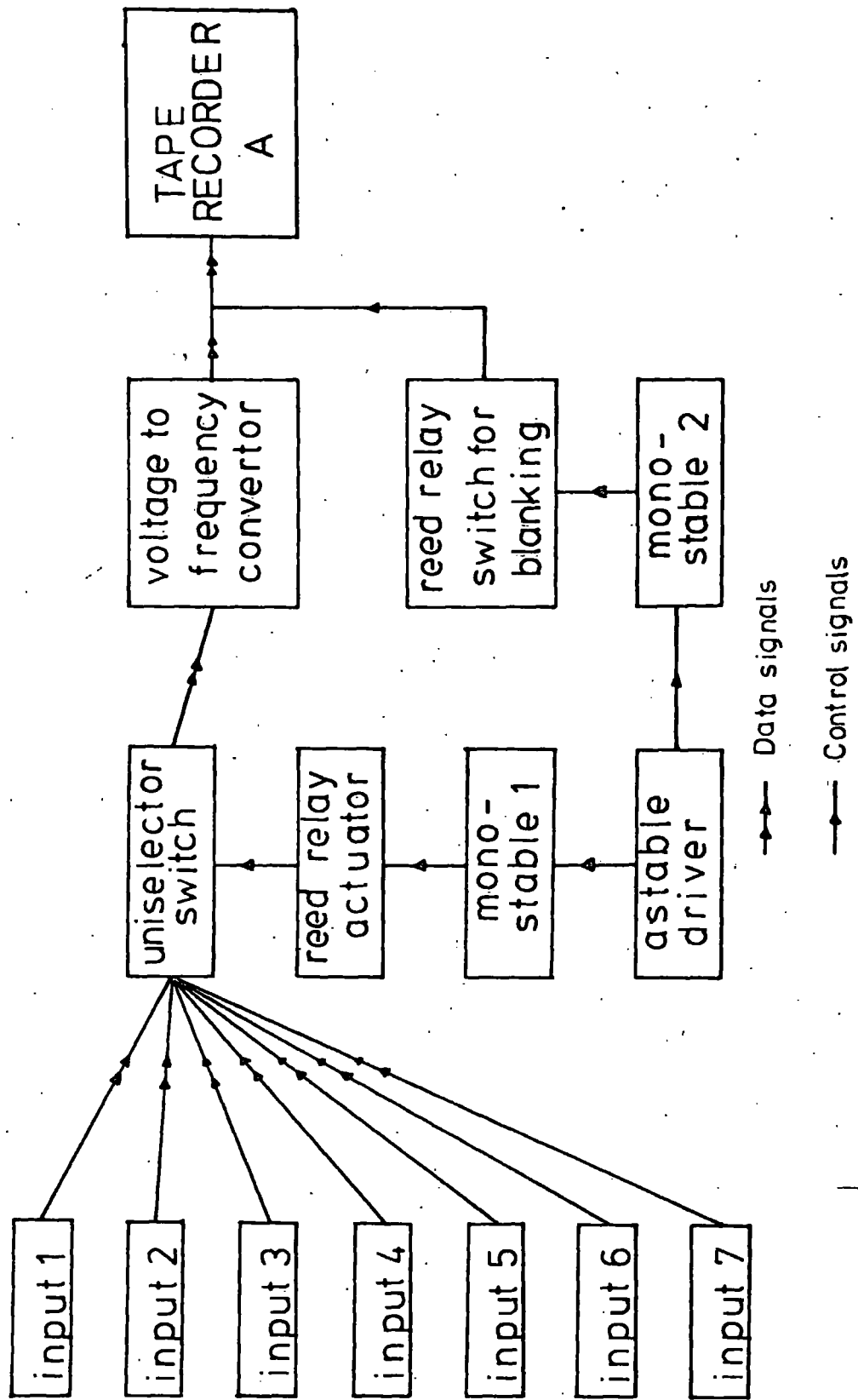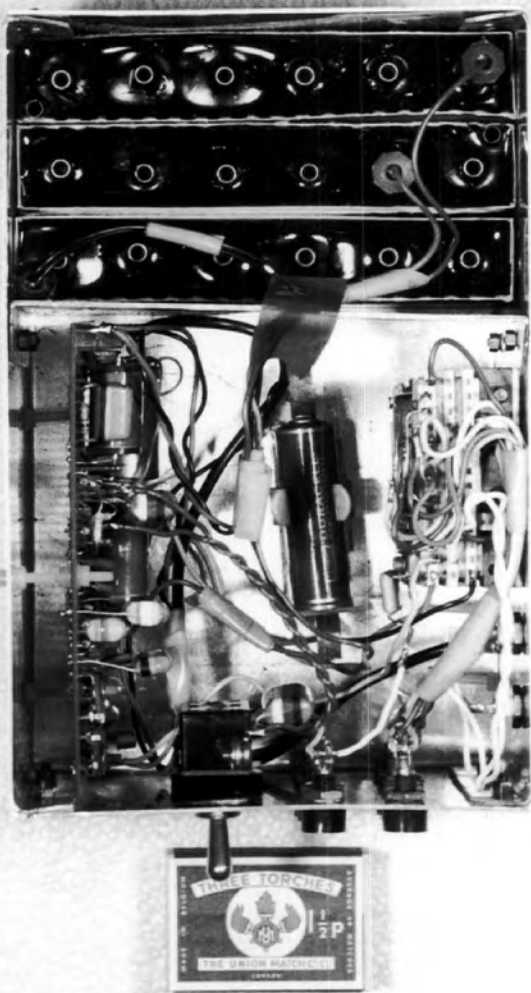
THE SAMPLING UNIT

The Sampling System

ASPINALL (1969) suggested that future sampling systems might be designed employing integrated circuitry. Following discussions with the electronics group at Durham, I realized that such techniques, whilst being eminently suitable for sampling AC signals, were not easily adaptable to sampling DC signals. It was recommended that the use of some type of electromechanical device would, most likely, be far simpler. ASPINALL had himself used reed relays and a quite complex logic system in his experiments. Frankly, the author found the prospect of designing and constructing a system involving twelve reed relays and associated logic a little daunting and was therefore led to consider simpler alternative systems.

The feasibility of employing a uniselector as the sampling device was consequently investigated. (A uniselector is a solenoid actuated multiway switch, a suitable current pulse causing it to advance to the next contact position). Fortunately, the Group already possessed a number of 12 way uniselectors and tests confirmed that such devices could be made to switch at the required speeds.

Fig. 5.2. shows the system that was constructed employing the uniselector. The sampling rate of the system is determined by the pulse repetition frequency of the astable driver. The output square wave from the driver was used to trigger monostable 1 and this, in conjunction with a reed relay, supplied pulses to advance the uniselector.

During the marking interval standard conditions were established in the voltage to frequency convertor by switching a

10·K resistance in parallel with its input.

5.3.3
The Voltage to Frequency Convertor

The ouput from the uniselector consisted of an ordered sequence of DC voltages and could therefore be connected directly to a suitable voltage to frequency convertor.

Previous workers at Durham have employed the circuit of DE'SA and MOLYNEUX (1962) for voltage to frequency conversion. However, the rather small range of output voltage of the measuring instruments used here required that either a different type of convertor be employed or that the signals were suitably amplified. The latter alternative was rejected as trouble had already been experienced with DC amplifiers. None of the published circuits appeared suitable and consequently it was necessary to develop a convertor specifically for this project.

It was known that the pulse repetition frequency of an astable multivibrator is very dependent on the voltage applied to the base timing resistors. The possibility of this voltage to frequency dependence being applied to the solution of the present problem was therefore explored. Suppose V_s was the supply voltage applied to the collector, whilst an excess voltage V were applied to the base timing resistors. This is shown in Fig. 5.2. (In this case the base resistors are R_5 and R_6, the collector resistors being R_7 and R_8). Simple theory indicates that the pulse repetition frequency, f, of such an arrangement is given by the expression

$$f = \frac{1}{2RC \ \ln\left(\frac{2V_s + V}{V_s + V}\right)}$$

(5.1)

THE SAMPLING AND RECORDING SYSTEMS — Circuit Diagram

5.2
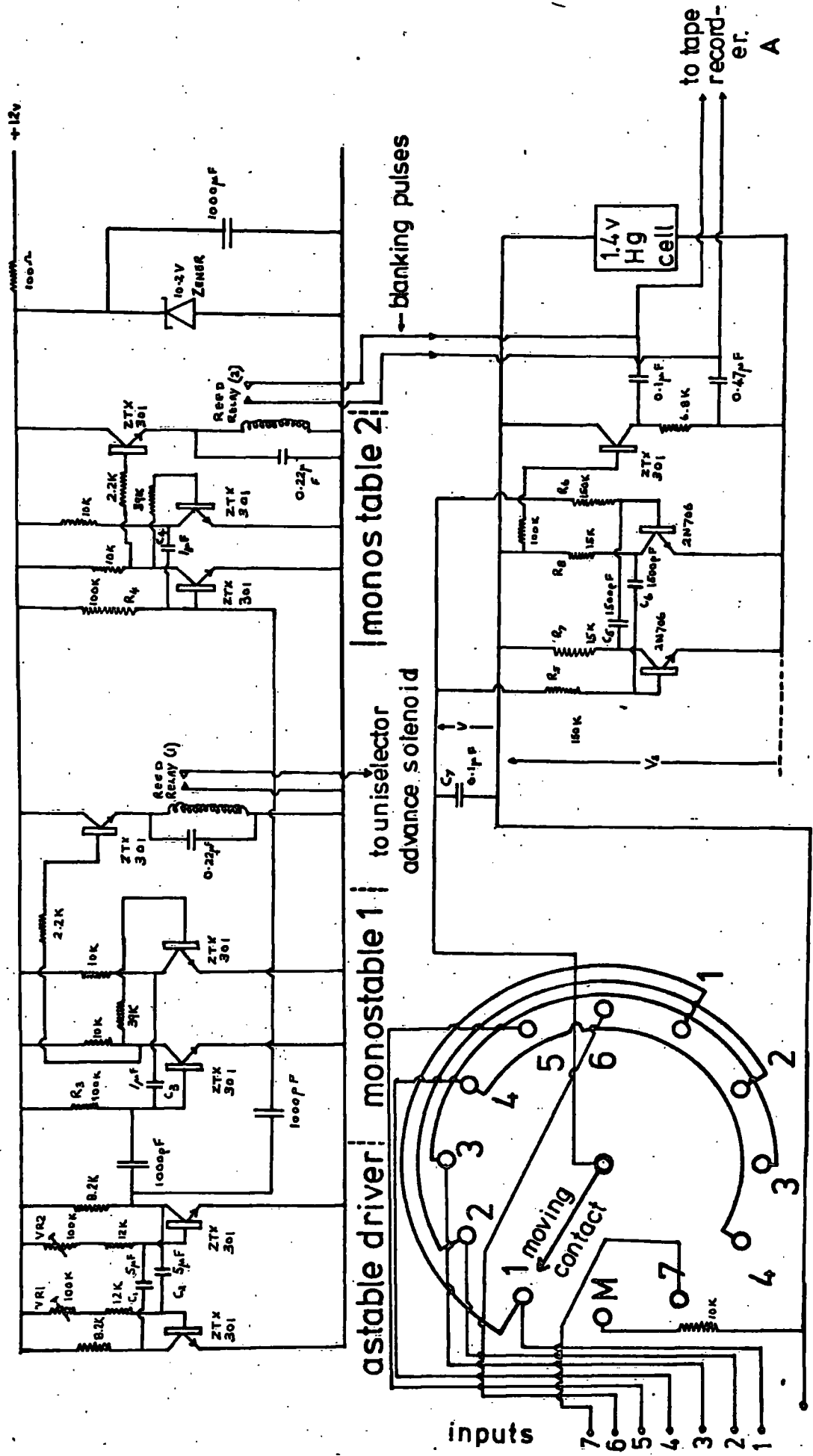
where R is the base timing resistance

and C the timing capacitor value.

(It is worth noting that equation (5.1) reduces to

$$f = \frac{1}{2RC \ln 2} \qquad (5,2)$$

when V = 0. This latter expression, of course, represents the relation between frequency and circuit values for a conventional astable multivibrator).

At this stage a trial circuit was constructed to establish the validity, or otherwise, of expression (5.1). Tests revealed that, not only was the theoretical relation closely adhered to, but also, by a suitable choice of V_s , the collector supply voltage, the voltage-frequency characteristic could be made virtually linear. It was found that, for this project, the optimum value of V_s was about 1.4V It should be noted, however, that as the frequency is also dependent upon the value of V_s , as well as of V , the V_s supply would need to be very stable. High stability was achieved in practice by specifying a mercury cell for this supply. (A mercury cell has a very flat voltage-time discharge curve, thus rendering it eminently suitable for the application in view). A further, and very useful, feature of this design of converter was its minute current consumption, this being typically about $150 \mu A$.

A computed voltage to frequency characteristic for the particular circuit values employed here is shown in Fig. 5.3.

5.3.4
The Blanking Circuits

Early trials with the sampling system revealed that considerable contact noise and other interference was present on the output signal of the voltage to frequency convertor during interchange between input channels. Various attempts to eliminate this interpference were unsuccessful, and therefore it was necessary to blank off the output signal during these changeover periods. Later, it was realized that the blanked interval in the signal could be used to trigger the printer on the digital voltmeter and thus make a separate synchronized trigger pulse unnecessary. The blanking signal was generated by monostable (2) (see Fig. 5.2.) The signal, after being passed through a driving transistor, was used to close a reed relay for a suitable length of time during the interchange. After trials the blanking pulse length was set to 70 ms.

Fig. 5.4 shows the types of wave form present in the voltage to frequency convertor and sampling system.

5.4
The Design and Operation of the Playback System
5.4.1
Preliminary remarks

During recordings each parameter was sampled for approximately 0.28 s, the exact duration depending on the setting of the astable driver circuit in the sampling unit. Consequently, if a tape were played back at the same speed as it had been recorded at, then the resultant output signal would consist of a series of tones each about 1/4 s in length. However, the fastest speed at which the digital voltmeter could reliably operate was one value per 3 s. It was decided, therefore, that a second tape recorder would be needed in order to playback

Computed voltage to frequency convertor characteristic

$$f = \frac{1}{2RC \ln(\frac{2V_S + V}{V_S + V})}$$

Where:-

V_S = supply voltage
R = timing resistance
C = timing capacitance

and in this convertor

V_S 1,46v
R   150K
C   1,5nF

Output signal frequency (KHz), (f)

Input voltage (v)
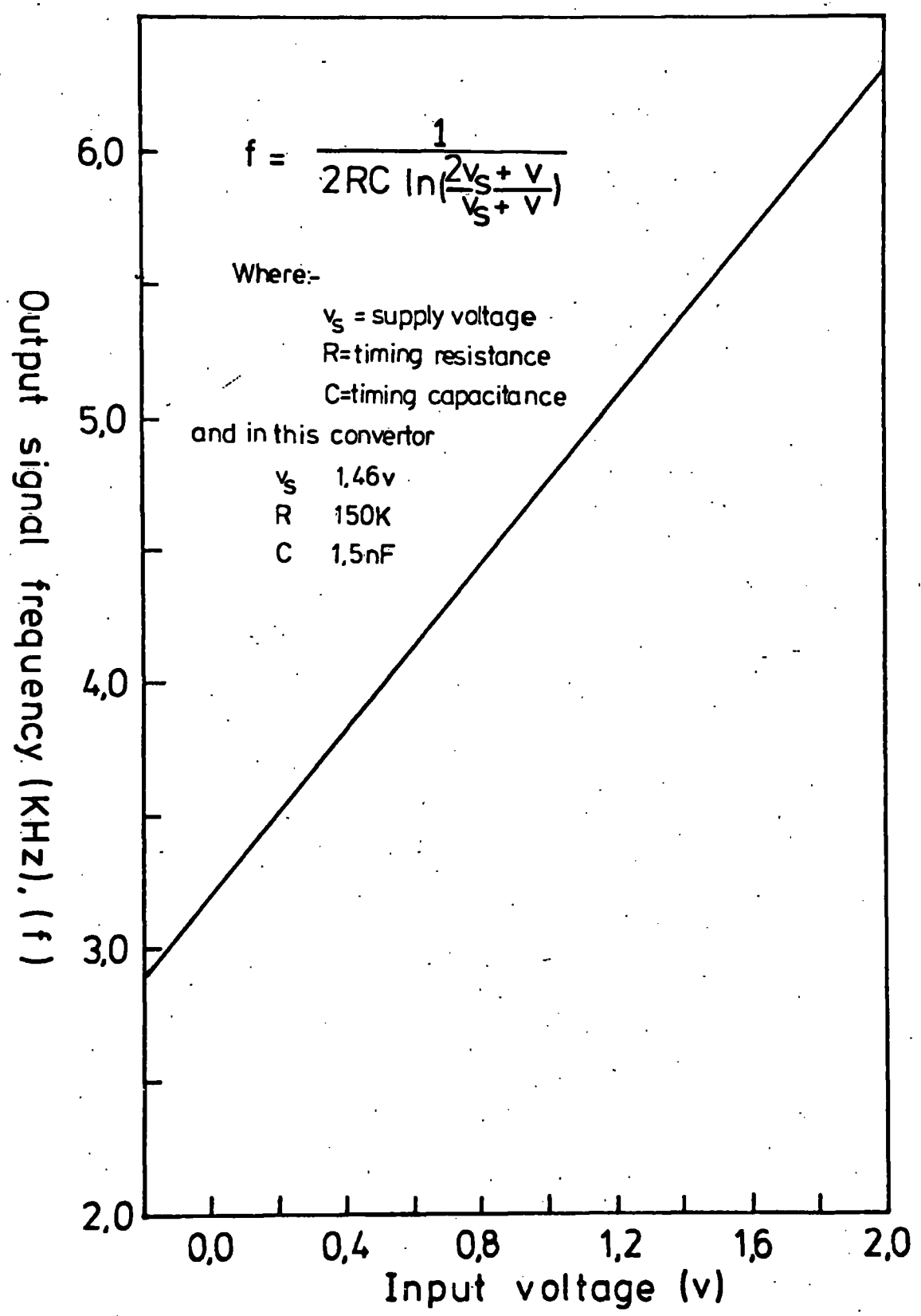
THE WAVEFORMS IN THE SAMPLING

AND RECORDING SYSTEMS (not to scale)

(a) Astable driver output (clock pulses)
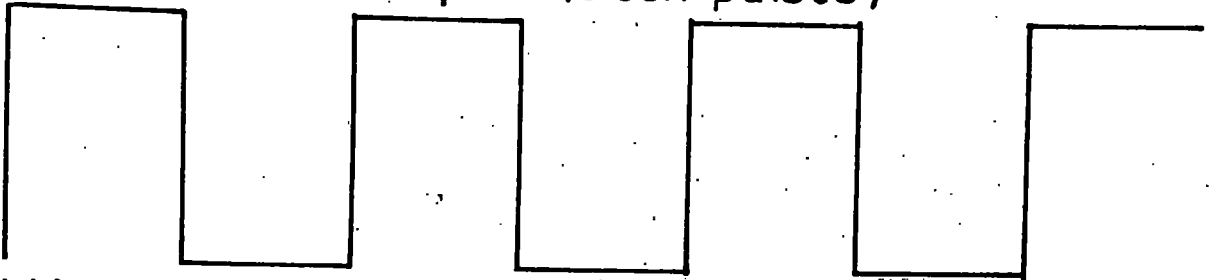
(b) Monostable 1 output (advances uniselector)
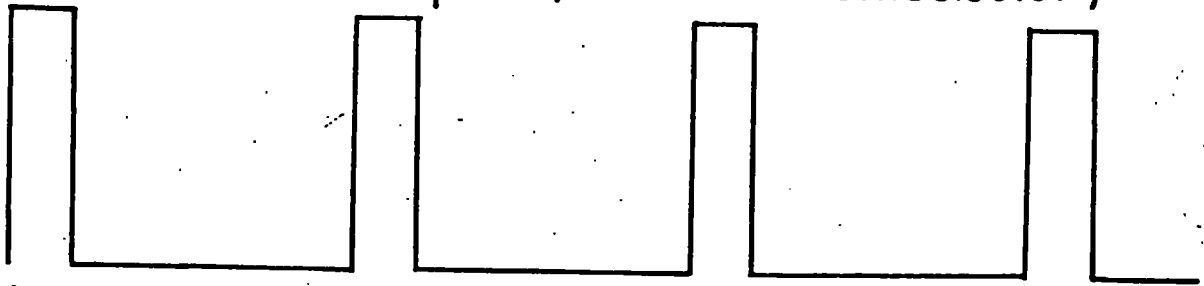
(c) Monostable 2 output (blanking pulses)

V
O
L
T
S
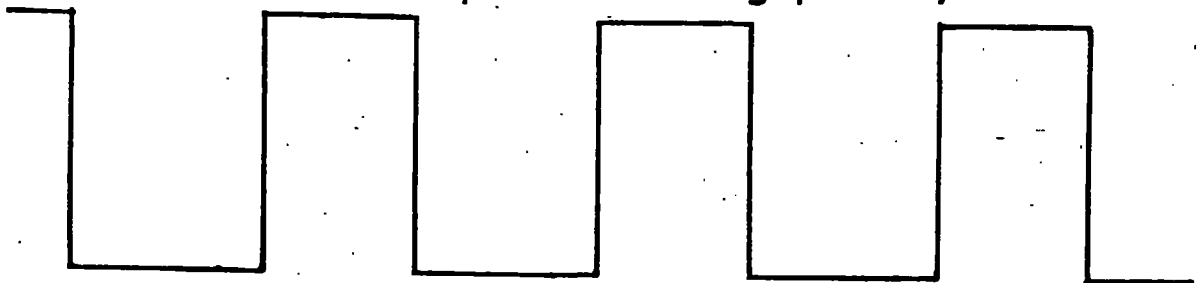
(d) Voltage to frequency convertor output after blanking

input 1   input 2   input 3   input 4

—————time————→
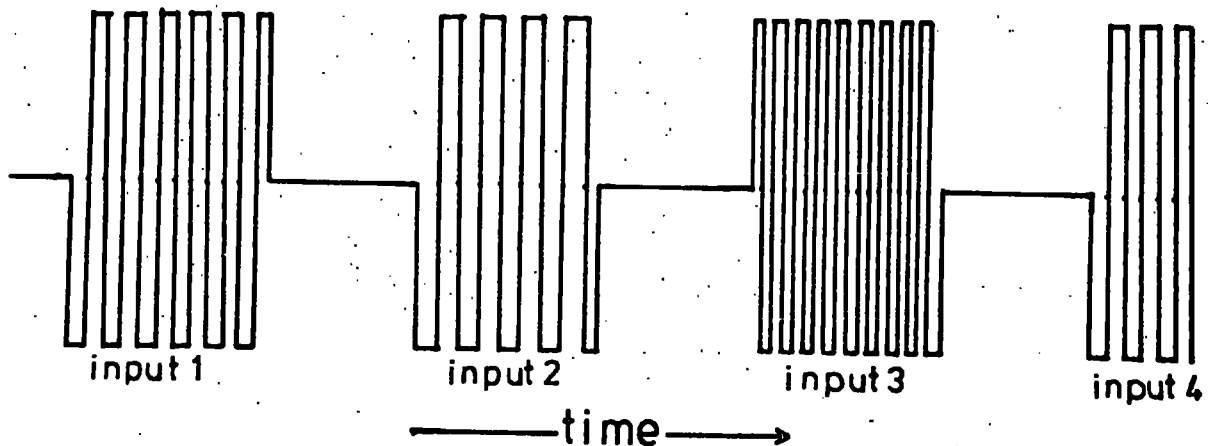
N.B.   IDEALISED   WAVEFORMS

tapes at a speed sufficiently low for the digital voltmeter to work satisfactorily. The portable tape recorder used for recording in the field operated at 7 1/2 IPS (inches per second) and consequently, in order to dilate the recorded signals sufficiently, it was necessary for the second tape recorder to operate at 0.6 IPS or less. A possible alternative might have been to record data tapes at speeds much higher than 7 1/2 IPS but this was regarded as unsatisfactory because, amongst other problems, vast amounts of tape would be required for any reasonable duration of recording.

A conventional mains-powered domestic tape recorder was obtained, and, by carefully modifying the drive system, it was possible to achieve a tape speed of just under 0.5 IPS. This was done by attaching additional reduction pulleys between the motor and existing systems and by carefully grinding down the capstan shaft to half its original diameter. A very high degree of concentricity needed to be maintained in the ground down capstan because any error would have caused tape speed variations. Wow and flutter would hence be created on the playback signal and this would result in a serious loss in the accuracy of the system.

This specially modified tape recorder will henceforth be referred to as tape recorder B. To emphasise this distinction, the portable tape recorder employed in the field will be termed tape recorder A.

5.4.2

The Frequency to Voltage Convertor

The function of this system was to convert the series of tones appearing at the output of tape recorder B into a sequence of DC voltages suitable for logging by the digital voltmeter. The rôle of the convertor is represented schematically in Fig. 5.5.

The voltage to frequency convertor in the recording system operated in the range 2 - 6 KHz. The tape speed during play-back was about 1/15th of that during recording and hence the frequency of the playback signals was in the range 130 - 400 Hz. This wide difference between the recording and the playback signal frequencies had, of course, to be borne constantly in mind when designing both systems. Setting the voltage to frequency convertor range too low would not have allowed the frequency to voltage convertor to operate correctly. Alternatively, if the voltage-frequency convertor range had been set too high the limited response of the portable tape recorder would have inhibited the performance of the system. In practice, the choice of frequency ranges proved quite satisfactory for both convertors.

The operation of the frequency to voltage convertor is briefly as follows. Incoming trains of pulses from tape recorder B are fed into the Schmitt trigger circuit (see Fig. 5.6.). This serves to increase the squareness of the pulses and to remove unwanted noise. The shaped pulses are then allowed to trigger monostable A. The output of this circuit consisted of a series of pulses of constant width, their frequency, of course, being equal to that of the incoming signal. These pulses are then clipped in the emitter follower circuit by a zener diode. After clipping, the pulses are integrated by an RC network, and

THE PLAYBACK SYSTEM

tape recorder B

frequency to voltage convertor

digital volt meter

printer

print command unit

Data signal

Control signal

Circuit Diagram

THE PLAYBACK SYSTEM —

+12v

REED READY

to printer

to DVM
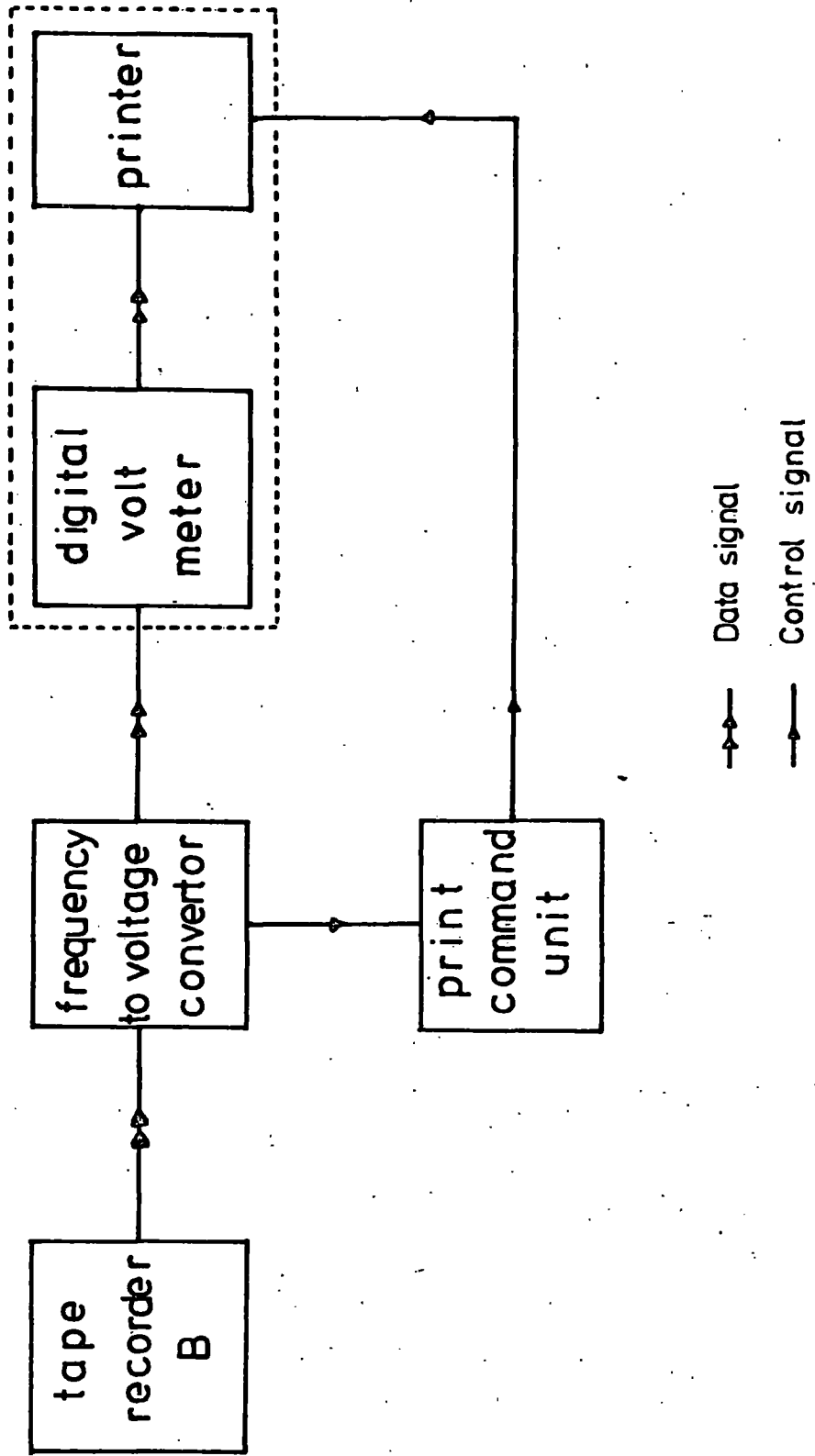
FREQUENCY TO VOLTAGE CONVERTOR   PRINT COMMAND UNIT
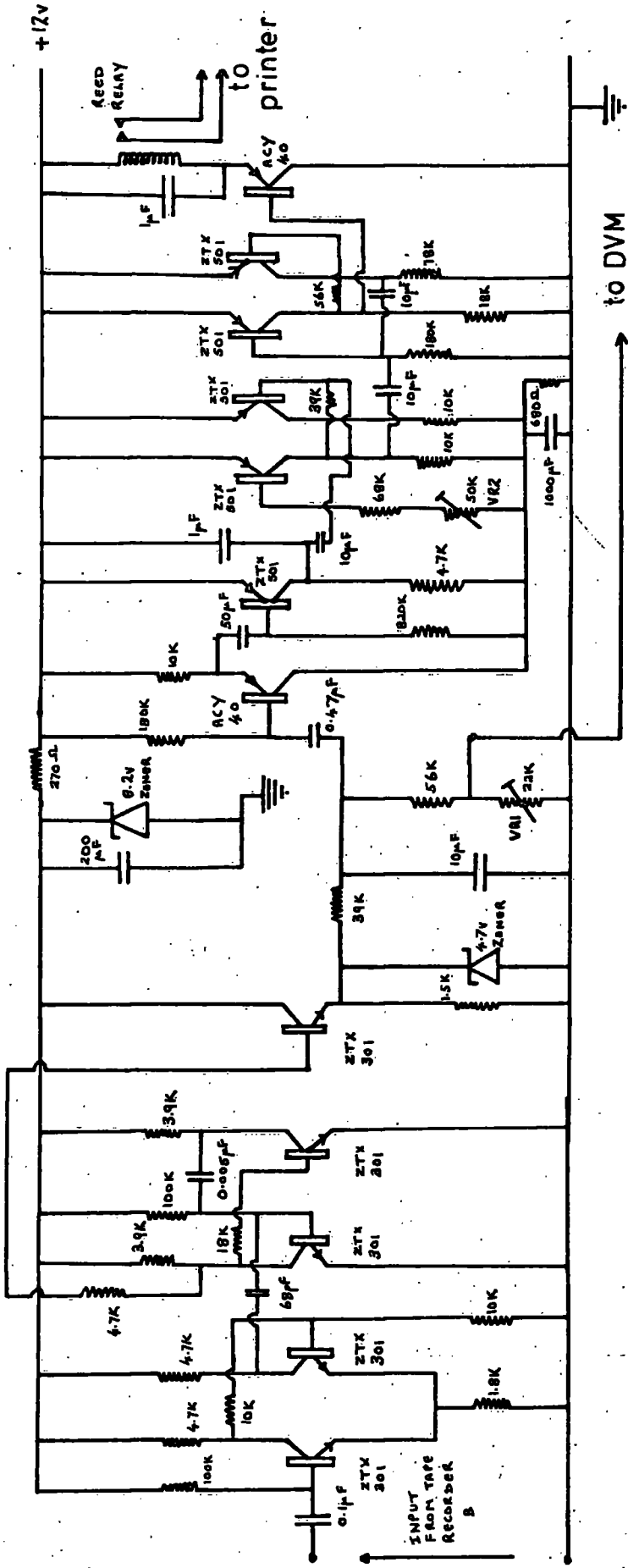
| Schmitt Trigger | Monostable A | Emitter follower & pulse-rate integrator | Differentiator | Monostable B | Monostable (Delay) | Output C | Driver |

INPUT FROM TAPE RECORDER
B

ZTX 301

ACY 40

ZTX 501

ZTX 501

ZTX 501

ZTX 501

ZTX 501

ZTX 501

ZTX 301

ZTX 301

ZTX 301

ZTX 301

VR1 22K

VR2 50K

100K

4·7K

4·7K

4·7K

10K

1·8K

10K

3·9K

3·9K

18K

100K

0·005µF

68pF

0·1µF

34K

1·5K

4·7v ZENER

270Ω

6·2v ZENER

200µF

180K

56K

10µF

0·47µF

10K

50pF

1µF

8·2K

4·7K

10µF

69K

10K

10K

1µF

10µF

34K

56K

18K

18K

680Ω

1000pF

1µF

16K

because of the constant height and width of the pulses, the output of this circuit depended only on the pulse frequency.

The time constant of this integrating circuit is of crucial importance to the correct functioning of the convertor. Too long a value would not have allowed the output voltage to have reached its final value within the span of the pulse train, whilst too short a time constant would have resulted in there being unnecessary ripple on the output voltage. In the present system the value of this time constant was set to 0.3 s. This ensured that the output voltage was within 1 per cent of its ultimate value before it was printed by the digital voltmeter. The form of the integrator output voltage, together with other waveforms, is shown in Fig. 5.7.

5.4.3
The Print Command Unit

It proved possible to derive a print trigger signal from the output of the integrator in the voltage to frequency convertor. This output, after being taken through a buffer amplifier, was differentiated by a long time constant CR network. The type of output produced by this circuit is shown in Fig. 5.7(c). It will be noted that a positive pulse is produced on the arrival of each train of pulses from tape recorder B. Consequently, if a suitable delay circuit were triggered by the arrival of these positive pulses then it should be straightforward to provide a trigger signal at an appropriate time. The optimum moment for such trigger pulses to occur is indicated by the X's in Fig. 5.7(b). A satisfactory delay circuit was developed employing, as is conventional, a monostable multivibrator, the trimming resistor VR2 being used to adjust the delay to the desired

value (monostable B). A further monostable (C) was then employed to supply the reed relay coil with a suitable current pulse, the digital voltmeter printer operating on closure of the relay contacts.

It should be mentioned here that the use of p-n-p transistors in this unit, instead of the n-p-n types as elsewhere, was a result purely of availability, the unit having been originally designed to use the n-p-n variety.

5.5
The Calibration of the Data Handling System and its Subsequent Performance in the Field

5.5.1
Considerations affecting the Accuracy of the System

System accuracy would depend largely on the following factors:

    (i) The performance of the voltage to frequency and frequency to voltage convertors.

and (ii) the constancy of tape speed in both tape recorders.

It was decided, before any attempt be made to calibrate the system as a whole, that those units on which the accuracy depended most heavily should be individually assessed.

The voltage to frequency convertor was already known to be satisfactory in terms of linearity and stability of output, these features having been closely investigated during the development of a suitable circuit. It was, however, dis- covered that, with the design of convertor being used, a small reverse voltage was generated across its input terminals. The origin of this voltage was traced to the effect of the base current flowing to the transistors in the convertor. This current, when flowing through the output resistance of voltage source connected to the convertor, produced the small reverse

WAVEFORMS IN THE PLAYBACK SYSTEM (not to scale)

(a) Output from the Schmitt trigger.
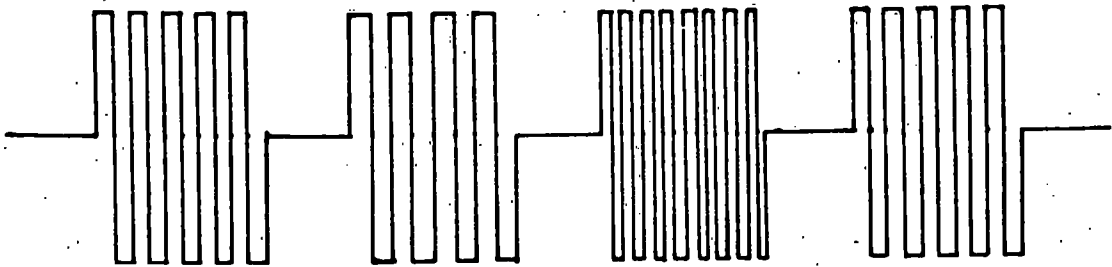
(b) Output to DVM
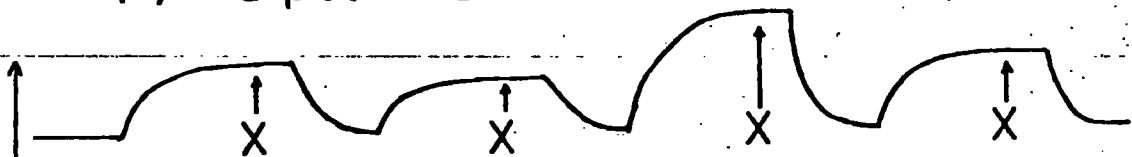
(c) Input to Monostable B
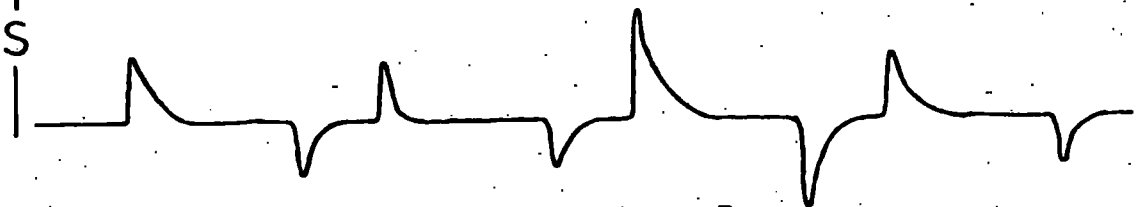
(d) Output of Monostable B

(e) Signal to reed coil (print trigger)

VOLTS

X   X   X   X

——time——→

N.B.   IDEALISED   WAVEFORMS
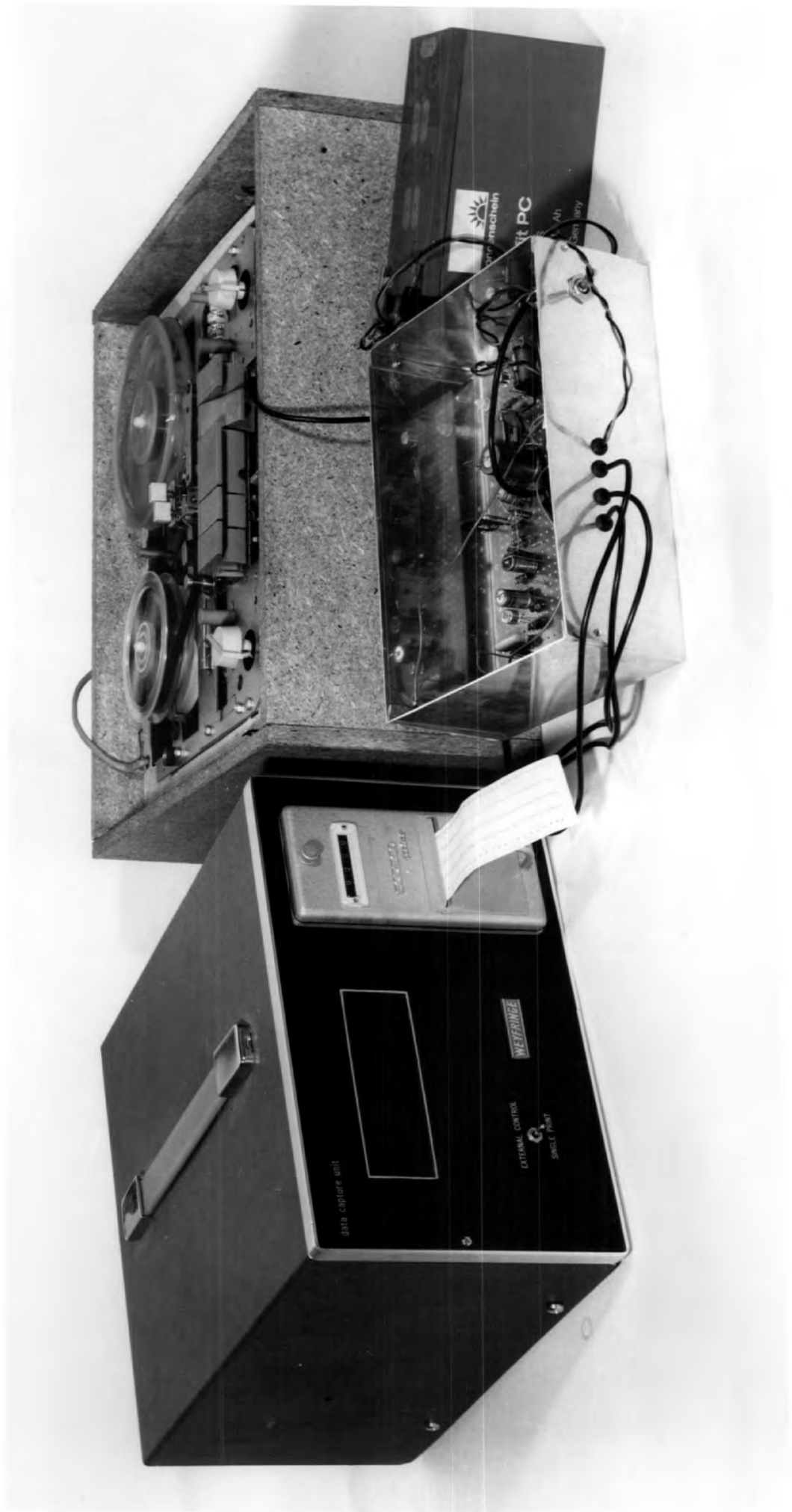
Playing-back a data tape

voltage. Typically this voltage was no greater than 0.1V and, once its existence was appreciated and understood, no further difficulty was experienced.

The frequency to voltage convertor was tested directly by applying a square wave signal, whose frequency could be varied, and monitoring the output voltage. The results of such a test are shown in Fig. 5.8(a) and indicate a very satisfactory performance.

The tape recorders were checked by the following method. A constant frequency signal of suitable amplitude, provided by a high quality signal generator, was recorded onto magnetic tape by one of the tape recorders. The tape recorder under test was then made to playback the recorded tape into the frequency to voltage convertor, the output being connnected to a pen recorder. During playback some small random variations were apparent in the outputs of both recorders, the large fluctuations being, as expected, in tape recorder B. The magnitude of these speed variations was never greater than 2 per cent of the average value and thus caused only a minor loss of accuracy.

It was possible, with all but the earliest observations, to provide some compensation for these minor tape speed variations. This was achieved during computer processing of the data, the ratio of the actual value of the marker signal (see Sec. 5.2.) to its value during calibration being used as a correction factor. The use of this technique, whilst not completely eliminating errors from speed variations, provided a convenient and effective means of substantially reducing them.

5.5.2
Calibration of the Data Handling System

Attention was now directed to establishing the characteristics of the data handling system as a single entity. The relationship of principal interest was, naturally, that between the input voltages presented to the sampler unit (and recorded as tones on magnetic tapes) and those voltages ultimately printed out by the digital voltmeter during playback. It was evident from previous work that the relationship would be closely linear, but a feature of equal, if not more, importance, was the long-term stability of the entire system.

The most obvious method of calibrating the data handling system appeared that of maintaining a number of stable and accurately known voltage inputs to the sampling unit, recording a tape, and then playing that tape back over the playback system. Standard voltages were obtained from three potentiometer networks supplied by a stable voltage source. The voltages chosen for the tests were 0, 0.5, 1.0 and 1.5, these values representing the full working range of the system. The stability was better than 1 mV for the duration of a recording. The recorded tape was played back in the normal manner.

After this test it was possible to accurately determine the voltage transfer characteristic of the system. The values printed out by the digital voltmeter were punched onto computer cards, and with the aid of a suitable computer program, their means and standard deviations found. The mean output voltages versus the input voltages are shown in Fig. 5.8(b). The standard deviations, which are too small to be illustrated

RECORDING AND PLAYBACK SYSTEM

(a) Frequency to voltage convertor performance
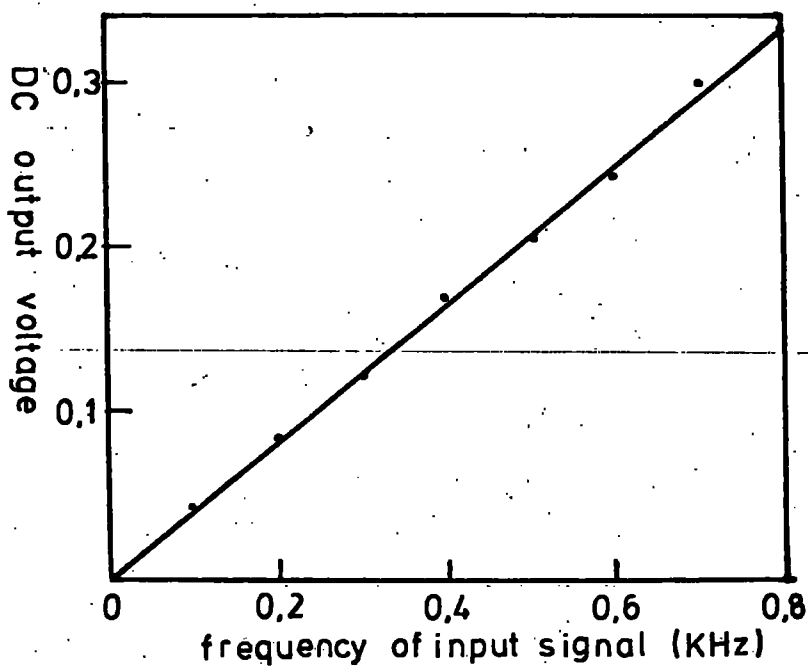
(b) Over-all performance
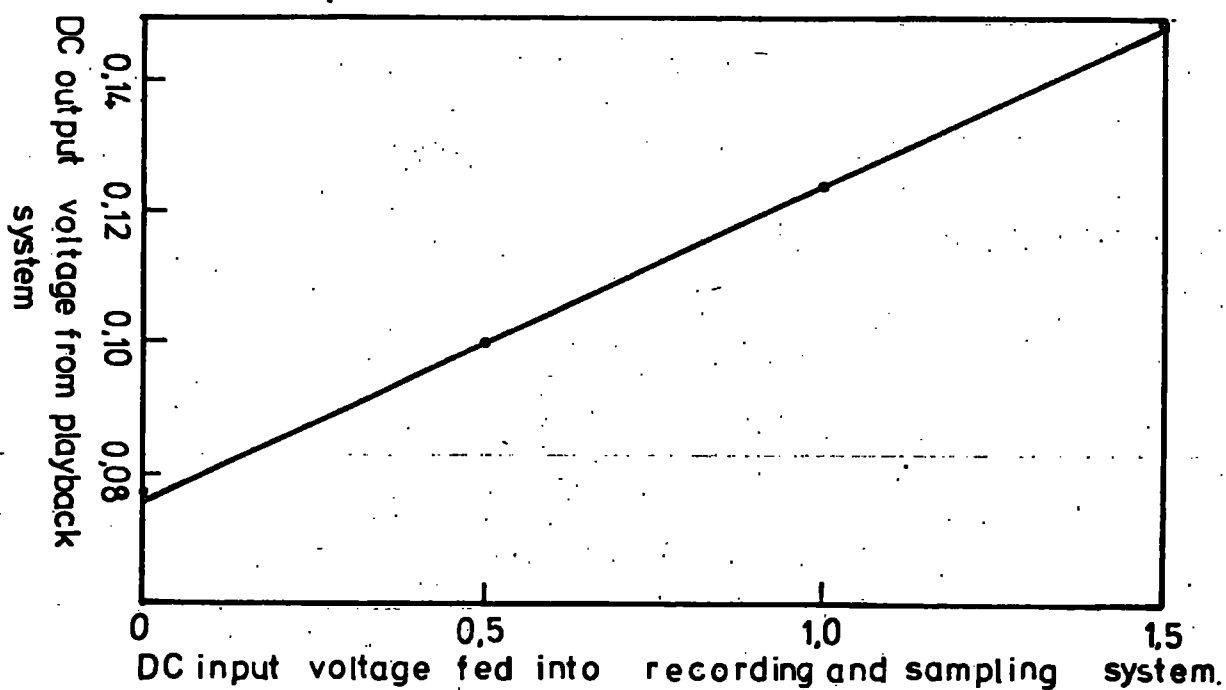
in the figure, were less than 1 per cent of the mean values
at all four calibration points. This was most satisfactory
and, at this point the data handling system was considered
ready for service in the field.

As a precaution the entire calibration procedure was repeated
at monthly intervals. After a few months it was found that
departures from the original calibration were quite negli-
gible, and because of this, subsequent calibration checks
were only considered necessary at three monthly intervals.
It emerged, as a result of these periodic tests, that the
long-term stability was only marginally less good than the
short-term performance.

5.5.3
The Performance of the System in the Field
Despite the careful design and rigorous testing of the system
in the laboratory prior to field work, some irritating,
though relatively minor, faults did appear.

Upon analysis of the recorded data it became clear that the
voltage to frequency convertor was more sensitive to tempera-
ture variations than had been expected. This posed problems,
particularly during intermittent sunshine, as the temperature
of the convertor could change by as much as $20^{\circ}C$. In total
these shifts in characteristic never exceeded 3 per cent and
were therefore not too serious. Once the effect had been
noticed the sampling and recording unit was always placed in
a shady position. The problem did not recur once this action
was taken.

After some use the uniselector switch contacts became dirty
and this resulted in erratic voltages being transmitted to the
voltage to frequency convertor. The application of a proprie-
tary contact cleaning fluid at regular intervals cured this
problem.

Apart from the occasional difficulties mentioned above, the
system functioned extremely well, and, once recording had
been started, could be relied upon to function without fur-
ther attention. This was ideal as it enabled the author to
undertake any supplementary observations needed or to check
that other equipment was working efficiently.

Chapter 6: <u>TECHNIQUES USED TO ANALYSE THE OBSERVED DATA</u>

6.1
Introductory Topics

6.1.1
The Series I and II experiments

The relationship between the behaviour of a plume and the pre-
vailing atmospheric stability was discussed in Sec. 2.7., whilst
particular electric field patterns that might be associated with
various plume configurations were mentioned in Sec. 3.6. Field
work was therefore directed, at least initially, to the recording
of electric fields under ion plumes in various conditions of
stability. The electric fields were measured by four field mills
whilst the atmospheric stability was monitored by the two anemo-
meters and thermistor system. The wind speed and temperature
gradient measurements would ultimately be used to compute the
Richardson number, thus allowing comparisons between different
field runs to be made.

After considerable experimental work of the type described above
had been undertaken it emerged that the results, though excellent
in themselves, were not really providing as much information as
was hoped. However, it had been realized by then that the intro-
duction of a recording bivane could be of considerable assistance
in understanding ion plume behaviour (see Sec. 2.8.). Consequently
such a device was constructed and employed in all later field work.
In practice, it proved necessary to sample the bivane readings as
frequently as possible and, in order to provide sufficient input
channels, the existing instrumentation arrangements were modified.
In fact, the number of field mills had to be reduced to three,
only one anemometer could be used and the differential temperature
system was dispensed with.

These two instrumental arrangements described above will be
referred to subsequently as the Series I and Series II systems
respectively.

The form of the data and the need for statistical analysis

In both the Series I and II field work all data was recorded
on magnetic tapes by the methods described in Ch.5. These
data tapes, once recorded, were returned to the laboratory
for processing by means of the playback system. During recor-
ding, parameters were sampled in cyclic order, and therefore
the series of values printed out by the digital voltmeter on
playback would be in a corresponding sequence. The actual
sequence depended, in practice, on the nature of the particu-
lar run and, of course, on whether a Series I or II type of
experiment was being conducted.

During any particular field run, most of which lasted 24 min.,
a different parameter was sampled every 0.28 s and, as a result,
in the region of 6000 'values' would be recorded on a single
tape. On playback the same number of values was printed on the
paper roll, there being approximately 1000 values per double
channel and 500 each for the remaining single channels (see
Sec. 5.2.).

The direct analysis of such a large amount of data, particularly
in the form of a long roll, was almost impossible. Therefore
techniques had to be devised to cope ultimately with many similar
volumes of data. The need for a statistical treatment of some
type was quite evident from the sheer quantity of data. However,
it was hoped that the recorded data could also be processed to
render graphical records so that the behaviour of the various

quantities could be examined visually. A further possibility
was that of comparing the observed data with results obtained
from the plume models. This is discussed in Sec. 6.4.

6.2
The Application of Statistical Techniques to the Analysis of
Observed Data

6.2.1
The choice of suitable methods

There was little doubt that the electric field under an ion
plume would vary in complex manner with time and space, the
variations being, of course, the result of both the localized
nature of the ion plume and the fluctuations of concentration
within it due to turbulence. It was expected that, whilst
the nature of the field variations themselves would be compli-
cated, certain of their overall characteristics might depend
in a fundamental way on the atmospheric stability and other
experimental circumstances.(Here, the term 'overall charac-
teristics' is used to refer to the general impression one
might gain by a casual glance at a potential gradient record.
Thus, for example, one would be immediately aware of the pre-
sence of large oscillations in the potential gradient values).

In order to compare the results of experimental runs made in
different conditions, it was obviously necessary to devise
methods of assessing this overall character of the recorded
variations. Graphical presentations of the data might have
been useful in this respect but it was felt that comparisons
between records would be very tedious and, as a result, time
consuming. Consequently, statistical methods were regarded

as being more suitable. Incidentally, it was hoped that inspection of graphical records would serve better as a means of analysing particular events rather than entire runs. In view of this we shall now consider how we can expect the electric field to depend on various parameters, and after arriving at some simple conclusions, propose a scheme of statistical analysis.

It seems obvious that, close to an ion plume, the mean electric field would be considerably larger than at a distance. Further, because of the erratic behaviour of all plumes, the variations of electric field would most likely also be greater near the plume. Thus, in statistical terms, the values of the mean and standard deviations of the electric field should depend, to a considerable extent, on the closeness of the measuring point to the ion plume. Of course, at large distances downwind, where the artificial ion concentration would be very low, both the mean and standard deviation of the electric field will approach their natural values.

The mean and standard deviation, although clearly of great importance in characterizing the electric field, tell us nothing about the speed with which the variations occur. The rapidity of the field changes depends on many factors, but principally on the height of the moving charges and their velocity. In practical terms this implies that the frequency of the electric field variations should be largely determined by the ion source height and the wind speed.

As well as the importance of the time scale of the variations, it would often be useful to be able to estimate the connexion between sets of observations taken at different locations. This is important because the relationships between such measurements

were expected to reveal considerable information about the
nature of the ion plume (this aspect is discussed further in
Sec. 3.6.).

Initially therefore, the means, standard deviations and corre-
lations would be computed for each set of data. Later it was
expected that, in the light of experience, certain additions
and refinements to the techniques would be required. A dis-
cussion of the statistical methods, including the later modi-
fications, now follows.

6.2.2
A synopsis of the statistical methods
6.2.2.1
Introduction

The application of statistical techniques to the analysis of
geophysical data is by no means novel. In studies of atmos-
pheric turbulence particularly, statistical approaches have
been regarded as virtually standard since the classical work
of TAYLOR (1935). In atmospheric electricity statistical
methods have also been applied but their use has not been so
widespread as in the previous case. Several workers at
Durham, e.g. SHARPLESS (1968), have used simple statistical
concepts in their data analysis. However, ASPINALL (1969)
extended these methods in analytical work on frontal precipi-
tation. In fact, his techniques have much in common with mine,
even though, of course, they were devised for a very different
purpose. ASPINALL includes a comprehensive discussion of the
statistical methods he employed and therefore only a summary
is presented here.

6.2.2.2
Means and standard deviations

Mean values were computed in the usual manner, that is by a calculation of the type

$$\overline{X} = \frac{1}{n} \sum_{i=1}^{n} X_i \qquad (6,1)$$

Here, as before, the overbar denotes the mean value, while X_i , $i = 1, 2, 3, 4 \ldots\ldots n$, represents the series of values whose average is required.

The standard deviation, σ_x , of the values of X was computed as is usual, by the following relation

$$\sigma_x^2 = \frac{1}{n} \sum_{1}^{n} (X_i - \overline{X})^2 \qquad (6, 2)$$

The quantity σ_x^2 is known as the variance, and both this and the standard deviation indicate the amount of variation present in the values of X.

Sometimes it is of interest to consider the relative, rather than the absolute, variation in a quantity. A useful measure of this, known as the coefficient of variation, CV , is defined by the ratio

$$CV = \frac{\sigma_x}{\overline{X}} \qquad (6,3)$$

6.2.2.3
Cross-correlation techniques

The application of cross-correlation techniques to establish the relationship between pairs of variables is well known, see for example RACTLIFFE (1962). As a first step the cross-

covariance C_{xy} of the variables X and Y is formed by using
the relation

$$C_{xy} = \frac{1}{n} \sum_{1}^{n} (X_i - \bar{X})(Y_i - \bar{Y})$$

(6.4)

A cross-correlation coefficient, R_{xy}, can then be obtained by
normalising C_{xy} by the product of the standard deviations of
each variable. The modulus of R_{xy} varies between zero, in
which case the variables are essentially uncorrelated, and unity
which implies perfect correlation - either in phase or in anti-
phase depending on the sign. Expressing this mathematically we
have

$$R_{xy} = \frac{C_{xy}}{\sigma_x \, \sigma_y}$$

(6.5)

It will be observed in equations (6.4) and (6.5) that correspon-
ding elements of each series have been correlated. That is the
i^{th} element of the X series has been correlated with the ith
element of the Y series. Suppose the electric field were being
recorded at two points downwind of the ion plume. This is shown
diagrammatically in Fig. 3.11(a). It is clear from the electric
field records depicted in the figure that a maximum cross-
correlation will occur when either of the records is displaced
in time by an amount equal to the transit time of the feature
causing the field variations. Thus we could profitably extend
the calculation of the 'simple' cross-covariance in equation
(6.4) to include cases where the two sets of variables have
been displaced with respect to each other. We now express this
idea mathematically, denoting the cross-covariance at a dis-
placement of l intervals by the quantity $C_{xy}(l)$. Hence

$$C_{xy}(l) = \frac{1}{n-l} \sum_{i=1}^{n-l} (X_{i+l} - \bar{X})(Y_i - \bar{Y}) \qquad (6,6)$$

The quantity l is usually known as the lag number and for meaningful results to be obtained it should not exceed $i/10$.

In a similar way we can normalise equation (6.6) to obtain the cross-correlation coefficient $R_{xy}(l)$ at lag number l. Thus

$$R_{xy}(l) = \frac{C_{xy}(l)}{\sigma_x \; \sigma_y} \qquad (6,7)$$

As a particular, but very important, case of cross-correlation analysis we can compute the correlation of a particular variable with itself at various time lags. Denoting this autocovariance, as it is known, by $C_x(l)$ we can write

$$C_x(l) = \frac{1}{n-l} \sum_{i=1}^{n-l} (X_{i+l} - \bar{X})(X_i - \bar{X}) \qquad (6,8)$$

Similarly we may normalize $C_x(l)$ by the variance of X to produce the autocorrelation coefficient at lag number l, $R_x(l)$ hence

$$R_x(l) = \frac{C_x(l)}{\sigma_x^2} \qquad (6,9)$$

The importance of $R_x(l)$ is that as it expresses the correlation of a variable with itself at various time lags it is consequently a sensitive measure of the time scale of the variations present in X.

In order to assist the reader various types of auto- and cross-correlation behaviour are shown in Fig. 6.1, together with notes concerning the nature of the variations giving rise to them.

It should be noted here that the lag number l is related to the displacement time τ, by the expression

$$\tau = s\,l$$

where s is the sampling interval.

6.2.2.4
Spectral analysis

It is intuitively reasonable to expect that a connexion might exist between the shape of an auto-correlation function and the variations when expressed in the form of a spectrum. Thus for example, in Fig. 6.1(a), the auto-correlogram which falls off the more rapidly (A) would obviously contribute a greater proportion to the variance at higher frequencies than the less rapidly varying autocorrelation function (B). It can be shown, subject to certain limitations which need not trouble us here, that the autocorrelation function and spectral density can be expressed as Fourier transforms of each other. In mathematical terms we have

$$G_x(f) = 4 \int_0^\infty C_x(\tau) \cos 2\pi f \tau \, d\tau \qquad (6, 10)$$

where $G_x(f)$ is known as the power or variance spectral density of the variate X. In fact, $G_x(f)\,\delta f$ represents the contribution to the variance of X arising from variations

within the frequency range f to $f+\delta f$. It should be noted that in the evaluation of $G_x(f)$, the quantity $C_x(\tau)$ is, by implication, a continuous function of τ . This may be so in some cases but in this project, owing to the discrete nature of the recorded data, the autocorrelation can only be calculated at those time intervals which are multiples of s , the sampling interval. Further, as the upper limit of integration is infinity, we apparently need to know the variation of $C_x(\tau)$ for all time. Clearly this is a practical impossibility, for we can only obtain realistic values of $C_x(\tau)$ up to a time equal to $ns/10$. The practical effects of these limitations are twofold, firstly the spectrum can only be evaluated within a particular range of frequencies and secondly, the contributions to the variance must be estimated in discrete bands. Actually by a suitable choice of sampling interval and running time, which controls n , these limitations need in no way be detrimental to the results.   --

A further source of trouble resulting from discrete data is that it can give rise to an effect known as aliassing. Variations which occur at frequencies higher than $1/2s$ cannot be resolved from those which occupy slightly lower frequencies. Consequently when a variance spectrum is computed from such data, contributions arising from frequencies higher than $1/2s$ are 'folded' into the spectrum near this high frequency limit. In view of this, caution must be exercised when considering the magnitude of the spectral density function near the high frequency limit. For a fuller discussion on this and related topics the reader is referred to BENDAT & PIERSOL (1966).

Typical auto- and cross-correlation patterns

(a) autocorrelation behaviour

B, less rapid variations, but indication of a weak periodicity

A, rapidly varying quantity

(b) crosscorrelation behaviour

A, variables behaving similarly but displaced in time by an amount τ_m

B, variables in 'antiphase' but only partially correlated

C, variables virtually uncorrelated
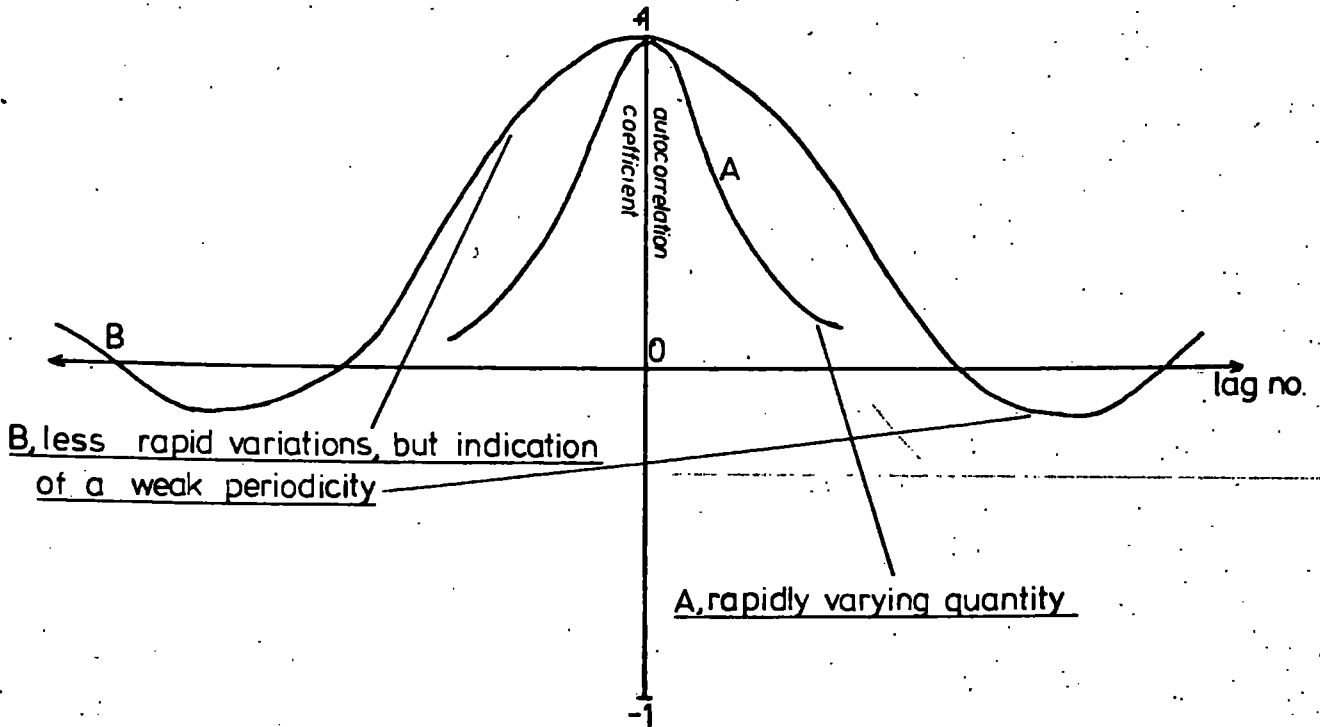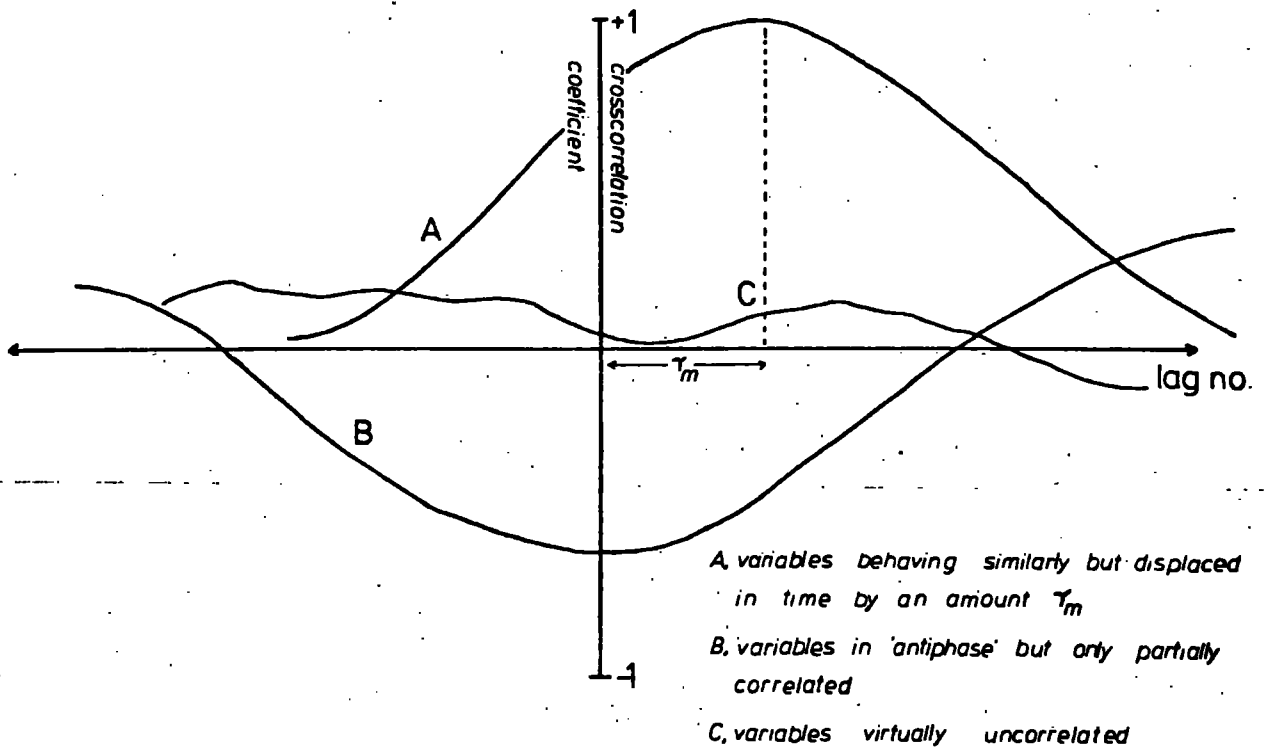
It is also possible to form spectra by applying Fourier transform techniques to the *cross-covariance* functions. In this case, however, the situation is more complicated because of the mathematical nature of the cross-covariance. It is found, on taking the Fourier transform, that the resulting spectrum is a complex quantity and has the general form

$$G_{xy}(f) = Co_{xy}(f) - j\, Q_{xy}(f)$$

The real part is known as the cospectral density function whilst the imaginary part is referred to as the quadrature spectral density function. A discussion on the significance of $Co_{xy}(f)$ and $Q_{xy}(f)$ is beyond the scope of this thesis and in any case is well documented in the literature.

The quantity

$$Coh_{xy}(f) = \frac{\left[G_{xy}(f)\right]^2}{G_x(f)\, G_y(f)}$$

(6,11), which is

known as the coherence of the variables X and Y at the frequency f, does however, have a simple physical interpretation. It represents, in fact, the relative contribution made to the total cross-correlation by variations occurring at the frequency f. As the value of such a concept may not be immediately obvious we shall illustrate its use by means of an example.

At a given wind speed and ion source height the rapidity of an electric field variation will depend on the dimensions of the charge system being blown past the measuring point. Obviously

a larger system will cause lower frequency variations than a smaller one. Suppose now we consider the connexion between the electric fields measured at two points separated in space. It should be clear that similar low frequency variations are likely to appear on both records because of the large scale charge systems producing them. (This argument, of course, only applies when the separation between the two points is not too great.) However, the high frequency variations, which arise from the movement of more local and smaller-scale charges are unlikely to be similar at both measuring stations. Expressing this idea in statistical terminology we would say that, in the above situation, the coherence between the records is larger at the low frequency end of the spectral range. The use of coherency analysis, which enables us to quantify the variation of cross-correlation with frequency, might therefore be of assistance in establishing the dimensions of the charge systems causing the field changes.

In a similar manner we may also consider the relative phase between the two electric field variations as a function of frequency. This is expressed mathematically by the relation

$$\phi_{xy}(f) \quad = \quad \tan^{-1} \frac{Q_{xy}(f)}{Co_{xy}(f)} \qquad (6.12)$$

the quantity $\phi_{xy}(f)$ being known as the phase spectrum of the variables X and Y.

6.2.2.5
Shape Analysis

After a number of graphical records of electric field had been examined it was evident that the variations were often of a characteristic shape. The larger electric field peaks were relatively narrow with sharp maxima, whilst the smaller peaks were broader and rounder. We may readily explain this by considering the behaviour of the electric field variations caused by two similar moving charges, one of which passes close to the measuring point, the other remaining more distant. The vertical electric field, due to a given charge, is proportional to $(\sin\phi)/R^2$ (see Sec. 3.3.). In the case of the more distant charge both the $\sin\phi$ and $1/R^2$ terms change only slowly, the $1/R^2$ term never becoming large. On the other hand, these terms change rapidly during the passage of a charge near the measuring point, and at the minimum distance of separation, the $1/R^2$ term can attain large values.

The effects described above result in the electric field variations being asymmetrically distributed about their mean value, rather in the manner shown in Fig. 6.2(a). It is, in fact, possible to quantify this 'skewness' of a variation by computing its third moment about the mean, and then normalizing by division with the cube of the standard deviation. (Further details can be found in LUMLEY & TENNEKES (1972)). Expressed mathematically the skewness, S, is given by

$$S_x = \frac{\sum_i (x_i - \overline{x})^3}{n\ \sigma_x^3} \qquad (6,13)$$

A further quantity of interest is the kurtosis or flatness factor. This function 'weighs the tails' of the distribution and responds strongly to the different types of variation

shown in Fig. 6.2(b). The kurtosis is expressed by the formula

$$K_x = \frac{\sum_i (X_i - \overline{X})^4}{n \, \sigma_x^4}$$

(6.14)

(Again further details may be found in LUMLEY & TENNEKES).

This completes the discussion on the statistical methods.

6.3
The computer programmes used to process the data

6.3.1
Introduction

It is not the intention of this section to consider the 'text'
of the computer programmes as such a discussion would be
inappropriate in this thesis. Copies of the programmes,
which were written in FORTRAN IV, are, however, included for
reference (see appendix).

A computer programme, once written, was transferred onto punched
cards and then, together with the appropriate data and control
cards, was submitted to the computer. After the programmes
were known to be functioning satisfactorily they were 'stored'
under their 'name' on magnetic discs. During subsequent com-
puting, access to any particular programme could be obtained
by referring to that name. It was also found worthwhile to
store programmes in compiled form as this saved considerable
computer time when processing data.

A valuable additional feature available at Durham was that of
computer plotting facilities. The 'plotter' which worked in
a similar manner to a conventional chart recorder, enabled both
observed data and theoretically derived results to be presented
graphically. Extensive use has been made of this facility

The skewness and kurtosis of a varying quantity

(a) skewness

a function with positive skewness
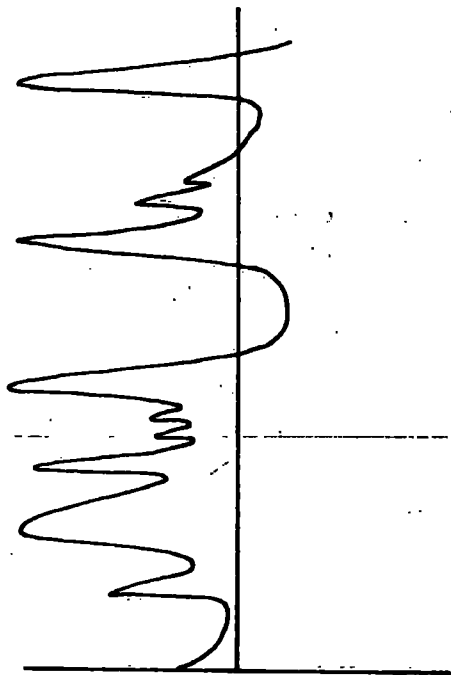
a function with negative skewness
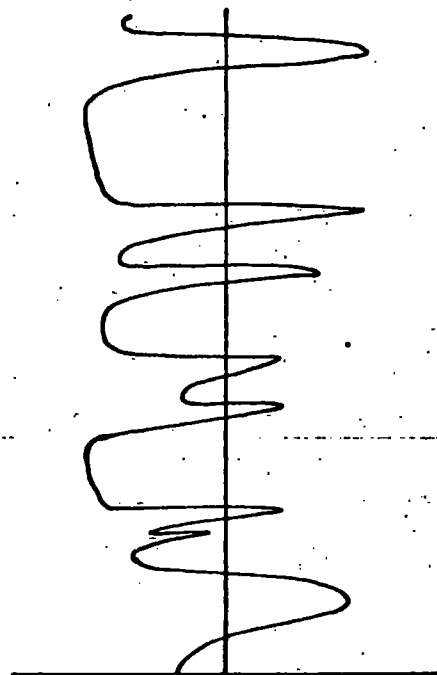
(b) kurtosis

a function with small kurtosis
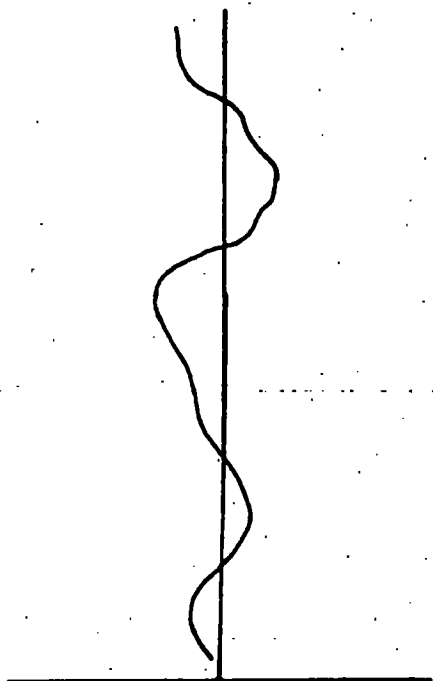
a function with large kurtosis
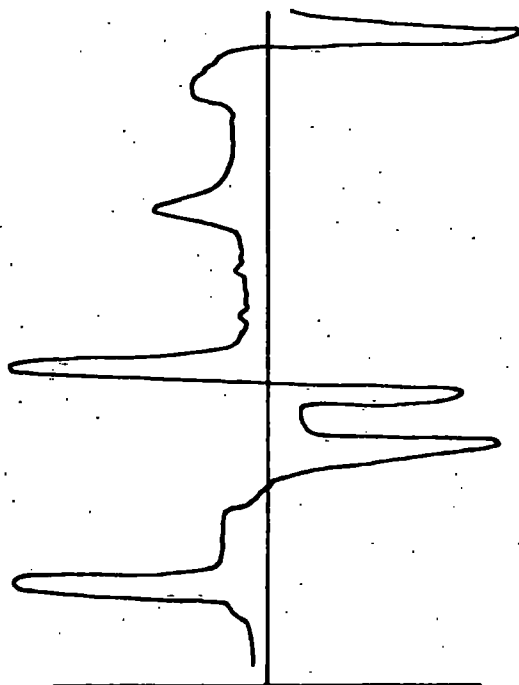
in preparing the observed data for analysis.

6.3.32
The Series I Programmes

The elements of these programmes are shown in Fig. 6.3.,
little additional comment being required here. Originally
all analysis was undertaken using DATAPROG. Later, when
interest was centred on the spectral and shape aspects of
the data further analysis was performed with SUPPROG (supple-
mentary programme).

The rôle of the digital filter will be discussed in Sec. 6.3.4.

6.3.3.3
The Series II Programmes

The basis of the two programmes used to process this data is
shown in Fig. 6.4., the bulk of the computing being undertaken
with BIVANEPROG.

Final experiments in this series involved the visual comparison
of computed plume configurations, derived from bivane data, with
those obtained directly from the cine photography of a smoke
plume. In order to facilitate these comparisons the derived
plume configurations were plotted with the aid of PLMPOSNPROG
(plume position programme). Details of this experimental
technique are given in Sec. 4.7., whilst results obtained with
it are discussed in Sec. 8.2.4.

It was felt worthwhile, having already determined values for
the three wind velocity components u , v and w , to compute the
magnitude of the surface stress. This quantity was calculated
using equation 2.7., and the reader is asked to consult
Sec. 2.3. for the details. The numerical value of this stress,

while having little direct bearing on this work, is neverthe-less of considerable interest. A great deal of published data exists on the surface stress and comparisons between these values and those observed might indicate, if nothing else, whether the bivane system was working satisfactorily. As observed values of the surface stress are presented in Ch. 8., comments on the bivane performance are reserved until then.

6.3.4
The use of digital filters

It should be understood that the rôle of a digital filter is essentially no different from any other type of filter, the idea being, in all cases, to suppress unwanted features of incoming data or signals.

It was found that spectral analysis of the electric field data often revealed the existence of very large variance con-tributions from the lowest frequencies. These contributions were, in fact, the result of large scale charge systems, e.g. clouds, passing over the field work area. Such very low fre-quency variations were of little relevance to this project but unfortunately their presence detracted from the overall quality of the computed spectra. This problem also confronted ASPINALL (1969) and his remedy was to filter the data prior to spectral analysis. A similar approach was discovered to be equally satisfactory in this case and ultimately a high pass filter of the type

$$X(K) = X(K) - P.X(K+1) \quad \text{(as in FORTRAN usage)}$$

Computer processing of Series I data

Computer processing of Series II data


```
┌─────────────────────────────────┐
│ Raw data on punched cards       │
│   observations from  3 mills,   │
│   anemometer and   bivane.      │
└─────────────────────────────────┘
                │
                ▼
┌─────────────────────────────────┐
│ conversion to actual values     │
│                                 │
└─────────────────────────────────┘
                │
                ▼
┌───────────────────────┐      ┌──────────────────┐
│ compute  u,v and w    │ ───► │ compute means,   │
│ velocity component    │      │ correlations,    │
│ values                │      │ surface stress   │
└───────────────────────┘      └──────────────────┘
                │
                ▼                  ┌ ─ ─ ─ ─ ─ ─ ─ ─ ┐
┌───────────────────────┐           ┌──────────────┐
│ compute plume config- │ ──►      │ plot plume   │
│ urations  using  the  │         │  configurations │
│ 'bivane data model'   │           └──────────────┘
└───────────────────────┘         └ ─ ─ ─ ─ ─ ─ ─ ─ ┘
                │
                ▼                  ┌──────────────────┐
┌───────────────────────┐ ───►    │ plot predicted   │
│ optional digital filter │       │ and actual field │
└───────────────────────┘         │ values           │
                │                  └──────────────────┘
                ▼
┌───────────────────────┐
│ correlate predicted and │
│ actual electric field │
│ values                │
└───────────────────────┘
```
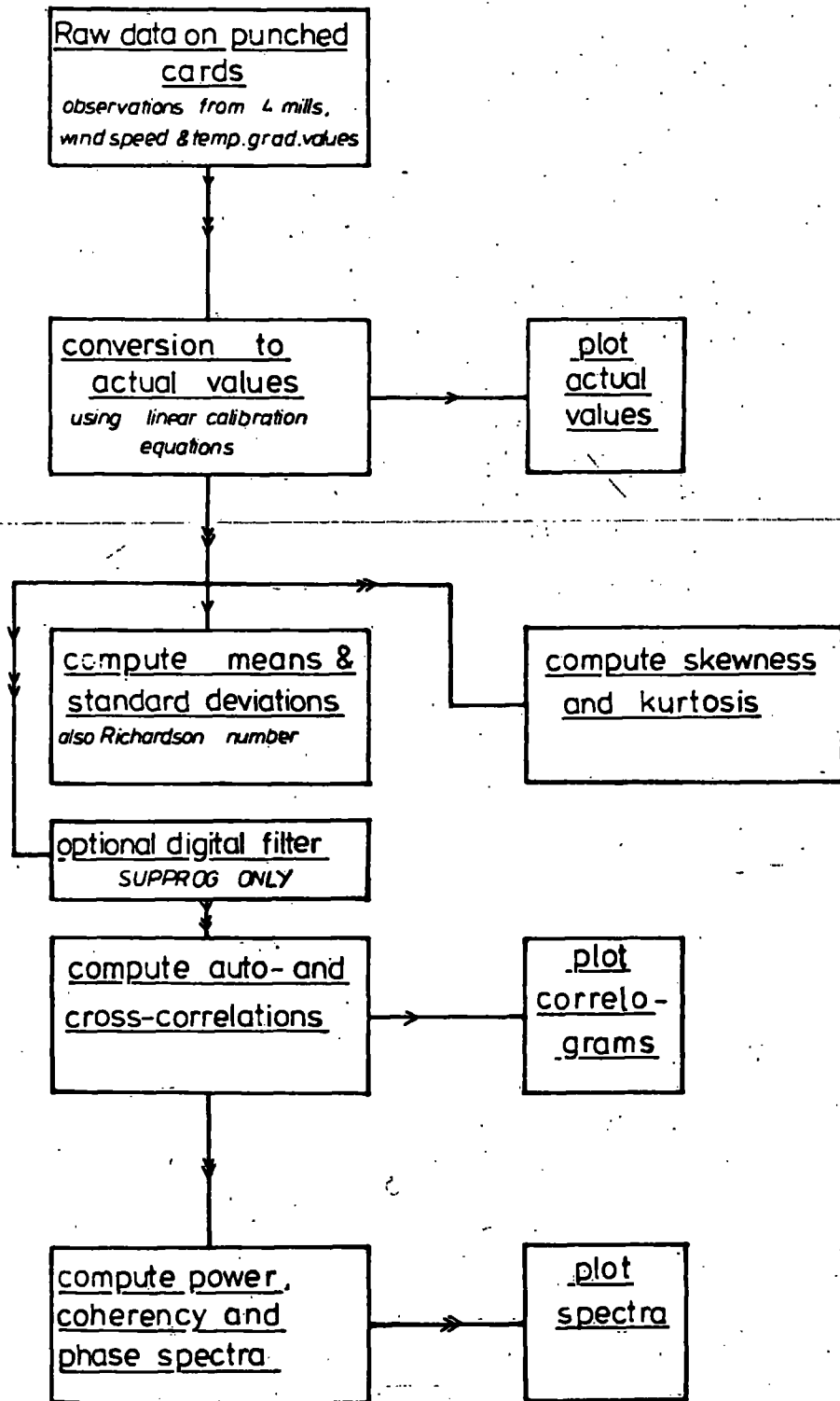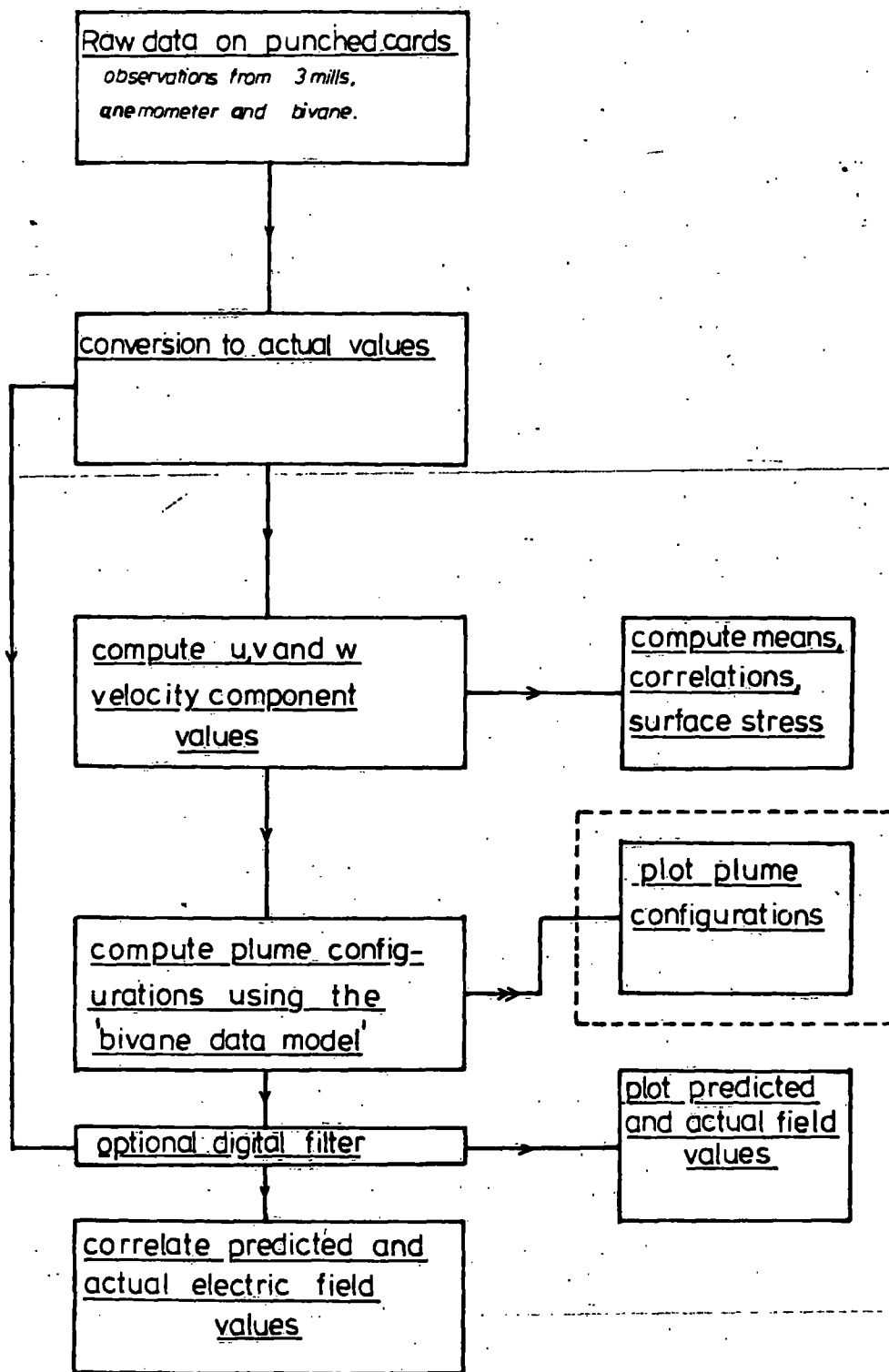
PROGRAMMES ——►— BIVANEPROG ——⇒— PLMPOSNPROG

was chosen. (See ACKERMANN (1964)). (Here $X(K)$ represents the Kth value in a sequence of values of X). Filtering action was obtained here by subtracting out any trends which were present in the data. The coefficient P , which must be ascribed a value between zero and unity, is used to control the degree of filtering. In practice, its value was adjusted empirically to obtain balanced spectra.

In the case of the Series II data analysis, inspection of the predicted and actual electric field records revealed that most of the disagreement between them was in the 'fine structure' of the variations. This was, of course, only to be expected, because the bivane data model, with its relatively coarse integration steps, could not possibly predict the details of the field variations. Thus, to suppress the higher frequencies, where it was unrealistic to demand good agreement, the two sets of values were put through a suitable low pass digital filter. The type of filter employed, which was originally intended for smoothing spectral estimates, is *of* the form

$$X(K) = 0.25.X(K-1) + 0.5.X(K) + 0.25.X(K+1)$$

and, in effect, takes a running mean of the quantity to be filtered. Further details of the method, which was originally due to HANN, can be found in BLACKMAN & TUKEY (1958).

6.4
Typical results obtained with the steady-state and oscillating plume models

6.4.1
Introduction

In practical terms, the steady-state and oscillating plume models proved rather disappointing. Neither model was capable of imitating the most important feature of all turbulent motion - its irregularity. Although the existence of this randomness was appreci ated from the outset its importance was underestimated and this resulted in the models being, frankly, rather unrealistic. More successful models of turbulent diffusion have been based on numerical techniques used in conjunction with a random number generator, e.g. THOMPSON (1971). Originally it was hoped to compare observed electric field data with that obtained from the models but in many cases this was a rather futile exercise. However, despite their inherent limitations, the results obtained from the models are of some interest and demonstrate, at least in a general way, certain features which do occur in reality.

6.4.2
The steady-state model

The electric field under the 'steady-state' plume was calculated in the manner detailed in Sec. 3.4.2. Fig. 6.5. shows results, in typical conditions, of such calculations made at various points under an ion plume. (The validity of assuming a plume configuration of this type has already been considered elsewhere and no additional comments are needed here - see Sec. 2.8.)

If the plume were treated as a line charge then the electric field would continue to increase as one moved downwind

Computed electric field values obtained with the 'steady-state' plume model
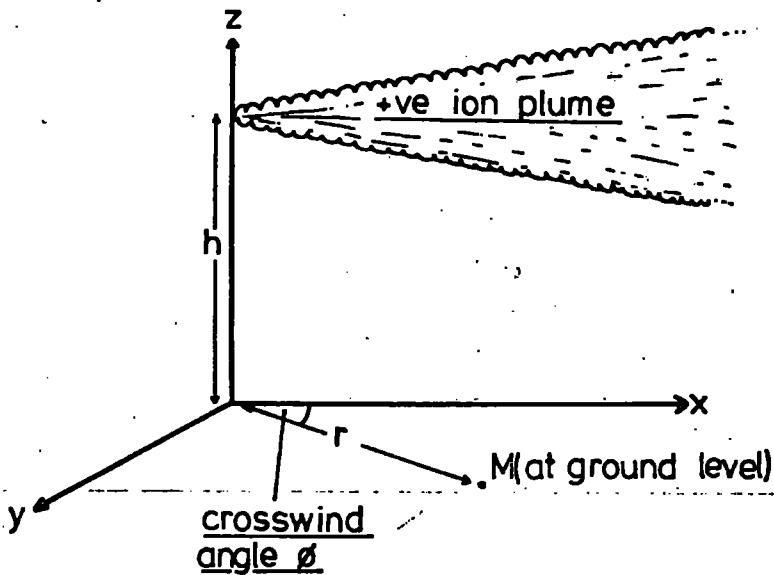
Conditions for this run:-
ion source +0,3uA 10m
wind speed   1ms^{-1}
plume dimensions were
appropriate to neutral
conditions

+ve ion plume

M(at ground level)

crosswind angle ø

crosswind angles

0°
2°
4°
6°
8°

Electric field (Kvm^{-1}) at M

downwind distance, r (m) ——➔
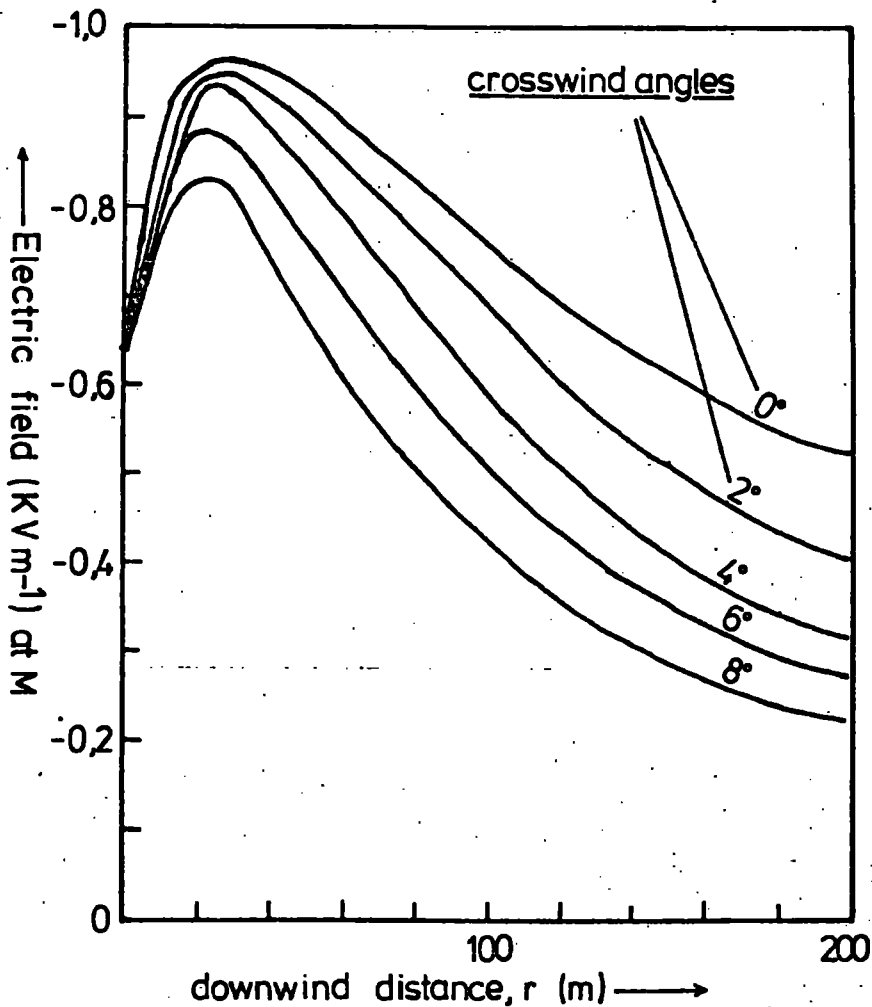
directly beneath it; however, in reality this effect must be offset against those of turbulent diffusion and electrostatic forces which tend to broaden the plume. In practice, and in the model, the combination of these various factors results in the electric field attaining a maximum value at a definite distance downwind.

It was found, after a number of computer runs with the steady-state model had been completed, that certain useful conclusions could be drawn. At any particular point, M say, the electric field E_m , for a given eddy diffusivity, depended on the source height h , the source current i and the wind speed u , in the following way

$$E_m \propto i$$
$$E_m \propto 1/u \qquad \text{VERY APPROXIMATE}$$
$$E_m \propto 1/h$$

(These relations could, in fact have been deduced on the basis of the relevant equations in Chs. 2 and 3). The main use of such relations was that they permitted electric field values to be determined, at least approximately, in other conditions without recourse to the computer.

Also of interest, though only indirectly in this work, are the values of electric field away from the surface. In these circumstances, of course, the horizontal components are no longer zero, the total electric field at any point being the vector sum of its three components. A calculation, using a steady-state model, was undertaken for a plume of the type found in stable conditions, some results being shown in Fig. 6.6. It should perhaps be emphasised again that the magnitudes of the electric field values obtained with this model

are not realistic because electrostatic expansion effects
have been ignored. However, the various trends shown in
the behaviour of the field components should persist regard-
less of the plume width. No further comments are included
here as unfortunately it was not possible to actually
measure the horizontal components and therefore comparisons
with observed data cannot be made.

6.4.3
The oscillating plume model

This model, which has been described in detail in Secs.
2.8.3. and 3.4.4., was an attempt to simulate the looping
plume characteristic of unstable conditions. Thus, in the
sense that the computed electric field was not constant but
varies with time, this model was more realistic than the
steady-state model. The main weakness of the model was, as
expected, the omission of crosswind and vertical diffusion
in the modelled plume. The importance of this factor was
appreciated at the outset, but it was estimated that a single
computer run, incorporating these diffusive effects, might
take longer than one hour. Unfortunately, such amounts of
computing time were not easily available and therefore the
limitations of the model had to be accepted. (Perhaps this
is an appropriate point to emphasise that the concept of a
looping plume with crosswind and vertical diffusion is
thought to approximate quite closely to reality).

A set of results which typify those obtained using this model
are now discussed. The values of electric field underneath a
plume executing vertical loops are shown in Fig. 6.7. The
electric field is, of course, a varying quantity and, in con-

Some results obtained using the 'steady-state' plume model
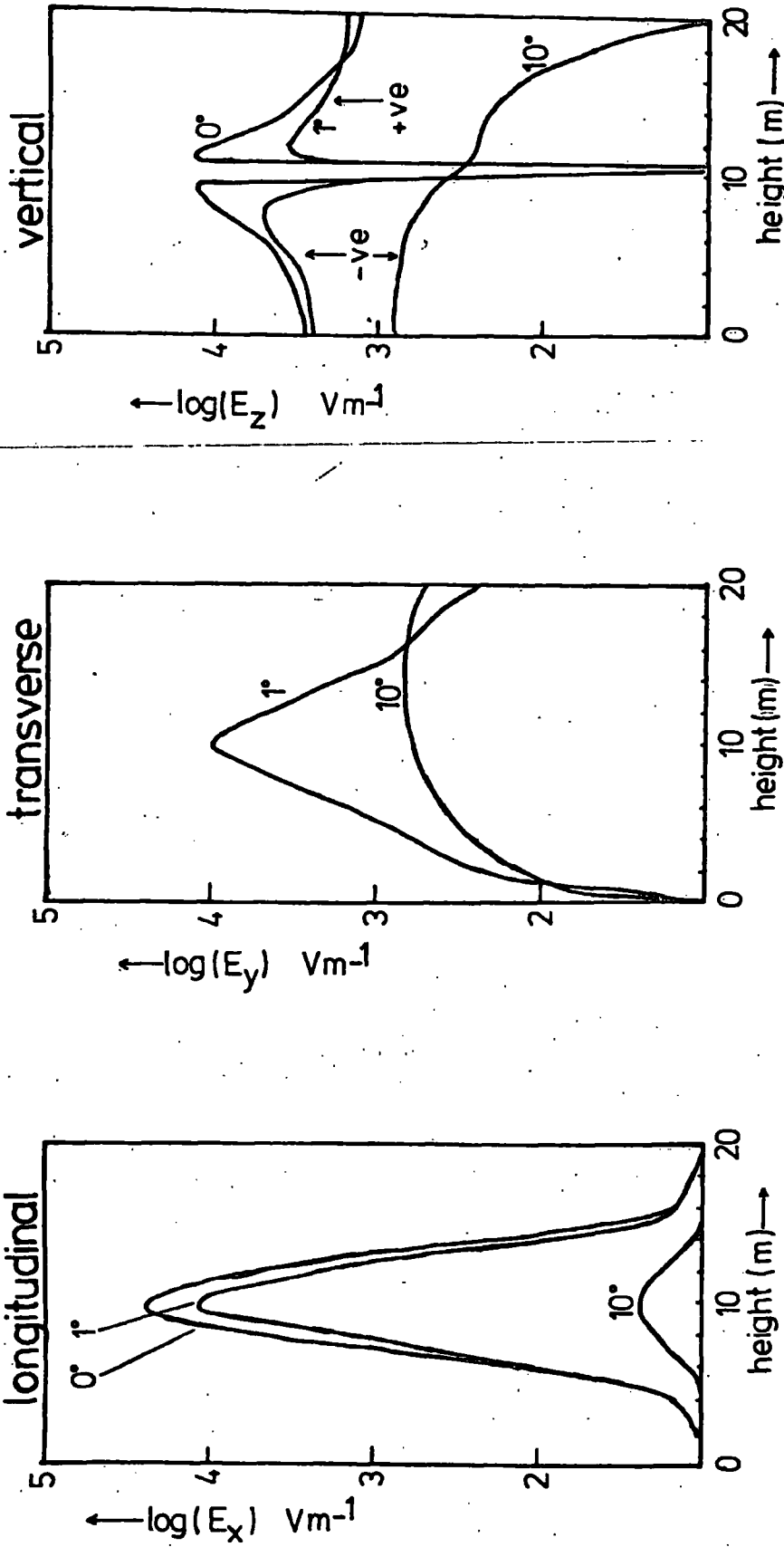
Computed electric field components near an ion plume

ELECTRIC FIELD VALUES ARE AT 100m DOWNWIND. CROSSWIND ANGLES AS SHOWN.

ION SOURCE: 1μA at 10m WIND SPEED 1ms⁻¹

PLUME DIMENSIONS APPROPRIATE TO STABLE CONDITIONS

Some typical results obtained using the 'oscillating plume model' (see also fig 2.5)

This run simulated a plume with vertical loops. Values ascribed to the various parameters were:-
$A_y=0, A_z=0{,}17, F_y=0, F_z=0{,}03, U=1ms^{-1}, H=10m$, 1µA ion source
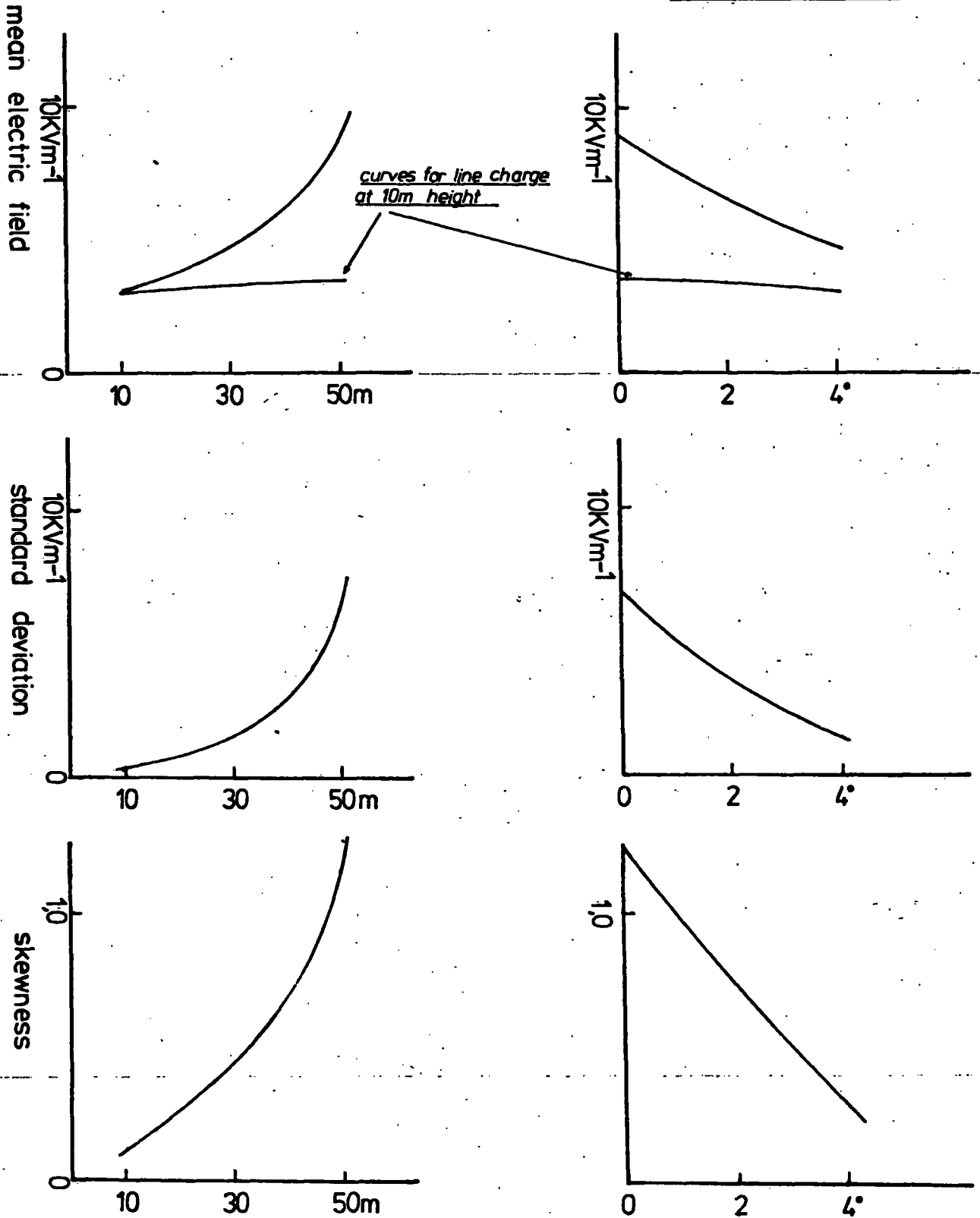
sequence, we may calculate its mean, standard deviation and other statistical quantities. In this example the field has been computed at 10, 30 and 50 m downwind of the ion source and also for crosswind angles of 2° and 4° at the 50 m position. The value of the constant A_z was chosen so as to make the plume descend, in its looping action, to within 1.5 m of the 50 m downwind point. In the model the amplitude of the oscillations was arranged to increase linearly with downwind distance and therefore at 10 m and 30 m the amplitude is correspondingly smaller. The efect of this increasing amplitude of the loops is shown by the dramatic increase in the mean, standard deviation and skewness (see Sec. 6.2.2.5.) of the electric field as one progresses downwind. It is, of course, not very meaningful to enquire how the electric field behaves at greater distances downwind, where the plume may reach the ground, because at that stage the concept of a line charge becomes totally unrealistic.

Many of the features described above actually occur in practice and further reference to them will be made in the next chapter. The magnitudes of the electric fields predicted, even taking into consideration the $1\mu A$ source used in the model, are larger than was measured. There can be little doubt that the reason for this was that the charge was too localized in the model. This again emphasises the need for the inclusion of crosswind and vertical diffusion in the model.

Chapter 7: THE SERIES I EXPERIMENTS

7.1
Introduction

The field work had to be conducted with portable equipment because there was no suitable site at which to install a permanent system. The lack of a permanent installation required that all equipment had to be erected before and dismantled after each series of experimental runs, a complex and lengthy procedure. Normally it took about an hour to erect the mast, attach the meteorological instruments and ion generator, and place the field mills at their allotted positions. Early field work was undertaken at the Oxen Law site (see Ch. 1.), approximately 20 miles from the University, and thus a further half hour was necessary to transport the equipment to this destination.

Once operational conditions were established, five or six field runs would be attempted. Each recording only lasted 24 min , but in between runs, field mills might have to be re-sited, or the height of the ion generator altered. As a result of these, and other, adjustments the total time required to perform the field runs was sometimes as much as five hours.

The complexity of the experimental system at times required the expenditure of considerable effort, both mental and physical, to assure its correct functioning. It was found that these human factors were restricting the amount of field work that could be done and to ameliorate this an experimental site nearer the University was sought. Later field work was,
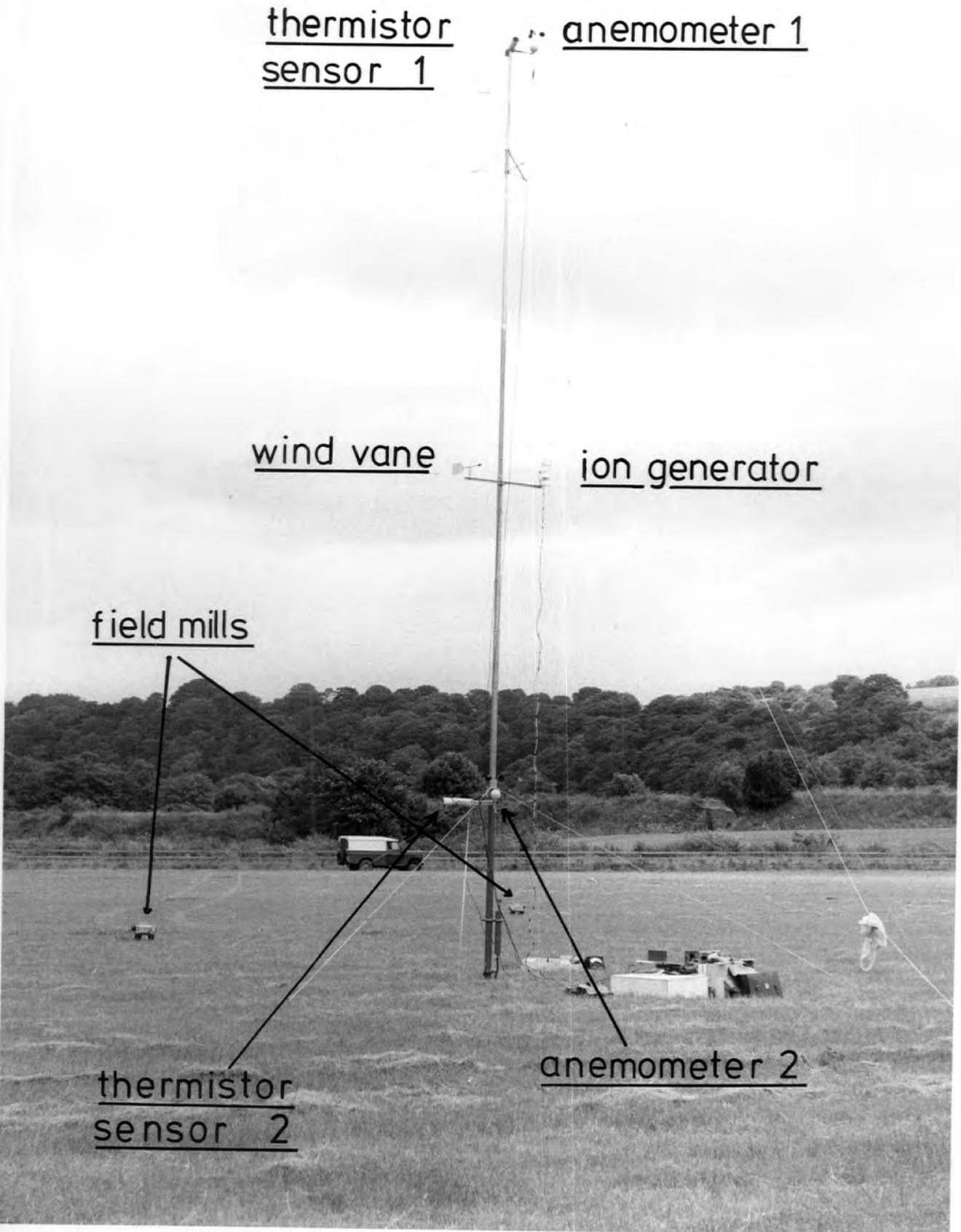
thermistor sensor 1   anemometer 1

wind vane   ion generator

field mills

thermistor sensor 2

anemometer 2

FIELD WORK IN PROGRESS   1

in fact, carried on in one of the playing fields at the University Sports Centre, Maiden Castle, (see Ch. 1.). In many ways this was an ideal site being only half a mile from the laboratory. However, one or two minor disadvantages did become apparent and these are mentioned in the next section.

7.2
The nature of the experiments and choice of weather conditions

The aims of the experiment were quite simple, being first to explore the electric field in the vicinity of ion plumes and then secondly to relate these results to the prevailing micro-meteorological conditions.

The ion source, anemometers and differential thermistor sensor were placed at standard heights on the Clarke mast. In practice the standard heights were 9 m and 2 m, whilst the ion generator could be attached at any of three heights, namely 9 m, 5 m and 2 m. The retracted mast, 2 m high, was held vertically by guy ropes and the various items of equipment bolted to it. The mast was then extended to its full height by means of the hand pump provided and the top guy ropes secured. After this the anemometers, thermometers and ion source were connected into their appropriate electronic systems and functional checks performed.

It was found very helpful to attach a small wind vane to the mast at the same height as the ion generator. Observation of this vane enabled the local wind direction to be accurately determined thus facilitating the correct placing of the field mills. Generally the mills were set in arcs or lines downwind of the ion source, the exact arrangement depending both on the

meteorological conditions and the particular objectives of the experiment. As a rule, field mills were not placed more than 100 m from the source, because, although ions could certainly be detected at much greater distances, the time involved in setting out cables of such lengths would have proved detrimental to the experiments as a whole.

A typical experiment is shown in progress Fig. *P10* , whilst additional details are presented in Sec. 6.1.1.

During the period 21st April 1972 to 10th August 1972, forty-seven 24 min. data recordings were made - mostly at Maiden Castle. Nine of these recordings were of the natural potential gradient whilst the remainder was concerned with the ion plume.

Ideally it was hoped to obtain results in as wide a variety of meteorological conditions as possible. There were however certain limitations to be considered, both in the performance of the equipment and in the technique itself. In particular, field work was impossible in rain or snow for reasons explained in Ch. 4. The equipment, notably the ion source, could be damaged by anything more than a light shower and therefore this eventuality had to be avoided. Consequently all field work was restricted to lightly clouded conditions so that there was little likelihood of any precipitation. Choosing such conditions also meant, conveniently, that the natural potential gradient variations would be small and therefore not interfere with the experiments. Occasionally, at the Maiden Castle site, diesel fumes from local land reclamation operations resulted in large fluctuating potential gradients being

measured (see also OGDEN (1967)). There was no choice but to abandon field work in these circumstances.

Positive ions were used throughout this series of experiments to avoid any ambiguities in the sign of the potential gradient downwind of the ion source. (The results of the Series II experiments indicate that the behaviour of ions of both signs is substantially the same). In many later experiments the natural potential gradient was not actually recorded because, if a field mill were reserved for this task, only three would remain for recording under the ion plume. Thus, in order to make maximum use of the equipment, all four field mills were sited for recording under the plume, the natural potential gradient being monitored at the beginning and end of each run to ensure that it was close to its normal value.

The complicating effects of topography and changing synoptic conditions were mentioned in Ch. 2. In practice by far the largest problem was that caused by the arrival of a sea breeze, the onset of which, usually about noon, could ultimately change the wind direction by as much as 90°. Further, the character of the sea breeze was such that after its arrival the atmosphere tended to be less unstable than previously. This disturbed the continuity of any experiments because, under these circumstances, the field mills had to be completely re-sited. Later, as experience was gained, the likelihood of a sea breeze could be anticipated and, by deploying the equipment appropriately, any irritating effects minimised.

The Summer of 1972, during which this field work was conducted, was rather cloudy and consequently stable and unstable condi-

tions occurred only infrequently. Nevertheless, some quite successful field runs were performed during unstable conditions, but obtaining results in stable conditions presented something of a problem. It will be recalled (see Sec. 2.6.) that stable conditions usually occur at night. The operation of the equipment in darkness would have been extremely difficult and was not seriously contemplated. Despite these obstacles, some useful data was obtained late one evening in thoroughly stable conditions.

7.3
Presentation and Discussion of the Experimental Results

7.3.1
Initial Considerations

The field data was processed in accordance with the analytical procedures described in the previous chapter, two computer programmes (DATAPROG and SUPPROG) being written for this purpose. Statistical techniques were of undeniable value as their use enabled a particular run to be precisely characterized and thus compared with other field runs. However, such methods did not necessarily convey to best advantage certain features present in the records themselves. It was thought preferable therefore, by way of introduction, to briefly describe those important and recurrent characteristics which were immediately apparent even from a visual examination of the records. It is hoped that the results of the more complex analyses will then be more easily understood once the reader has a clear idea of the nature of the variations themselves. Unfortunately, space does not permit the inclusion of entire records here but selected portions are presented in Figs. 7.1. and 7.2.

SIMULTANEOUS POTENTIAL GRADIENT RECORDS AT FOUR POINTS
IN A LINE DOWNWIND OF THE ION SOURCE
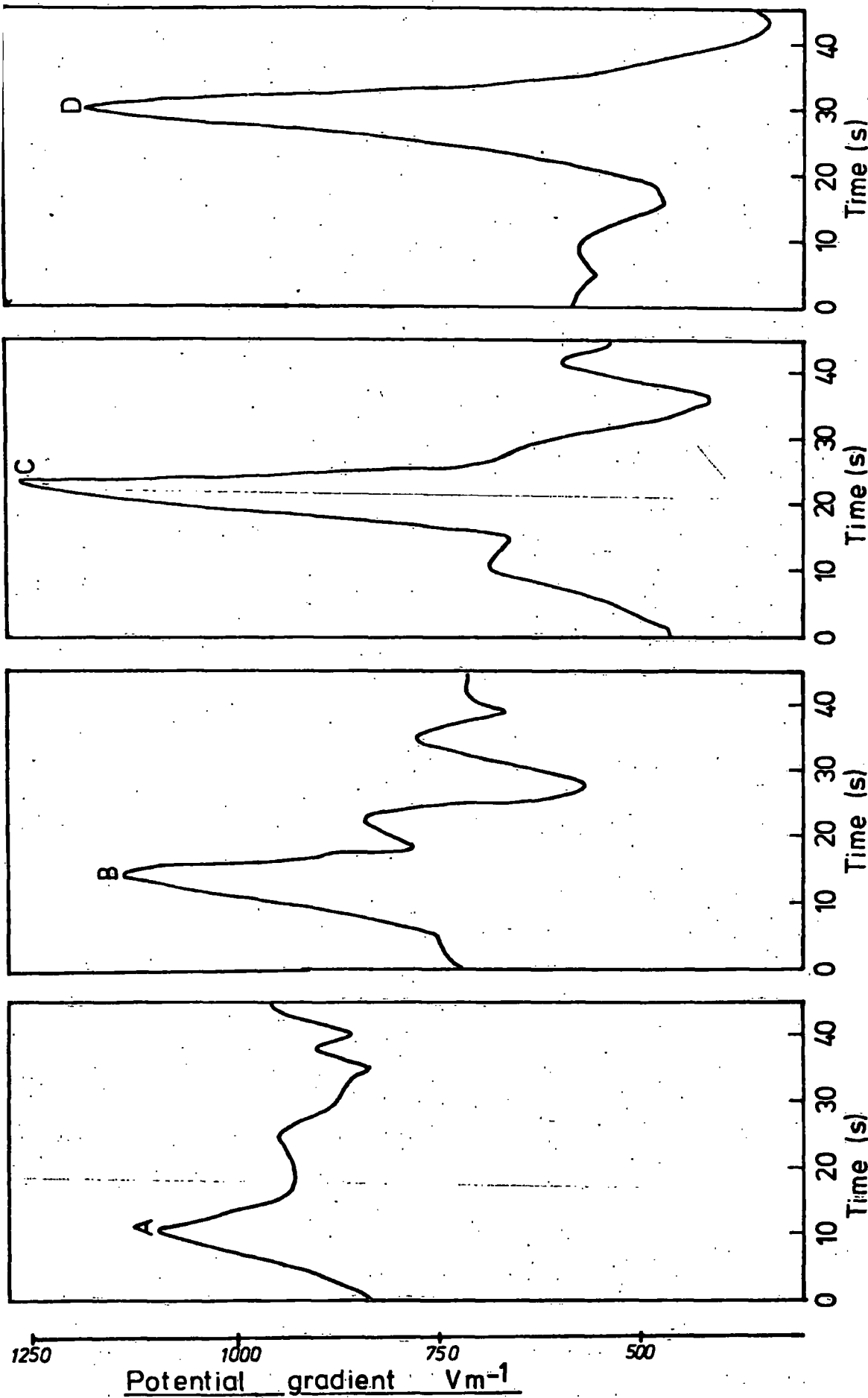
Mean wind speed 4.4 ms^{-1}

90m downwind

60m downwind

Ion source height 9m

30m downwind

15m downwind

Part of 8.7.72 (2)

Potential gradient Vm^{-1}

1250   1000   750   500

Fig. 7.1. shows a series of simultaneous potential gradient
records taken at various distances downwind of the ion source.
In this run (No. 4, 8.7.72) the ion source was at a height of
9 m, whilst field mills were placed at distances of 15, 30,
60 and 90 m downwind. We note that, in the record taken at
15 m from the source, a small peak (A) of potential gradient
occurs 11 s after recording commenced. It should be remarked
that the maximum value of potential gradient attained here,
1100 Vm^{-1} , was far in excess of the natural value.

We now make the reasonable assumption that, whatever the
charge distribution was that caused the peak A to occur, that
charge would inevitably be blown along by the wind. This idea
was, in fact, introduced in Ch. 3 and the reader is referred
there for further details. In accordance with this assump-
tion we might reasonably expect similar peaks (B, C and D) to
occur in records taken at greater distances downwind, but of
course, at correspondingly later times. We can estimate the
velocity of travel of the charge parcel on this basis, and in
this case, it was found to be 4.4 ms^{-1} . The fact that this
figure is <u>exactly</u> the same as the mean wind speed for the run
is fortuitous but the agreement does indicate the plausibility
of the above hypothesis. Also of interest is the fact that
the peak attains a maximum size in the record taken 60 m down-
wind of the source. It seems from this that the charge parcel,
as well as travelling along with the wind, appears to change
as it does so. In practice, it was thought that the parcel
moved gradually nearer the ground, possibly under the action of
image forces (see Sec. 3.5.5.), as it was blown along. Naturally
the parcel was also dispersed, both by turbulent and electro-

static agencies, as it moved downwind and therefore at greater distances the electrical effects begin to diminish.

An additional feature of relevance was the behaviour of the background, as distinct from the natural, potential gradient in these records. In fact, we can observe a systematic decrease in this as the downwind distance increases. This is substantially in accordance with the steady state model discussed in Ch. 6 and is, of course, a result of the general increase in ion plume dimensions as it travels downwind.

Typical results obtained with the alternative arrangement of field mills, i.e. across the width of the plume, are shown in Fig. 7.2. In this record, part of No. 3, 13.7.72, the ion source was at a height of 4.85 m, the mean wind speed being 2.3 ms^{-1} . As anticipated in Sec. 3.6. the relationship between the potential gradient records is now quite different, although their individual character is much the same. We note that in the record of mill 3 a peak (A) occurs at the same time as a trough (A') in the mill 2 record. A similar, but more pronounced, example of this is demonstrated by the features B and B'. It is clear, that in order to produce these out-of-phase variations, the ion plume (or part of it) must have moved toward mill 3 and away from mill 2. This movement could occur in two ways. Firstly, as shown in Fig. 3.11, a horizontal loop could have passed over mill 3, or secondly, if the plume were already nearer mill 3, then the passage of a vertical loop would have produced the same effect.

SIMULTANEOUS POTENTIAL GRADIENT RECORDS AT THREE POINTS IN A CROSSWIND LINE DOWNWIND OF THE ION SOURCE

Part of   13.7.72(3)   Ion source height   4.85m

Mean wind speed   2.3 ms⁻¹
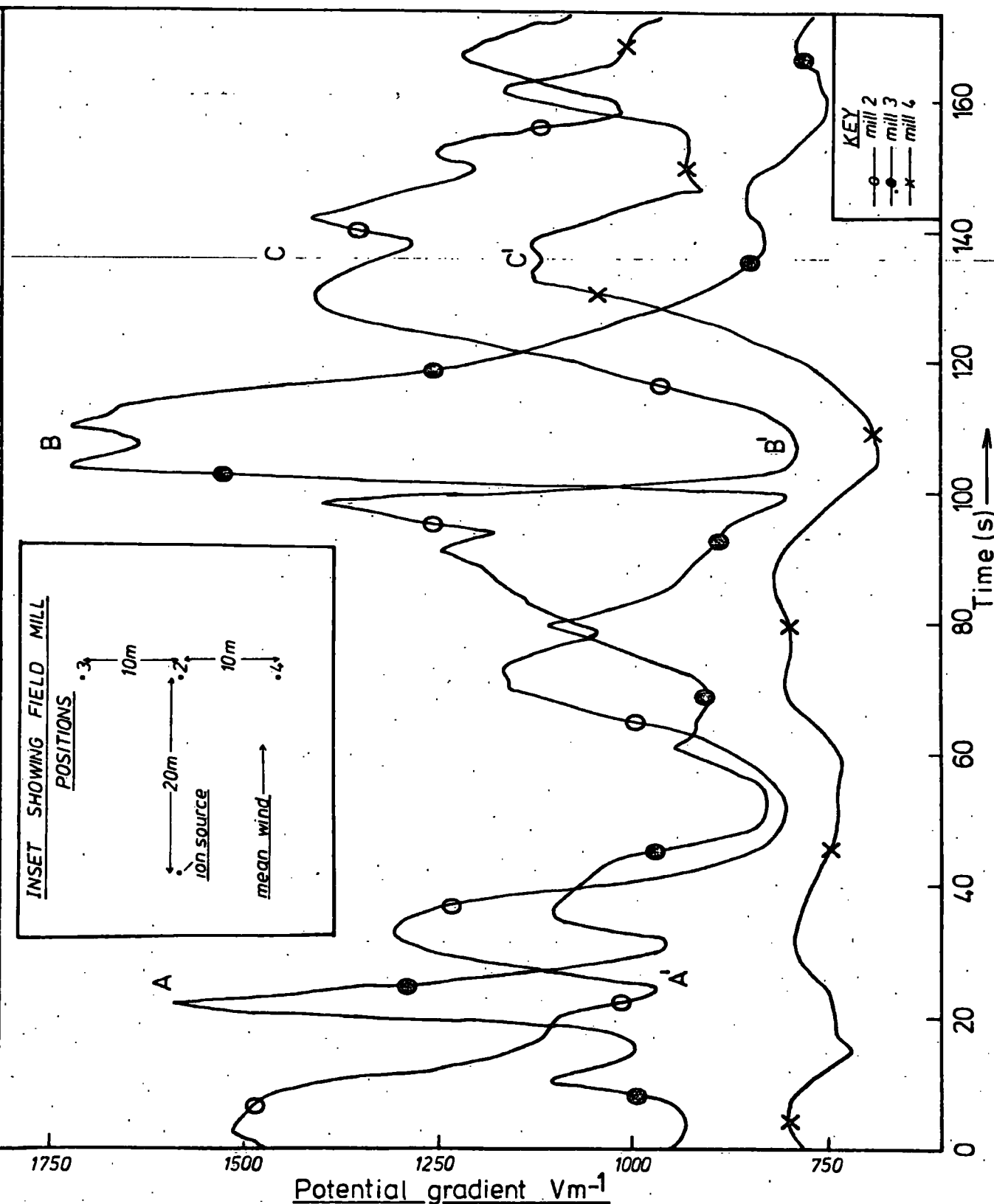
A different type of behaviour is indicated by the in-phase peaks C and C'. Here the charge parcel must have been moving nearer both field mills simultaneously and again there are a number of ways in which this could have occurred. Calculations show, however, that in order to produce these two peaks of roughly the same size, it is most likely that a charge parcel passed between field mills 2 and 4 rather than to one side of them.

Unfortunately, as can be seen, it is not possible to specify precisely the type of movement that produces these potential gradient variations, but the indications are that, because of the out-of-phase nature of some of the variations, the size of the features causing them is relatively small. The statistical analyses, to be discussed next, do, however, give a clearer idea of the size of these charge features.

7.3.2
The Statistical Analyses

7.3.2.1
Purpose of the Analysis

The main purpose of this investigation was to establish the basic features of ion plume behaviour. Consequently it was thought more appropriate to take a collective view of the statistical results rather than attempting to ascribe too much significance to any particular run. It seemed obvious that the meteorological conditions and ion source height would profoundly affect the potential gradient variations and therefore the statistical results were considered in relation to these, and other, factors. Further, the existence of the

electrostatic effects, described in Ch. 3, could also be clearly demonstrated by such an approach. The results of the statistical analyses are presented graphically in Figs. 7.3. - 7.11., verbal comments being included below.

7.3.2.2
Mean potential gradient v. distance downwind

This is shown in Fig. 7.3., distinction between runs with different source heights being made by the use of the symbols indicated. The mean values are widely scattered but, nevertheless, certain general trends are apparent. The lines, drawn by eye, indicate the overall tendency of the mean potential gradient as a function of distance downwind. Reference to Fig. 3.10. shows, that for the 9 m plume, we would not expect either image or repulsion effects to be large, except in the lightest winds, and thus the behaviour of the plume is largely determined by the meteorological conditions. The values of the mean potential gradient are, in this case, in reasonable agreement with those predicted by the steady-state model (see Fig. 6.5.) but it should be emphasised that this does not necessarily imply that the actual ion plume was in a steady state. However, when the ion source was at 2.3 m, Fig. 7.3. shows that, in winds of a few metres per second, image effects appear capable of bringing the plume down to ground level within about 50 m of the source. It is not possible to be categorical here because of the paucity of data but the results *do* seem to indicate an abrupt disappearance of the plume at about 50 m downwind.

MEAN POTENTIAL GRADIENT versus DISTANCE
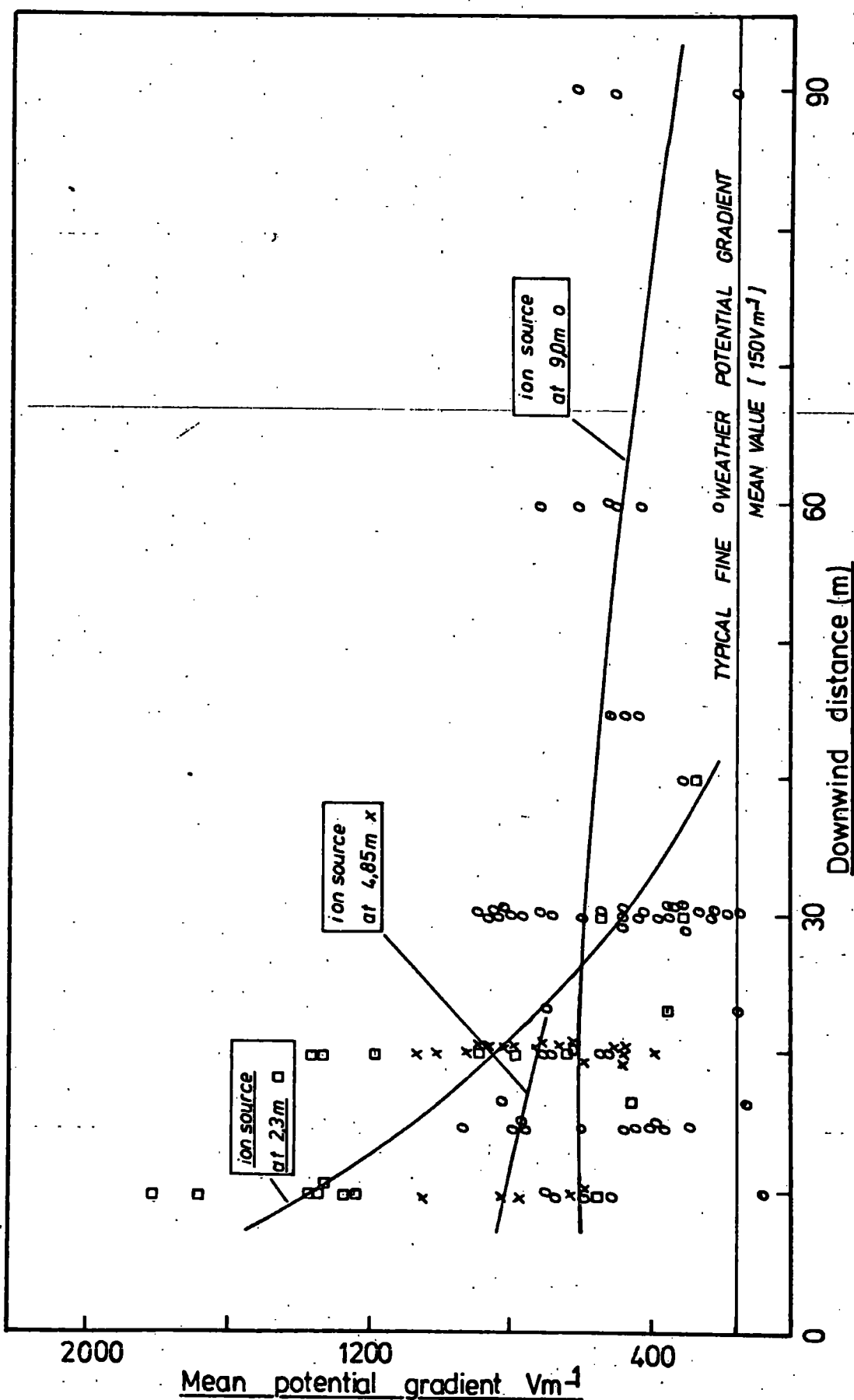
DOWNWIND FROM ION SOURCE (all runs)

ion source at 9,0m o

ion source at 4,85m x

ion source at 2,3m □

TYPICAL FINE WEATHER POTENTIAL GRADIENT

MEAN VALUE (150 Vm⁻¹)

Downwind distance (m)

Mean potential gradient Vm⁻¹

STANDARD DEVIATION OF POTENTIAL GRADIENT versus
DISTANCE DOWNWIND FROM ION SOURCE (all runs)
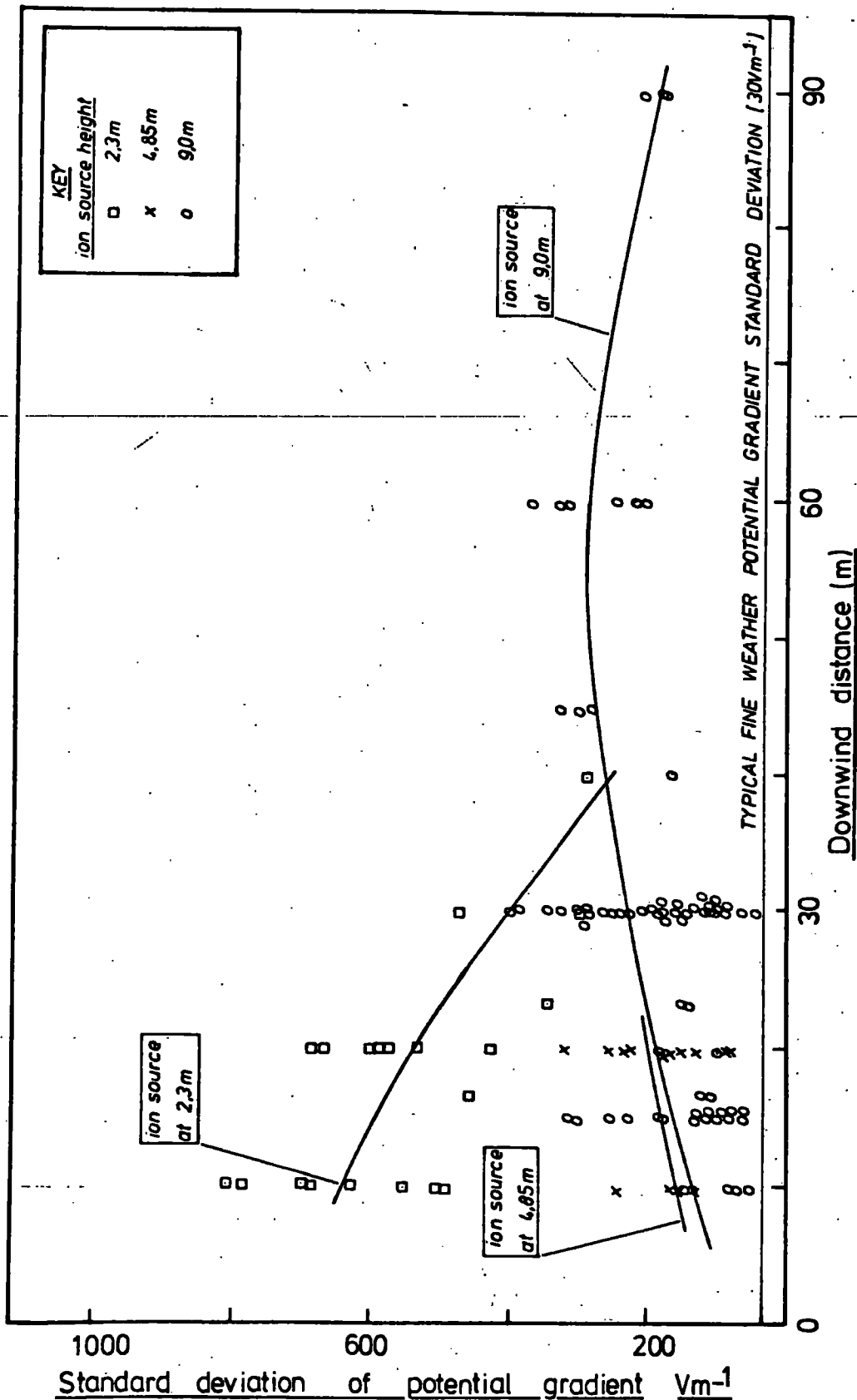
7.3.2.3
<u>Standard deviation of potential gradient v. distance downwind</u>

This is shown in Fig. 7.4., and again there is considerable scatter in the results, but as before, trends are apparent. It can be seen that, in those cases when the ion source was at 9 m, the standard deviations show a broad peak at about 50 m downwind. The existence of this peak is thought to be a result of two opposing effects. Firstly, the gradual motion of some plume elements toward the ground, caused both by image forces and certain larger scale turbulent motions (e.g. looping - see Sec. 2.7.), results in the potential gradient variations increasing in magnitude with downwind distance. Secondly, and in opposition, are the diffusive effects of turbulence and electrostatic repulsion. Thus, at a certain distance downwind, the field variations attain a maximum of intensity.

The rapid decrease of variance of potential gradient downwind of the ion source at 2.3 m is in accordance with the image effects discussed previously.

7.3.2.4
<u>Standard deviation of potential gradient v. mean wind speed</u>

This analysis, shown in Fig. 7.5., indicates a weak trend in the data obtained with the ion source at 2.3. m. It appears in this case that potential gradient variations tend to be largest when the wind speed is about 4 ms^{-1} . This can also be explained in terms of opposing effects, namely those of image forces and dilation of plume material by the wind. It was shown in Sec. 3.5.3. that the charge per unit length of the plume was inversely proportional to the wind speed. Consequently, at the higher wind speeds, the plume segments are likely to be more sinuous and dilute, and as a result, the

potential gradient variations smaller.

7.3.2.5
Standard deviation of potential gradient v. Richardson number

In contrast with previous results, this analysis, which is
shown in Fig. 7.6., displays a very marked trend. We note
that much lower standard deviations occur during unstable and
stable, *rather than* neutral, conditions. This is, in fact, a
direct result of the lessening of turbulent diffusion activity
in the stable conditions; whilst on those occasions when it
was unstable there was so little wind that any turbulence was
almost entirely thermal. Consequently, in both circumstances
the weather was very quiet and this allowed the electrostatic
effects to dominate the ion plume behaviour. It was shown in
Ch. 3 that, in very low wind speeds, these effects result in
a very broad plume being formed with very little variation of
concentration within its boundaries. We may, therefore, con-
jecture that an ion plume of this nature would not be capable
of producing large potential gradient variations.

7.3.2.6
Cross-correlation between potential gradient records at
different downwind distances

Previous reference to the evolution of plume elements has been
made when discussing the correspondence between potential
gradient peaks obtained when the field mills were arranged in
a line downwind. It is possible *to* estimate relative changes
in the charge distribution by the use of cross-correlation ana-
lysis, the results of such techniques being shown in Fig. 7.7.
Further details of the method can be found in Secs. 3.6. and
6.2. In the results here, the cross-correlations are expressed

STANDARD DEVIATION OF POTENTIAL GRADIENT AT VARIOUS

DISTANCES DOWNWIND OF THE ION SOURCE versus

MEAN WIND SPEED
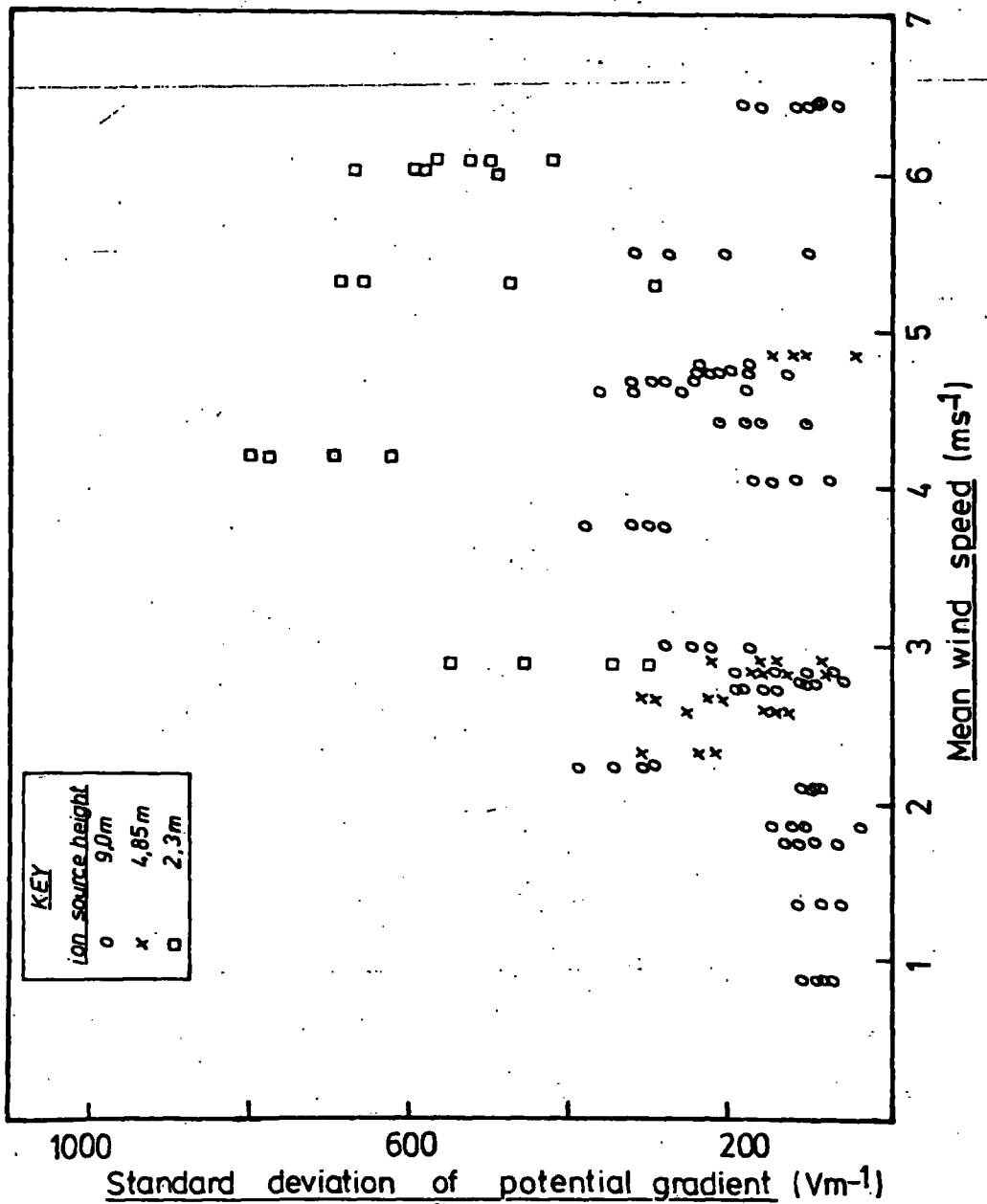
STANDARD DEVIATION OF POTENTIAL GRADIENT AT VARIOUS

DISTANCES DOWNWIND OF THE ION SOURCE versus

RICHARDSON NUMBER
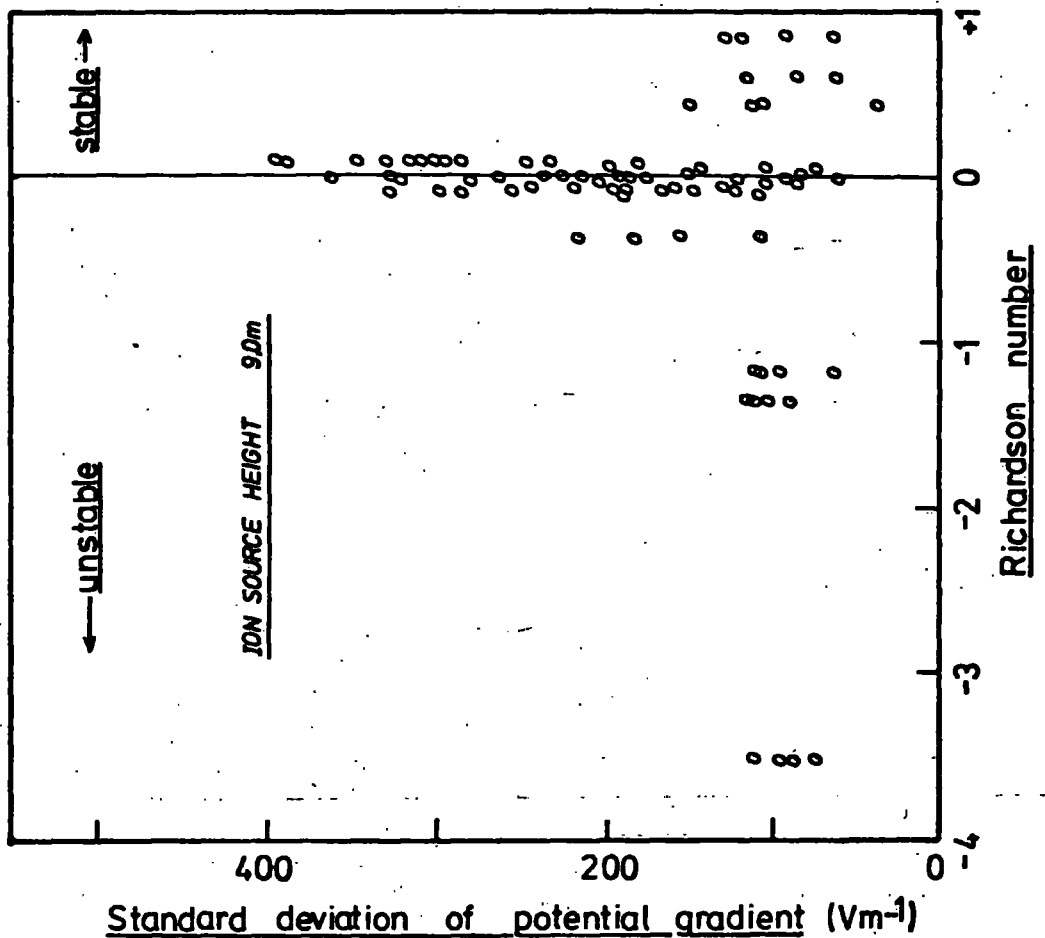
with reference to the field mill nearest the ion source, which in all cases was either 10 or 15 m downwind. The effects of time displacements between the records have been eliminated by considering the maximum cross-correlation coefficient provided that it occurred at an appropriate lag number. As we would expect the potential gradient records were almost fully correlated, about 0.99 in practice, when the field mills were together. With increasing downwind separation the cross-correlation gradually decreases, the height of the ion source having, rather surprisingly, little effect on the correlation decline. A very approximate estimate suggests that, at mill separations of greater than 200 m, the potential gradient records would be virtually uncorrelated. This does not necessarily imply that all the ions have recombined, or otherwise disappeared in this distance, but that the mixing effects of turbulence have resulted in a thorough re-distribution of the charge.

The results of the investigation of the fine weather natural potential gradient are included for reference and indicate, as anticipated, a much slower decline in cross-correlation with field mill separation. This is interpreted as being a direct result of the considerably larger scale of the natural charge elements.

7.3.2.7
Cross-correlation between potential gradient records taken at various cross-wind angles

It was only possible to draw tentative conclusions when discussing the downwind cross-correlation behaviour in the previous section. However, in this case, shown in Fig. 7.8.,

the indications are more definite. The basis of the approach
has already been described in Secs. 3.6. and 6.2. and there-
fore only the implications of the results are dealt with here.
The analyses, rather as expected, showed that, in normal condi-
tions the ion plume width was about 20°. This is, in fact,
somewhat larger than an uncharged plume and is, most likely, a
result of the electrostatic expansion effects referred to in
Ch. 3. Of particular interest is the ion plume behaviour in
unstable and stable conditions, where the much slower decline
of cross-correlation with angular separation strongly rein-
forces the opinions expressed in Sec. 3.3.

7.3.2.8
Relation between time-lag at maximum cross-correlation, wind
speed and separation distance of field mill pair

It was pointed out in Sec. 3.3. that certain features of the
potential gradient records were the result of charge parcels
being blown along by the wind. One may investigate this in a
more rigorous way by considering the relationship between the
time lag at maximum cross-correlation, wind speed and mill
separation. Such an analysis, depicted in Fig. 7.9., indi-
cates conclusively that the potential gradient variations were
caused either by features of the entire ion plume or plume
segments travelling along with the wind.

7.3.2.9
Potential gradient variance spectra

Although a considerable number of variance spectra were computed,
the results, though interesting, did not reveal as much as was
hoped. The data was passed through a digital high pass filter,
described in Sec. 6.3.4., prior to spectral analysis in order
to remove any low frequency trends that might have been present.

THE CROSS-CORRELATION BETWEEN POTENTIAL GRADIENT
RECORDS TAKEN AT VARIOUS DISTANCES DIRECTLY
DOWNWIND OF THE ION SOURCE (VARIOUS RUNS)

KEY
ion source height
o 9,0m
□ 2,3m

TYPICAL FINE WEATHER POTENTIAL GRADIENT BEHAVIOUR

Separation between field mill pair (m)

Cross-correlation coefficient maximum
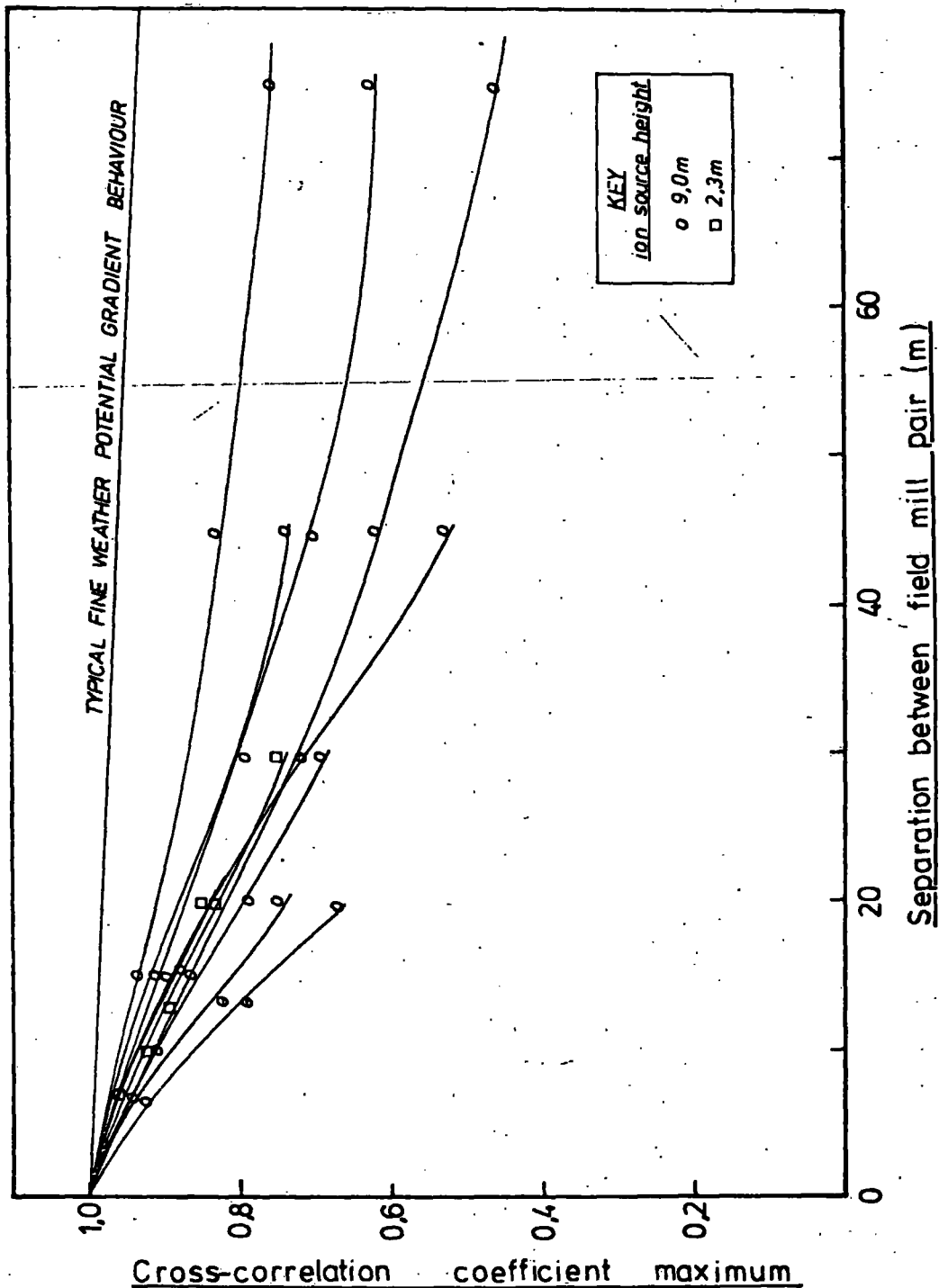
THE CROSS-CORRELATION BETWEEN POTENTIAL GRADIENT RECORDS TAKEN AT POINTS WITH VARIOUS CROSSWIND ANGULAR SEPARATIONS
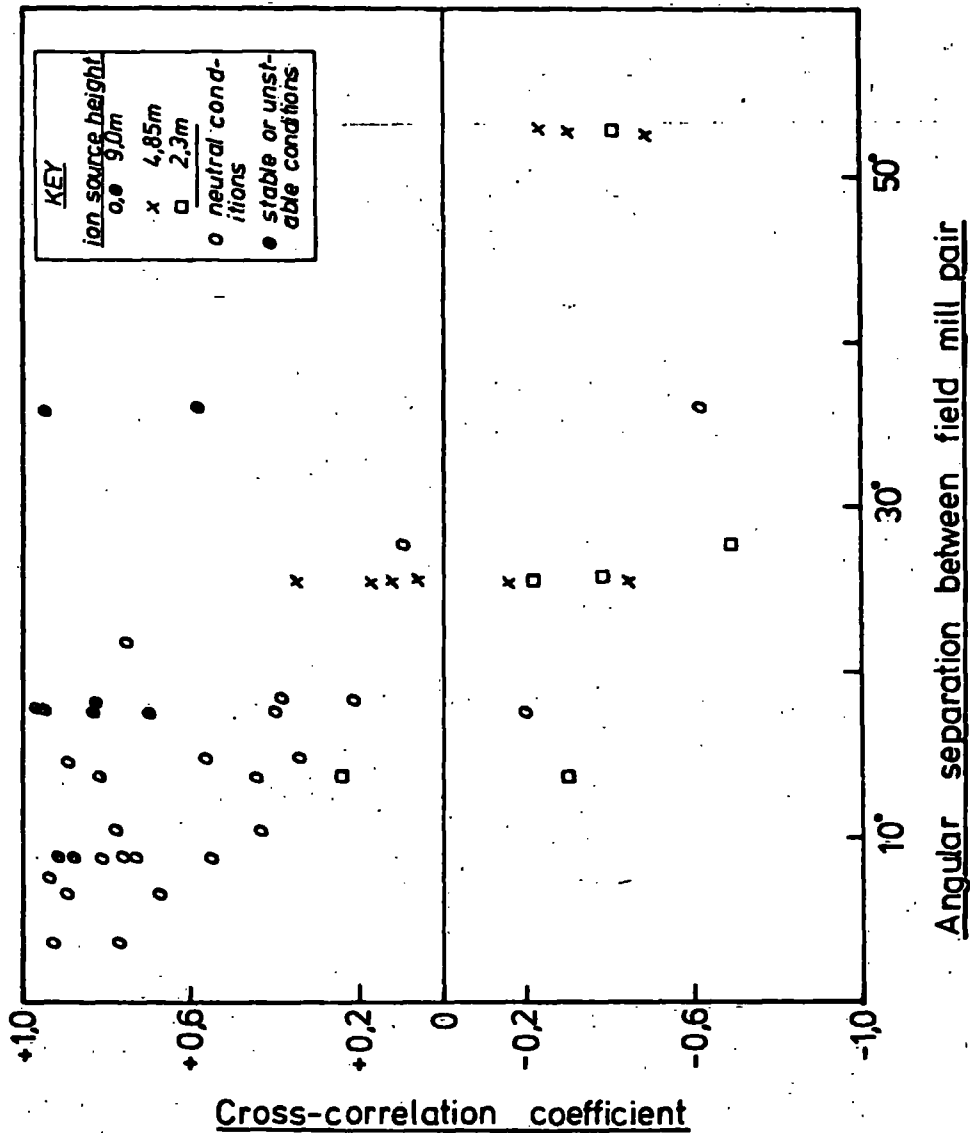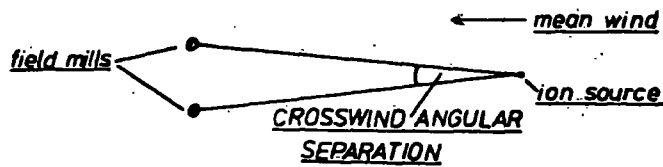
THE RELATION BETWEEN TIME-LAG AT MAXIMUM CROSS-CORRELATION, WIND SPEED AND SEPARATION DISTANCE OF FIELD MILL PAIR (Field mills directly downwind of the ion source)

Time lag for maximum cross-correlation *multiplied by* mean wind speed for run, (m)
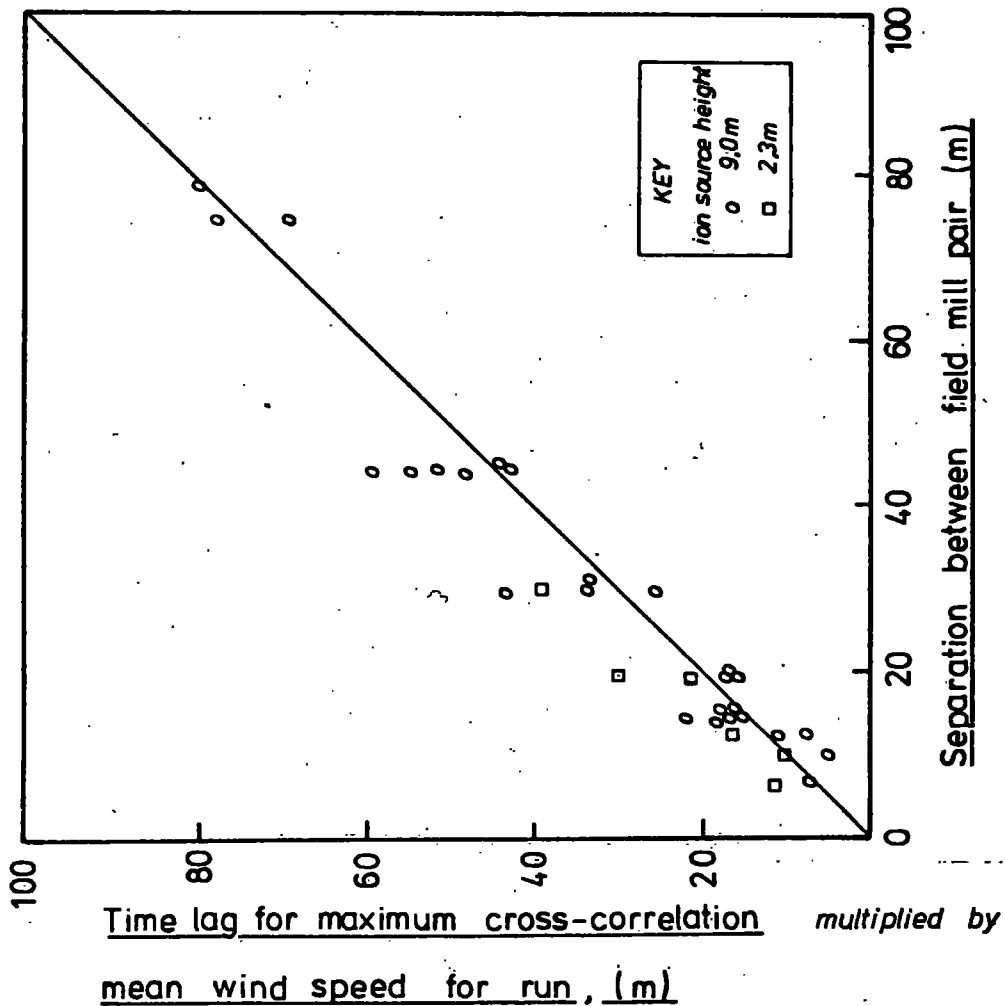
Typical results are shown in Fig. 7.10. and these bring out clearly the considerable effects that the plume has at all frequencies. The effect of the ion source height on the variance spectrum is also shown, indicating that the potential gradient variations are larger throughout the frequency range with a lower source.

A feature not revealed by the spectra was a tendency, in similar conditions, for the autocorrelation of the potential gradient to fall off faster when the ion source was lower. This implied the presence of relatively more high frequency energy in that case and follows directly from the elementary reasoning regarding moving charges presented in Sec. 3.3. It remains obscure why this point is not evinced by the variance spectra.

Finally, it should be mentioned that there is still a considerable variance contribution at the high frequency limit of the spectra and therefore it would be advantageous if the frequency response of the field mills and recording system could be extended in future investigations.

7.3.2.10
Potential gradient coherence and phase spectra
Typical spectra are shown in Fig. 7.11. not because they convey any new information but rather the spectra indicate the complexity of the processes operating. Despite the intricacy of the spectra, certain general features can be distinguished. Firstly, the coherence was greater at all frequences when the field mills were closer together and also, in that case, it fell-off more slowly with frequency., Secondly, the phase

difference increased much more rapidly in the case of the widely separated mills. These general trends can, in fact, be deduced from simple geometrical arguments but the complex nature of the actual spectra was thought to be a result of two additional factors. On *the occasion shown* a very wide variety of eddy sizes was present in the wind and this would naturally result in there being a similarly sized assortment of ion plume segments moving downwind. Further, whilst the plume segments were travelling between the field mills, the action of turbulence was constantly re-arranging the ion distribution within them.

7.3.2.11
Skewness and Kurtosis analysis

The potential gradient records were subjected to the skewness and kurtosis analysis proposed in Sec. 6.2.2.5. The skewness of the potential gradient under the ion plume was invariably a small positive value which did not vary systematically with the meteorological conditions, ion source height or any other parameter. The sign of the skewness was a direct result of the fact that a positive ion plume had been used in this investigation. Inspection of the potential gradient records indicates that, although occasionally highly skew peaks do occur, it seems most likely that, statistically speaking, these peaks would be masked by the large number of small and much less skew peaks present in most of the data.

The result of the kurtosis analysis was similarly inconclusive.

Typical potential gradient variance spectra

THESE SPECTRA WERE OBTAINED IN SIMILAR

METEOROLOGICAL CONDITIONS AND ARE

THEREFORE COMPARABLE

Variance spectral density $(V^2 m^{-2} Hz^{-1})$

*ion source height 2.3m
field mill 10m downwind
10.8.72(5)*

*ion source height 9.0m
field mill 10 m downwind
16.6.72(3)*

*TYPICAL FINE WEATHER POTENTIAL
GRADIENT BEHAVIOUR 23.5.72(4)*

Frequency (Hz)
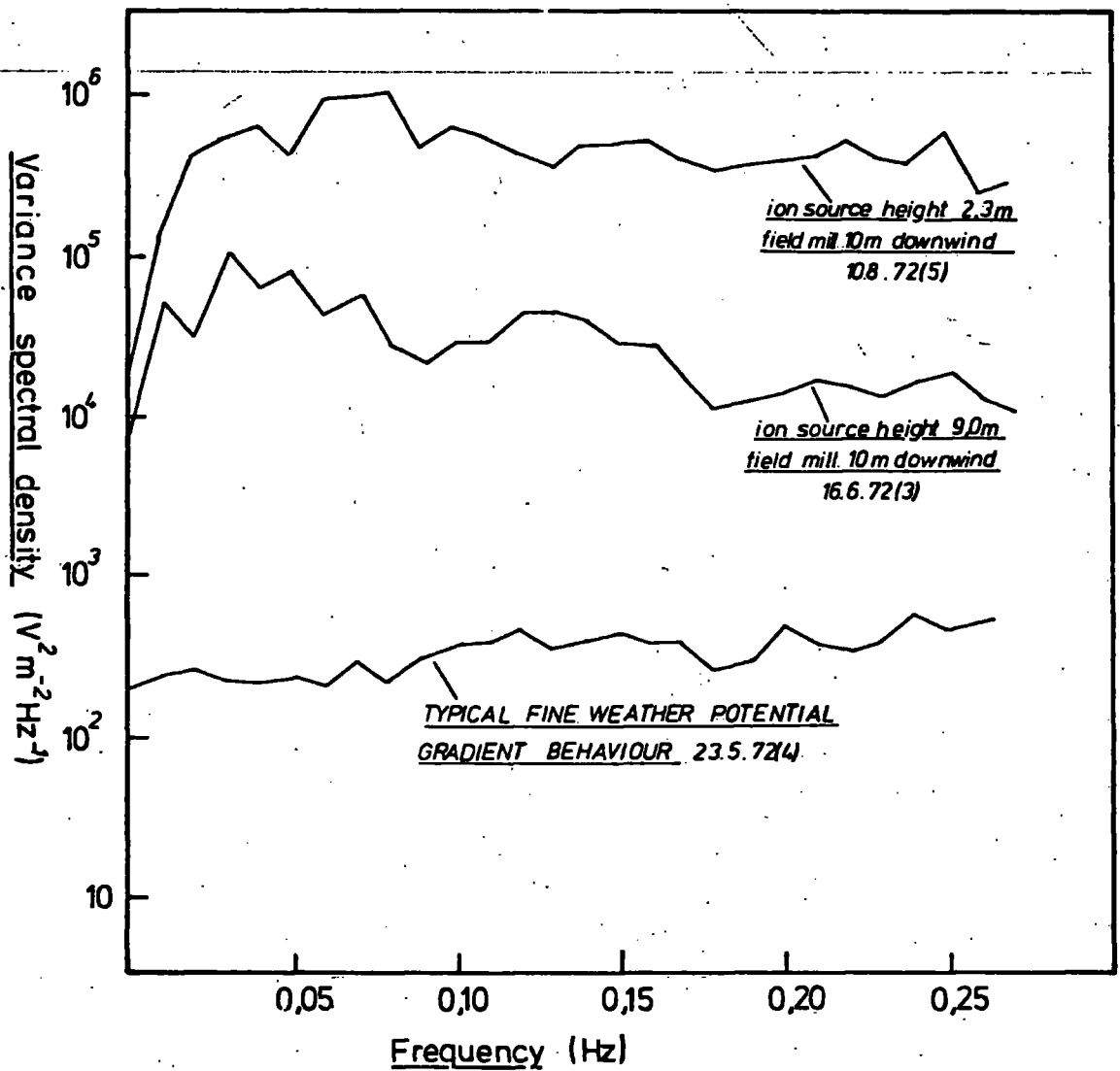
Coherence and phase spectral analysis of potential gradient records
obtained from field mills at various distances downwind of the ion source

ION SOURCE HEIGHT 9,0m
5.6.72 (4)
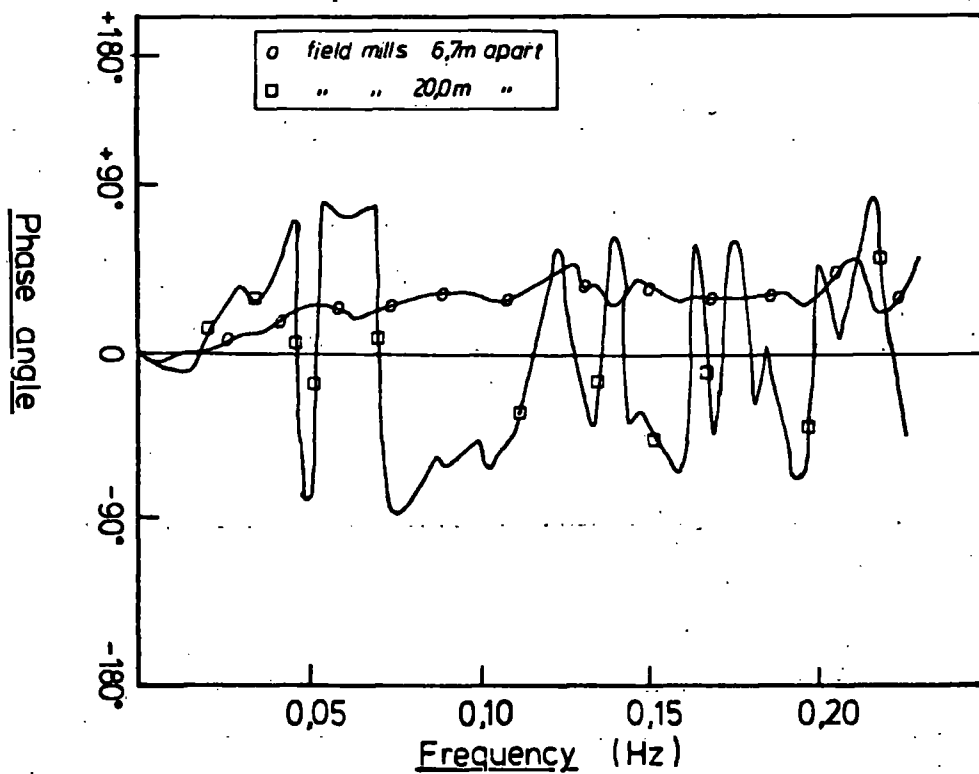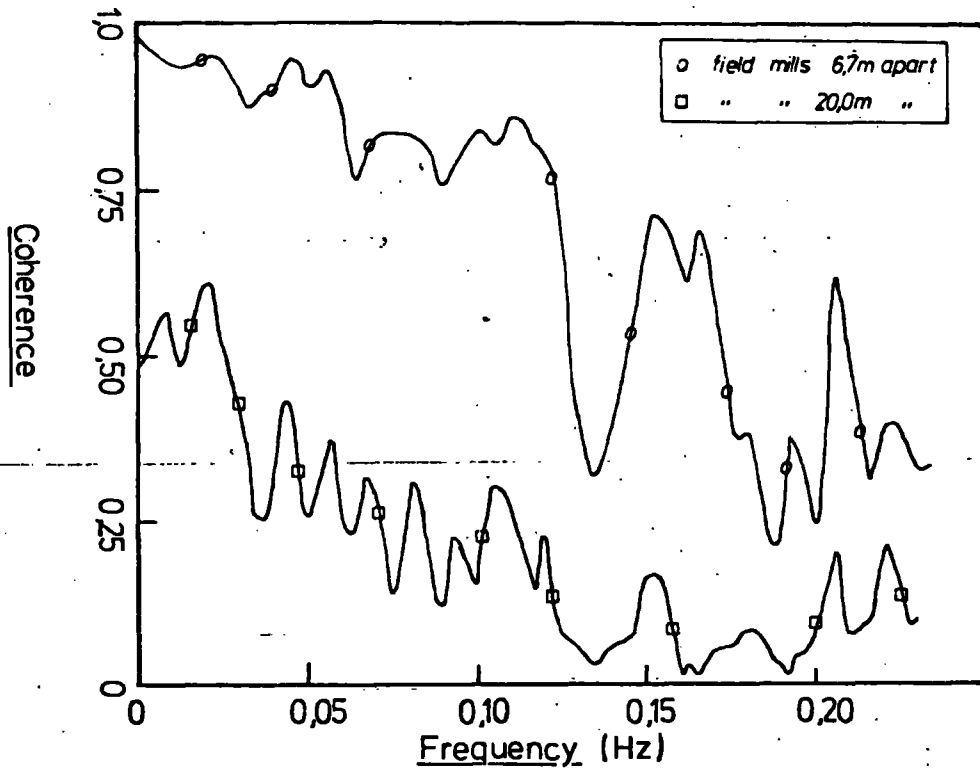
7.4
Criticisms and Conclusions

The results indicate that the potential gradient variations are caused by a haphazard sequence of charge distributions passing over the measuring point. In certain conditions it would appear that portions of the ion plume become virtually detached from the main system. These charge parcels are capable of maintaining their identity over considerable distances and result in characteristic electric field patterns as they pass over an array of field mills. Cross-correlation analysis has indicated that these detached portions are of quite small size - typically a few metres across. The configuration of the ion plume and the behaviour of the detached portions is largely controlled by the meteorological conditions, as are the characteristics of a smoke plume. Two important exceptions to this must be noted however. Firstly, ions released at a low level (less than 2 m) are rapidly attracted to the ground by images forces and presumably absorbed therein. Secondly, in very light winds, less than 3 ms^{-1} or so, ion plume behaviour is dominated by the electrostatic effects discussed in Ch. 3.

It was clear at the outset that the Series I experiments would only provide general data on the ion plume. In particular, the instantaneous ion plume configuration could not be ascertained and thus the details of the charge distribution were not known. The Series II experiments, using the bivane, largely resolved this difficulty.

Chapter 8: <u>THE ION COLLECTOR, SERIES II AND OTHER RESULTS</u>

<u>8.1</u>
<u>Introduction</u>

The experimental results presented in the previous chapter
enabled one to make various, rather general, deductions
about ion plume behaviour. It would obviously be useful
if a more penetrating technique were available to investi-
gate these plumes. Reference has already been made to
bivane techniques and thus the justification for the choice
of this method is not discussed here. Bivane readings taken
near the ion source were used to predict the changing ion
plume configuration, from which values of the potential
gradient were evaluated at various points and compared with
those actually measured. Certain shortcomings, both in the
equipment and the bivane data model, became apparent, and, in
a further series of experiments, the predicted plume configu-
rations were checked against results obtained directly from
cine photography of a smoke plume.

Two related investigations were also conducted. The region
near the source, that is within 10 m, was explored with the
ion collector, whilst field mills set at distances of up to
1/2 km downwind were used to determine the "long-range
behaviour" of the plume.

8.2
The Series II (Bivane) Results

8.2.1
General Remarks

The arrangement of apparatus in the field was broadly similar to that of the previous series of experiments. The main difference, of course, was the inclusion of the recording bivane near the ion source (see Sec. 6.1.1.). Certain difficulties had been experienced from sea breezes at Maiden Castle and consequently the Series II experiments were conducted at Oxen Law. (As these experiments were performed in the Autumn the much weaker insolation would probably have caused little difficulty with sea breezes anyway.)

Thirteen 24 min. data tapes were recorded on two slightly unstable clear days in October 1972. The predicted and measured values of potential gradient downwind of the ion source were then compared statistically. However, inspection of the graphical records also produced by the computer indicated that much of the disagreement between the values was attributable to the short-period variations. In this context the term short-period refers to variations lasting no longer than two or three seconds. The sampled nature of the bivane data implied it was clearly impossible for the computer model to predict these short-term variations accurately. In order to obtain a more realistic assessment of the value of the model, the predicted and actual potential gradient data was therefore passed through a low pass digital filter prior to statistical analysis. Before discussing these results, however, we shall consider by way of introduction, a typical section of potential gradient data obtained during this series of experiments.

Discussion of a Section of Typical Potential Gradient Record

Fig. 8.1. shows part of a record obtained 10 m downwind of the ion source which, on this occasion, was at a height of 5 m. The predicted and actual potential gradient variations are shown, the nature of the records being much the same as those presented in the previous chapter. The overall agreement between the predicted and actual values is self-evident and, with some relatively minor exceptions, this was so in most of the other records. Certain features are worth noting, however. Firstly, nearly everywhere on this record, the predicted values are somewhat less than the actual readings, although the magnitude of the variations is much the same. The virtually constant difference is attributed to the presence of the natural potential gradient which is, of course, superimposed on any values measured near an ion plume. The natural potential gradient, as monitored by a field mill placed well upwind of the ion source, was found to be about 250 Vm^{-1} , this figure according well with the difference between the predicted and actual data. Secondly, this record, which has not been filtered, exhibits the discrepancies in the short-term variations referred to previously.

To illustrate the nature of the ion plume motion causing the potential gradient variations two computed configurations are shown in Figs. 8.2. and 8.3. In these figures small black dots have been used to indicate the positions of successive plume elements, whilst the lines joining the dots depict the geometry of the plume as a whole. The position coordinates were obtained with the bivane data model. It should be remembered that in the calculation of potential gradient with this
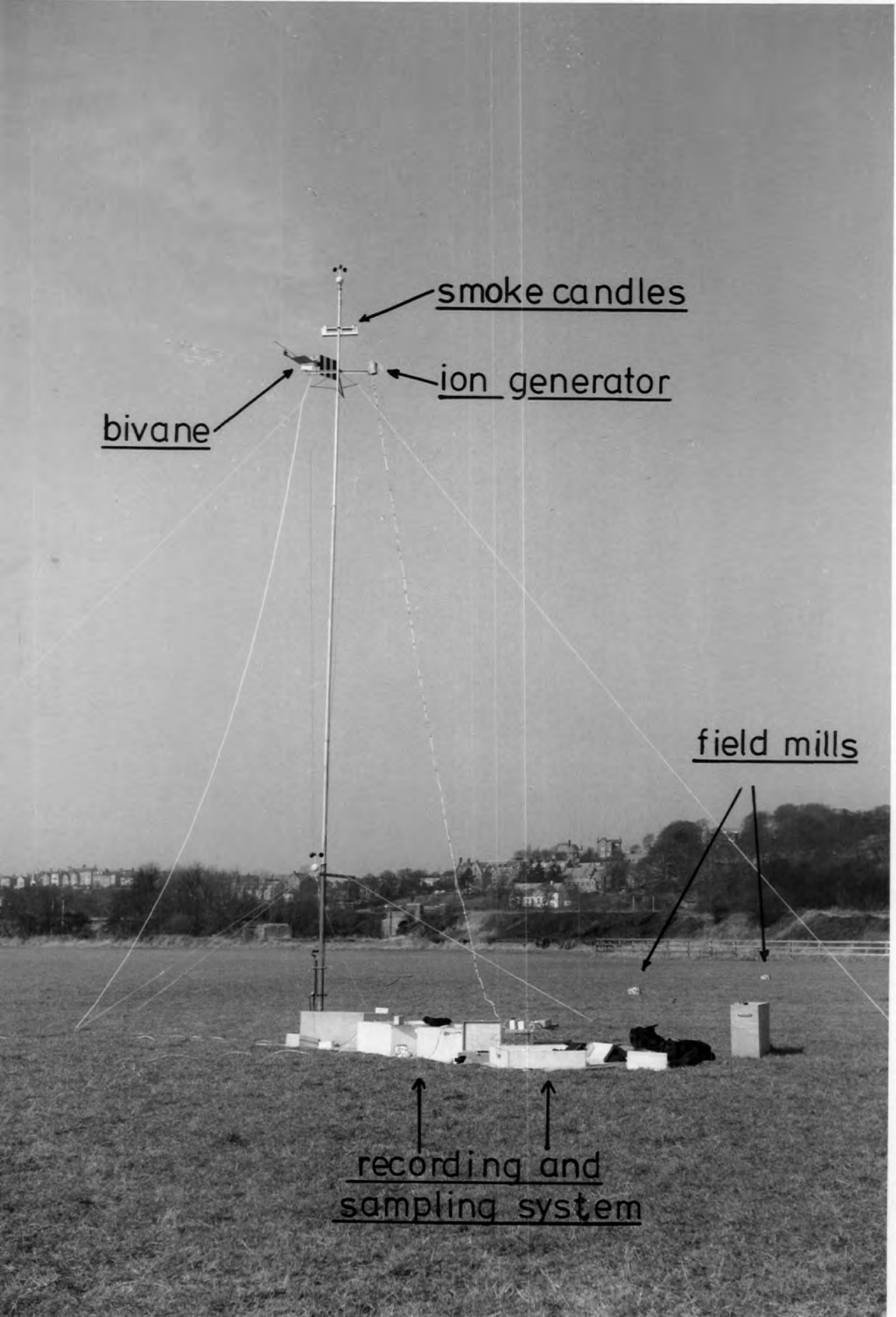
smoke candles

ion generator

bivane

field mills

recording and sampling system

FIELD WORK IN PROGRESS 2

TYPICAL MEASURED VALUES OF POTENTIAL GRADIENT COMPARED WITH THOSE COMPUTED FROM BIVANE DATA

PART OF 4.10.72(6)   ION SOURCE HEIGHT 5m   MEAN WIND SPEED 3.4 ms⁻¹
CONDITIONS: slightly unstable, sky clear
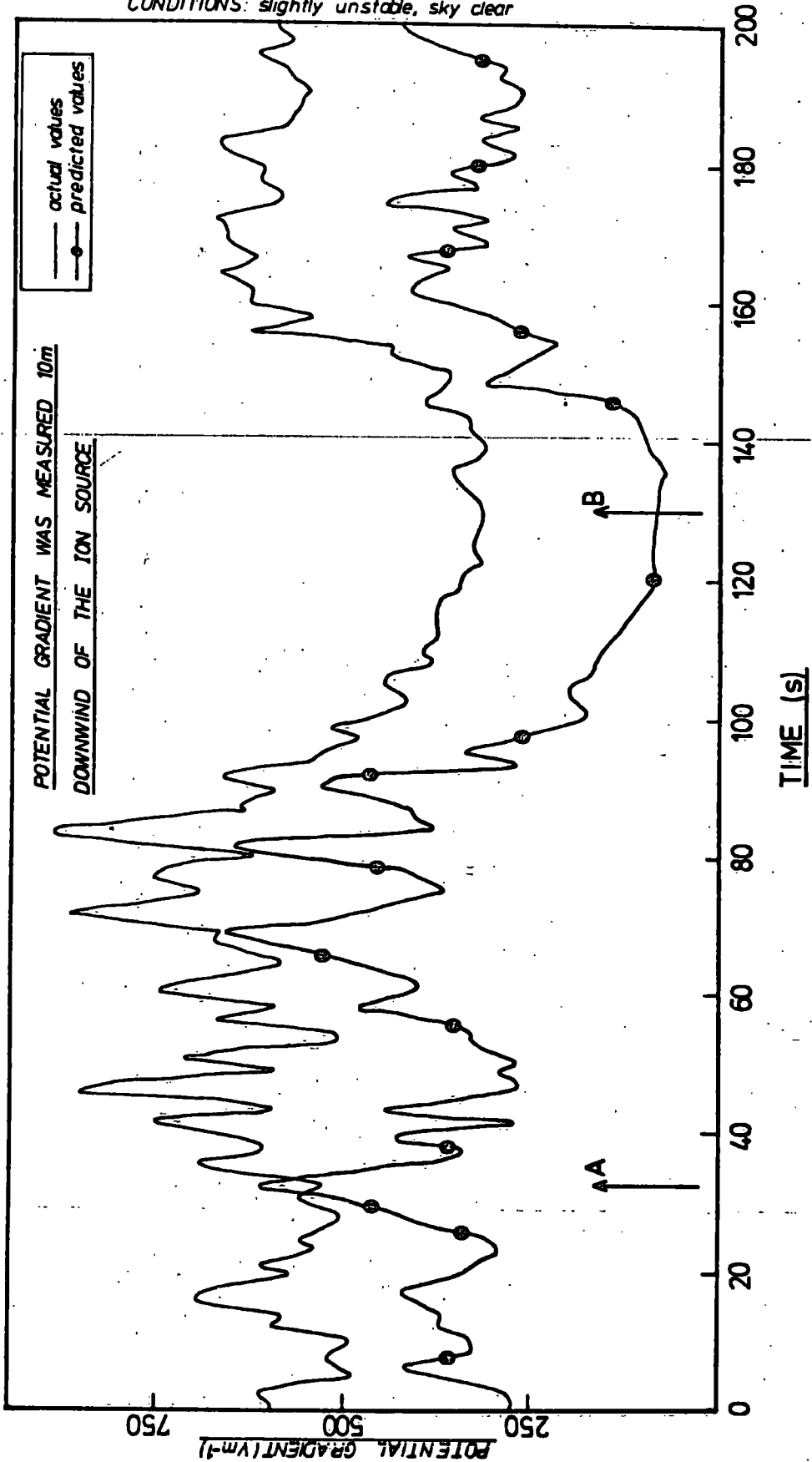
Example of computed ion plume configuration

(1) AT TIME 'A' (see fig. 8,1)

ELEVATION

PLAN
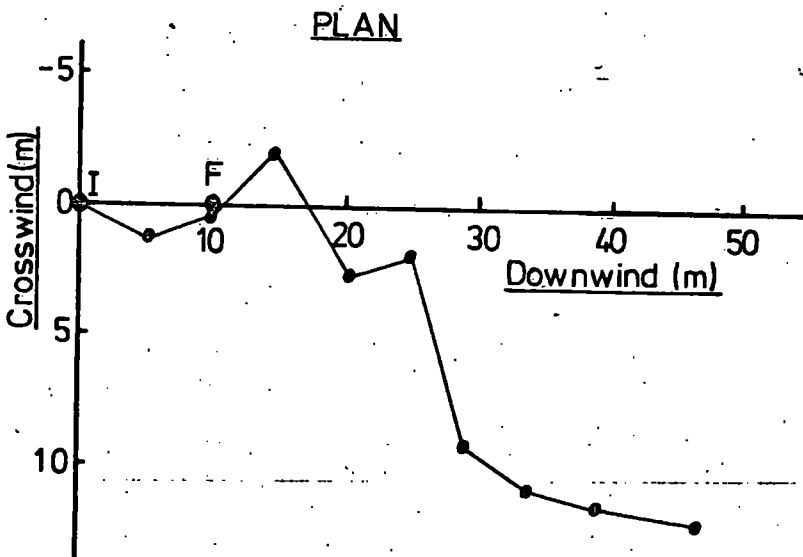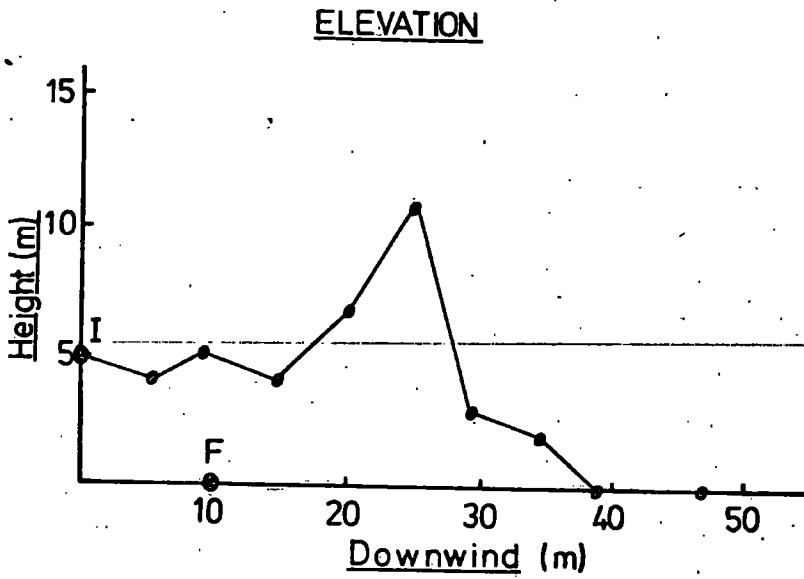
I   ION SOURCE   F   FIELD MILL

Example of computed ion plume configuration

(2) AT TIME 'B' (see fig. 8,1)

ELEVATION

PLAN
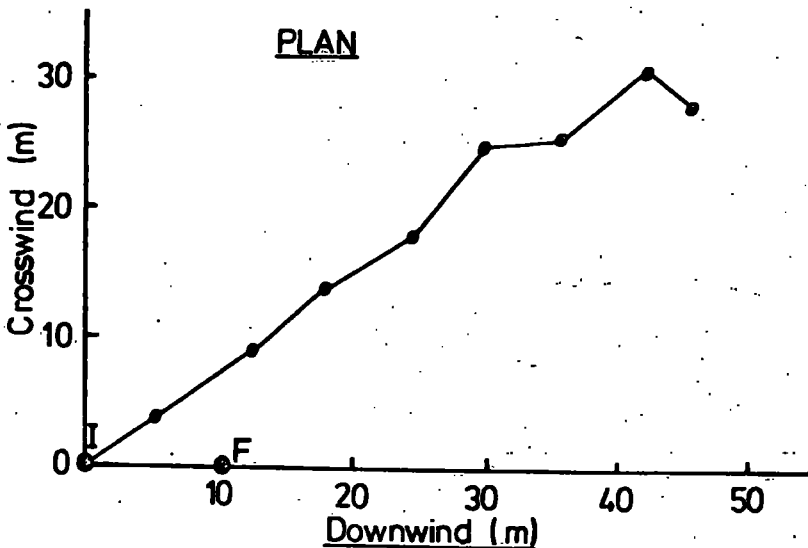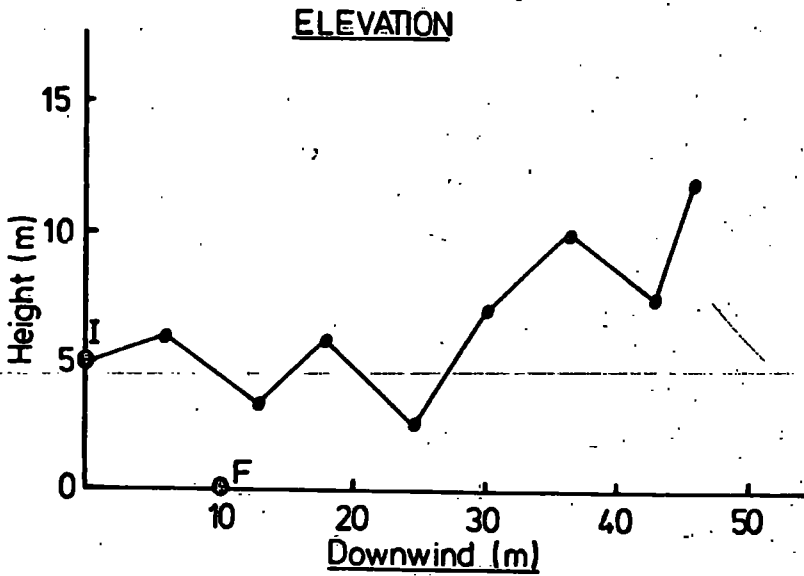
I   ION SOURCE   F   FIELD MILL

model appropriately sized space charge parcels were supposed to reside at the plume element positions. The validity of this assumption is discussed later.

At time A (see Figs. 8.1. and 8.2.) we observe that three charge elements of the plume are almost directly above the field mill (F) and, *because* of the inverse square law, it is these three local charges which make by far the largest contribution to the predicted potential gradient. During this time the actual potential gradient behaved similarly and we thus conclude that, in all probability, the actual plume configuration was not too different from that predicted. In marked contrast with this is the situation of the ion plume at time B (see plan in Fig. 8.3.). Here the projection of the entire plume is at an angle to the mill-source line, possibly due to the passage of a large horizontal eddy or similar feature. The predicted potential gradient is, as we would expect, much lower because nowhere is the ion plume near the field mill.

8.2.3
Discussion of the Statistical Results

8.2.3.1
Opening remarks

The data obtained from the bivane, anemometer and field mills was processed by the computer in the manner described in Sec. 6.3. The cross-correlation coefficient between the predicted and actual potential gradient values was of most interest because its magnitude indicated the validity or otherwise of the bivane data model and the extent, if any, of the electrostatic effects. The standard deviations of the predicted

and actual potential gradient were also computed and in many cases the agreement was quite good. In fact, the best agreement was obtained when the source current in the model was set to $+0.3\,\mu A$ and, taking into account the Series I results, this figure was accepted as being the best available. Observations with the ion collector indicated that the ion source produced negative ions rather more copiously, see Sec. 8.3. Values of the turbulent surface stress obtained with this relatively simple equipment, although of little direct relevance to this project, were nevertheless of interest in that they provided a check on the bivane and recording system. Actually, the results obtained for the stress were close to the accepted figures and this was quite encouraging.

It will be noted from Fig. 8.4., which gives a summary of the Series II results, that negative ions were used in some of the runs. The implication of this is that near or under the ion plume the sign of the potential gradient would, at times, most likely be reversed. Unfortunately, sign discrimination was *never* incorporated on the field mills as had been originally intended and consequently there were inevitably occasions when the polarity of the recorded potential gradient was uncertain. This effect, which is discussed in more detail later, caused certain difficulties both when interpreting the graphical records and in understanding the value of cross-correlation obtained.

SUMMARY OF SERIES II DATA

DATE	RUN No	SOURCE HEIGHT m	ION TYPE	MEAN WIND SPEED ms⁻¹	Surface stress N m⁻²	STANDARD DEVIATION OF POTENTIAL GRADIENT Vm⁻¹ actual values mill 1	actual values mill 2	predicted values mill 1	predicted values mill 2	Correlation coefficient of actual and predicted mill 1	mill 2
4.10.72	3	9,0	+ve	2,8	0,15	160	160	82	180	0,04^a	0,52
	4	"	"	2,5	0,11	140	150	84	240	0,09^a	0,42
	5	5,0	"	3,4	0,14	91	140	180	240	0,40	0,34
	6	"	"	3,3	0,08	110	160	200	240	0,49	0,40
	7	2,3	"	3,7	0,04	410	260	460	230	0,63	0,62
	8	"	"	4,0	0,09	320	71	520	310	0,19^a	0,34
	9	"	"	2,9	0,07	430	220	530	370	0,43	0,49
13.10.72	3	9,0	-ve	1,4	0,02	54	200	130	270	0,57^b	-0,04^b
	4	"	+ve	1,7	0,13	110	350	60	62	0,60	-0,43^a
	5	5,0	+ve	1,5	0,08	150	160	600	87	0,40	0,35
	6	"	-ve	2,7	0,10	190	44	330	10	0,10^a	-0,41^c
	7	2,3	-ve	2,5	0,16	220	68	630	8,4	0,20^b	0,18^b
	8	"	+ve	2,8	0,12	180	100	390	17	0,21^a	0,49

Notes

1. METEOROLOGICAL CONDITIONS - clear skies. slightly unstable on both occasions

2. FIELD MILL POSITIONS

   4. 10. 72   mill 1   10m   Downwind
            " 2   30   "

   13.10.72   both mills 30m Downwind but 50 apart

3. Predicted values of potential gradient obtained from bivane data model. Actual and predicted values were passed through a digital low-pass filter prior to statistical analysis. Ion source in model was 0,3μA.

4. Low cross correlations are superscripted by a,b or c, the letters being used to refer to the various effects causing the poor results. SEE TEXT.

8.2.3.2
The nature of the cross-correlation between predicted and actual potential gradient data

We shall now consider firstly how this cross-correlation might be expected to depend on various factors and secondly any likely sources of discrepancy between measured and predicted values of potential gradient.

The cross-correlation should be better when

    (a) the wind speed is higher,

    (b) the ion source height is greater, and

    (c) the field mill is placed near the source.

Under circumstances (a) and (b) we would anticipate that the ion plume configuration would adhere more rigorously to the bivane data model because any electrostatic effects would be minimal. However, in conditions of high wind speed, because the sampling interval is constant, the plume elements used to evaluate the potential gradient in the model are relatively widely spaced. Inevitably, this large spacing will, at least to some extent, detract from the accuracy of any predicted electric field values. In the case of (c) above it would seem reasonable that, whatever the exact nature of the turbulence causing the potential gradient variations, the model would be more applicable nearer the source. This is because the departure from the straight line effect (on which the bivane data is based) would be less near the source than at greater distances downwind (see Sec. 2.8.).

Sources of discrepancy between the predicted and actual values of potential gradient were thought to be:

(a) Departure from the straight line effect - see Sec. 2.8.2.,

(b) Discrete, i.e. sampled, nature of the data,

(c) Omission of crosswind and vertical diffusion in the model,

(d) Disregard of electrostatic effects,

(e) Instrumental errors, principally those of bivane alignment
    and anemometer accuracy, and

(f) Lack of field mill sign discrimination.

The existence of the straight-line effect is, of course, funda-
mental to the success of the bivane data model and any depar-
ture from it would inevitably affect the results adversely.
Of equal importance was the sampled nature of the data, it being
suspected that many small scale features of the plume were being
missed. This suspicion was confirmed in some later experiments
with smoke plumes (discussed later in this chapter) during which
the validity of the straight-line hypothesis was also thoroughly
explored. Initially it was hoped to include the effects of
crosswind and vertical diffusion in the bivane data model but
this was not possible for reasons detailed in Sec. 8.3.3.2.
For similar reasons, the effects of electrostatic forces had
also to be omitted from the model.

Considerable effort was taken to carefully align the bivane
by a procedure involving the use of compass and binoculars,
more details of the technique being given in Sec. 4.6.4. Des-
pite these precautions it is felt that, together with inaccu-
racies in the data transfer system, the bivane observations
could have been as much as 5° in error. Naturally, if the
anemometer system also gave inaccurate readings, this would
detract further from the reliability of the computed wind com-
ponent values.

We now consider the analytical results, shown in Fig. 8.4., in the light of the previous comments. An examination of the cross-correlation coefficients indicates that if any tendencies are apparent, they would seem to be in contradiction to the proposals made above. That is, the correlation appears rather better when the ion source height was low and in light winds. However, a visual inspection of the graphical records suggested that the predicted and actual potential gradient values agreed rather better than their correlation coefficients would indicate and, in fact, on most occasions the agreement was quite good. Further, visual analysis also substantiated that any discernible trends in this agreement did apparently conform to the criteria originally suggested.

The reason for the disparity between the two methods of analysis is quite simple and is as follows. It must be remembered that the value of the correlation coefficient is very sensitive to the position of the largest peaks and, because of the nature of the system being investigated, it was in the prediction of these large potential gradient variations that the maximum error was likely to arise. The largest variations are, of course, caused by space charges passing close to the field mill and when such a variation has to be predicted the accuracy of the bivane and anemometer as well as the validity of the computer model are both severely challenged. Consequently, it was hardly surprising that whilst the agreement between the small peaks, associated with the movement of more distant charges, was frequently excellent, that between the large peaks was often disappointing. In view of this it appears that correlation analysis, in the mathematical sense, produces unnecessarily pessi-

mistic results and thus more importance was attached to the
visual analysis of the potential gradient records.

Certain additional effects contributed to the poor cross-
correlation obtained in some cases. The particular instances
where this is applicable have been superscripted with the
letters a, b or c so that the various factors causing these
low figures can be discussed separately.

In the case of those values labelled with an 'a' the poor
correlations were substantially a result of the effects des-
cribed immediately above combining in an unfavorable manner.

The poor results carrying 'b' or 'c' labels were all obtained
when negative ions were being used and we therefore suspect
immediately that this may be a result of the lack of sign dis-
crimination on the field mills. In fact, this turns out to be
so but the lack of sign discrimination causes, not one, but two
related effects. Let us suppose, as was the case in fact, that
the natural potential gradient was small and positive through-
out these field runs. Firstly, if the negative ion plume is
relatively distant from the field mill, then any motion toward
the mill, provided that the motion is not too large, will result
in the measured potential gradient being decreased slightly.
However, the possibility of computations involving negative ions
(and hence negative potential gradients) was, rather stupidly,
not allowed for in the bivane data model computer programme and
as a result the sense of the predicted potential gradient varia-
tions was incorrect in the circumstances detailed above. That
is, when the ion plume is executing motions relatively far away

from the field mill the predicted and actual potential gradient values will be in antiphase. Consequently, if this type of situation is maintained throughout a field run then the overall cross-correlation between the values will be negative. This is referred to as effect 'c'.

Secondly, a more complex situation arises if the negative ion plume moves much nearer the field mill. The potential gradient will, in all probability, be reversed, but, because of the failure of the mills to descriminate between positive and negative values, the actual negative potential gradient will be recorded as positive. Therefore, in this case the larger, but usually less common, peaks would be in phase with their predicted counterparts. However, as before the smaller, but invariably more numerous, peaks will be in antiphase. This state of affairs will lead to either a small positive or negative cross-correlation depending on which factor is dominant. This is referred to as the effect 'b'.

8.2.3.3
Concluding notes

The 'bivane method' of investigating ion plumes has been reasonably well established despite considerable instrumental problems and difficulties with data analysis. Cross-correlation techniques proved rather disappointing but careful visual examination of the results indicated that, with relatively few exceptions, the agreement between predicted and actual potential gradient values was good. The physical complexity of operating the experiments in the field was such that only a small number of runs could be attempted. Conse-

quently the coverage of various meteorological conditions was nothing like as comprehensive as in the case of the Series I experiments. Nevertheless, it was possible to discern, as anticipated, that the bivane data model was more reliable at moderate wind speeds and with the ion source well above the ground.

The results of these experiments also indicated that there was little difference between the behaviour of positive and negative ions, although investigation of negative ion plumes was, to some extent, frustrated by the lack of sign discrimination on the field mills.

A photographic technique was devised to re-examine the validity of the bivane approach in an attempt to discover the reason for the occasional disagreements between the predicted and actual potential gradient values. The details of this method and the results obtained are now discussed.

8.2.4
Smoke plume photography

Suppose a smoke plume were generated by a suitable source placed as close as possible to the ion generator. Then, ignoring electrostatic effects, the smoke and ion plumes should be coincident. Further, the position of the smoke, and hence the ion, plume could be determined directly by photography and the computed configurations obtained from the bivane could be compared with these photographic results. In this way the reality of the bivane data model could be critically assessed. It would also be possible, if time permitted, to compute the expected potential gradient from the photographs, and departures from the actual values indicating the

magnitude of the electrostatic effects present. However, the success of such experiments depended entirely on two factors. Firstly, the smoke must be electrically uncharged, and secondly, the ions and smoke particles must not interact. In the first case field mills placed downwind of a smoke candle indicated that the smoke was, fortunately, electrically neutral. The magnitude, if any, of an ion-smoke interaction was not investigated.

The experimental technique, briefly described in Sec. 4.7., was an extension of the method used in the previous investigations with the bivane. Two 8 mm cine cameras were placed at suitable distances upwind and crosswind of the smoke candle. These cameras, which were mounted on sturdy tripods, could be remotely controlled and were connected into the recording system by a specially designed interface system. In order that accurate synchronisation could be maintained between the photographic and recording systems, small lamps were situated near the cameras and within their field of view. These lamps were arranged to light during that part of the recording cyle in which bivane data was being sampled.

Initially, it was hoped to ignite the smoke candles electrically. It became apparent, however, that the mast, already overloaded, would not support any additional wiring and thus an alternative method of igniting the smoke generators had to be found. In practice the only method appeared to be that of attaching time fuses to the candles and lighting these with the mast retracted. Once the fuses were burning the mast was pumped to its maximum height and the top guy ropes secured. Clearly, this was a somewhat tedious procedure and the diffi-

culties were increased by the fact that once the fuses were
lit no further control could be exercised over the time of
ignition.

The type of smoke candle used burned for approximately 4 min.
and produced a dense white smoke. Despite the relatively
high opacity of this smoke, on some occasions the contrast
between plume and sky was rather poor. This led to difficul-
ties when trying to discern the position of the plume on the
cine films. In an attempt to alleviate this more powerful
smoke generators were tested but these appeared to produce
a much hotter smoke and considerable convective activity
was observed. Unfortunately, this precluded their use in
this project.

Despite all these difficulties quite useful results were
obtained and these are now discussed briefly.

In these experiments the correlation between the predicted and
actual potential gradient values were examined as before.
Although the duration of the runs was now much shorter, only
4 min., the cross-correlation coefficients were similar in
value to those obtained from the previous 24-min. recordings.
However, this correlation was not the primary concern here,
the main interest being centred on the relation between the
plume configurations obtained photographically and those com-
puted with the bivane data model. Experiments were performed
with the ion and smoke sources at two heights, namely 9 m and
2.3 m. In the case of the higher sources, however, the plume-
sky contrast was so poor that very little could be learnt from
the cine film record. Thus the conclusions listed below derive

mainly from results obtained with the sources at 2.3 m.
These experiments were performed on a clear day in March
1973 with near-neutral conditions and a wind speed of about
4 ms^{-1} . The general conclusions are as follows:

(a) The bivane data model appeared to exaggerate the veri-
cal motions. This might conceivably explain the occa-
sional large peaks found in the predicted potential
gradient records which apparently bore little relation
to the actual values. Presumably, it is the presence
of the ground which is inhibiting these vertical motions.
(See Sec. 2.6.)

(b) The discrete nature of the model resulted in, as had
already been suspected, quite important features pre-
sent in the actual plume being omitted entirely in the
computed version.

(c) It was clear that vertical and crosswind diffusion must
have had a considerable effect on the charge distribu-
tion even at distances of a few tens of metres from
the source.

(d) As expected, the bivane data model was more accurate
at short distances downwind of the source.

Although the above are fairly harsh criticisms of the bivane
data model it should be pointed out that, at times, there was
little discrepancy between the actual and computed plume con-
figurations, and thus the effects causing the departures from
the predictions were not by any means always operative.

It should, of course, be noted that the above comments are based on the detailed analysis of only a few runs and therefore any conclusions are inevitably tentative. Nevertheless, in a first attempt at understanding the dynamics of ion plumes the 'bivane method' would seem a simple and quite effective approach.

8.3
Experiments with the Ion Collector

The use of an ion collector was considered at the inception of this project but reasonably priced solid state amplifiers of the type required were not then available. During the later stages of the work such items did appear on the market and an ion collector was constructed. The collector, which is described in Sec. 4.5., did not work as well as had been hoped. Whilst the performance was quite satisfactory on the less sensitive range, a considerable amount of noise was present on the output signal on the higher gain setting. Some efforts were made to cure this problem, but as the noise appeared to originate from brush interference in the impeller motor, little could be done without completely rebuilding the instrument.

In the field the device was placed directly downwind of the ion source. The mean wind direction was obtained from a light wind vane mounted close to the ion source as before. A special metal gantry of variable height was constructed to support the ion collector. The collector-source distance was altered by moving the gantry and collector as a single unit. OGDEN (1967) has pointed out that such structures may disturb the ion distribu-

tion because of electrode effects. The alternative proposi-
tion, i.e. to construct the gantry out of an insulating material,
seemed equally unsatisfactory as quite possibly   non-conduc-
ting materials would become electrically charged and thus
also disturb the ion distribution.

The ion collector output was taken to a small mains-driven
chart recorder. The mains supply was obtained from the Group's
portable generator, considerable care being needed when siting
the latter. The exhaust gases from the generator engine could
be quite highly ionized, and to avoid the possibility of any
interference with the experiments, the AC generator was placed
well downwind of both ion source and collector.

The ion concentration, at least near the source, fluctuated
considerably with time at any particular point. The character
of these fluctuations was, of course, much the same as those of
smoke concentration that would be measured near a smoke source
and is a direct indication of the turbulent nature of the
wind. However, if mean values of the ion concentration are
taken over periods of several minutes, then quite definite
trends can be discerned in the recorded data. These results
are shown in Fig. 8.5. and were obtained on a day when there
was little vertical motion and the ambient ion concentration at
various heights and distances downwind of the ion source.
Unfortunately, insufficient data was available to draw concen-
tration isopleths but, by carefully inspecting the results, the
following somewhat tentative conclusions can be drawn.

Firstly, particularly very near the ion source, it is evident
that the ion plume width is much greater than that of a smoke

plume in similar conditions. This is taken as direct evidence of the electrostatic repulsion effect described in Sec. 3.5.

Secondly, the mean values at 5 m downwind suggest that the axis of the ion plume is tilted downward. In this case the effect is attributed to image forces.

Thirdly, the ion source produces considerably more negative than positive ions, some indication of this having already been seen in the field mill records. It is estimated that when the ion generator was connected so as to produce negative ions its output was about twice that obtained when set to generate positive ions.

8.4
Experiments at longer distances from the ion source

This work was intended to be a preliminary study. The main objective was to establish, at least approximately, the characteristics of the electric field several hundred metres downwind of the ion source. In practice, a number of difficulties arose in the execution of these long-range experiments. Equipment had to be checked frequently to ensure it was working satisfactorily and as a result a great deal of time was spent walking between the various items of apparatus. Also at large distances downwind of the ion source the correct placing of a field mill presented problems. It was necessary to observe the wind vane, placed near the ion generator, with powerful binoculars and considerable skill was needed to keep the image steady for a sufficient time. It is recommended that any future experiments along these lines be carried out by at least two persons, and that an efficient means of communication be provided between them.

SPOT MEAN VALUES OF ION CONCENTRATION DIRECTLY

DOWNWIND OF THE ION SOURCE

(RESULTS OBTAINED WITH THE ION COLLECTOR)

DATE 8. 11. 72   TIME 1200 - 1500   WIND SPEED 4 ms⁻¹

(a) ion source producing positive ions
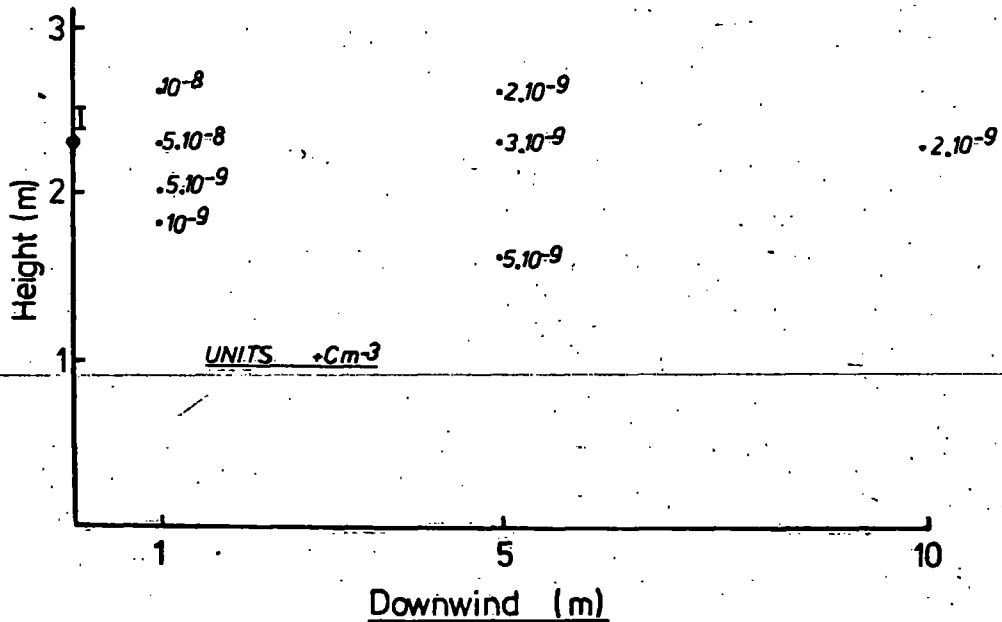
I = ION SOURCE

(b) ion source producing negative ions
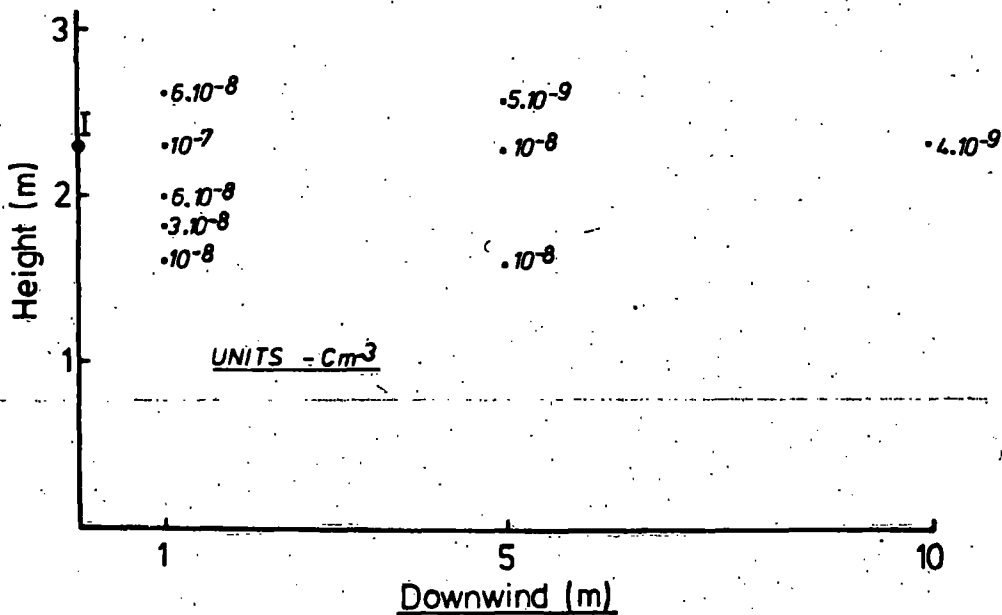
POTENTIAL GRADIENT VARIATIONS RECORDED 140m DOWNWIND OF THE ION SOURCE

(ion source was pulsed 45s on, 45s off)

ion source height 5m   23.3.73
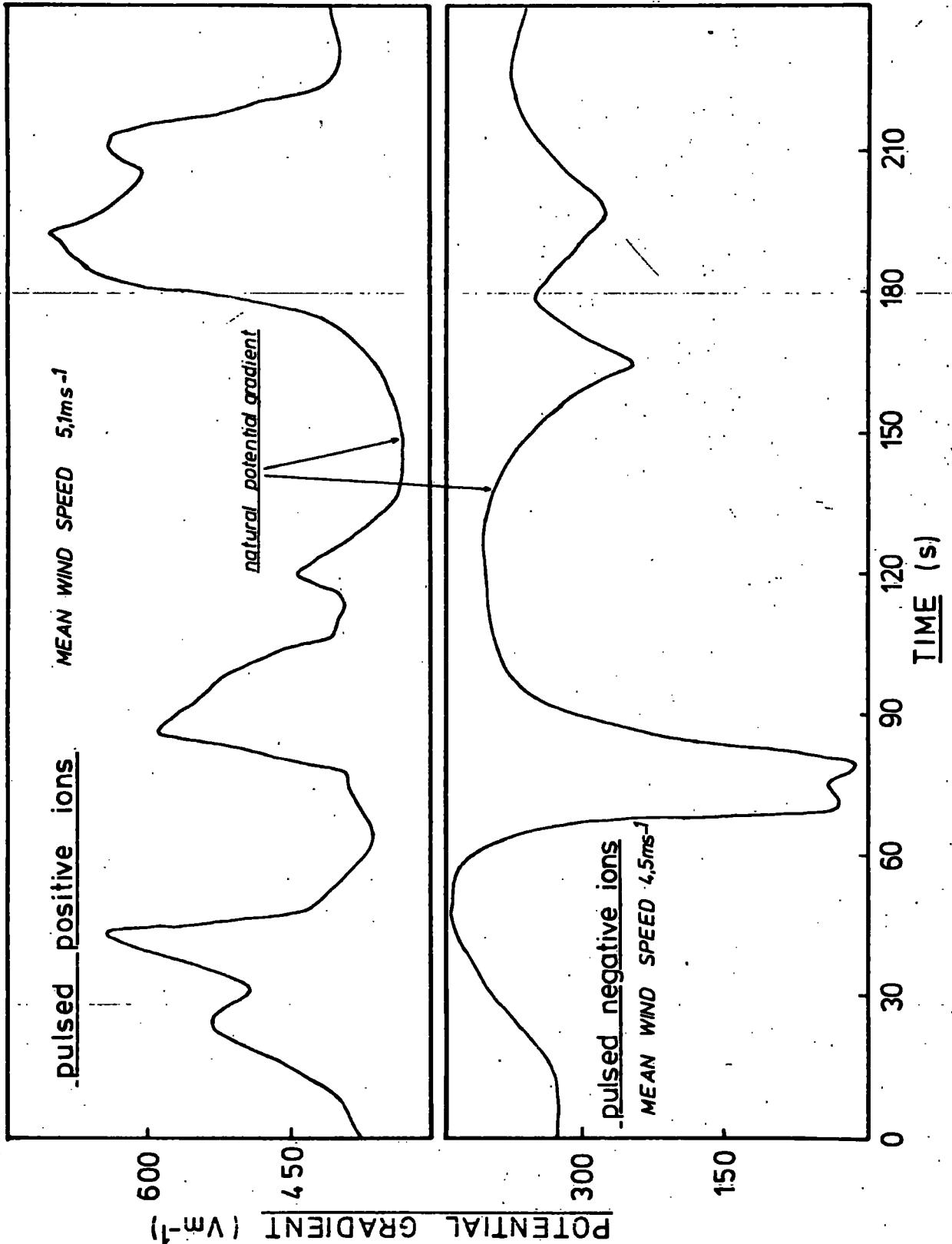
It would be reasonable to expect the character of the potential gradient to be different, in several ways, from that nearer the source. Firstly, because of the longer distance of travel the ion plume will be more diffuse and hence the potential gradient fluctuations will be smaller. Secondly, at these longer distances any small scale variations in concentration will be 'smeared out' by diffusion and therefore variations of potential gradient will tend to be slower. In fact, it was thought that at three or four hundred metres from the source the artificially produced variations would not be much larger than those occurring naturally. It was known that pollutants, even in low concentrations, could markedly affect the potential gradient and, as a precaution, initial trials were carried out at a site where pollution levels were known to be low. The site chosen was a large flat-topped hill about 1 km north of Lanehead, County Durham. Previous workers, particularly SHARPLESS (1968), had already established that pollution effects were minimal at a station in the village and thus at the site itself one could be certain that the air was clean.

In the initial work quantities of negative and positive charge were released (separately) 300 m upwind of a field mill. On the occasion chosen the wind speed was very low being about 1 ms^{-1}. Several peaks (or troughs) having amplitudes between 60 and 200 Vm^{-1} were detected downwind of the source, the larger variations being associated with the negative ions. Also at this distance the general time scale of the potential gradient variations was much longer, as expected.

It was already known that the ion source produced negative ions more copiously than positive ions but negative ions were

thought to be more numerous for an additional reason. At
large distances from the source the ion concentration levels
are, of course, relatively low. Small concentrations of posi-
tive ions would serve to slightly enhance the natural potential
gradient, whereas similar concentrations of negative ions
would diminish the prevailing value. If the negative ion
concentration were not large enough to reverse the natural
potential gradient then a negative ion cloud would be driven
upward by electrostatic forces. Nearer the ion source where
negative ion concentration is larger the potential gradient
will be reversed and thus the ion cloud will move downward
under the action of image forces. For these reasons we may
expect the negative ions to remain airborne for longer periods.

Further experiments were planned at the Lanehead site but were
abandoned for the following reason. In order to save time
and effort in placing the field mill and ion source the Land
Rover was often used as a means of transport. Most moorland
regions, and this site was no exception, often possess exten-
sive boggy areas. Experiments were discontinued when the Land
Rover was inadvertently driven into such a waterlogged area,
considerable difficulty being encountered in freeing the
vehicle. In view of this a less ambitious project was attemp-
ted at the Maiden Castle site.

In these experiments a slightly different approach was adopted
as trouble had already been experienced with polluted air. The
method consisted of cyclically switching the ion generator on
and off thereby producing 'packets' of ions which travelled
downwind. Potential gradients measured downwind of such a
pulsed source should therefore possess a markedly periodic

character and it was hoped this would enable the artificially produced field variations to be readily distinguished.

Some results were obtained 140 m downwind of the ion source, a typical section of the records being shown in Fig. 8.6. The 'pulsed' nature of the measured potential gradient is evident in the diagram and, at this distance downwind, the size of the variations is quite substantial.

It was hoped initially to estimate a value for the ionic recombination rate from the long range potential gradient measurements. However, as a result of the experimental difficulties referred to earlier, very little data was actually obtained and therefore estimates of the recombination rate were not feasible. Further, it was felt that rather more extensive experiments, both in terms of distance and equipment, would be necessary to obtain reliable information on this quantity. Nevertheless, the results given above are interesting because they clearly indicate that a significant fraction of the ions generated, particularly if negative, can persist in the lower atmosphere for at least 5 min.

Chapter 9: <u>CONCLUSIONS AND SUGGESTIONS FOR FURTHER WORK</u>

9.1
Summary of Important Results

The experimental results have, broadly speaking, substantiated the ideas about the behaviour of ion plumes developed theoretically in Chs. 2 and 3. The central feature of these ideas was that with the strength of ion source being used in this project, ion movement and dispersion would largely be determined by the pattern of the local air motion. However, two important exceptions to this statement were deduced theoretically and later established experimentally. Firstly in very light winds the electrostatic repulsion effect (see Sec. 3.5.) operating between the ions comprising the plume caused a larger crosswind and vertical spreading than did the effects of turbulence. Secondly, image charge effects, also discussed in Sec. 3.5., resulted in downward forces being exerted on the ion plume, particularly when it was near the ground.

Later experiments with the bidirectional vane enabled the shape of the ion plume to be deduced theoretically. In this way it was possible to compare the values of potential gradient obtained by measurement with those arrived at by computation. The plume model used in this reconstruction took no account of electrostatic forces, or indeed of crosswind and vertical diffusion, but nevertheless on most occasions the agreement between predicted and measured potential gradient values was good. These results also suggested that the plume behaviour was determined by atmospheric motion and turbulence except in low wind speeds or with low source heights.

It would be unwise to quote any hard and fast rules about
when or when not small ion behaviour reflects the true charac-
ter of atmospheric turbulence. With wind speeds of $4 \ ms^{-1}$
or greater and ion plume heights in excess of 10 m the effects
of electrostatic forces are small. Of course, it must be
remembered that these figures apply to an ion source of $0.3 \mu A$
output and these results should be amended accordingly when
sources of different strengths are under consideration (see
Sec. 3.5.).

9.2
Implication of the Results

The importance of these results is evident. In all but
light winds and at the lowest levels the ion plume behaviour
is determined by the characteristics of the local air motion.
Consequently, there would seem to be no reason why small
ions could not be used as a tracer in small-scale atmos-
pheric diffusion experiments. The advantages of such a
choice would be as follows. Ions are cheap and easy to pro-
duce and have minimal physiological effects. The detection
of ions and measurement of ion concentration, either indirec-
tly by electric field methods or by the more direct approach
using ion collectors, does not require elaborate techniques.
The response time of many conventional detectors to changes
in concentration whether it be sulphur dioxide or some other
pollutant is often relatively slow and the alternative of an
entirely electrical detection system offers the attractive
possibility of designing rapid response instruments.

Whilst the behaviour of ions within a hundred metres or so of
the source has been fairly well established, it should be

pointed out that further downwind, recombination and other effects may be of major importance in determining the fate of the ion plume. Thus it should be emphasised that the results of this project only indicate that the use of ions for short range (i.e. up to 100 m) diffusion studies would be feasible. Before longer range investigations using the method can be attempted, further research into ion plumes is necessary. At larger distances downwind particular care should be taken to determine the nature of the ambient variations, both of electric field and ion concentration.

9.3
Difficulties with the Present System

Apart from one or two minor exceptions, the equipment detailed in Chs. 4 and 5, functioned very satisfactorily in the field. One of the main problems was caused by the sheer complexity of the system. On arrival at a site considerable time was required to set out the field mills, attach the instruments and ion source to the mast and connect up the sampling and recording systems. Once operational conditions were established, provided no special circumstances arose, the equipment could be relied upon to operate automatically. Nevertheless, it was thought prudent to make frequent checks to ensure that each item of equipment was working correctly. This was done as often as possible so that if a fault did arise minimum recording time was lost. The more advanced experiments using the bivane and later the cine cameras were even more complicated and were, at times, almost too much to cope with single-handed.

Turning now to the instruments themselves, several refine-
ments and alterations can be suggested in the light of opera-
tional experience. Firstly, the omission of sign discrimina-
tion on the field mills should have been remedied at an early
stage. Some technical difficulties do exist here but it is
not thought they are insuperable. In particular, the bias
plate would need to be supplied with a highly stable, yet
adjustable, DC voltage. With portable equipment,carrying
batteries of limited power,care would be required in the
design of such a voltage supply system. Secondly, a higher
speed sampling system would have been advantageous, particularly
when taking bivane readings. This would have greatly facili-
tated the development of a more accurate bivane data model.
Naturally, the response time of the field mills and other
instruments should be decreased in order to take full advan-
tage of the higher speed sampling.

Considerable difficulty was experienced in accurately aligning
the bivane, see Sec. 4.6. The procedure described in that
section to effect this alignment was both tedious and time
consuming and a better method should be devised. It is felt
that the only really satisfactory system would be to rigidly
attach the bivane and other instruments to a fixed mast.
Apart from any improvements in accuracy a large amount of time
would be saved when setting out equipment for field work.

Recently considerable advances have been made in integrated
circuit techniques and as a consequence the entire electronics
system could well be redesigned to take advantage of these
innovations. Two points are particularly worth noting.
Firstly, very high input *impedance* amplifiers are now available

and these would serve ideally as field mill amplifiers. This is an attractive possibility because the construction of large numbers of mills (e.g. for use in arrays) having standard performance would now be feasible. Secondly, the appearance of high precision voltage to frequency and frequency to voltage convertors could replace the existing transistor systems. The use of VHF radio links to replace the long cables between field mills and the central recording system would also be of great assistance. (The reader's attention is drawn to the fact that a Post Office Licence must be obtained before radio techniques are used.)

9.4
Suggestions for Future Work

9.4.1
Experimental Work

A number of points raised by the current investigation require elucidation. These are now discussed.

The fate of the ions at large distances downwind of the source is not clear but it appears to depend in a sensitive manner on the ambient small and large ion densities and also on the prevailing nucleus concentration. A logical extension of this project would therefore be to place small and large ion collectors, together with nucleus counters, downwind of the ion source. In this way it should be possible to establish the behaviour of the ion plume reasonably conclusively.

A method involving the use of a ground level collector plate might be used to assess the effect of image forces. Ions arriving at the ground, by whatever cause, constitute a current

and, provided the ambient ionization were low, the magnitude
of this current could be related to the effects of image
forces. The ion concentration and electric field would also
have to be measured simultaneously but this would not pose
any difficulties. Some arrangement would need to be made
for displacement current compensation and, with the large
and rapidly changing electric fields that would inevitably
be present, this might present something of a problem.
KASEMIR (1955) has developed a method of compensation which
might be suitable.

Measurements of the electric field at ground level have
already provided very valuable information concerning the
behaviour of ion plumes. Whilst the technique could be exten-
ded by employing more field mills at ground level it might be
more productive, certainly more interesting, to consider the
possibility of total vector measurements using elevated field
mills. By measuring the three field components of the elec-
tric field a great deal more information could be obtained,
particularly about plume movements in the vertical plane.
Some theoretical calculations, results of which are given in
Sec. 6.4.2., indicate that near the ion plume very large hori-
zontal electric fields would be present. From the technical
standpoint considerable difficulties would arise in the design
and operation of elevated three component field mills; never-
theless, it is not thought these problems are insurmountable.
IMIANITOV (1949) has reported a design for a device apparently
capable of measuring the three components of the electric field.

In the later stages of this project, a technique involving the
comparison of computed ion plume configurations with those

obtained directly by cine photography of a smoke plume was developed. Lack of time did not permit this method to be properly exploited. The indications are that the photographic approach could be a very useful adjunct to the understanding of ion plume behaviour.

9.4.2
Theoretical Work

There appear to be three areas where further theoretical effort could usefully be directed.

The treatments of both image and repulsion forces, presented in Ch. 3, are, to say the least, somewhat simplified and it is felt that considerable refinement would be most desirable. A rigorous analytical approach to the problem would be very complex mathematically and possibly numerical techniques involving the use of a digital computer might be a more feasible alternative. In particular, the interaction of electrostatic and turbulent effects has only been considered very superficially and further theoretical work should be aimed in this direction.

On a more practical level the bivane data model, although capable of yielding good results, did possess a number of faults. The effects of certain of these could be minimised by a more sophisticated experimental arrangement whereas the remaining defects require modification of the computer model for their elimination. As previously mentioned, a higher sampling rate should greatly increase the accuracy of the bivane data model as it would correspondingly decrease the separation of the computed plume elements (see Sec. 3.4.).

On the theoretical side incorporation of the effects of electrostatic forces and those of turbulent diffusion would considerably enhance the realism of the model. In practice, considerable restriction might be placed on the researcher by the limitations of the computer. No doubt, the speed of computers will be further improved and the inclusion of these suggested modifications would ultimately present little difficulty. One might also be able to allow for certain more subtle features of atmospheric turbulence. For instance, the bivane data model derives its results from 'Eulerian', i.e. fixed point measurements, whereas, of course, the ion plume travelling downwind is essentially in a 'Lagrangian' environment. Possibly, this feature may be catered for by the inclusion of the Lagrangian-Eulerian time scale ratio in a later model, see PASQUILL (1961).

Finally, it should be remarked that as employing ions as a tracer does appear to be a potentially useful method of studying short-range diffusion, such an approach may stimulate further theoretical investigations into turbulence by revealing factors hitherto unsuspected from experiments using more conventional techniques.

REFERENCES

ACKERMANN, B. The application of variance spectrum
analysis to cloud measurements
TECH. NOTE NO. 34.
DEPT. OF GEOPHYSICAL SCIENCES,
UNIVERSITY OF CHICAGO

ASPINALL, W.P. 1969 Ph.D. THESIS
UNIVERSITY OF DURHAM

BENDAT, J.S. and 1966 Measurement and analysis of Random
PIERSOL, A.G. Data
WILEY

BENT, R.B. 1964 Ph.D. THESIS
UNIVERSITY OF DURHAM

BEST, A.C. 1935 Transfer of heat and momentum in
the lowest layers of the atmosphere
Met. Office Geophysical Memoirs No. 65

BLACKMANN, R.B. 1958 The measurement of power spectra
and TUKEY, J.W. DOVER PUBLICATIONS

BLEANEY, B. I. and 1965 Electricity and Magnetism 764 p.
BLEANEY, B. C.U.P.

BRUNT, D. 1939 Physical and Dynamical Meteorology
C.U.P.

CARSLAW, H.S. and 1959 Conduction of heat in solids 510 p.
JAEGER, J.C. OXFORD, CLARENDON PRESS

CHALMERS, J.A. 1963 Taking the mystery out of Gauss's
theorem
Contemp. Physics $\underline{4}$, 456-8

CHALMERS, J.A. 1967 Atmospheric Electricity 515 p.
PERGAMON

I.

CRAMER, H.E.,
GILL, G.C. and
RECORD, F.A.

1954

Research into atmospheric turbulence
and associated diffusion of aerosols
and gases near the Earth's surface

MIT. Report under contract AF19. (604
- 145

CRAMER, H.E.,
GILL, G.C. and
RECORD, F.A.

1957

Heated thermocouple anemometers and
light bivanes

Exploring the Atmosphere's First Mil
edited by H. LETTAU and B. DAVIDSON
1, 233 - 242

PERGAMON

CROZIER, W.D.

1963

Electrode effect during night-time
low wind conditions

J. Geophys. Res. 68, 3451-8

DAVIDSON, B. and
HALITSKY, J.

1958

A method of estimating the field of
concentration from tower bivane data

J. Air. Poll. Contr. Ass. 7, 316 - 3

DAYARATNA

1969

Ph.D. THESIS

UNIVERSITY OF DURHAM

DEACON, E.G.

1955

The turbulent transfer of momentum
in the lower layers of the atmospher

Tech. Paper No. 4. Melbourne
CSIRO Div. Met. Phys.

DE'SA, O. and
MOLYNEUX, L.

1962

Electronic Engineering, 34, 468 - 46

A transistor voltage to frequency
convertor

EBERT, H

1901

Aspirations Apparat zur Bestimmung
des Ionen Gehaltes der Atmosphäre

Phys. Z, 2, 662-6

EBERT, H

1904

Über die Ursache des normalen atmos-
phärischen Potentialgefälles und der
negativen Erdladung

Phys. Z., 5, 135-40

ELSTER, J and
GEITEL, H.

1899

Über die Existenz elektrischer Ionen
in der Atmosphäre

Terr. Magn. Atmos. Elect. 4, 213-34

HOPPEL, W.A. and   1972   Experimental determination of the
GATHMAN, S.G.   eddy diffusion coefficient over the
                           open ocean from Atmospheric Electric
                           Measurements

                           J. Phys. Oceanog. Vol. 2, No. 3,
                           248-254

IMIANITOV, I.M.   1949   Measuring the horizontal component
                           of the atmospheric-electric field

                           IZV. AKAD, NAUK. SSSR. Ser. Geog.
                           Geofiz 13, 320-40

KAWANO, M   1957   The coefficient of eddy diffusivity
                           estimated by the method of Atmospheric
                           Electricity

                           J. Met. Soc. Japan Series II
                           35, No. 6, 29-32

KELVIN, LORD   1860   Electricity Atmospheric

                           Nichol's Cyclopaedia 2nd Ed.,
                           Paper on Elec. and Magn.   192-208

LANGEVIN, P.   1905   Sur les ions de l'atmosphère

                           C.R. Acad. Sci. Paris, 140, 232-4

LARGE, M.I. and   1957   The dependence of point discharge
PIERCE, E.T.   currents on wind as examined by a new
                           experimental approach

                           J. Atmos. Terr. Phys. 10, 251-7

LEMONNIER, L.G.   1752   Observations sur l'électricité de l'air

                           Mem. Acad. Sci. 2, 233

LOEB, L.B.   1968   Electric coronas - their basic prin-
                           ciple mechanisms   694 p.

                           UNIVERSITY OF CALIFORNIA PRESS

LUMLEY, J.L. and   1964   The structure of atmospheric turbulence
PANOFSKY, H.A.   239 p.

                           WILEY

LUMLEY, J.L. and   1972   A first course in turbulence
TENNEKES, H.   300 p.

                           MIT PRESS

MAPLESON, W.W.   1955   Apparatus for accurate and continuou
and WHITLOCK, W.S.   measurement of the Earth's electric
                                field
                                J. Atmos. Terr. Phys. 7, 61-72

MAUND, J.E.   1958   Ph.D. THESIS
                                UNIVERSITY OF DURHAM

MÜHLEISEN, R.   1953   Die luftelektrischer Elemente in
                                Grossstadtbereich
                                Z. Geophys. 29, 142-60

OGDEN, T.L.   1967   Ph.D. THESIS
                                UNIVERSITY OF DURHAM

PASQUILL, F.   1962   Atmospheric Diffusion   297 p.
                                Van NOSTRAND

PRIESTLEY, C.H.B.   1959   Turbulent transfer in the lower atmo
                                phere   130 p.
                                UNIVERSITY OF CHICAGO PRESS

PROJECT PRAIRIE   1956   Detailed description of the techniqu
GRASS   used can be found in:
                                CRAMER, H.E., GILL, G.C. and
                                VAUGHAN, H.C. (1958)
                                The study of the diffusion of gases
                                or aerosols in the lower atmosphere
                                MIT. Dept. of Meteorology, Final Repo
                                under contract AF 19 (604) - 1058

RACTLIFFE, J.F.   1962   Elements of Mathematical Statistics
                                202 p.
                                O.U.P.

RICHARDSON, L.F.   1925   Turbulence and vertical temperature
                                differences near trees
                                Phil. Mag. 49, 81-90

ROBERTS, O.F.T.   1923   The theoretical scattering of smoke i
                                a turbulent atmosphere
                                PROC. ROY. SOC. (LONDON) A 104, 640-6

IV.

SCHMIDT, W. 1918 Wirkungen des Luftaustauches aus des Klina und der taglichen Gang der Lufttemperatur in der Höhe

Sitzber. Akad, Wisserisch. Wien 127, 1942-1957

SCRASE, F.J. 1930 Some characteristics of eddy motion in the atmosphere

Met. Office Geophys. Memoirs No. 52

SHARPLESS, G.T. 1968 Ph.D. THESIS
UNIVERSITY OF DURHAM

SUTTON, O.G. 1953, Micrometeorology 333 p.
McGRAW-HILL

TAYLOR, G.I. 1935 Statistical theory of turbulence Parts 1-4

Proc. Roy. Soc. A 151, 421-478

THOMPSON, R 1971 Numerical Calculation of turbulent diffusion

Q.J. ROY. MET. SOC. 97, 93-98

TORRESON, O.W. 1939 Condensation nuclei in the atmosphere in Peru, and their relation to atmospheric-electrical and meteorological observations

Terr. Magn. Atmos. Elect. 44, 59-74

WHITLOCK, W.S. and CHALMERS, J.A. 1956 Short period variations in the atmospheric electric potential gradient

Q.J. ROY. MET. SOC. 82, 325-36

WILSON, C.T.R. 1900 On the leakage of electricity through dust free air

Proc. Camb. Phil. Soc. 11, 32

WRIGHT, H.L. 1936 The size of atmospheric nuclei, some deductions from measurements of the number of charged and uncharged nuclei at Kew observatory

PROC. ROY. SOC. (LONDON) 48, 675-689